ON THE DEVELOPMENT OF NUMERICAL ALGORITHMS FOR THE CLINICAL ANALYSIS OF THE SINGLE BREATH NITROGEN WASHOUT CURVE

Kevin O'Mara

A Thesis

In

The Faculty of

Engineering and Computer Science

Presented in Partial Fulfillment of the Requirements
for the degree of Master of Computer Science at
Concordia University
Montreal, Quebec, Canada

August 1981

ABSTRACT

ON THE DEVELOPMENT OF NUMERICAL ALGORITHMS FOR THE CLINICAL ANALYSIS OF THE SINGLE BREATH NITROGEN WASHOUT CURVE

Kevin O'Mara

This thesis describes the development of a special purpose computer-aided medical diagnostic system which uses numerical methods to tackle a clinically important pattern recognition problem.

My thesis describes a discrete non-linear least squares algorithm suitable for the automated analysis of the single breath nitrogen washout test. This quick, sensitive, non-invasive test of lung function assesses small airway pathology and may be of use in the diagnosis and management of early obstructive lung disease.

The first two chapters of this thesis present various aspects and models of pulmonary mechanics and airway structure that are believed to underly the significance of this test.

A major difficulty in the manual application of the single breath washout tests to the clinical evaluation of lung function is that visual examination is a very subjective method for determining the onset of airway closure. More reliable techniques involving the mathematical analysis of these curves are essential for the quantitative evaluation

of closing volume curves in the study of small airway function.

This thesis presents numerical methods for the discrete linear, discrete non-linear and continuous linear analysis of these curves. Details of the implementation of the most sophisticated of these algorithms are presented. Preliminary results of work are described along with a discussion of the clinical applicability and comparative value of this algorithm.

ACKNOWLEDGEMENTS

My first introduction to Concordia University and its Department of Computer Science was through Rod Vokey, who was at that time a student of Professor Terrill Fancott. I have profited greatly from that introduction. In fact, were it not for Dr. Fancott's advice and support, thrbugh both the good and the hard times, I would not have entered the M. Comp. Sci. program, let alone finished this thesis. I am thankful to Dr. Fancott for his supervision and guidance in which he has emphasized perseverence and stamina in the pursuit of quality.

Sections of this thesis, particularly Chapter Two, owe their clarity of thought to a very stimulating and productive afternoon spent with Dr. Jere Mead.

Anyone who has had the pleasure of working with the late Dr. K.V. Leung will notice his handiwork and style reflected in many of the mathematical formulations presented in this thesis. I am very lucky to have known K.V. as a teacher, colleague and friend.

There are many others who have consistently offered me encouragement and guidance. Of these I have been productively influenced by the philosophies of Professors M.W. Jaworski, P.S. Digby, M.N. Oğuztöreli and E.J. Stansbury, while I have been helped, when it was needed most, by Drs. A.W. McLeod, H. Frank, S. Klasa and M. Becklake.

This is an excellent time to also thank both Kent Farrell and Libero Ficocelli for their thoughtful discussions and criticisms of

the various drafts of this work. I shall not forget the many ways in which their kindness has aided me.

I wish to express my gratitude to Beverley Abramovitz who has cheerfully typed and corrected a difficult manuscript. I am thankful for the quality and speed of her work.

Finally, I would like to thank my parents, who have taught me, more than anyone, through their altruism, patience, and understanding. I dedicate this work to them.

PREFACE

Computer-aided medical diagnosis using the techniques of pattern recognition and numerical methods in conjunction with graph and game theory is rapidly changing the scope and quality of modern medicine. These changes are also influencing our view of computer science as it progressively integrates with the mainstream of scientific endeavour.

This thesis describes the development of a special purpose computer-aided medical diagnostic system which uses numerical methods to tackle a clinically important pattern recognition problem.

I have attempted to describe this problem, its relevance, and a possible solution, in a way that will be understandable to a scientist whether he or she be a medical or computer expert. As such, I have used mathematics and graphics as an adjunct to the text.

Considering the scope of this undertaking I have used the bibliography to point to review articles and texts in specialized areas. This thesis does not offer a comprehensive overview of either the subject matter or the literature. The area is simply too wide. In fact, for each reference listed in the bibliography there are two others that I have deleted.

Similarly, this thesis is an inappropriate place to present the detailed results of an epidemiological study of the algorithm's clinical performance. Hence the technical details of the algorithm's design [90] and modification [126] are published separately from the results of a clinical trial [127].

TABLE OF CONTENTS

List of Symbols and Abbreviations*

INDEX

*These symbols and abbreviatons conform where possible to those recommended in the literature [110].

1.1 Upper Case Roman Script Symbols

Symbol	Meaning	Function of:	Equation
E	Pulmonary Elasticity	$V,\dot{V},\dot{V}\dot{V},t$	2.7
R	Pulmonary Resistance	$V,\dot{V},\dot{V}\dot{V},t$	2.8
I	Pulmonary Inertance	$\ddot{V},t$	2.5
C	Pulmonary Compliance	$V,\dot{V},\dot{V}\dot{V},t,1/E$	

1.2 Upper Case Roman Symbols

Symbol	Parameter	Function of	Given in Equation
A	Integral	$\lambda(b)$	4.16
B	Integral	$\mu(b)$	4.17
C	Sum	ξ,N	3.11
F	Fractional Concentration		
G	Aerodynamic Inertia	T	2.14
H	Aerodynamic Resistance	T	2.15
I	Linear Continuous Model	α,β,η,ξ	4.2
J	Volume of Expired Nitrogen	$V,\Delta,\nabla,[N_2]$	5.1
K	Fiducial Number of Points	ξ	3.3
M	Sum	K,ξ	3.12
N	Total Number of Discrete Points		
P	Pressure	t,τ	2.6
Q	Sum of Squares	K,ξ	3.13
$\dot{Q}$	Blood Flow or Perfusion		
R	Sum	$(N-K),\xi$	3.14
S	Sequence		
T	Sum of Squares	$(N-K),\xi$	3.15
U	Sum	ξ,N	3.10
V	Volume	t,P	2.3
$\dot{V}$	Flow	t,P	2.1
$\ddot{V}$	Acceleration	t,P	2.5

Symbol	Parameter	Function of	Given in Equation
W	Work	$P,\dot{V}$	2.18
$\dot{W}$	Rate of Work	γ,W	2.20
X	Sequence of Discrete Nitrogen Concentration Values		3.1
Y	Sequence of Discrete Lung Volume Values		3.1
Z	Generation		2.17

1.3 Independent Lower Case Roman Symbols

Symbol	Meaning	Function of	First Given in Equation
a	Boundary points		3.1
b	Boundary points		
c	Integral	$\nu(b)$	4.18
d	Airway diameter	z	2.17
e	$[N_2]$ Intercept for Phase II		5.2
f	See Operators		
f_1	Elasticity term	$V,\dot{V}$	2.7
f_2	Resistance term	$V,\dot{V}$	2.8
f_3	Inertiance term	$\ddot{V}$	2.5
i	See Lower Case Subscripts		
j	See Lower Case Subscripts		
ℓ	Airway length	Z	2.16
m	Slope of the initial part of Phase III		5.2
n	See Lower Case Pointers		
q	See Symbols Modified by Subscripts		
r	See Lower Case Pointers		
t	Time		
u	See Lower Case Pointers		
v	See Lower Case Pointers		
w	See Lower Case Pointers		
x	See Symbols Modified by Subscripts		
y	See Symbols Modified by Subscripts		

1.4 Lower Case Roman Symbols Modified by Subscripts

Symbols	Meaning	Subscript
$\dot{v}$	Regional Airflow	j
$\dot{q}$	Regional Bloodflow	j
x	Lung Volume Reading	1,2,3,...n....N
y	Nitrogen Concentration Reading	1,2,3,...n....N
ℓ	Airway Length	0
d	Airway Length	0

2.0 Greek Symbols

Symbol	Meaning	Function of	First Found in Equation
γ	Frequency of breathing		2.20
ρ	Density		2.13
χ	Viscosity		2.13
Ψ	Complement of Ω		5.5
Ω	Angle between α and β		5.5
ω	Angular frequency		2.13
ν	Integral	ξ	4.15
μ	Sum or Integral	ξ	3.17,4.14
λ	Sum or Integral	ξ	3.16,4.13
η	Nitrogen concentration	ξ	3.18
ξ	Lung volume	Φ	3.20
Φ	Non-linear discrete model parameter	K,N-K,α,β,η,ξ,X,Y	3.19
Λ	Continuous model parameter	η,ξ,ϕ_1,$\phi 2$	4.10
ϕ_1	Continuous model parameter	ξ	4.11
ϕ_2	Continuous model parameter	ξ	4.12
T	Womersley parameter	d,w,ρ,χ	2.13
α	Slope of Phase III	(n,ξ)	3.8
β	Slope of Phase IV	(n,ξ)	3.9
κ_1	Coefficient of laminar flow in Rohrer's model		
κ_2	Coefficient of turbulent flow in Rohrer's model		

Symbol	Meaning	Function of	First Found in Equation
τ	Time lag term		2.6
α_1	Coefficient of flow		2.2
α_2	Second order Coefficient of flow		2.2
α_3	Coefficient of flow-volume interaction		2.2
α_4	Coefficient of volume		2.4
α_5	Second order coefficient of volume		2.4
α_6	Coefficient of volume-flow interaction		2.4
α_7	Coefficient of inertia		2.5
α_8	Equilibrium pressure point		2.6

3.0 Special Symbols

Symbol	Meaning	Equation
$\not\equiv$	Radioactive gas molecule	5.1
Δ	Boundary points on the SBN_2 curve	5.1
∇		5.4
$\bullet$		

4.0 Upper Case Roman Subscripts Used to Modify Parameters

Subscripts	Meaning	Parameter
A	Alveolar	P,V,F
D	Deadspace	V
E	Expiratory	VC,F,V
I	Inspiratory	VC,F,W,V
L	Lung	P

4.1 Lower Roman Case Subscripts

Symbol	Meaning	Equation
ao	Mouth	2.0
eL	Elasticity	2.0
es	Esophageal	2.6
pL	Pleural	2.0
res	Resistance	2.0
i	Inertia	2.0
j	jth region	
o	Initial	

4.2 Second Order Roman Subscripts

Subscript	Used to Modify Subscript
N_2	A,E
anat	D

4.3 Lower Case Roman Pointers

Pointers	Meaning	Parameter
u	Start of sequence	S
v	Sequence pointer $u \leq v \leq w$	S
v(1)	Sequence pointer 1st position	S
v(2)	Sequence pointer 2nd position	S
w	End of sequence	S
r	Value of present iteration	ξ
r-1	Value of previous iteration	
r+1	Value of next iteration	
n	Value of persent iteration	ξ
n-1	Value of previous iteration	
n+1	Value of next iteration	

5.0 Pulmonary Abbreviations

Lung Volumes and Capacities (See Figure 1.0 on page 10)

Abbreviation	Meaning
RV	Residual volume
TLC	Total lung capacity
CV	Closing volume
CC	Closing capacity
VC	Vital capacity
VC_I	Inspired vital capacity
VC_E	Expired vital capacity
FRC	Functional Residual capacity
FVC	Forced vital capacity

Gases

O_2	Oxygen
N_2	Nitrogen
CO_2	Carbon Dioxide

General Terms

BTPS	Correction factor to account for body temperature and atmospheric pressure effects on pulmonary parameters
SBN_2	Single breath nitrogen washout procedure
NHLI	United States of America National Heart and Lung Institute

7.0 Program Acronyms

Algorithms	Use
A1	Main non-linear least squares algorithm
A2	Data selection algorithm
A3	Algorithm for the computation of lung volumes
A4	Anatomical dead space algorithm
A5	Flow rate monitor algorithm
A6	Quality control algorithm
A7	Segmentation algorithm

Restraints	
R1	Arithmetic restraints on division by zero
R2	Convergence restraint on Epsilon 2
R3	Arithmetic restraint on the recursive algorithm
R4	Slow convergence restraint on solution
R5	Restraint on data selection procedure
R6	Restraint on the minimum significant size of the data file

Constraints	
C2	The slopes of Phase III and Phase IV are equal
C1	The slope of Phase III > the slope of Phase IV

General Terms

Abbreviation	Meaning
COPD	Chronic obstructive pulmonary disease
phase I	Anatomical dead space gas
phase II	Mixed alveolar and dead space gas
phase III	Alveolar gas plateau
phase IV	Regionally sequestered alveolar gas

6.0 Operators

Symbol	Operation	Operand
$\vdots$	Permutation	S
[ ]	Concentration	CO_2, N_2, O_2
| |	Absolute value	VC_I, VC_E, P, V
Δ	Difference	P,V
Γ	Sum of squares	f
f	Function	.....
dx	First derivative of x	V,t
∂x	Partial derivative of x	$\Gamma, d, \beta, \eta, \xi, v, t$
$\dot{x}$	First derivative of x	W,V
$\ddot{x}$	Second derivative of x	V
$\hat{x}$	Predicted value of x	$\bar{d}, \bar{\ell}, N_2$
x^n	nth power of x	n = 1,2...6
$\bar{x}$	Mean value of x	$d, \ell,$
$\Big\|_y^x$	Evaluated between x and y	$V_{E_{N_2}}$

Parameters	Use
Epsilon 1	Significance threshold for $\phi \neq 0$
Epsilon 2	Minimum improvement threshold
ITMAX	Maximum number of iterations
INUM	Minimum number of data points

Behavior	Meaning
LIFO	Stack like: Last-in-first-out
FIFO	Queue like: First-in-first-out

8.0 Abbreviated Units of Measure

mL	milliliter
sec	second
msec	millisecond
µm	micrometer

LIST OF FIGURES

CHAPTER ONE

INTRODUCTION

The human cardio-pulmonary circuit is a complex, hierarchical and highly interactive system. It has evolved to successfully effect gas exchange for cellular metabolism in a terrestrial environment. As such, it would naively appear that the only germain and meaningful tests of cardio-pulmonary performance are measurements of arterial gas tensions. In the ultimate sense this view is correct. Consequently, arterial blood-gas measurements have become a very common and useful aid in the diagnostic assessment and management of cardio-pulmonary status within critical care units [43,5,111,163]. Computer aided systems have been developed to facilitate the clinical interpretation [124,163,155], technical analysis [58,78,35] and measurement [4,35] of blood gas tensions and hydrogen-ion balance. While arterial blood gas measurements can provide essential information on the viability of an individual, they are relatively insensitive to anything less than very severe cardio-pulmonary abnormalities [5,142].

The physiological reserves and compensatory mechanisms of the cardio-pulmonary system are efficient enough to maintain its perfusion and gas exchanging abilities even in cases where the organ system is severely compromised by disease [103,5,21]. In fact, there is no known single parameter that can measure or reflect all aspects of respiration [103]. For this reason, a multiplicity of

tests have been used to assess pulmonary and cardio-pulmonary function. Each of these tests has its own unique advantages and disadvantages. These tests have sought to evaluate the precise aspects of pulmonary mechanics that determine lung pressures [70,53,12], volumes [161,86], flow rates [166,19,86], and gas diffusion capacities [88, 133,136,131] on the entire, intact human lung. Such in vivo tests are often used to infer the structural or morphological abnormalities believed to underly the observed physiological data [27, 103, 17, 96, 145, 134].

Thus, in order to achieve a comprehensive overview of cardio-pulmonary function, it is necessary to perform a battery of tests on an individual [121]. Clinical expertise has made it possible to interpret patterns of abnormalities in the results of these diagnostic procedures even when the integrity of the system's gas exchanging abilities has not been compromised [121,97,116,135,120]. Consequently, multifactoral pattern analysis is often used in preference to a more specific or technically precise diagnostic measurement [123]. Some computer aided diagnostic systems have been developed to exploit the multifactoral analysis [44,145] and assessment [3,66,100] of pulmonary function. Statistical [100,156] and syntactic [123,152,150] algorithms have been developed for this type of diagnosis [155,156] and prognostic assessment [125,79] of the pulmonary patient.

The diagnostic success of such multifactoral pattern analysis can be attributed to the fact that disease processes often involve

the lung tissue, or parenchyma, and airways nonhomogeneously. From a nonhomogeneous assault on this system, often only a fuzzy pattern emerges from the lumped, or global, measurement of the many parameters of pulmonary mechanics. The more nearly homogeneous the lungs are, the more precise are the facile interpretations of such global measurements. Thus, for the analysis of the normal human lung, the approach is simplified since the tests can be more realistically thought of as dealing with a complex but homogeneous structure. In the normal individual, the lung parenchyma and airways may be successfully analysed [88,19,96,12] and modeled [71,69,20,89,166] in terms of gas flow as the consequence of a single driving pressure. In such models, the various lung volumes and capacities of the system are treated as indices of its overall geometry. Such a lumped circuit analysis based on a single degree of freedom is a gross oversimplification for a system as complex as the human lung. Paradoxically, however, the very complexity of this system contributes to the validity of such a gross analysis. Thus, for example, in spite of large differences in path lengths and bifurcations in the bronchial tree of the normal human lung, the alveoli have been observed [130] to empty and fill in synchrony throughout the lung. Thus, lumped circuit analysis has provided the clinician and biophysicist both practical and basic information.

Irregardless of their specific characteristics, almost all tests of pulmonary mechanics are interpreted in terms of current paradigms

of lung mechanics. The limitations and hypotheses underlying these models are discussed in the first section of chapter two. The latter half of chapter two contains a brief, essential, overview of the form and function of the human bronchial tree.

The techniques that are currently in use in a lumped circuit analysis of pulmonary mechanics can be divided into invasive and non-invasive measurements. Today, the medical and research community try to use invasive techniques sparingly and only when the information they provide is important and unobtainable by safer means.

Pulmonary function tests may be subsequently subdivided into those that employ submaximal or maximal respiratory effort on the part of the subject. The latter were among the first measurements to be developed for the purpose of studying lung function in health and disease [108,103,5]. While such maximal efforts may be easily monitored by relatively simple equipment, they only indirectly assess the state of patency, or caliber, of the airways [3,103]. These tests are also heavily dependent on patient co-operation and the lung volume at which they are taken.

On the other hand, some submaximal techniques such as dynamic compliance [162,77] and resistance measurements [9,112] can be recorded during spontaneous tidal breathing and provide a direct assessment of the impedance to ventilation [103,166]. However, many of these submaximal effort techniques require expensive, sophisticated equipment as well as a fair degree of time and effort to perform.

Some of these techniques are believed to preferentially assess small airway function [68,95,94,81]. The significance of such tests is that they appear on the grounds of morphological and physiological evidence [27,134,102] to be the first sites of the pathology associated with early obstructive lung disease. As a result of the rapidly increasing incidence of both chronic obstructive lung disease and pulmonary carcinoma, a significant degree of attention has been devoted to the development of quick non-invasive tests capable of determining the onset of early obstructive lung disease. Such a test should be suitable for the mass screening of the population at risk [6,62,28,84,82]. The single breath nitrogen washout test has been proposed as an efficient and reliable [38,37] measure for this task. The second section of chapter three references a synopsis [6] of the various epidemiological and morphological considerations involved in the assessment of the specificity, sensitivity, acceptability, precision and validity of this test.

The single breath gas washout curve was first described by Fowler [49] and has classically been used to estimate various aspects of gas distribution in the human lung.

In 1967 Dollfuss, Milic-Emili and Bates [36] described a modification of this manoeuvre using ^{133}Xe as a tracer gas. They were the first to realize that this test could potentially be used to determine the lung volume in gravitationally dependent airways at the onset of their closure. This volume is referred to as the

lung's closing volume. Since then other gases such as helium, argon, and nitrogen have been used in extensive studies of single breath washout curves [16], their reproducibility [7,99], and their diagnostic uses [16,138] in health and disease. The physiological basis of this test and its interpretation will be discussed in the first section of chapter three.

The closing volume determination is of clinical interest in that it is an easily performed, non-invasive measurement related to small airway function. As such it has been proposed as a simple but sensitive test for the detection and assessment of early obstructive lung disease [102,95].

While this test has been shown to be well suited for use in a respiratory disease screening program, the prognostic implications of an abnormal closing volume tracing are not yet known [14,48,134]. In fact, while the closing volume test parameters may be considerably more sensitive than any other single test of small airway function, it remains to be shown that individuals with abnormally large closing volumes will eventually manifest irreversible airway obstruction [16,102].

A major difficulty in the use of the single breath gas washout test in the clinical evaluation of lung function is that the visual examination required is an extremely subjective method for determining the onset of airway closure [99,91]. More reliable techniques involving the mathematical analysis of these curves are essential

for the quantitative evaluation of closing volumes in the study of small airway function [39].

It seemed appropriate therefore to develop a numerical technique for the analysis of the single breath gas washout curve based on an exact theoretical formulation of this problem. Four other groups of researchers have developed numerical techniques for the analysis of the single breath nitrogen washout curve, SBN_2. Two of these groups [53,61] have developed computer programs for estimating the slope of the alveolar plateau, or phase III component, of this curve.

Both of these programs made use of the method of least-squares to evaluate the best numerical fit of a straight line to a portion of the washout curve that they considered characteristic of the alveolar plateau. These programs then located the onset of the subsequent portion, or phase IV, of the curve in accordance with the literal definition of closing volume as "the last point of departure of the expired nitrogen concentration curve from a straight line fitted to the latter part of phase III" [51].

The two other groups [34,33] have implemented computer programs that calculated the onset of closing volume as the point of intersection of the two straight lines independently fitted to the phase III and IV segments of the tracing. These programs calculated CV in accordance with the methodology proposed by Hamosh and Taveira da Silva [64] rather than following that outlined in the standardized guideline [51].

While these groups of researchers reported similarly encouraging results on generally reliable computer programs with good clinical applicability, they also noted the need for an improvement of their techniques [53,61]. Cramer and Miller [33], in their work on perhaps the most sophisticated algorithm to-date, have acknowledged the need for further theoretical work on the problem of pinpointing the beginning of closing volume.

Chapter Two of this thesis gives a brief overview of the lung's structure and discusses various models that have been used to describe its form and function.

Chapter Three addresses some specific problems of gas distribution within this structure and describes the theoretical developemnt of a numerical method for the analysis of the single breath washout curve. This method, which has been accepted for publication [127], involves the discrete simultaneous non-linear least-squares estimation of the slopes of the phase III and phase IV components of the curve.

A copy of an earlier paper [90] involving the discrete linear analysis of this data may be found in Appendix 1 of this thesis, while a continuous linear analysis of this curve is presented in Chapter Four.

Chapter Five describes the implementation of the most sophisticated of these algorithms: the discrete non-linear analysis.

Chapter Six presents a preliminary study of the results obtained by this algorithm. These results were obtained on test cases [146] which were provided by Dr. Margret Becklake of McGill University's Epidemiology Department.

Chapter Seven presents a discussion of the protocols proposed for the analysis of the single breath nitrogen washout curve in light of our results. Appendix 2 of this thesis contains a copy of the protocol proposed by the American National Heart and Lung Institute for the measurement and analysis of this test.

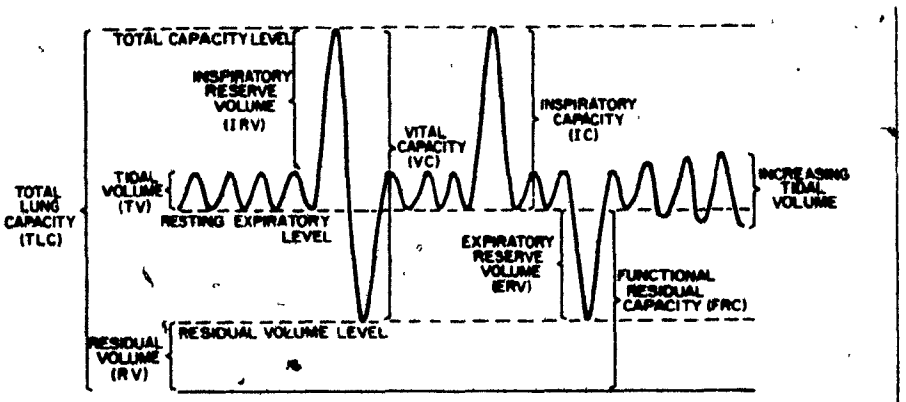

Figure 1.0. The volumes and capacities of the lung can be appreciated from a study of the diagram. There are four volumes: (1) the tidal volume (TV), which is the amount of gas moving in and out of the lung with each respiratory cycle; (2) the residual volume (RV), which is the amount remaining in the lung after a maximal expiration and is the only lung volume that cannot be measured directly by spirometry; (3) the inspiratory reserve volume (IRV), the additional gas that can be inspired from the end of a quiet inspiration; and (4) the expiratory reserve volume (ERV), the additional amount of gas that can be expired from the resting or end-expiratory level.

There are also four capacities, each of which contains two or more volumes: (a) total lung capacity (TLC), which is the gas contained in the lung at the end of a maximal inspiration; (b) vital capacity (VC), which is the amount that can be expired after a maximal inspiration; (c) inspiratory capacity (IC), which is the amount of gas that can be inspired from the end of a quiet expiration; and (d) functional residual capacity (FRC), which is the volume of gas remaining in the lungs at the end of a quiet expiration. From [50].

CHAPTER TWO

The first section of this chapter provides an overview of respiratory mechanics and the models that have been used to analysis and predict the macro-behaviour of this system.

The second section of this thesis presents a short synopsis of the structure and function of the lung's bronchial tree.

Section 2.1

An eighteenth century physiologist, the Rev. Stephen Hales, appears [158] to have been the first scientist to attempt to quantitatively correlate function and structure in the lung. Since then a great many scientists have contributed to our knowledge of the inter-relation between the lung's morphology and it's physiology [71,158]. Today most tests of pulmonary mechanics may be easily interpreted in terms of the basic paradigm of lung mechanics proposed by Mead [106] in 1961.

This paradigm involves the use of an equation of motion to describe the manner in which transpulmonary pressure develops sufficient force to overcome the elastic, frictional and inertial properties of the lung. Each of these three properties may be considered [108] in terms of the pressure, or force per unit area, needed to overcome them. The applied pressures considered in this model are equal to the pressure differences observed across the anatomical structures of the lung.

The total trans-pulmonary pressure of the lung, P_L, may be considered to be partitioned into its elastic, frictional and inertial components by segmenting the total pressure differences across the lung, P_L into the component terms in Mead's paradigm [67]. Thus, as is shown in figure 2.1, P_L may be segmented into:

$$P_L = P_{ao} - P_{pl}$$

$$= (P_{ao} - P_A + (P_A - P_{pl}) + P_i \qquad (2.0)$$

$$= P_{res} + P_{el} + P_i$$

where

P_{ao} is the pressure at the mouth,

P_A is the alveolar pressure,

P_{pl} is the pleural pressure and

P_{res} is the pressure required to overcome frictional resistance, P_{el} is the pressure required to overcome elasticity and P_i is the pressure required to overcome the inertial elements of the lung.

P_{el} is proportional to lung volume, $V(t)$, at time t, while P_{res} is proportional to its velocity, $\dot{V}(t)$ and P_i is proportional to its acceleration, $\ddot{V}(t)$.

Rohrer first described the P_{res} in terms of the expression:

$$P_{res} = \kappa_1 \dot{V}(t) + \kappa_2(V(t)^2) \qquad (2.1)$$

The term $\kappa_1 \dot{V}(t)$ accounts for the resistance to laminar flow to the lung's airways, while the term $\kappa_2(\dot{V}(t)^2)$ accounts for the effects of non-uniform, turbulent flow in the conducting airways. Experimentation [1,166,80] has shown that while equation 2.1 provides a

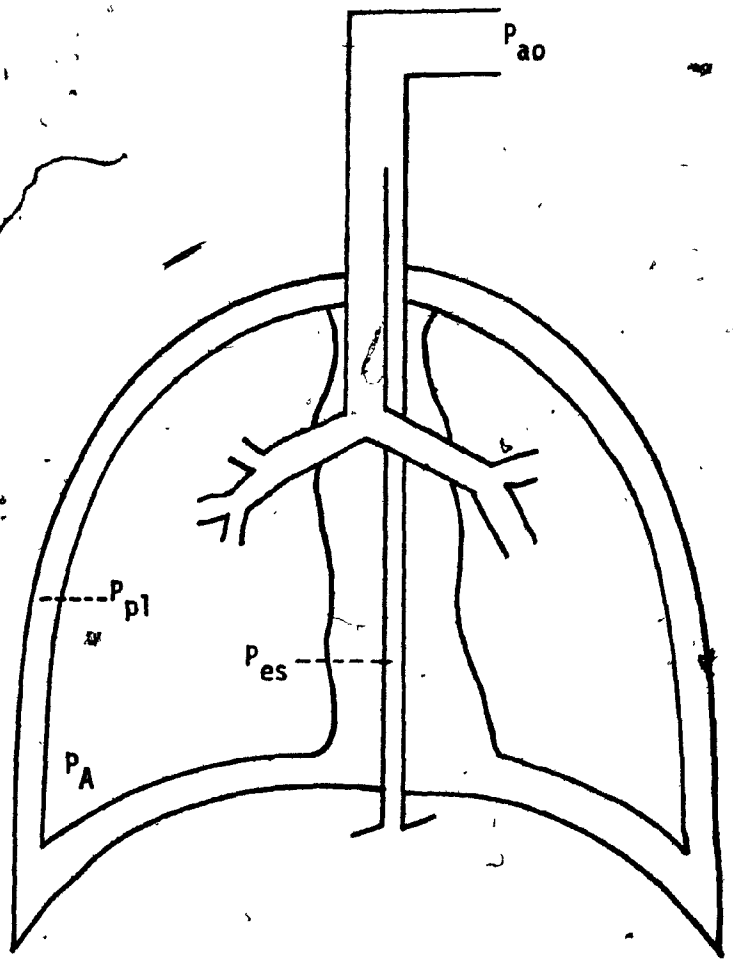

Figure 2.1. Schematic Diagram of the Pressure Differences Across the Lung. See Text for details.

Pressures pertinent to analysis of respiratory function. Pressures which are measured relative to an arbitrary reference, usually atmospheric pressure.

The thoracic cavity is divided by the mediastinum into 2 major chambers which contain the right and left lungs. The right lung has 3 lobes (upper, middle and lower) separated into a total of 10 segments, and is supplied with air via 3 lobar bronchi which branch to form 10 segmental bronchi. The left lung is divided into 2 lobes (upper and lower) comprising 9 segments. After [67].

reasonably good fit of the dynamic pressure-flow curve, P-$\dot{V}$, the coefficient κ_1 in equation 2.1 is inversely proportional to lung volume [166], while κ_2 appears to be independent of variation in lung volume. Rohrer's interpretation of κ_1 and κ_2 is most likely wrong [80].

Considering: $\kappa_1 = (\alpha_1 - \alpha_3 V(t))$ equation 2.1 may be expanded to give:

$$P_{res} = (\alpha_1 + \alpha_3 V(t))\dot{V}(t) + \alpha_2(\dot{V}(t)^2)$$

$$= \alpha_1 \dot{V}(t) + \alpha_2(\dot{V}(t)^2) + \alpha_3(V(t)\ \dot{V}(t)) \qquad (2.2)$$

where α_2 has been found to range [112,166] in value from 0.15 to 0.38 and α_3 is a small negative number [104].

The elastic properties of the lung have historically been considered in term of either dynamic or static pressure-volume, P-V, plots. The dynamic analysis of elasticity of the lung describes the instantaneous pressure-volume relationship encountered through the entire range of flow velocities which existsduring breathing. The static P-V curve is obtained by measuring the pressure-volume relationship under conditions of zero flow and zero frequency. Under conditions of low flow over relatively small lung volumes, resembling those of tidal breathing, the dynamic P-V curve approaches that obtained for the static case. Figure 2.2 describes the details of this procedure. Thus, while P_{el} has been considered to be a simple function of V(t) [109],.

$$P_{el} = \bar{C}V(t) \quad \text{where} \quad C = \Delta V/\Delta P \qquad (2.3)$$

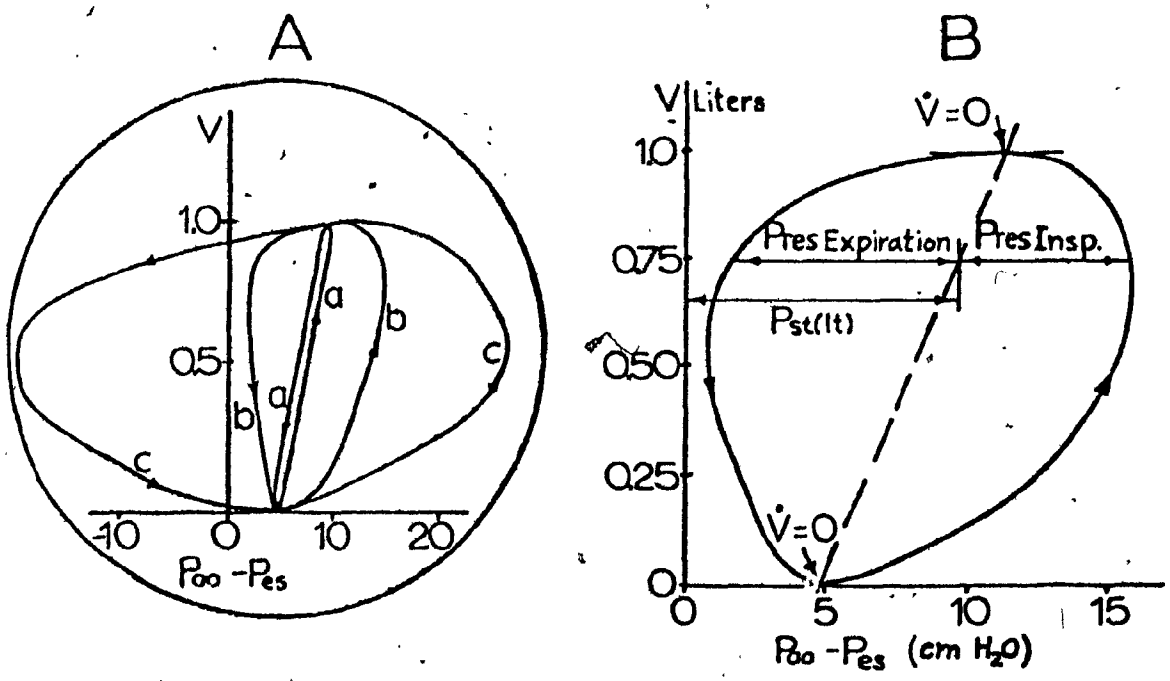

Figure 2.2. Analysis of Dynamic v-p Loops of the Lung.

A, these oscilloscopic tracings were made by simultaneously recording tidal volume from a spirometer on the vertical axis and transpulmonary pressure (Pao-Pes) on the horizontal axis at three breathing rates: (a) very slow breathing, about 3 breaths per minute, (b) moderately rapid breathing, about 40 breaths per minute, (c) near maximal breathing rate. In (a) the flow resistive pressure is negligible.

B, A line joining the two points at which $\dot{V} = 0$ gives the dynamic elastic v-p curve of the lung. Pst (lt) is due to the elastic lung retractive force while Pres is due mainly to gas flow resistive and partly to tissue resistive forces. From [67].

it is in fact a function of both $V(t)$ and $\dot{V}(t)$ in that C is in fact a function of $V(t)$ and $\dot{V}(t)$.

Thus, while the static compliance curve shown in figure 2.3 has been successfully used for diagnostic purposes [5, 67], it provides only a first-hand approximation of P_{el}. A more refined approximation may be provided by equation 2.4, which contains a quadratic term in $V(t)$ and an interaction term $(V(t)\dot{V}(t))$

$$P_{el} = (\alpha_4 + \alpha_5 V(t) + \alpha_6 \dot{V}(t))V(t)$$

$$= \alpha_4 V(t) + \alpha_5 (V(t)^2) + \alpha_6 (\dot{V}(t)V(t)) \qquad (2.4)$$

where α_4 may be obtained from the static P-V curve.

Finally, we shall briefly consider the pressure required to overcome the inertial elements of the lung. Experimentally, once zero flow conditions have been met in the determination of quasi-static compliance, E^{-1}, lung volumes tend to creep for some time in the same direction as the immediately preceding dynamic volume change [70]. Such a phenomenon could be simply accounted for by the inclusion of a term describing P_i as a function $\ddot{V}(t)$

$$P_i = \alpha_7 \ddot{V}(t) \qquad (2.5)$$

where α_7 would be small and negative. A related effect, involving trans-pulmonary pressure changes with time, once zero conditions (i.e., zero volume change) are met, has been referred to as 'stress adaptation' [70]. This effect has been coined 'stress relaxation' when it diminishes trans-pulmonary pressure and 'stress recovery'

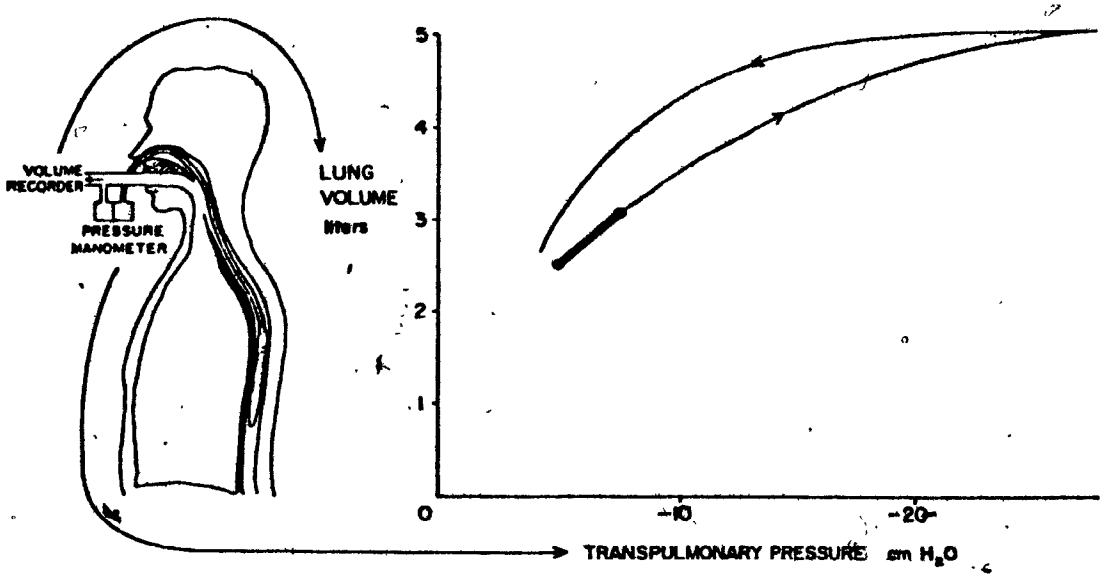

$$\underline{\text{STATIC}}\ \text{COMPLIANCE} = \frac{\Delta V}{\Delta P} = \frac{0.500}{2.5} = 0.200\ \text{liter/cm}$$

Figure 2.3a. The static compliance, expressed as liters per centimeter of water, is the ratio of volume change, shown on the ordinate, to pressure change, shown on the abscissa. The heavy line marks the normal range of tidal volume during a quiet inspiration, where the relationship between volume and pressure change is approximately linear. This is the value commonly used to describe the elastic properties of the lung. Note, however, that even in the normal subject, the relationship changes over the inspiratory range and that there is a difference between the inspiratory and deflation curves. From [5].

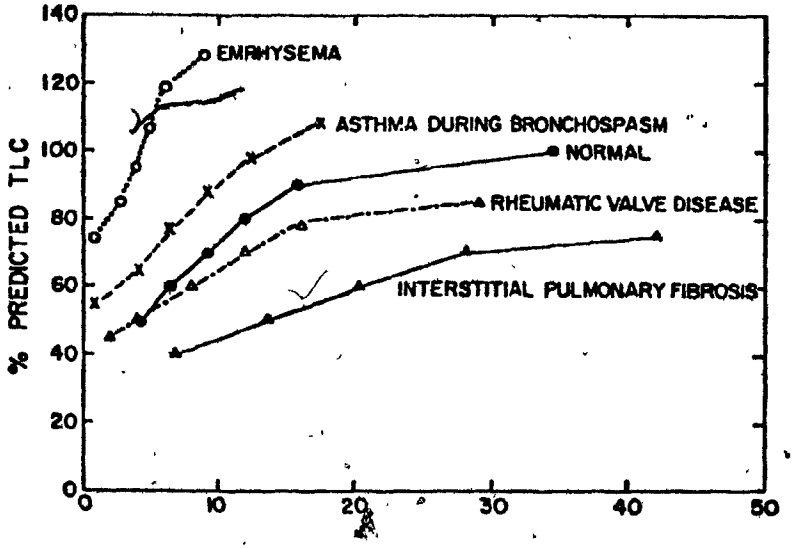

Figure 2.3b. Static deflation pressure-volume curves in emphysema, asthma during bronchospasm, normal subjects, rheumatic valve disease. The curve for interstitial pulmonary fibrosis was obtained furing inflation. From [5].

when it increases trans-pulmonary pressure. Stress adaptation usually occurs as a pressure change opposite to that immediately preceding it and is in accordance with a model of pulmonary mechanics which contains an acceleration term with negative weight [70]. Thus the model of pulmonary mechanics described here [89] may be written as:

$$P_{es}(t-\tau) = \alpha_1\dot{V}(t) + \alpha_2(\dot{V}(t)^2) + \alpha_3(V(t)\dot{V}(t)) + \alpha_4 V(t) + \alpha_5(V(t)^2) + \alpha_6(V(t)\dot{V}(t)) + \alpha_7\ddot{V}(t) + \alpha_8 \quad (2.6)$$

where τ is a bias term that has been incorporated into the model to account for the fact that the eosophageal pressure, P_{es}, measurements used to approximate pleural pressure in this model are not in phase with the lung volume and flow measurements made at the mouth. α_8 is a constant that has been added to the equation 2.6 to account for the equilibrium pressure point about which the system oscillates.

The coefficients α_1, α_2 and α_3 are used to quantify the system's response to airflow while the coefficients α_4, α_5 and α_6 portray the system's response to lung volume. The term involving α_7 in equation 2.6 accounts for the effects of inertia , I, on trans-pulmonary pressure. In this model both elasticity, E, and resistance R, are functions of lung volume and flow:

$$E = f_1(V(t),\dot{V}(t)) \quad (2.7)$$

$$R = f_2(V(t),\dot{V}(t)) \tag{2.8}$$

while I remains a simple function of acceleration

$$I = f_3(\ddot{V}(t)).$$

Hence, Mead's equation:

$$P(t) = E\,V(t) + R\,\dot{V}(t) + I\,\ddot{V}(t) \tag{2.9}$$

which may be rewritten in terms of equation 2.7 and 2.8 as:

$$P(t) = [f_1(V(t),\dot{V}(t))]V(t) + [f_2(V(t),\dot{V}(t))]\dot{V}(t) + I\,\ddot{V}(t) \tag{2.10}$$

Thus, equation 2.10 is really a simple expansion of that proposed by Mead [106].

The states of a simple volume-elastic system can be represented by a surface in the three dimensional space V-$\dot{V}$-P. Fry and Hyatt [53] were the first to introduce the use of such a diagram, shown in figure 2.4, to describe the states of the respiratory system. They found that, this system's cyclical behaviour approximates a surface in V-$\dot{V}$-P space. There also appears to be [80] special surface characteristics in this space, for inspiratory and expiratory phases of breathing. These findings imply that the respiratory system normally behaves in a manner adequately described by equation 2.10. This is a remarkable finding in light of the constraints imposed on the system by mechanical properties of the lungs and chest cage as well as those imposed by the various regulatory systems that control respiration.

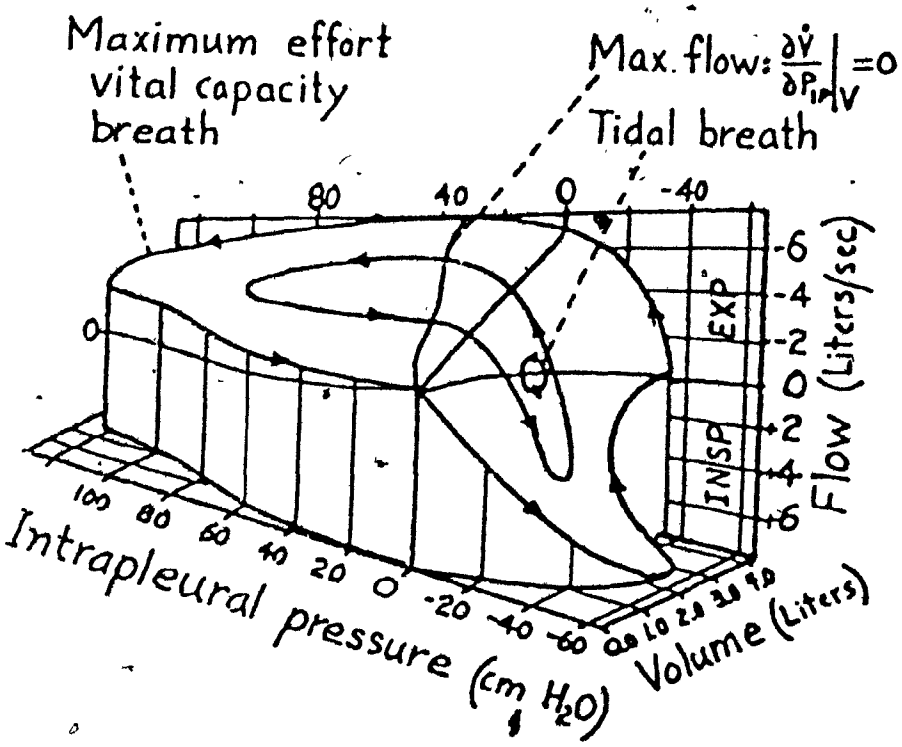

Figure 2.4. The Dynamic Pressure-Volume-Flow Relationship.

If flow, considered as a function of intrapleural pressure and lung volume, is plotted on one of three perpendicular axes, a surface is obtained which describes the flow characteristics of a lung. Shown here are the data from a normal lung. Expiration is limited by airway collapse as indicated by the fact that the surface dips back down toward the PV plane for large positive pleural pressures. The intersection of the surface with the PV plane is the static PV curve of the lung, and the intersection with the $V\dot{V}$ plane is the passive expiration curve. After [53].

Other works [33] have applied the basic principles of fluid mechanics to the analysis of airflow in the lung. Detailed theory of oscillatory airflow in a long straight tube of diameter, d, and length, ℓ, shows that the resistance term, R, and the inertance, I, of equation 2.10 may be given by [13]:

$$R = \frac{16\,\chi\ell}{\pi d^4}\,H(T) \qquad 2.11$$

$$I = \frac{16\,\chi\ell}{\pi d^4\omega}\,G(T) \qquad 2.12$$

where T is the Womersley parameter given as:

$$T = \tfrac{1}{2}d\sqrt{\frac{\omega\rho}{\chi}} \qquad 2.13$$

and χ is the substance's viscosity

ρ is the substance's density

ω is the angular frequency of oscillation

where both H and G are functions of T. These functions may, in turn, be approximated as [33]:

$$G(T) \cong T^2 \qquad 2.14$$

$$T<6 \mid H(T) \cong 8 \qquad 2.15$$

$$T>6 \mid H(T) \cong T\sqrt{2}$$

A detailed and realistic analysis of airflow through the bifurcating structure of the human bronchial tree is very difficult. As we shall see in section 2.2 the architecture of the lung's conducting airways is both elegant and complex.

Section 2.2

We know that since the sixteenth century, western physicians such as Vesalius [60] have been intrigued by the investigation of pulmonary anatomy. The quantitative anatomical studies of such early scientists as DaVinci appear to be the first to point to the role of environmental agents, such as dust, in pulmonary disease [140].

It was not until the pioneering work of Weibel and Gomez [158,159,157] that the statistical and sampling techniques essential to quantitative morphology were refined to the point where it was possible to provide accurate and reliable data on the structure of the static human bronchial tree.

The airways of this tree form a system of branching tubes whose diameters and lengths decrease from the trachea to its periphery in a strictly systematic way [141,166]. This tree provides a sophisticated mechanism for ventilating the 60-80 meter^2 surface area of the lung. This extensive area is achieved by partitioning the lung's total volume into over 300 million volumetric units, or alveoli. These alveoli are approximately spherical, 200 μm in diameter and octagonally arranged in a helical manner [167] shown in Figure 2.5.

The terminal branches of the bronchial tree are provided with alveoli. Each alveolus receives a supply of air; while each alveolar wall is perfused by a supply of blood [21]. These

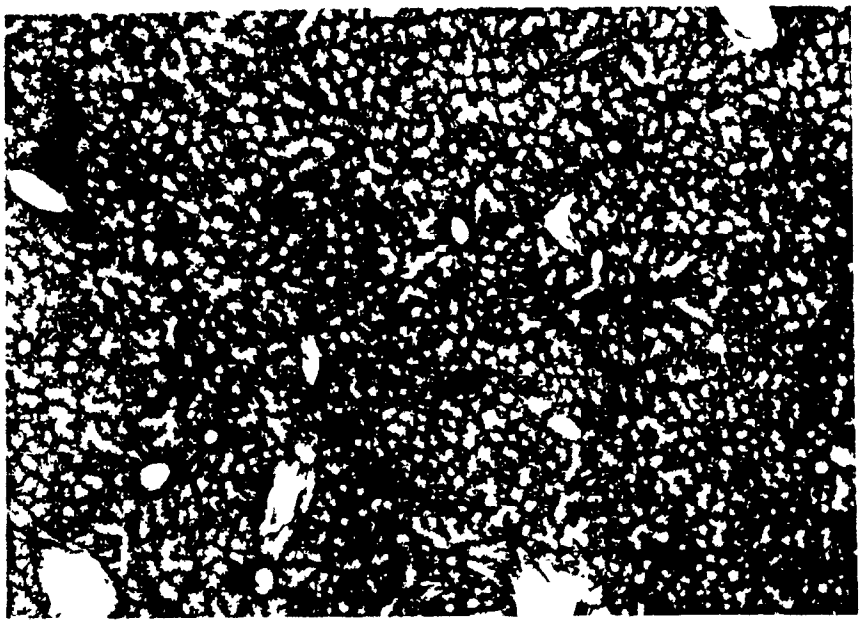

Slice of inflated lung cut about 300 μ thick. Note interlocking coils of lacy pattern occupying almost all the area (volume). (Original magnification x20).

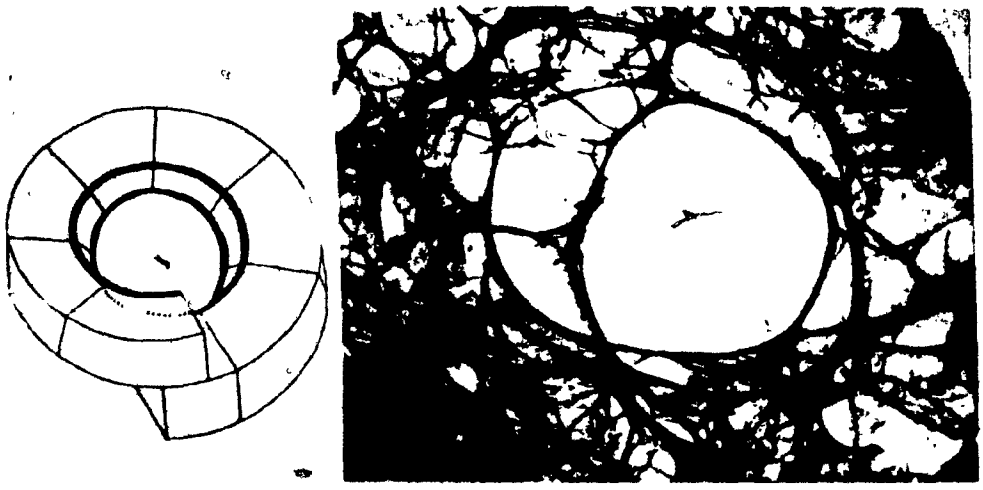

Diagram and microradiograph of a small section of a respiratory unit to show how the alveoli are arranged in spiral tiers around a central helical framework. (Original magnification x300).

Figure 2.5. The Form of the Alveolar Macro-Structure. From [167].

Figure 2.6. Left Bronchial Tree (Frontal Projection). A, Normal bronchogram of a 39-year-old woman. From [50].

alveoli along with the pulmonary capillary networks contained in their walls comprise the parencyhyma, or respiratory zone of the lung. The intermediate or transition zone of the lung contains airways so closely associated with alveoli that they cannot be easily separated form them. The airways more distal to the transition zone of the lung are collectively referred to as the conducting zone of the lung. The airways in the lung's conducting zone are not in direct contact with the pulmonary capillaries and are thus not active sites in the actual process of gas exchange.

During breathing, airflow in the mammalian lung is intermittant and reciprocating. As such, the last portion of each breath that is shunted into and out of the lung's conducting airways never reaches a gas exchanging surface. Hence, the volume of the lung's conducting airways defines the minimum dead space of the lung. This volume is referred to as the lung's anatomical dead space, $V_{D_{anat}}$.

The bronchial tree, shown in the radiographs and casts reproduced in Figures 2.6, 2.7 and 2.8, is in fact a very complex stack which exhibits last-in first-out (LIFO) behaviour [14]. The volume of this stack corresponds to the anatomical dead space of the system. A schematic representation of the overall structure and composition of this system is given in Figure 2.9.

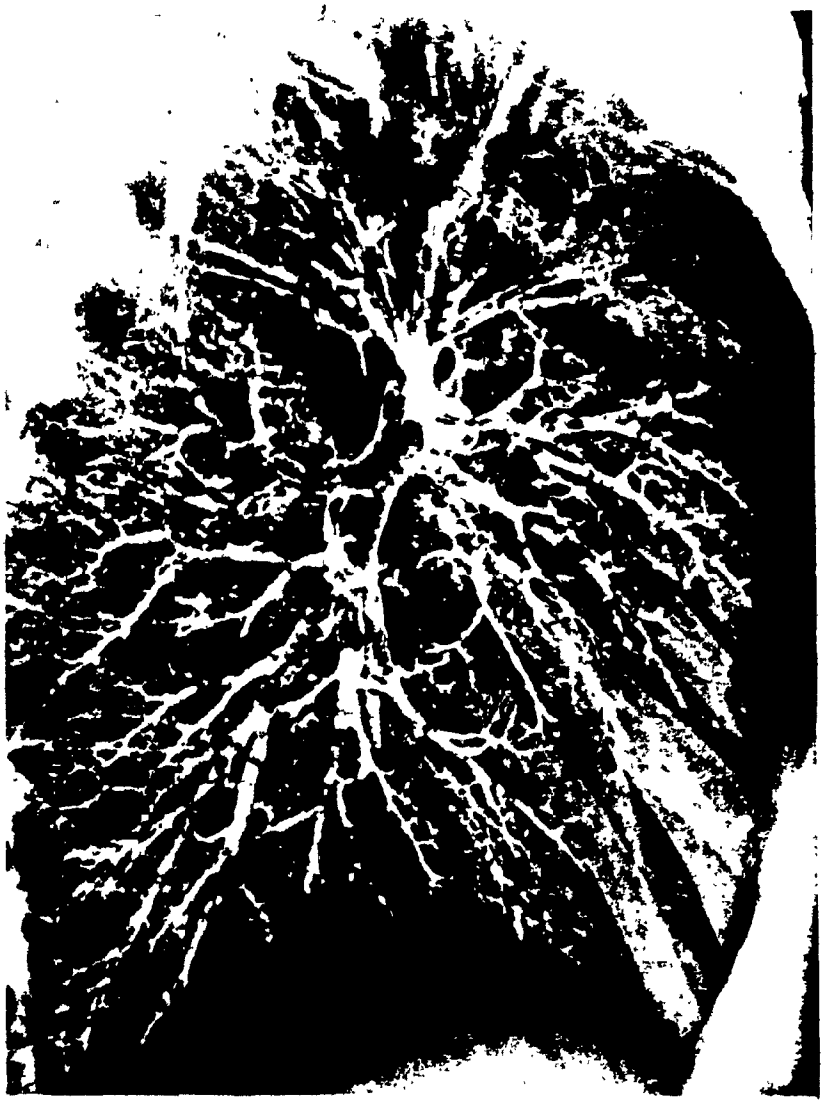

Figure 2.7. Left Bronchial Tree (Lateral Projection). A, Normal bronchogram of a 39-year-old woman. From [50].

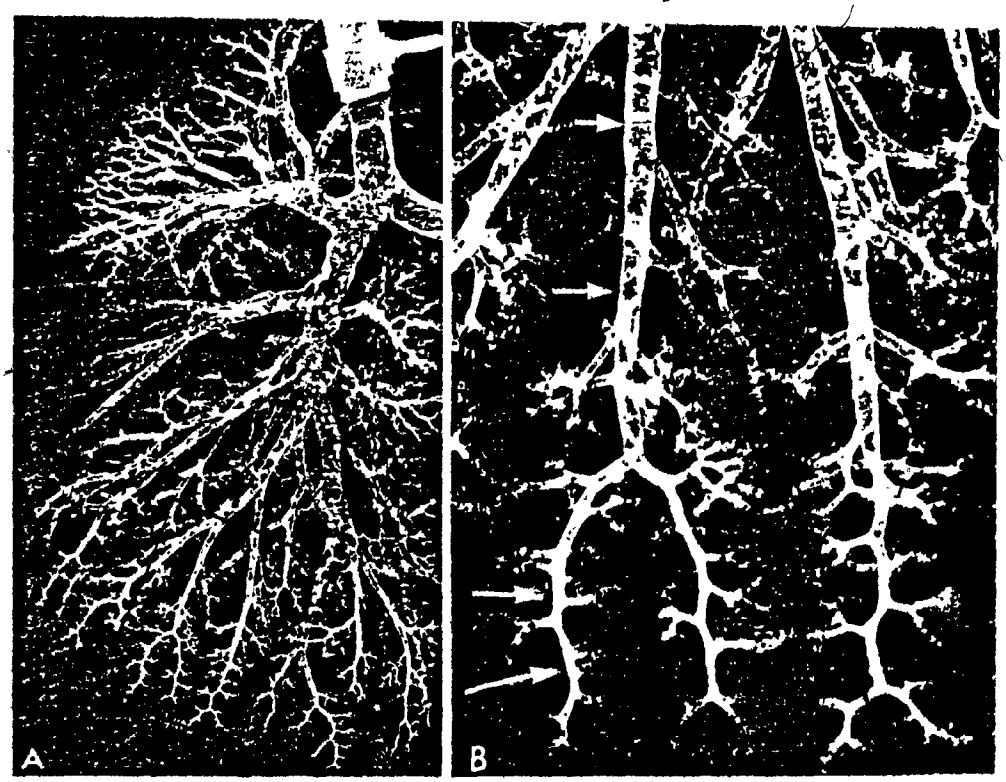

Figure 2.8. The Pattern of Bronchial and Bronchiolar Branching.

A, Roentgenogram of an excised right lung following insufflation of particulate lead into the tracheobronchial tree. B, Magnified view of the peripheral airways of the lateral basal segment; upper arrows point to the "centimeter pattern" of branching, lower arrows to the "millimeter pattern." From [50].

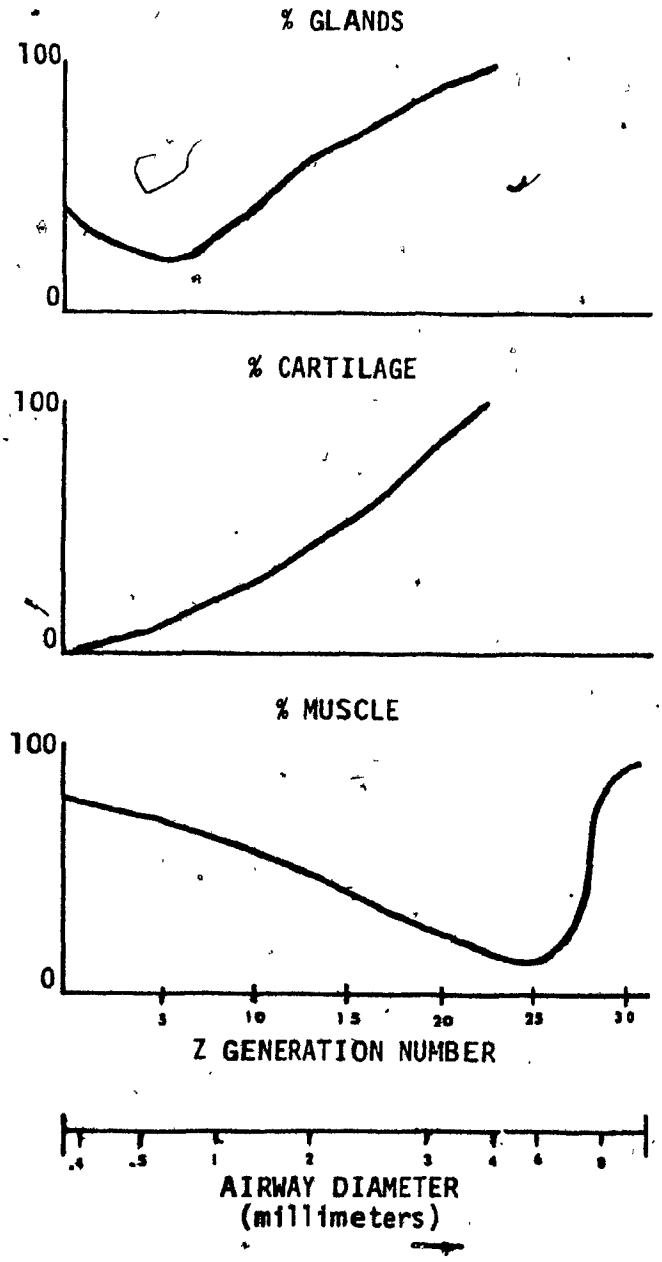

Figure 2.9a. Structure and Relative Composition of the Human Bronchial Tree. After [71].

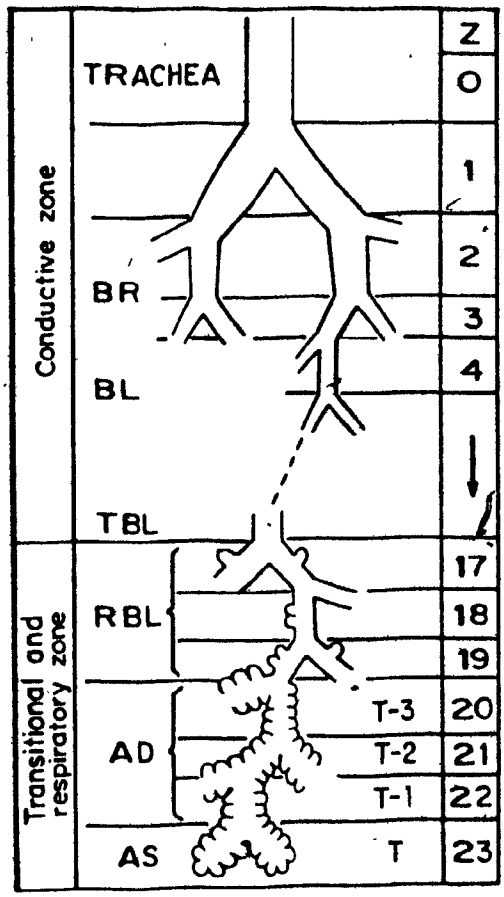

Figure 2.9b. Structure and Relative Composition of the Human Bronchial Tree.

Diagrammatic representation of the sequence of elements in the conductive and transitory zones of the airways. Z designates the order of generation of branching, T the terminal generation. Model of airway branching, BR = bronchus; BL = bronchiole; RBL = respiratory bronchiole; TBL = terminal bronchiole; AD = alveolar duct; AS = alveolar sac. After [158].

From a detailed analysis of the bifurcating architecture of the lung's conducting airways, Weibel [158] confirmed earlier workers' observations that these airways branch by irregular dichotomy. Thus while each branch gives rise to two daughter branches, which in turn become parent branches, these daughter branches often vary considerably in diameter and length. In this notation each generation of airway may be referred to by its order, Z.

Weibel presented his measurements in two forms [158].

In the first of these, he developed a model of airway structure that statistically accounts for the irregular dichotomy of the conducting zone.

In a second, symmetric model, he imposed a regular dichotomy on the structure of these airways. This symmetry may be simply achieved by taking the mean values of the lengths, $\bar{\ell}(Z)$, and diameters, $\bar{d}(Z)$, for all airways of each generation, Z. While Weibel's symmetric model is a gross simplification [71,73,74] of the system's structure, it offers a theoretical and computational structure which has often been exploited in the modeling [133, 165] and mathematical analysis [29,31,80] of airflow through the conducting zone.

Weibel's data, for a symmetric model of airway bifurcation, shows a geometric progression in airway length and diameter from the alveoli to the top of the bronchial tree. This progression, which is shown in Figure 2.10, has been given [58] as:

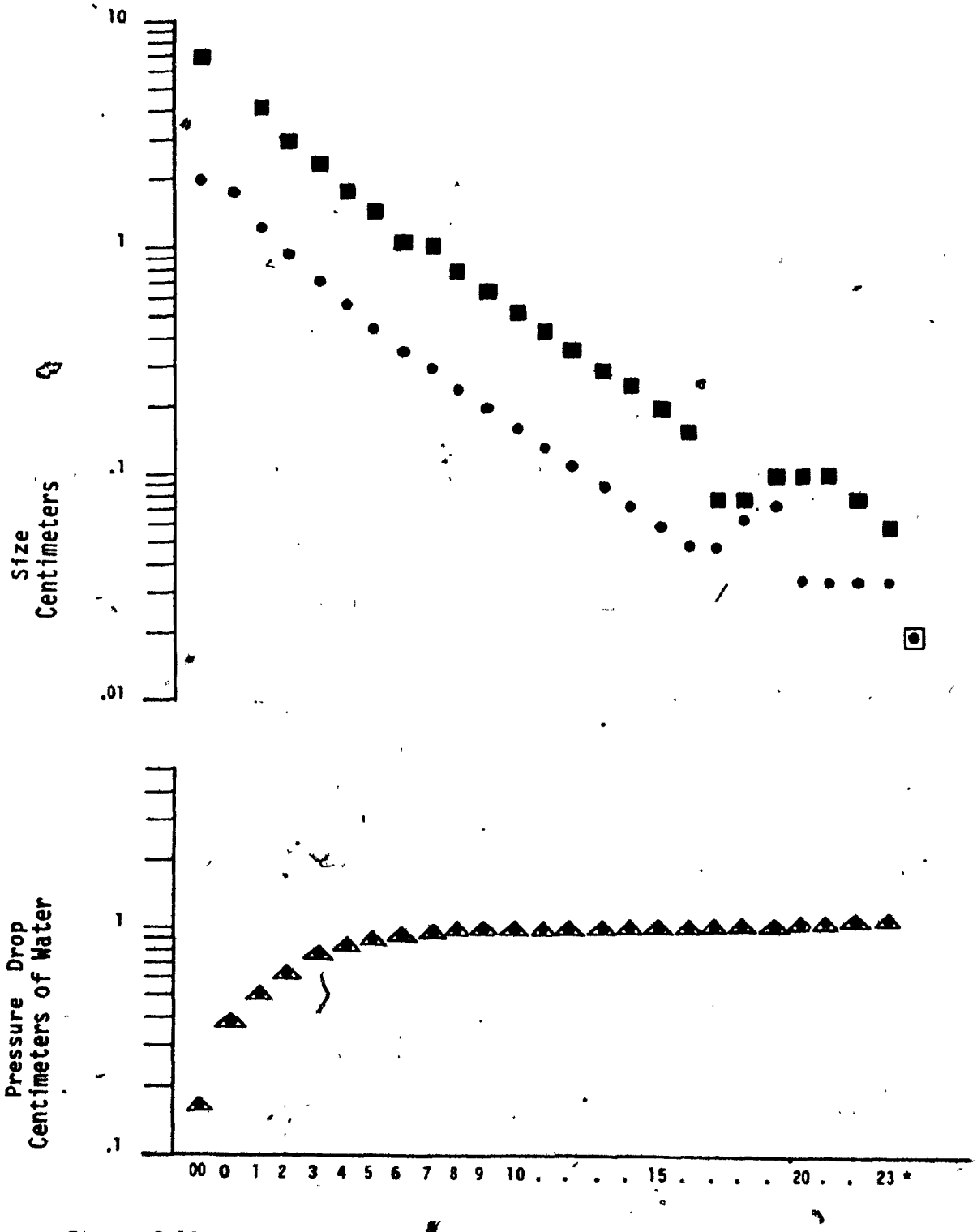

Figure 2.10. Observed Mean Diameters, , and Mean Lengths, , along with the Computed Pressure Drops, , for each Generation of Airway, Z, in Weibel's Symmetric Lung Model. After [122].

$$Z < 4 \mid \hat{\bar{\ell}}(Z) = \ell_0 e^{-0.92*Z} \qquad \ell_0 = 12.0$$

$$Z > 4 \mid \hat{\bar{\ell}}(Z) = \ell_{0'} e^{-0.17*Z} \qquad \ell_{0'} = 2.5 \qquad 2.16$$

$$Z < 4 \mid \hat{\bar{d}}(Z) = d_0 e^{-0.388*Z} \qquad d_0 = 2.0$$

$$Z > 4 \mid \hat{\bar{d}}(Z) = d_{0'} e^{-(0.293-0.0062*Z)Z} \qquad d_{0'} = 1.3 \qquad 2.17$$

From this data, it is easy to compute the cross sectional area [122] of each branch of the symmetric model. This information is shown in Figure 2.11. The cumulative total volume [122] of the airways is presented as a function of the tree's order, Z, in Figure 2.12.

An analysis of the aerodynamics [133, 122] and fluid mechanics [133, 122] of this model has provided estimates of the Reynold's numbers for these airways. These estimates are graphed as a function of Z in Figure 2.13.

From an aerodynamic analysis of a rigid symmetric structure defined by a regular dichotomy, it is possible to compute the minimum airway length at which laminar flow would resume after a bifurcation. This length is referred to as the airway's entrance length. The computed entrance lengths [122] for each generation, Z, of airway in Weibel's symmetric model are given in Figure 2.14. The mean observed airway length for each generation of this tree are also given in Figure 2.14. From this analysis it is possible to see the nature of the cumulative pressure drops in this system.

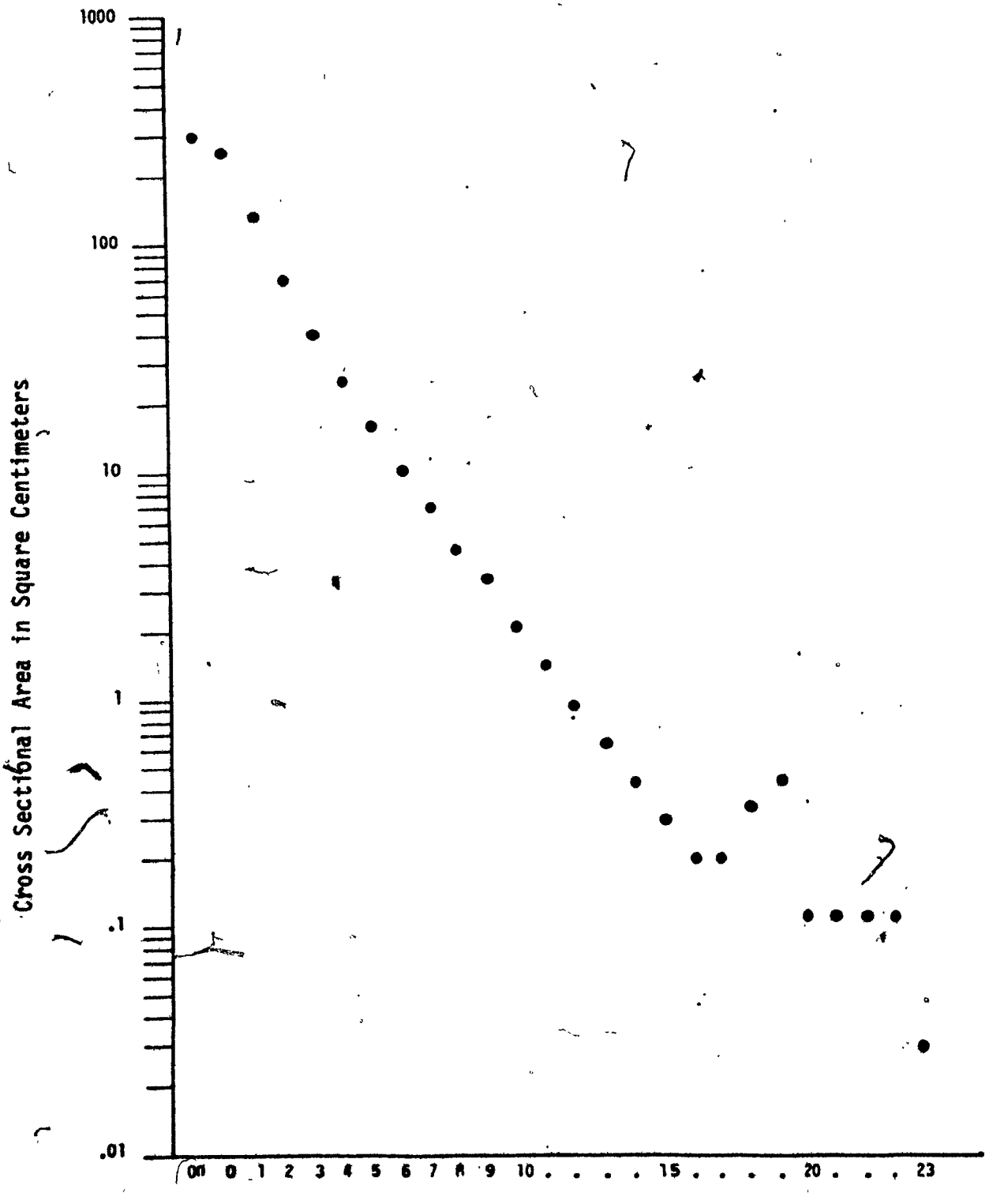

Figure 2.11. Computed Cross Sectional Area for each Generation of Airway, Z, in Weibel's Symmetric Model. After [122].

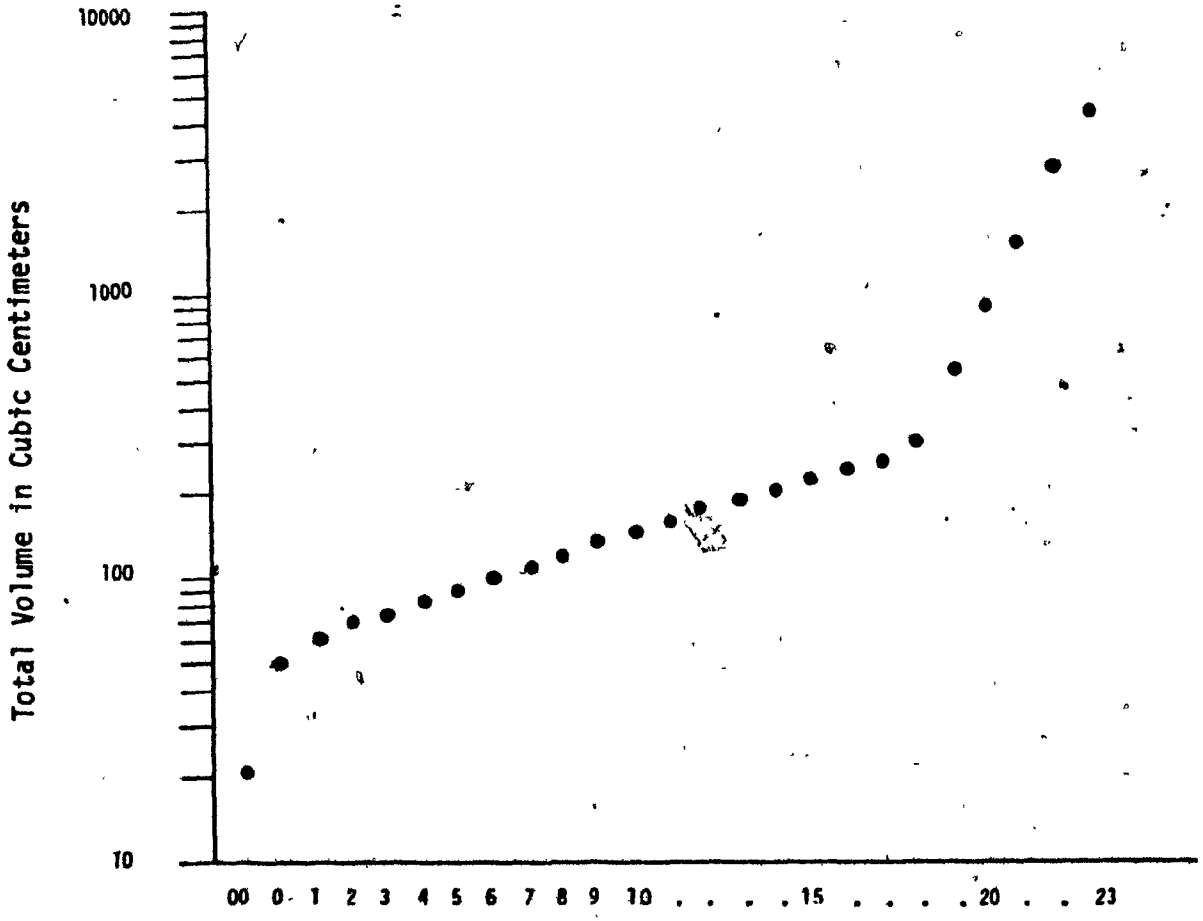

Figure 2.12. Computed Total Volume of the Lung as a Function of Airway Generation, Z, for a Symmetrically Bifurcating Lung. After [122].

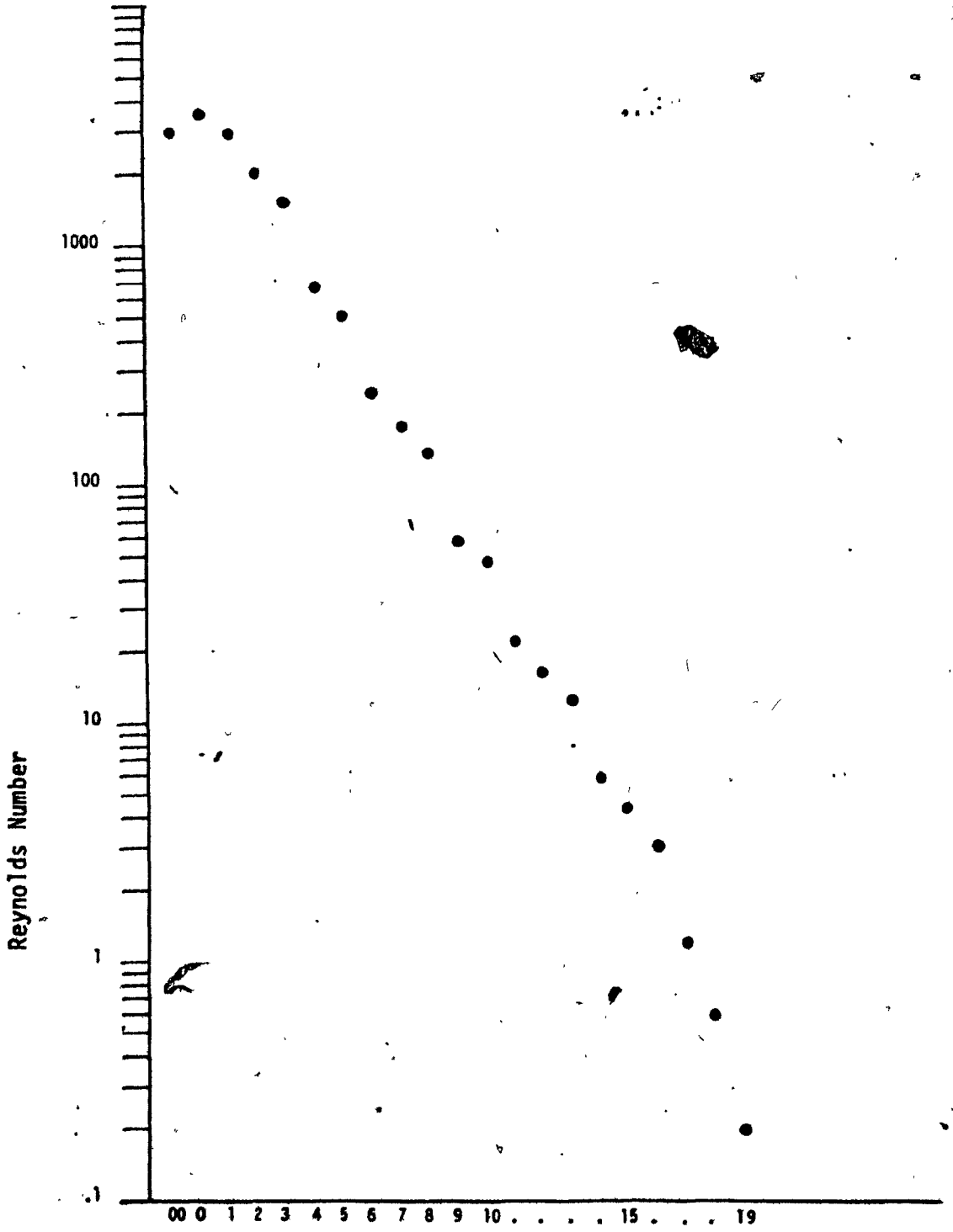

Figure 2.13. Computed Values of the Reynolds Number for Airflow in Each Generation, Z, of Weibel's Model of Symmetric Airway Bifurcation. After [122].

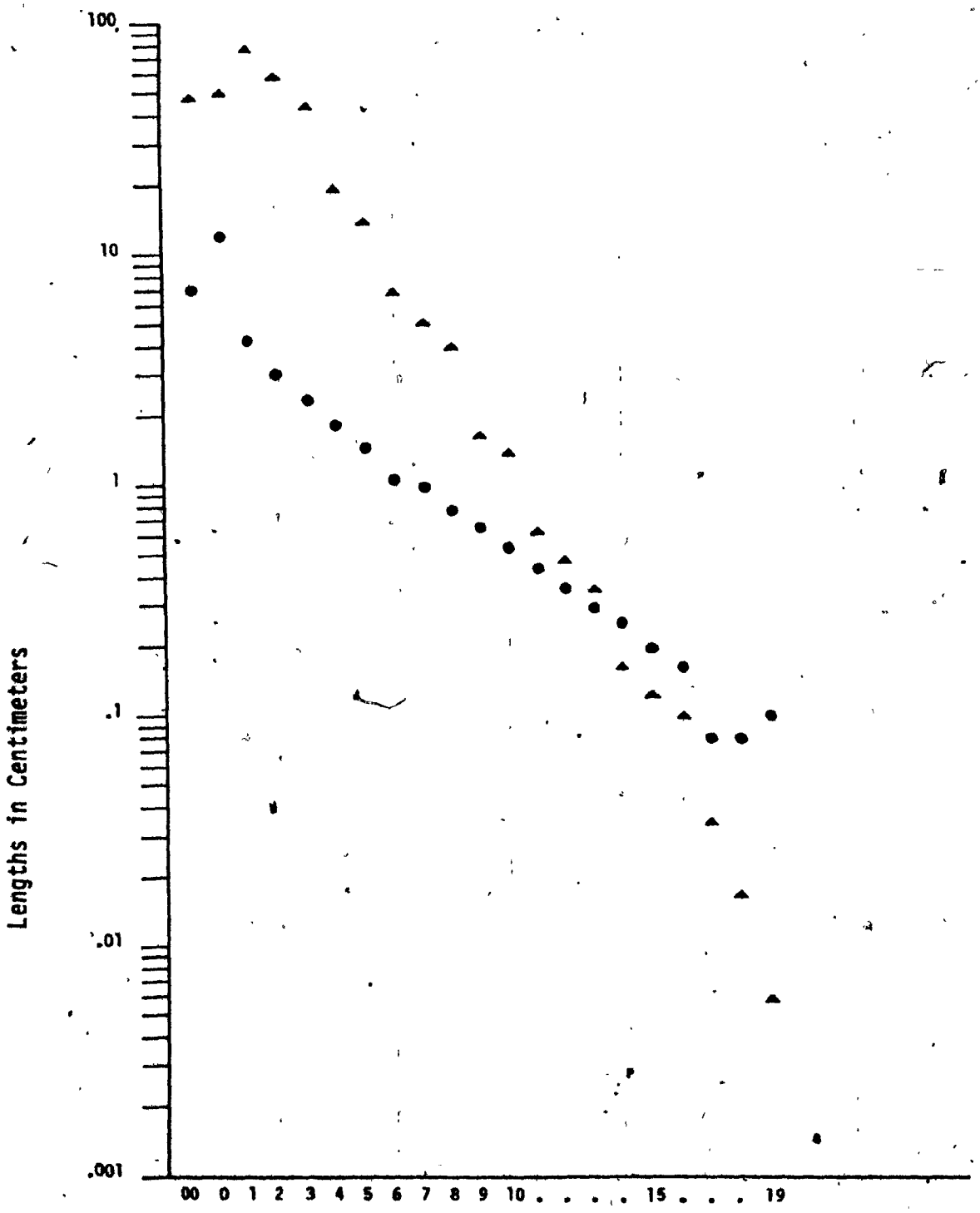

Figure 2.14. Comparison of the Computed Entrance Lengths and Mean Observed Airway Lengths for Each Generation, Z, in Weibel's Symmetric Model. After [122].

These computations are graphed in Figure 2.10. From these anatomical considerations, it is understandable that the lung's small airways contribute to less than 20% of the conduction zone's resistance [94].

Gomez [165] claims to have shown that the bifurcating structures of the lung are optimally defined by three conditions. These conditions are:

"1) The structural branches occur in such a way that the amount of dissipative energy which has to be developed to create air or blood flow through the system must be a minimum.

2) The mass of the structures involved must also be a minimum, so that the volume they occupy has to have the smallest possible value.

3) Finally these conditions must be such as to define, numerically, a prescribed apparent total length of the system."

For Gomez's first condition to be met it is necessary to show that the coefficients of the equation of motion of the lung allow the system to provide a given ventilatory volume with little work.

The work done during a breathing cycle may be represented as an area on the pressure-volume diagram presented in Figure 2.2. This simple representation is valid because the forces developed by the respiratory system are measured in terms of pressure differences, while displacements are expressed in terms of volume changes. The work, W_I, involved in the inspiration of a single breath is then

the integral of the lung's pressure excursions over its volume:

$$W = \int P(t)dV(t) \qquad 2.18$$

Ignoring the time lag, τ, in our formulation of equation 2.6 we may approximate W_I by rewriting equation 2.19 in terms of equation 2.6 as:

$$W_I = \int [\alpha_1 \dot{V}(t) + \alpha_2(\dot{V}(t)^2) + \alpha_3(V(t)\dot{V}(t)) + \alpha_4 V(t) + \alpha_5(V(t)^2) + \alpha_6(V(t)\dot{V}(t)) + \alpha_7 \ddot{V}(t) + \alpha_8]dV \qquad 2.19$$

Otis[ ] evaluated the rate of work involved in inspiration, $\dot{W}_I$, in terms of a lower order approximation of equation 2.19 as:

$$\dot{W}_I = \frac{\alpha_4}{2\gamma}(\dot{V}(t))^2 + \frac{\alpha_1}{4}\pi^2(V(t))^2 + \frac{2\alpha_2}{3}\pi^2(\dot{V}(t)^3)\gamma^3 \qquad 2.20$$

for sinusiodal breathing where V is the mean ventilation at the respiratory frequency, γ.

If exhalation is accomplished passively by energy stored during inspiration, equation 2.20 can be used to approximate the total positive work needed per unit time or the power for breathing.

If expiration is not achieved passively but requires the active participation of expiratory muscles, equation 2.20 becomes:

$$\dot{W}_I = 2\left[\frac{\alpha_1}{4}\pi^2(\dot{V}(t))^2 + \frac{2\alpha_3}{3}\pi^3(\dot{V}(t))^3\right] \qquad 2.21$$

In that the P-V relationship observed during inspiration usually traces a geometric figure resembling a semiellipse equation, 2.19 can be crudely approximated by the expression:

$$W_I \cong \frac{\pi}{4}|P||V| \qquad 2.22$$

where $|P|$ and $|V|$ are the amplitudes of the pressure and volume changes respectively. Similarly the figure of minimum work, representing elastic work only, can be approximated as the fraction, $\pi/2$, of equation 2.22 [109]. Maximum work can be similarly approximated as the simple product $|P||V|$.

Realistic computations of the work of breathing involves the additional considerations [129] of cost of breathing [105,98] and the relative proportion of alveolar to dead space ventilation, $\dot{V}_A/\dot{V}_{D_{anat}}$. The work of breathing is of great importance to our understanding of pulmonary function in health and disease [23,22, 98, 142,166].

While the exact mechanisms underlying the control of ventilation still evade us [92], experimental data [105] supports Gomez's first condition. Studies [115] of the mechanical work of ventilation on exercising subjects breathing at various frequencies are summarized in Figure 2.15. The frequency at which minimal work occurred, increased progressively with increased alveolar ventilation and corresponded closely at each level of alveolar ventilation with the frequency spontaneously chosen by the subject.

Gomez's second condition involves minimizing the mass and volume of the lung. Such a minimization would reduce the total work of breathing by giving the respiratory muscles an easier task [118,119,148].

Gomez's last condition assures a minimum anatomical dead space.

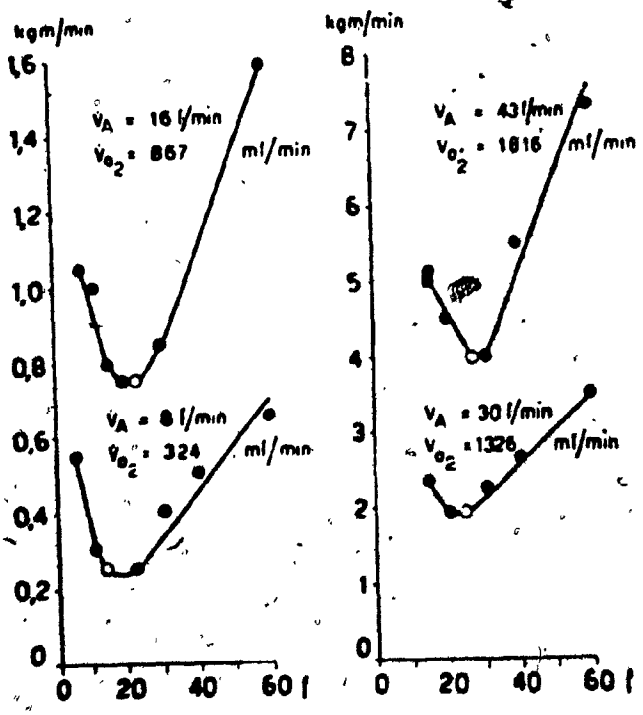

Figure 2.15a. Mechanical work of breathing in kg-m/min as a function of frequency of breathing in breaths/min at several constant rates of alveolar ventilation, $\dot{V}_A$. The open circles indicate the freqeuncies spontaneously chosen. From [15].

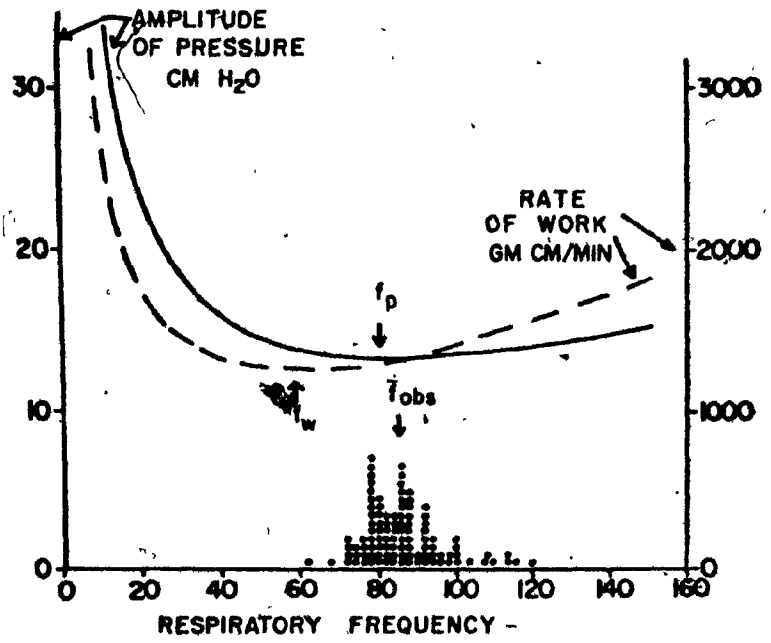

Figure 2.15b. Pressure amplitude (solid curve) and rate of work (broken curve) as a function of breathing frequency in a guinea pig. The points represent instantaneous frequencies of 103 individual breaths observed during a 3-hour period. The frequency for minimal work is indicated by f_w; that for minimal pressure amplitude by f_p. From [105].

The work involved in ventilating the lung's anatomical dead space is an entirely wasted expenditure that is necessarily incurred by the lung's architecture and reciprocating airflow. Hence the minimization of the apparent path length of the conducting airways in a symmetric dichotomous lung reduces the work of breathing.

Gomez's proof of the optimality of these conditions in the structure of the bronchial and pulmonary vascular trees has not been published. It was in one of his last articles [165], that he referred to an unpublished proof.

Further work [165] has shown that an architecture that optimizes mass gas transport is different from that which is needed to assure efficient molecular diffusion in the transition and respiratory zones of the lung. Figure 2.16 demonstrates the computed [165] range defined by mass transfer and molecular diffusion processes.

Figure 2.17, which is taken from Gomez's work [165], shows that these considerations also hold for the vascular perfusion of the lung. This result is very surprising, for the pulmonary vascular system perfuses the lung in a queue-like manner which exhibits first-in first-out, FIFO, behaviour. Furthermore, blood is brought to the alveoli by one system, the arterial, and returned by another, the venous. Thus the pulmonary vascular system has no anatomical dead space because the blood flow through

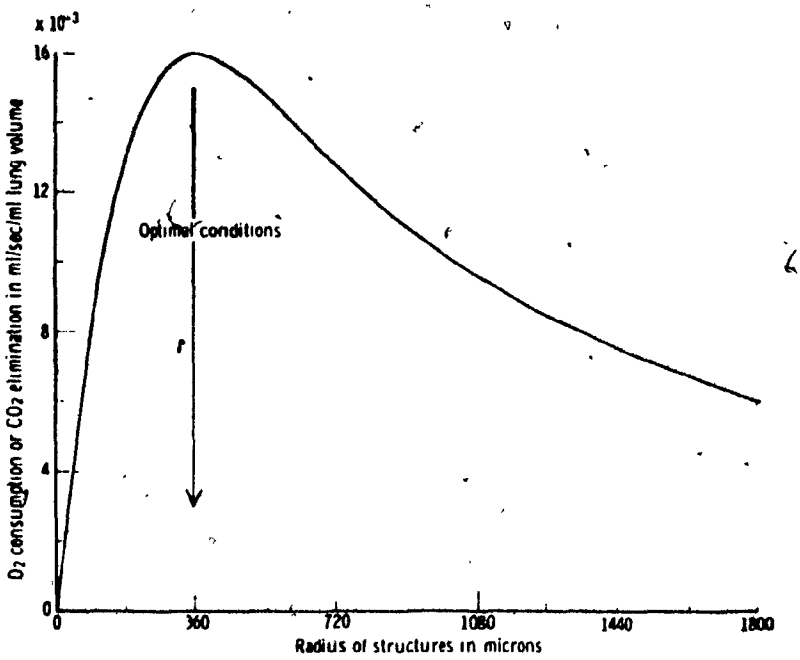

Rate of elimination of CO_2 per unit lung volume and in the unit of time (ordinates) as a function of the radius of the cylindrical structures of the diffusion fields of the lung.

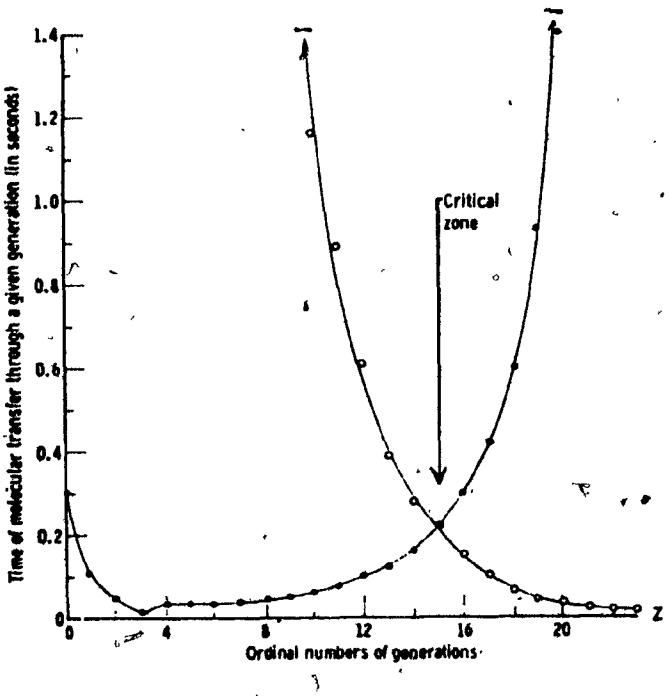

Time of transfer through either mechanical motion or molecular diffusion of a respiratory gas across successive generations of the lung structures.

Figure 2.16. From [165].

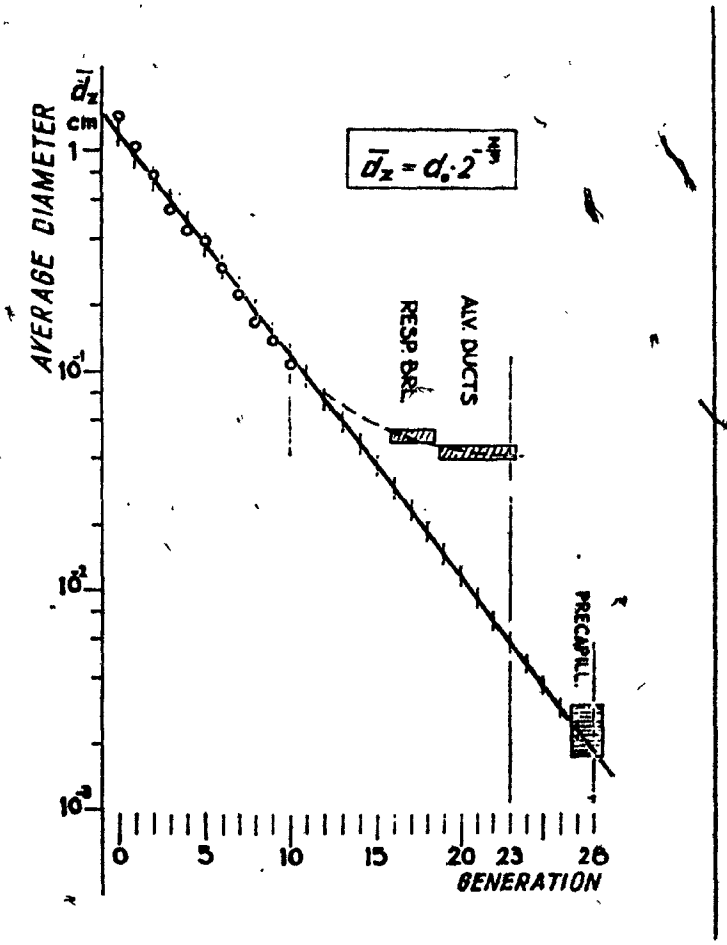

Figure 2.17a. Comparison of the Observed Vascular and Airway Diameters As a Function of Generation, Z, in the Pulmonary Vascular and Bronchial Trees. After [158].

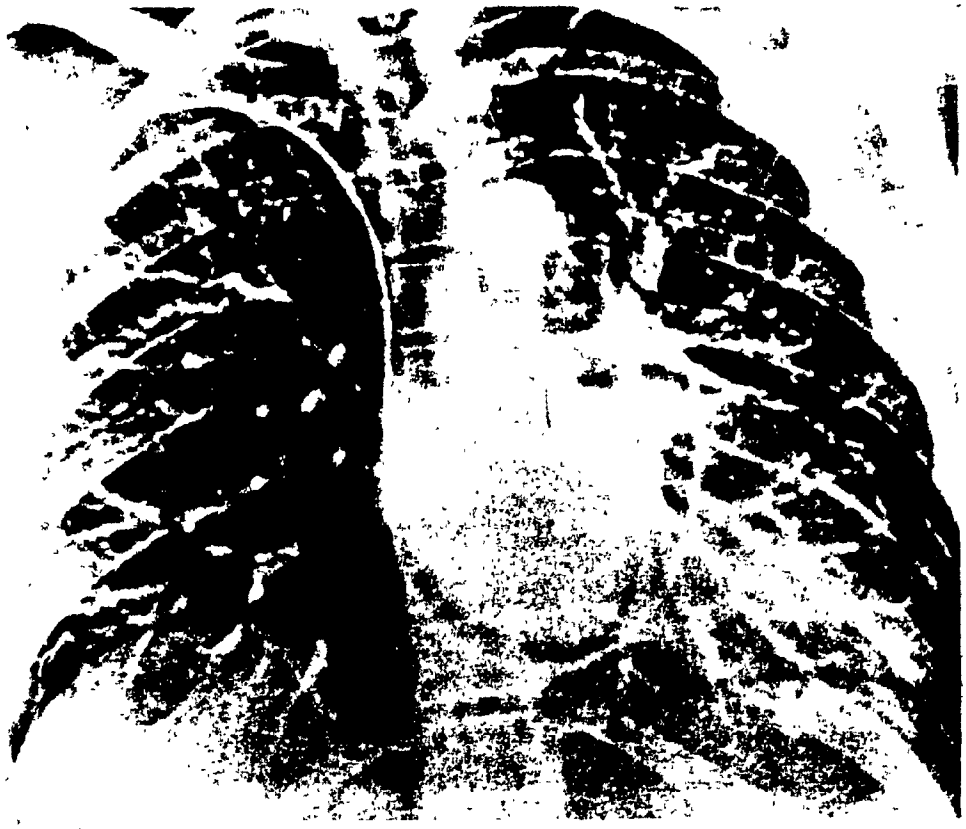

Figure 2.17b. Pulmonary Angiogram (Venous Phase) Showing the Pulmonary Vascular Tree. From [50].

the vascular tree that perfuses the lung is pulsitile and unidirectional.

It is also surprising that the same physical dimensions and structures have arisen from the constraints placed on blood flow through a queue-like vascular arboresence, with FIFO behaviour, as are observed for airflow which is shunted into and out of a stack-like arboresence with LIFO behaviour.

In the healthy individual, the complex asymmetric architecture of the lung's conducting airways allows it to fill and empty synchronously [130]. This behaviour occurs in spite of large differences in the actual path length from the trachea to the alveolar surface in different regions of the lung [133]. In health this synchronous behaviour is maintained over a wide range of respiratory frequencies by dynamic changes [133,70] in the diameters and lengths of the conducting zone's airways.

An analysis of the dynamics of the geometric transformations of the bronchial tree during breathing would be a very complex and fascinating task that is beyond the scope of this thesis. As we have observed in Figure 2.9 the relative composition of muscle and cartilage varies throughout each generation of the bronchial tree. Dynamic control is aided by sophisticated physiological and morphological changes in the structure [73,116] and composition [71,167] of each generation of the bronchial tree.

Before continuing on with our analysis of this system, we should consider more closely an important methodological point that was briefly introduced in the beginning of this section of chapter two.

In order to classify, analyse, and model the bronchial tree, two main methods of labelling the bronchi were developed [133]. The first [158] and easiest to understand, was developed by Weibel. He used what is in fact a breadth-first search [143,85] to label and provide the statistics which characterize each generation of airways in the bronchial tree structure. A breadth-first search proceeds from the top of a tree and sequentially visits all adjacent vertices at each subsequent order, or generation, Z.

Horsfield and Cumming [71,74] used, what is in fact, a post-order traversal of the bronchial tree to label and obtain the morphological statistics on which they characterized its structure. A post-order tree traversal effectively traverses the tree from its periphery up to the trachea. Figure 2.18 demonstrates the essential differences in labelling a given tree by these two traversal techniques.

Weibel used data labelled by a breadth-first search of the bronchial tree to compute the airway lengths and diameters for the symmetric model that we have considered in this chapter.

Other workers [71, 133] have forcefully argued that breadth-first labelling of the bronchial tree is an inappropriate manner to analyze and model its structure. From Figure 2.18 it appears that

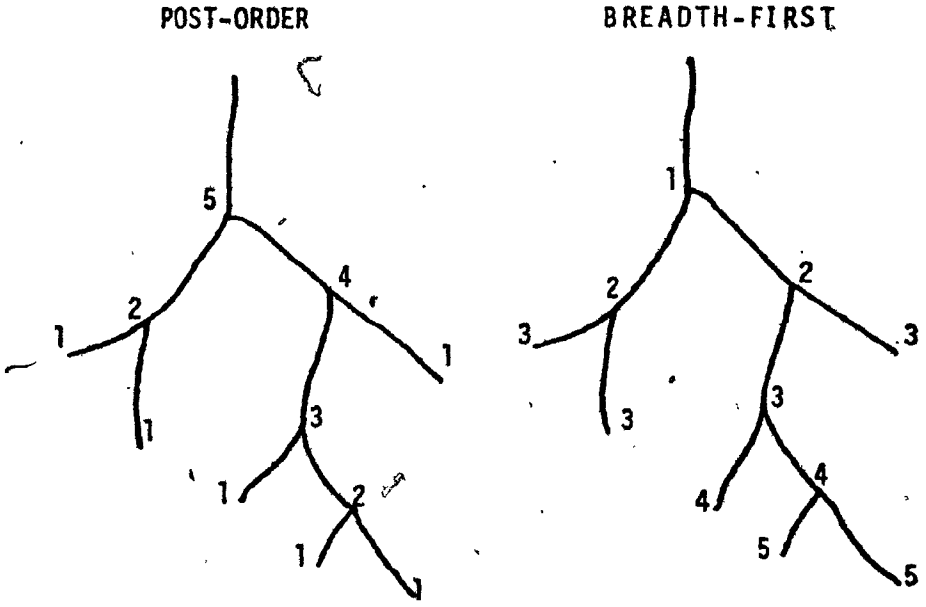

Figure 2.18a. Comparison of Binary Tree Labelling Using Both a Post-Order Tree Traversal and a Breadth-First Search Scheme.

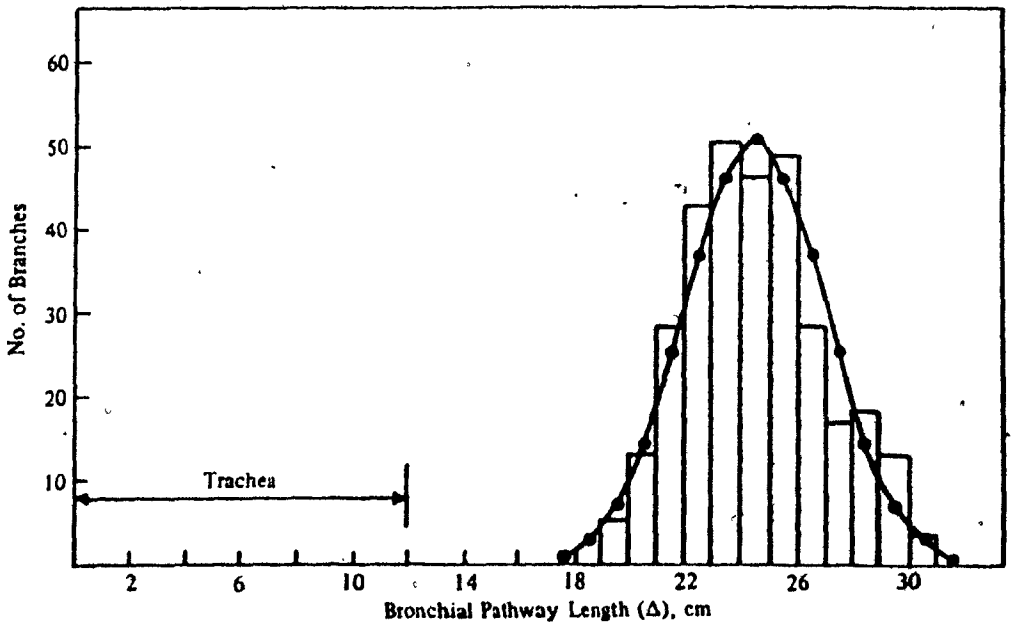

DISTANCE FROM CARINA OR LARYNX TO BRONCHIAL BRANCHES HAVING 2-mm DIAMETER

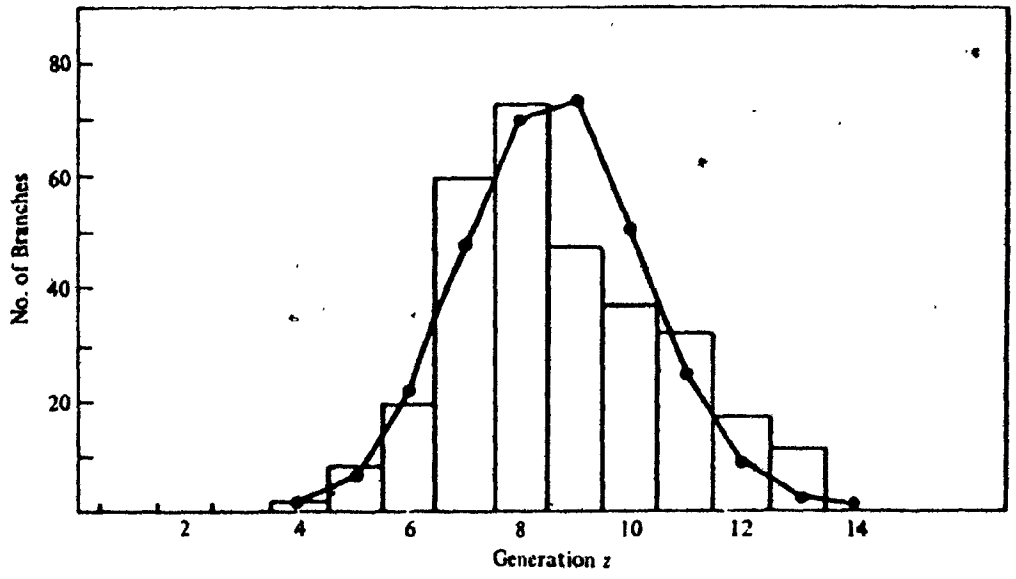

DISTRIBUTION OF BRONCHIAL BRANCHES HAVING 2 mm DIAMETER IN GENERATIONS OF DICHOTOMOUS BRANCHING

Figure 2.18b. From [165].

a post-order tree traversal does provide a better way of labelling the bronchial tree. Surprisingly, both analyses yield similar results [71]!

The necessary and sufficient structural characteristics of a binary tree that are needed to assure the equivalence of these two methods in labelling and analysing its structure remain, to my knowledge, an open question. However, experimental data indicates that these characteristics appear to be possessed by the human bronchial tree.

The analysis of the structure and physiology of the bronchial tree is very complicated in most disease states. There is evidence [117, 97, 166] to support the belief that various generations of airways are preferential sites involved in the deposition of particulate [97] as well as the accumulation [97] and production [97] of mucus. The literature also supports the belief that certain airways are critical to the aetiology of asthma [101] and chronic obstructive pulmonary disease [135,134]. In the next chapter of this thesis we shall consider the single breath nitrogen washout test as a non-invasive tool for the analysis of gas distribution and small airway function in the human lung.

CHAPTER THREE

The first section of this thesis provides an introduction to the many problems involving the regional, topographical distribution of perfusion and ventilation in the lung.

The second section of this chapter describes a non-linear numerical method for the automated analysis of single breath tests of ventilatory inhomogeneity.

Section 3.1

It is not possible to describe gas distribution in the human lung solely in terms of the structural and physiological models presented in chapter two, as these models address global or homogeneous aspects of the lung's form and function.

By their nature the models of pulmonary mechanics discussed in the last chapter implicitly consider the lung as a spatially homogeneous visco-elastic system whose exact structure is greatly influenced by the forces acting on it. Conversely the data and models of bronchial tree structure discussed in this thesis are valid under conditions of zero flow at a given, fixed, arbitrary lung volume and trans-pulmonary pressure. The bronchial tree's form is implicitly considered to be invariant to the pressure and volume excursions incurred throughout the breathing cycle. However, see Figure 3.1c.

In order to describe gas distribution within the lung, it is necessary to also consider some of the principal factors that have been shown to be concomitant to, or to affect, the functional topographical distribution of the lung's ventilation to the perfusion coefficient, v_j/q_j, for a given region, j. A simple description of the lung's overall ventilation to perfusion coefficient, $\dot{V}/Q$, in terms of its spatial average tells us nothing of the regional gas or blood distribution. Elegant studies [60,154,136,75] have shown the complexity of the homeostatic mechanisms that appear to optimize the lung's net overall gas transfer by interactively matching differences in regional

ventilation and perfusion in a synergistic manner. These studies have shown that regional vasoconstriction of the pulmonary capillary bed occurs whenever local oxygen levels fall. In this manner blood flow is cleverly shunted to areas of greater ventilation. This system is capable of assuring optimal gas transfer over a wide range of pathophysiology associated with structural and temporal, or asynchronous, disorders. The lung is perfused with blood in a manner which economizes the work involved in perfusing its alveolar surface under a given gravitational gradient [158]. The topographical distribution of blood flow through the pulmonary capillary bed is therefore greatly dependent on the body's position [160]. A teleologist would not be surprised to find out that there exists a similar gravitationally dependent topographical distribution of ventilation [136,10,114,41]. The mechanics controlling the gravitationally dependent regional distribution of ventilation may be partially attributed to the shape, mass and infrastructure of the lung which hangs within the body's pleural cavity [166, 160]. The pressure established within this cavity, by the effects of intercostal, scalenes and diaphramatic muscle activity, exerts complex topographical pressure gradients on the lung's surface [57,56]. It may be that these topographical pressure gradients in conjunction with the mechanisms that dynamically control the time constants of each branch of the bronchial tree are sufficient to effectively determine regional distribution of ventilation in the human lung [41,118]. If this were the case, then a physiologically

meaningful analysis of the aerodynamics of ventilation could be obtained from a weighted post-order traversal of the bronchial tree. The weights in such an analysis could account for the topographical pressure gradients attributable to gravity. Even with gross simplifications this task presents many theoretically challenging and computationally difficult problems [133]. Furthermore, any analysis of airflow through the bronchial tree is further hampered by the knowledge that each generation of the tree dynamically changes shape as a function of regional air flow [76,131], pressure gradients [9,57], cardiovascular dynamics [26] and overall lung volume [71,157]. In addition it is not clear, to my knowledge, that the bronchial tree expands and contracts isomorphically [72]. Hence the angles of bifurcation in the tree may also vary as a complex function of volume, flow, pressure and cardiovascular activity. These considerations tend to discredit any of the published mathematical analyses of airflow and gas distribution in the lung. For instance, the principles of fluid dynamics suggest that turbulent flow usually occurs within systems that exhibit Reynolds numbers in excess of 2300. Hence, if we consider the Reynolds numbers and computed entrance lengths for the rigid symmetric bronchial tree model given in Figures 2.13 and 2.14, it would appear that airflow within such a "cast-iron" bronchial tree would be mostly turbulent [133]. However, even this conclusion is not certain! In 1883 Reynolds [168] was able to carefully construct systems in which laminar flow was maintained at Reynolds numbers in

excess of 6,000 [133]. Should laminar flow be physiologically desirable, it would not be surprising to find such careful elegant design in the bronchial tree's structure.

In spite of the lack of a good mathematical analysis of this system, physiological tests of its behaviour have yielded some very interesting results. While inferential, these results support a belief that the human lung's structure is very well, if not optimally, adapted to its task. The belief that a biological system's structure is optimally adapted to task is referred to as Rashevsky's principle of optimum design [165]. This principle is a corollary of Darwin's paradigm of evolution [137]. Rashevsky's principle is of great value to the analysis of biological systems. It reduces a functional analysis of the system's structure to the task of demonstrating that the structure is in fact an optimal solution to the task at hand. When such an endeavour fails it is either because the system violates Rashevsky's principal or the analysis has failed to adequately model the task at hand and consider the range of its consequences.

Physiological experiments have shown that gas distribution within the lung varies as a function of its degree of inflation, or overall volume. As we see from Figure 3.1 this means that different topographic regions of the lung are preferentially sequestered as a function of the lung volume at which ventilation is occurring. The important ramifications of this effect can be easily understood in terms of a 'gedanken' experiment which reduces this effect to an elaborate

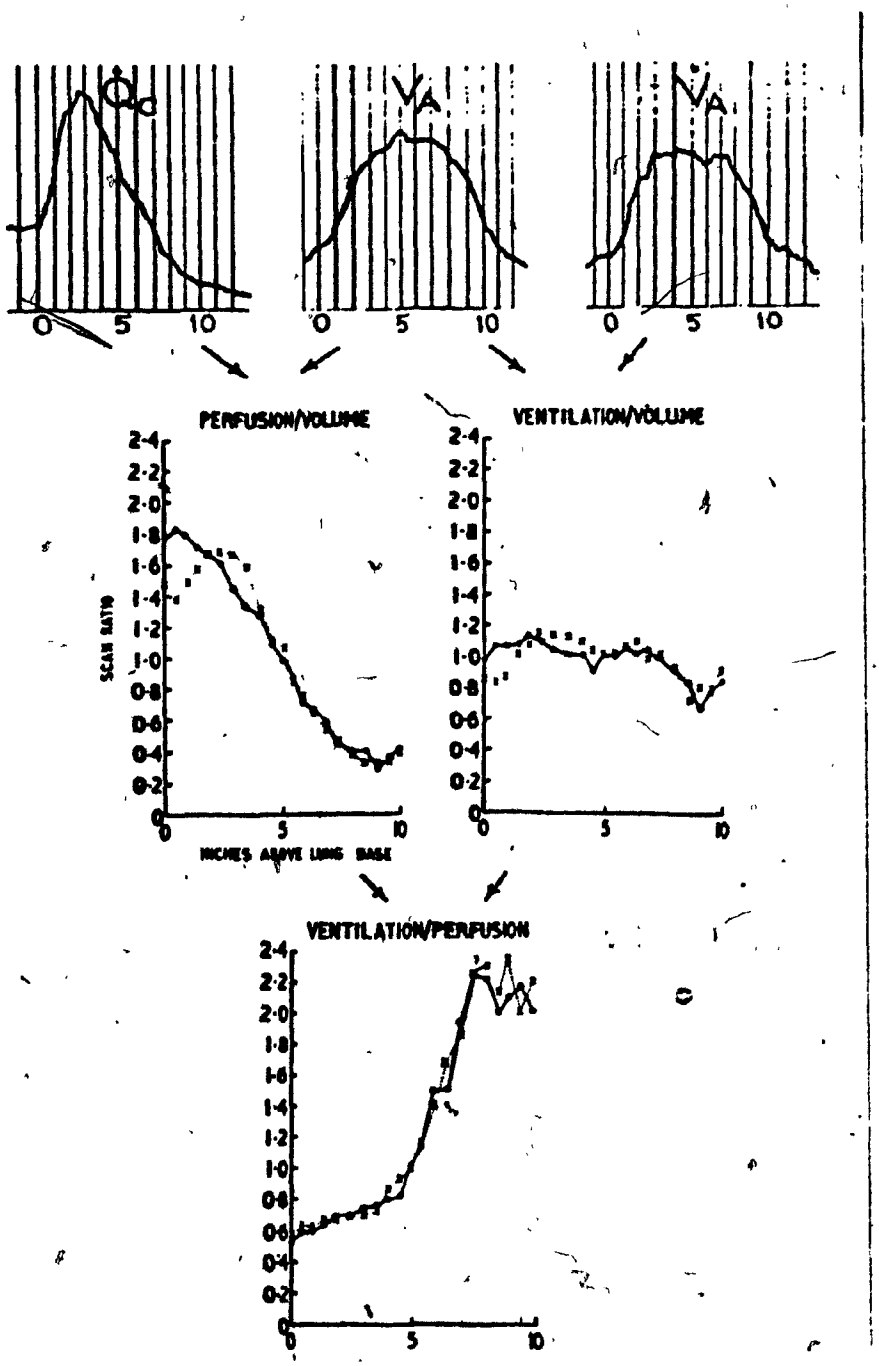

Figure 3.1a. Demonstration of regional inequality in ventilation-perfusion ratios. The common abscissa is distance from the bases of the lungs, in inches. The experimental data are shown at the top and indicate the radioactivity (obtained by rapid scanning method) at different lung heights following either a single breath, rebreathing, or intravenous injection of radioactive xenon. These procedures allow one to determine relative ventilation, volume, and perfusion, respectively, of the alveoli at any lung height. From the first two the ventilation per unit volume is obtained (center, left) and from the last two the perfusion per unit volume (center, right). These two can now be combined to obtain information on the ventilation-perfusion ratio (lower figure). Both ventilation and perfusion are increased as one moves down the lung, but since the perfusion changes more rapidly than the ventilation, large differences in $\dot{V}_A/\dot{Q}$ are developed. From [136].

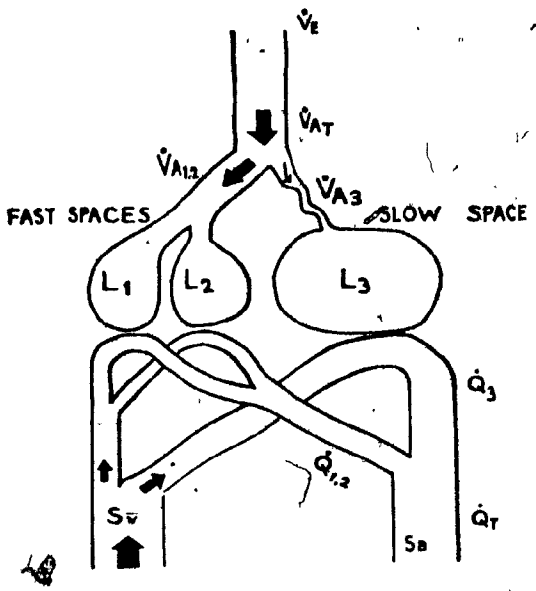

Diagram of the concept of the slow space in chronic obstructive lung disease. There are variously well ventilated fast spaces (L_1, L_2) with a collective volume $L_{1,2}$. There is a homogeneously poorly ventilated group of alveoli with volume L_3 called the slow space. The total of these various volumes, L_T, is the functional residual capacity. L_3/L_T is the volume of the slow residual space expressed as a fraction of the functional residual capacity. $\dot{V}_{AT}$, $\dot{V}_{A3}$, $\dot{V}_{A1,2}$ are alveolar ventilations, the different subscripts referring respectively to the total in all alveoli, to that of the slow space and to that of the fast spaces. $\dot{V}_E$ is minute ventilation at the mouth, including dead space ventilation. $\dot{Q}_T$, $\dot{Q}_3$, $\dot{Q}_{12}$ are the blood flows respectively to the whole lung (i.e. cardiac output), to the slow space and to the fast spaces. – $S\bar{v}$, Sa, S_{c3} and S_{c12} refer to oxygen saturation respectively of mixed venous blood, of mixed arterial blood, of blood partially oxygenated in the slow space and of blood fully oxygenated in the various fast spaces. – $\dot{V}_{A3}/\dot{Q}_3$ is the ventilation perfusion ratio in the slow space which determines the saturation of the blood oxygenated in these alveoli. $\dot{Q}_3/\dot{Q}_T$ is the fraction in cardiac output perfusing the slow space, and determines how much incompletely oxygenated blood mixes into the arterial blood.

Figure 3.1b. From [120].

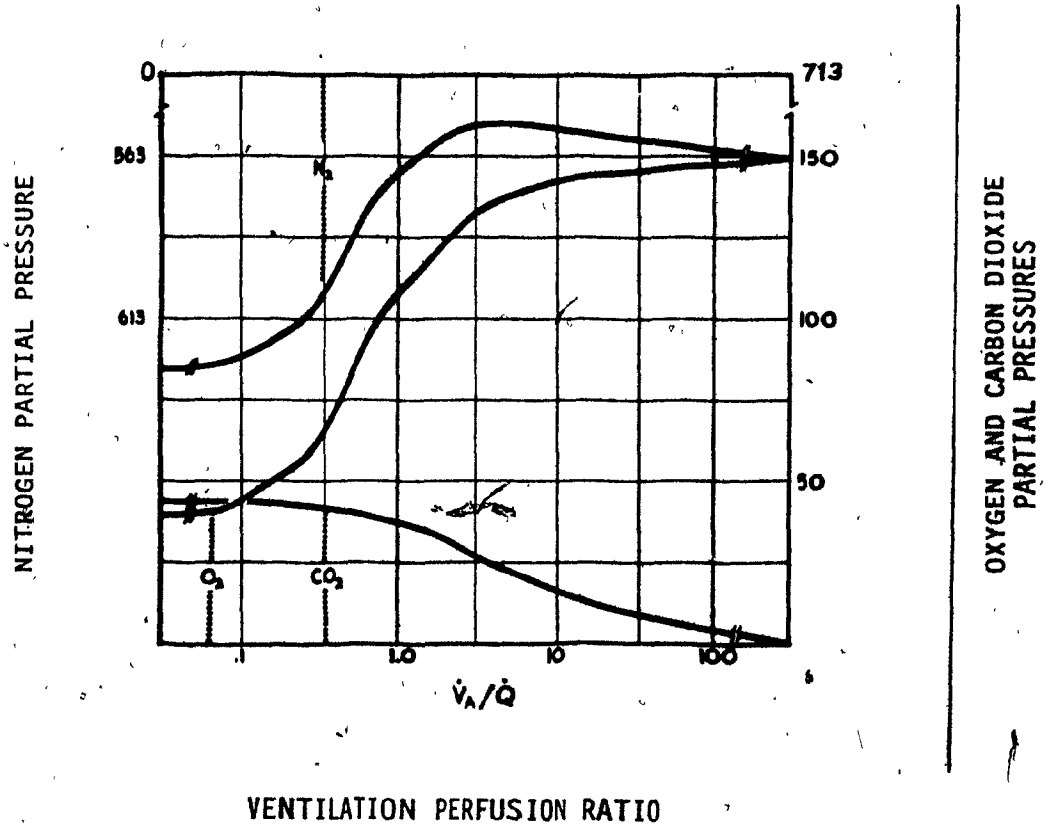

Figure 3.1c From [136].

scheme for recursively sorting the air we breathe.

In this experiment consider inhaling a single breath from a long thin tube. Pretend that we have labelled the sequence of gas molecules, S_{vs}, in this tube by their order of occurrence. Furthermore, assume that we can manipulate turbulent and laminar gas flow during inspiration in a manner that assures that there is no gross gas mixing of this ordered arrangement in the upper airways of the bronchial tree. Under these constraints we would expect the bronchial tree model shown in Figure 3.2 to fill in a manner which topographically distributes the breath of air specified by the sequence, S_{vw}, in a manner shown in Figure 3.2b. Now we know that the manner in which this tree is emptied depends on the length of the sequence, S_{vw}, and the length of the sequence, S_{uv}. In terms of this string notation, given in Figure 3.3, the total lung volume at the end of inspiration would be S_{uw}, while the volume of gas inspired during the breath is S_{vw}, where the volume of resident gas in the lung prior to this inspiration would be S_{uv}.

The effect of exhaling is to permute, or sort, the initial inspired gas sequence, S_{vs}, into some other order. Figures 3.2c and 3.2d conceptually demonstrate this effect for expiratory volumes of length $S_{wv(1)}$ and $S_{wv(2)}$ where $v(2) < v < v(1)$. Let us first consider the simple case of ventilating a corpse, where we may ignore the effects of carbon dioxide and oxygen transfer on this system. In such a case, the lung's stack-like first-in-first-out ventilatory

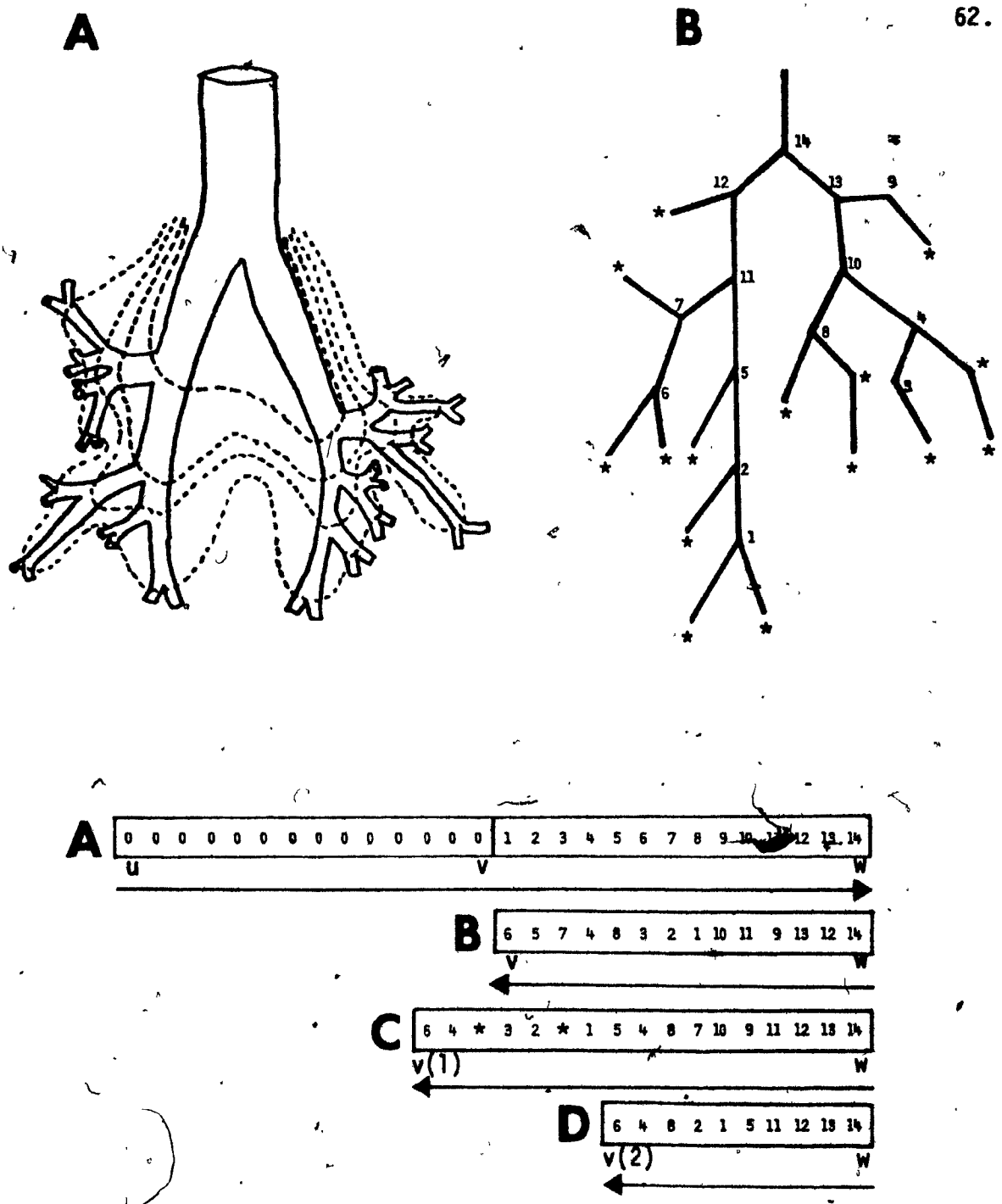

Figure 3.2. Hypothetical Ventilatory Distribution of Gas in a Non-Symmetric Binary Tree During Inspiratory and Expiratory Movements.

Figure 3.2a. First Four Generations of Airways of a Bronchial Cast Drawn to Scale in Two Dimensions. From [158].

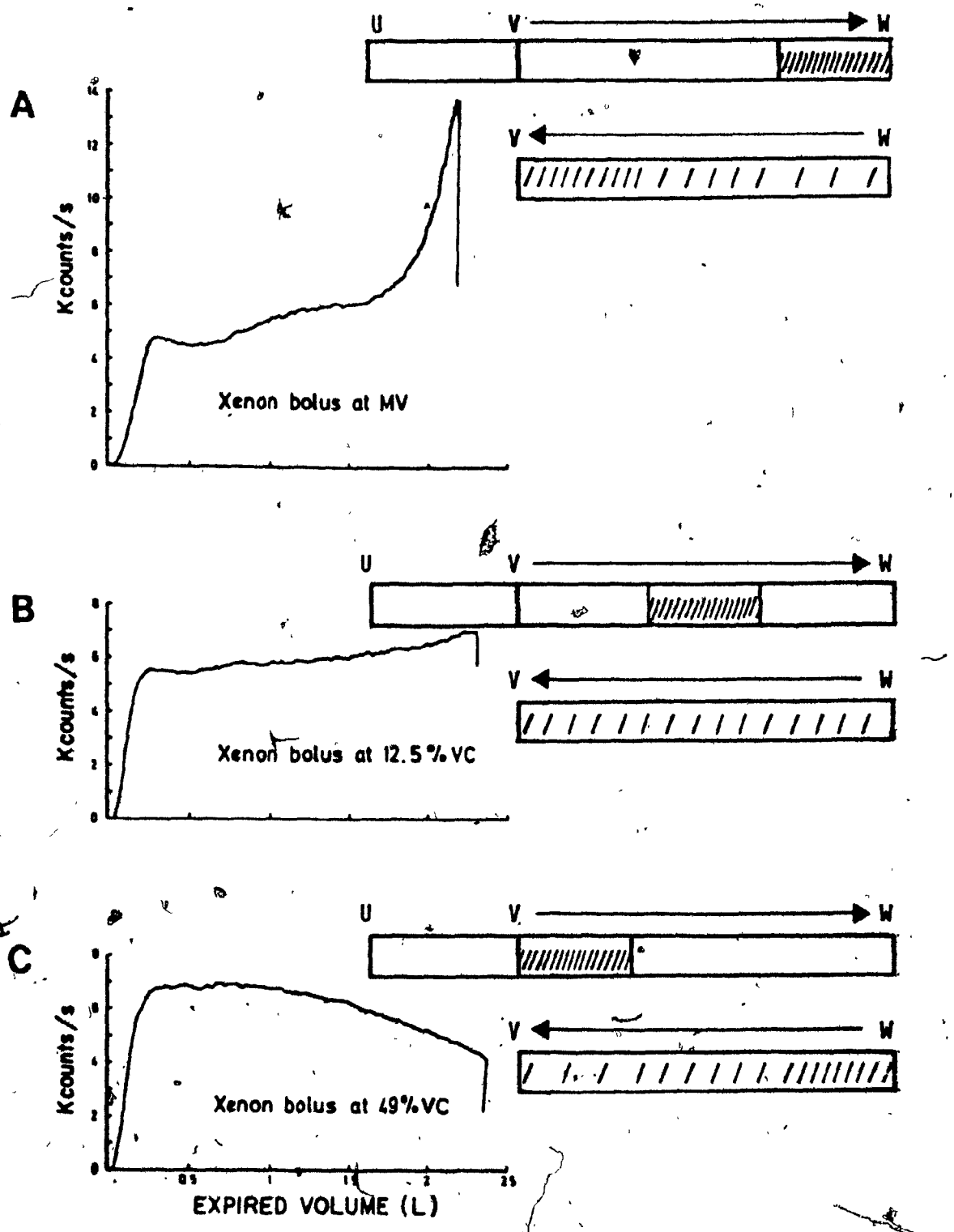

Figure 3.3. Washout Pattern for Xenon-133 Following Injection of a Bolus of Xenon-133 at the Indicated Volumes of a VC Inspiration. From [56].

behaviour could be described by the operation of a permutation $\vdots$ on S_{vw} as $\vdots S_{vw}$. It is much harder to analyse the effects of a permutation on S_{vw} when oxygen and carbon dioxide transfer occurs. Gas transfer involves making deletions, for oxygen absorption, and insertions, for carbon dioxide production, on the sequence, S_{vw}, prior to its permutation $\vdots$ during exhalation. The cumulative effects of random deletions and insertions on a string is a difficult theoretical problem [85,83].

If the gas molecules in the sequence S_{vw} were of different composition, for example: O_2, CO_2 and N_2, then we would expect their particular densities and viscosities to further influence their relative distribution within the tree.

Consider a simple case where we arrange an appropriate sequence of gaseous radioactive tracer molecules, denoted as $\neq$, at the beginning of sequence S_{vw}. Then we could count the number and position of these particles as they are exhaled in $\vdots S_{vw}$. In terms of our gedanken experiment we would expect to see a distribution like that shown in Figure 3.3a. Furthermore, if we were to exactly repeat this study with a different arrangement of radioactive gas molecules, we would expect to observe a different exhaled distribution than that found in Figure 3.3a. In fact if we were to arrange an equivalent sequence of radioactive tracer molecules at the end of the inspiratory sequence S_{vw}, then we would expect to observe the distribution shown in Figure 3.3c.

The single breath washout tests may be considered as approximations

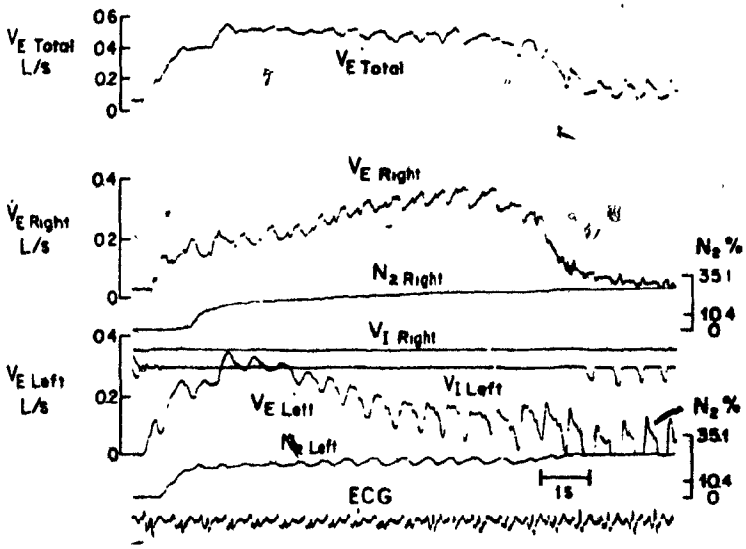

Inspiratory and expiratory flow rates and N_2 concentrations of individual lungs recorded as a function of time in *subject 3* (left lateral decubitus position). Cardiogenic oscillations in flow and intermittent inspiration of the left lung appeared after the right lung had apparently reached flow limitation. The amplitude and duration of the expiratory oscillations are larger than those of the inspiratory oscillations. $\dot{V}I_{Right}$, $\dot{V}I_{Left}$ = inspiratory flow rates of right and left lungs, respectively.

Figure 3.4. From [51].

of our gedanken experiment. These tests involve the analysis of the sequential gas distribution observed during a single exhalation. Various experiments [36,56,114] which involve inhaling an aliquot or bolus of radioactive gas at specific points during a carefully controlled inspiratory effort provide information on the distribution of gas over a range of lung volumes. Some results of these experiments are shown in the single breath washout curves seen in Figures 3.4a, b and c. The pattern of inhaled radioactive gas, ≠, is given above each of these curves in the sequence notation S_{uvw} used in our gedanken experiments along with a metric which is expressed in terms of the standard subdivisions of lung volume. The curves shown in Figure 3.4 were obtained from carefully controlled experiments on excised whole dog lung [56].

These curves are analysed in terms of the behaviour of the four phases shown in Figure 3.5. The first phase of these curves, I, results from the stack like behaviour of the upper airways. This structure insures that the last portion of gas to enter the lung's airways during inspiration is the first portion to leave during expiration. Hence phase I is composed entirely of dead space gas. If there was no mixing of dead space gas with alveolar gas, which has partaken in the process of gas transfer, then we would observe a step-function in gas concentration immediately after an individual had exhaled a cumulative volume equal to his anatomical dead space volume. The sigmoidal shape of phase II of this curve results from the

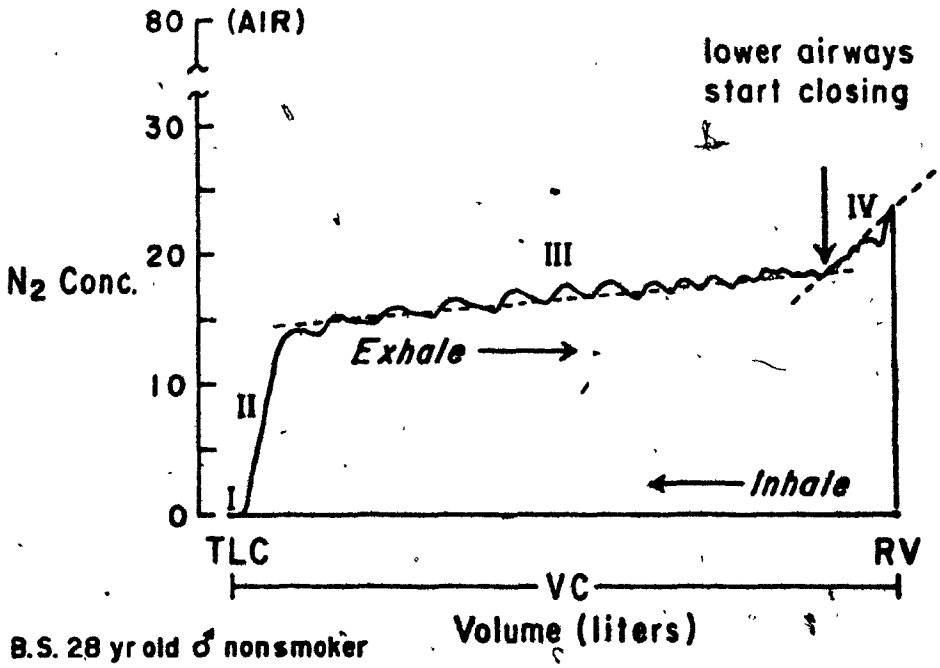

Figure 3.5.. Continuous record of expired nitrogen concentration obtained from a nonsmoker during exhalation after an inspiration of pure oxygen from residual volume to total lung capacity. The Roman numerals indicate the 4 phases of the nitrogen concentration record. From [15].

significant mixture of alveolar and anatomical dead space gas during this phase of expiratory washout. The third phase, III, or alveolar plateau, of this curve is indicative of the respiratory system's ability to achieve quasi-stationary concentrations of gas throughout a large sequential portion of the expired gas volume. Observed gas concentrations within the alveolar plateau often gently rise as successively higher regions, with increased $\dot{v}/\dot{q}$ ratios, contribute to the expired gas.

Towards the end of an expiration when over 80% of the inspired volume has been exhaled there is often a sudden increase in the slope of the alveolar plateau. This effect marks the beginning of phase IV of the expiration. The lung volume at which phase IV begins is called closing volume, CV, while the trans-pulmonary pressure at this point is called the closing pressure, CP.

At the start of phase IV the small airways to the basal, or bottom regions of the lung have closed or narrowed to a point where the regions downstream, or distal, to the point of closure can no longer contribute gas to the expirate. Thus any alveolar gas which is distal to the point of closure is effectively trapped. Through phase IV this effect occurs in successively higher regions of the lung. Hence as phase IV proceeds, the proportion of gas entering the expirate from the apical, or higher regions of the lung, progressively increases. If the apical regions are overventilated and underperfused then there is marked increase in the expired gas concentrations during phase IV as expiration proceeds.

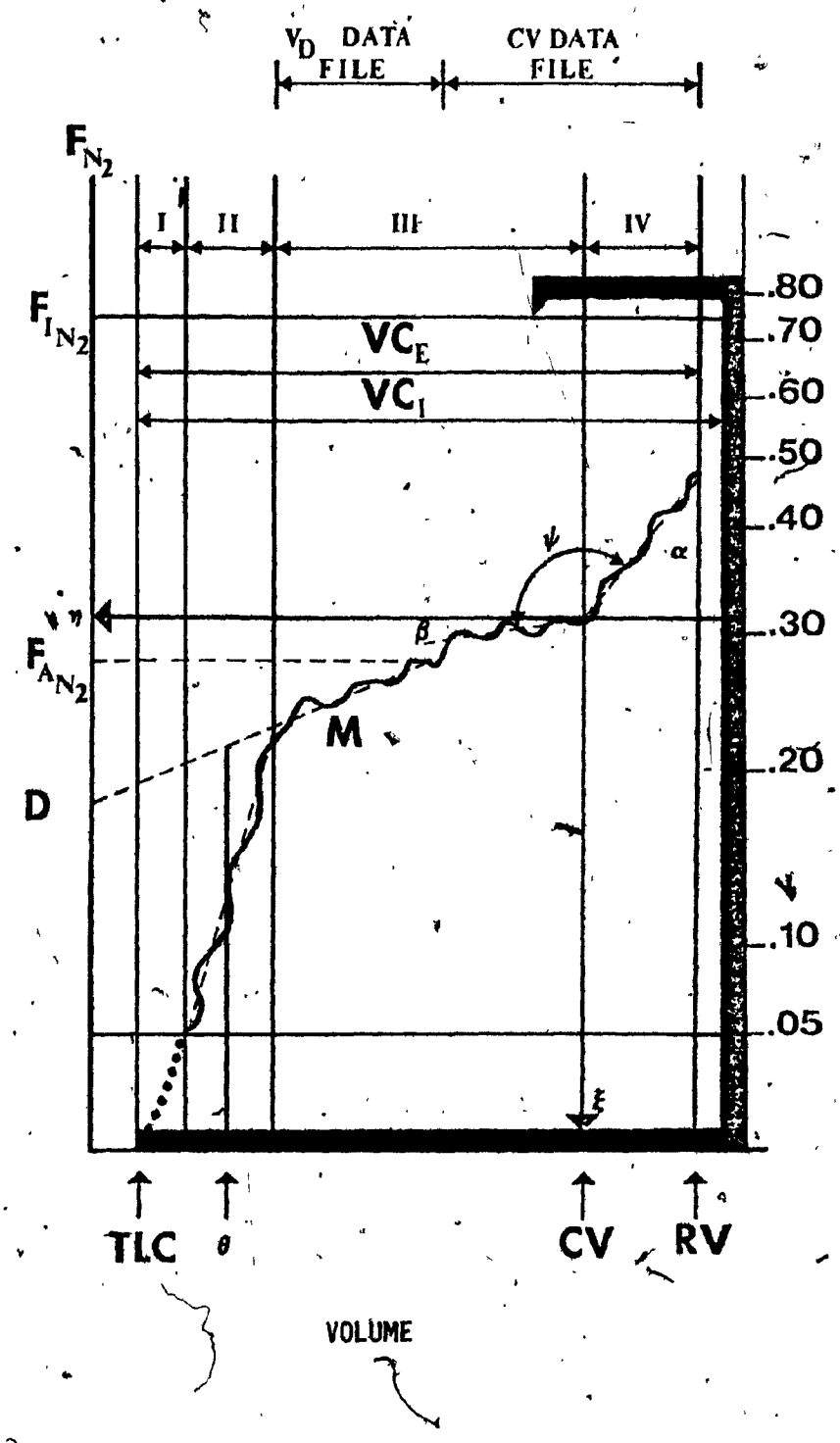

Figure 3.6. Detailed Characteristics of the SBN_2 Curve. From [126].

If this simple interpretation of the complex behaviour underlying this system were correct, then it follows that the pattern of xenon concentration in the expirate, which is shown in Figure 3.3a, would be reversed if the bolus was given towards the end of the inspired volume. As shown in Figure 3.3c that is exactly what occurs.

Section 3.2

The portion of the single breath nitrogen washout curve shown in Figure 3.6 will be considered for practical purposes to be a tabulated function of N discrete observations of nitrogen concentration, Y_n, at a given lung volume, x_n: (x_1,Y_1) $(x_2,Y_2),\ldots,(x_N,Y_N)$, with $x_1 \leq x_2 \leq \ldots, \leq x_N$.

We wish to estimate the nitrogen concentration at any lung volume within the domain specified by the phase III and phase IV components of the gas washout curve as:

$$y = \begin{cases} \alpha x + \eta - \alpha\xi & \text{if } a \leq x \leq \xi, \\ \beta x + \eta - \beta\xi & \text{if } \xi \leq x \leq b, \end{cases}$$

where α, β are the slopes of the phase III and phase IV segments of the washout curve, a and b are the boundary points of the experimental data, and η and ξ specify the nitrogen gas concentration and lung volume components at the onset of closing volume.

In order to obtain optimal estimates of the slopes of the phase III and phase IV components of single breath gas washout curves and the point of onset of closing volume, we wish to determine the parameters α, β, ξ, η so as to reduce their sum of squares of errors, $\Gamma(\alpha, \beta, \xi, \eta)$, to a minimum. The sum of squares of errors Γ, for a given set of parameters, α, β, ξ, η, may be calculated as:

$$\Gamma(\alpha, \beta, \xi, \eta, x_n, Y_n) = \sum_{n=1}^{N} [y(\alpha, \beta, \xi, \eta, x_n) - Y_n]^2 \qquad 3.1$$

$$= \sum_{n=1}^{K} [\alpha x_n + \eta - \alpha\xi - Y_n]^2 + \sum_{n=k}^{N} [\beta x_n + \eta - \beta\xi - Y_n]^2, \qquad 3.2$$

Leung and O'Mara [20] have previously described a technique for the linear least squares estimate of α, β, ξ, η outlined in equation 3.2. Due to both practical and theoretical considerations we wish to describe a refinement of this technique. This refinement balances the contribution of the two component sum of squares on the left hand side of equation 3.2 in accordance with the relative number of data points on either side of the estimated value of closing volume. This normalization procedure involves weighing the contribution of each component sum of squares by a

factor which is inversely proportional to the relative number of points on either side of the closing volume. The weights in question may be derived from equation 3.2 as $1/K$ and $1/(N-K)$.

By applying these weights in equation 3.2 we may obtain the refined estimates of α, β, ξ, η from a consideration of equation 3.3

$$\Gamma(\alpha, \beta, \xi, \eta, x_n, Y_n) = \frac{1}{K} \sum_{n=1}^{K} [\alpha x_n + \eta - \alpha\xi - Y_n]^2 \qquad 3.3$$

$$+ \frac{1}{(N-K)} \sum_{n=K}^{N} [\beta x_n + \eta - \beta\xi - Y_n]^2,$$

with K dependent on ξ such that $x_K \leq \xi < x_{K+1}$.

The set of parameters α, β, ξ, η that reduce equation 3.3 to a minimum is a solution of the following four non-linear equations:

$$\frac{1}{2} \frac{\partial}{\partial\alpha} \Gamma(\alpha,\beta,\xi,\eta,x_n,Y_n) = \frac{1}{K} \sum_{n=1}^{K} [(x_n - \xi)\alpha + \eta - Y_n][x_n - \xi] = 0, \qquad 3.4$$

$$\frac{1}{2} \frac{\partial}{\partial\beta} \Gamma(\alpha,\beta,\xi,\eta,x_n,Y_n)$$

$$= \frac{1}{K} \sum_{n=K+1}^{N} [(x_n - \xi)\beta + \eta - Y_n][x_n - \xi] = 0, \qquad 3.5$$

$$\frac{1}{2}\frac{\partial}{\partial\eta}\Gamma(\alpha,\beta,\xi,\eta,x_n,Y_n) = \frac{1}{K}\sum_{n=1}^{K}[(x_n-\xi)\alpha+\eta-Y_n] \qquad 3.6$$

$$+\frac{1}{(N-K)}\sum_{n=K+1}^{N}[(x_n-\xi)\beta+\eta-Y_n]=0,$$

$$\frac{1}{2}\frac{\partial}{\partial\xi}\Gamma(\alpha,\beta,\xi,\eta,x_n,Y_n) = \frac{1}{K}\sum_{n=1}^{K}\alpha[\alpha(x_n-\xi)+\eta-Y_n] \qquad 3.7$$

$$+\frac{1}{(N-K)}\sum_{n=K+1}^{N}\beta[\beta(x_n-\xi)+\eta-Y_n]=0.$$

These equations are obtained by evaluating each of the four partial derivatives of equation 3.3 with respect to our set of parameters and subsequently equating them to zero.

Solving equation 3.4 and 3.5 for α and β in terms of ξ and η, we obtain:

$$\alpha = \alpha(\xi,\eta) = -\frac{P(\xi)}{Q(\xi)}\eta + \frac{\mu(\xi)-\xi\lambda(\xi)}{KQ(\xi)}, \qquad 3.8$$

$$\beta = \beta(\xi,\eta) = -\frac{S(\xi)}{T(\xi)}\eta + \frac{[B-\mu(\xi)]-\xi[A-\lambda(\xi)]}{[N-K]T(\xi)}, \qquad 3.9$$

where

$$A = \sum_{n=1}^{N} Y_n \qquad 3.10$$

$$B = \sum_{n=1}^{N} x_n Y_n \qquad 3.11$$

$$P(\xi) = \frac{1}{K} \sum_{n=1}^{K} (x_n - \xi) \qquad 3.12$$

$$Q(\xi) = \frac{1}{K} \sum_{n=1}^{K} (x_n - \xi)^2 \qquad 3.13$$

$$S(\xi) = \frac{1}{(N-K)} \sum_{n=K+1}^{N} (x_n - \xi) \qquad 3.14$$

$$T(\xi) = \frac{1}{(N-K)} \sum_{n=K+1}^{N} (x_n - \xi)^2 \qquad 3.15$$

$$\lambda(\xi) = \sum_{n=1}^{K} Y_n \qquad 3.16$$

$$\mu(\xi) = \sum_{n=1}^{K} x_n Y_n \qquad 3.17$$

with $K = K(\xi)$ such that

$$x_K \leq \xi < x_{K+1}$$

Eliminating α and β from equation 6, we get η in terms of ξ only:

$$\eta=\eta(\xi) = \frac{\frac{P(\xi)[\mu(\xi)-\xi\lambda(\xi)]}{KQ(\xi)} + \frac{S(\xi)[B-\mu-\xi A+\xi\lambda(\xi)]}{[N-K]T(\xi)} - \frac{\lambda(\xi)}{K} - \frac{(A-\lambda(\xi))}{[N-K]}}{\frac{[P(\xi)]^2}{[Q(\xi)]^2} + \frac{[S(\xi)]^2}{[T(\xi)]^2} - 2} \quad 3.18$$

Hence from equations 3.8 and 3.9 α and β become functions of ξ only, and equation 3.7 may be rewritten as follows:

$$\Phi(\alpha(\xi),\beta(\xi),\xi,\eta(\xi),x_n,Y_n)$$

$$= \alpha^2 P(\xi) + \beta^2 S(\xi) + (\alpha+\beta)\eta - \frac{\alpha\lambda(\xi)}{K} - \frac{\beta[A-\lambda(\xi)]}{[N-K]} = 0. \quad 3.19$$

The zeros of equation 3.19 may then be obtained by an iterative algorithm employing the variable secant method [164]. This method uses two arbitrarily chosen values of ξ to generate a sequence of ξ that may then converge to the zeros of equation 3.19 by using the iterative formula:

$$\xi_{r+1} = \xi_r - \frac{\Phi(\xi_r)}{\Phi(\xi_r) - \Phi(\xi_{r-1})}[\xi_r - \xi_{r-1}]. \quad 3.20$$

The zero of equation 3.19 that reduces the sum of squares of errors $\Gamma(\alpha,\beta,\xi,n,x,Y)$, to a global minimum optimally specifies the unbiased value of ξ at the point of onset of airway closure.

CHAPTER FOUR

The portion of the single breath nitrogen washout curve considered in Figure 3.6 may be treated as a continuous function $y = f(x)$ with boundary conditions specified by $a \leq x \leq b$. In this case we may apply the method of least squares to approximate the continuous function by two intersecting straight lines

$$\tilde{y} = \begin{cases} \alpha x + \eta - \alpha\xi \\ \beta x + \eta - \beta\xi \end{cases} \tag{4.1}$$

The four parameters α, β, η, ξ in equation (4.1) are determined so as to minimize the squares of errors:

$$I = I(\alpha,\beta,\eta,\xi) = \frac{1}{(\xi-a)}\int_a^{\xi}[\tilde{y}(x)-f(x)]^2dx \tag{4.2}$$

$$+ \frac{1}{(b-\xi)}\int_{\xi}^{b}[\tilde{y}(x)-f(x)]^2dx = \frac{1}{(\xi-a)}\int_a^{\xi}[\alpha x+\eta-\alpha\xi-f(x)]^2dx$$

$$+ \frac{1}{(b-\xi)}\int_{\xi}^{b}[\beta x+\eta-\beta\xi-f(x)]^2dx$$

The values of α, β, η, ξ may be obtained by solving a system of four non-linear equations. These equations are derived from equating to zero each of the four partial derivatives of equation 4.2 with respect to α, β, η, ξ:

$$\frac{\partial}{\partial\alpha}I(\alpha,\beta,\eta,\xi) = 0 \tag{4.3}$$

$$\frac{\partial}{\partial\beta}I(\alpha,\beta,\eta,\xi) = 0 \tag{4.4}$$

$$\frac{\partial}{\partial\eta}I(\alpha,\beta,\eta,\xi) = 0 \tag{4.5}$$

$$\frac{\partial}{\partial\xi}I(\alpha,\beta,\eta,\xi) = 0 \tag{4.6}$$

or explicitly, as shown in sections 4.1, 4.2, 4.3, 4.4.

$$\alpha = \alpha(\eta,\xi) = \frac{3\eta}{2(\xi-a)} + \frac{3(\mu-\xi\lambda)}{(\xi-a)^3} \tag{4.7}$$

$$\beta = \beta(\eta,\xi) = \frac{-3\eta}{2(b-\xi)} + \frac{3[(\beta-\mu)-\xi(A-\lambda)]}{(b-\xi)^3} \tag{4.8}$$

$$\eta = \eta(\xi) = \frac{3(\mu-\xi\lambda)}{(\xi-a)^2} - \frac{3[(\beta-\mu)-\xi(A-\lambda)]}{(b-\xi)^2} + \frac{2\lambda}{\xi-a} + \frac{2(A-\lambda)}{b-\xi} \tag{4.9}$$

$$\Lambda(\xi) = \eta(\xi)\phi_1(\xi) + \phi_2(\xi) \stackrel{\xi}{=} 0 \tag{4.10}$$

where

$$\phi_1(\xi) = \frac{2f(\xi)}{\xi-a} + \frac{2\lambda}{(\xi-a)^2} + \frac{3[2\mu-\lambda(a+\xi)]}{(\xi-a)^3} + \frac{2f(\xi)}{b-\xi} - \frac{2(A-\lambda)}{(b-\xi)^2} - \frac{3[-2(\beta-\mu)+(A-\lambda)(\xi+b)}{(b-\xi)^3} \tag{4.11}$$

$$\phi_2(\xi) = \frac{[f(\xi)]^2}{\xi-a} - \frac{\nu}{(\xi-a)^2} \qquad (4.12)$$

$$+ \frac{6(\mu-\xi\lambda)[2\mu-\lambda(a+\xi)]}{(\xi-a)^5} - \frac{[f(\xi)]^2}{b-\xi} + \frac{c-\nu}{(b-\xi)^2}$$

$$+ \frac{6[(\beta-\mu)-\xi(A-\lambda)][-2(\beta-\mu)+(A-\lambda)(\xi+b)]}{(b-\xi)^5}$$

with

$$\lambda = \lambda(\xi) = \int_a^{\xi} f(x)dx \qquad (4.13)$$

$$\mu = \mu(\xi) = \int_a^{\xi} xf(x)dx \qquad (4.14)$$

$$\nu = \nu(\xi) = \int_a^{\xi} [f(x)]^2 dx \qquad (4.15)$$

$$A = \lambda(b) = \int_a^{b} f(x)dx \qquad (4.16)$$

$$\beta = \mu(b) = \int_a^{b} xf(x)dx \qquad (4.17)$$

$$c = \nu(b) = \int_a^{b} [f(x)]^2 dx \qquad (4.18)$$

The zero of equation (4.10) may then be obtained by an iterative algorithm employing the variable secand method. This method uses two arbitrarily chosen values of ξ to generate a sequence of ξ

that may then converge to the zeros of equation (4.10) by using the iterative formula:

$$\xi_{n+1} = \xi_n + \Lambda(\xi_n)\frac{\xi_n - \xi_{n-1}}{\Lambda(\xi_n) - \Lambda(\xi_{n-1})} \qquad (4.19)$$

SECTION 4.1

By equating the partial derivative of $I(\alpha,\beta,\eta,\xi)$ with respect to α to zero, as in equation (4.3), we obtain

$$\frac{\xi-a}{2}\frac{\partial}{\partial\alpha} I(\alpha,\beta,\eta,\xi) = \int_a^\xi [\alpha x-\eta-\alpha\xi-f(x)][x-\xi]dx$$

$$= \alpha\int_a^\xi x^2dx + [\eta-\alpha\xi-\alpha\xi]\int_a^\xi xdx - \xi[\eta-\alpha\xi]\int_a^\xi dx$$

$$+ \xi\int_a^\xi f(x)dx - \int_a^\xi x(fx)dx$$

$$= \frac{\alpha}{3}[\xi^3-a^3] + \frac{1}{2}[\eta-2\alpha\xi][\xi^2-a^2] - \xi[\eta-\alpha\xi][\xi-a]$$

$$+ \xi\lambda - \mu$$

$$= \frac{\alpha}{3}[\xi^3-a^3-3\xi^3+3a^2\xi+3\xi^3-3a\xi^2]$$

$$+ \frac{\eta}{2}[\xi^2-a^2-2\xi^2+2a\xi] + \xi\lambda - \mu$$

$$= \frac{\alpha}{3}[\xi-a]^3 - \frac{\eta}{2}[\xi-a]^2 + \xi\lambda - \mu = 0 \qquad (4.1.1)$$

where

$$\lambda = \lambda(\xi) = \int_a^\xi f(x)dx \qquad (4.1.2)$$

$$\mu = \mu(\xi) = \int xf(x)dx \qquad (4.1.3)$$

Equation (4.7) is then obtained by solving equation (4.1.1) for α in terms of η and ξ:

$$\alpha = \alpha(\eta,\xi) = \frac{3\eta}{2[\xi-a]} + \frac{3[\mu-\xi\lambda]}{[\xi-a]^3} \qquad (4.7)$$

in which λ and μ are defined by equations (4.1.2) and (4.1.3) as function of ξ.

SECTION 4.2

By equating the partial derivative of $I(\alpha,\beta,\eta,\xi)$ with respect to β, as in equation (4.4), we obtain:

$$\frac{b-\xi}{2}\frac{\partial}{\partial\beta}I(\alpha,\beta,\eta,\xi) = \int_\xi^b [\beta x+\eta-\beta\xi-f(x)][x-\xi]dx$$

$$= \beta\int_\xi^b x^2dx + [\eta-\beta\xi-\beta\xi]\int_\xi^b xdx - \xi[\eta-\beta\xi]\int_\xi^b dx$$

$$+ \xi\int_\xi^b f(x)dx - \int_\xi^b xf(x)dx$$

$$= \frac{\beta}{3}[b^3-\xi^3] + \frac{1}{2}[\eta-2\beta\xi][b^2-\xi^2] - \xi[\eta-\beta\xi][b-\xi]$$

$$+ \xi[A-\lambda] - [\beta-\mu]$$

$$= \frac{\beta}{3}[b^3-\xi^3-3b^2\xi+3\xi^3+3b\xi^2-3\xi^3]$$

$$+ \frac{\eta}{2}[b^2-\xi^2-2b\xi+2\xi^2] + \xi[A-\lambda] - [\beta-\mu]$$

$$= \frac{\beta}{3}[b-\xi]^3 + \frac{\eta}{2}[b-\xi]^2 + \xi[A-\lambda] - [\beta-\mu] = 0 \qquad (4.2.1)$$

where

$$A = \lambda(b) = \int_a^b f(x)dx \qquad (4.2.2)$$

$$\beta = \mu(b) = \int_a^b xf(x)dx \qquad (4.2.3)$$

Equation (4.8) is then obtained by solving equation (4.2.1) for β in terms of η and ξ:

$$\beta = \beta(\eta,\xi) = \frac{-3\eta}{2[b-\xi]} + \frac{3}{(b-\xi)^3}[(\beta-\mu) - \xi(A-\lambda)] \qquad (4.8)$$

in which λ and μ are defined by equations (4.1.2) and (4.1.3) as functions of ξ.

SECTION 4.3

By equating the partial derivative of $I(\alpha,\beta,\eta,\xi)$ with respect to η, as in equation (4.5), we obtain:

$$\frac{1}{2}\frac{\partial}{\partial\eta}I(\alpha,\beta,\eta,\xi) = \frac{1}{\xi-a}\int_a^\xi [\alpha x+\eta-\alpha\xi-f(x)]dx$$

$$+ \frac{1}{b-\xi}\int_\xi^b [\beta x-\eta-\beta\xi-f(x)]dx$$

$$= \frac{1}{\xi-a}\left[\frac{\alpha}{2}(\xi^2-a^2) + (\eta-\alpha\xi)(\xi-a)\right] - \frac{\lambda}{\xi-a}$$

$$+ \frac{1}{b-\xi}\left[\frac{\beta}{2}(b^2-\xi^2) + \eta - \beta\xi)(b-\xi)\right] - \frac{A-\lambda}{b-\xi}$$

$$= \frac{\alpha}{2}(\xi+a) + \eta - \alpha\xi - \frac{\lambda}{\xi-a} + \frac{\beta}{2}(b+\xi) + \eta$$

$$- \beta\xi - \frac{A-\lambda}{b-\xi}$$

$$= 2\eta - \frac{\alpha}{2}(\xi-a) + \frac{\beta}{2}(b-\xi) - \frac{\lambda}{\xi-a} - \frac{A-\lambda}{b-\xi} \qquad (4.3.1)$$

Eliminating α and β from equations (4.7), (4.8) and (4.3.1) we get η in terms of ξ only:

$$2\eta - \frac{1}{2}\left[\frac{3\eta}{2} + \frac{3(\mu-\xi\lambda)}{(\xi-a)^2}\right] + \frac{1}{2}\left[-\frac{3\eta}{2} + \frac{3[(\beta-\mu) - \xi(A-\lambda)]}{(b-\xi)^2}\right]$$

$$- \frac{\lambda}{\xi-a} - \frac{A-\lambda}{b-\xi} = 0$$

$$\frac{\eta}{2} - \frac{3(\mu-\xi\lambda)}{2(\xi-a)^2} + \frac{3[(\beta-\mu) - \xi(A-\lambda)]}{2(b-\xi)^2}$$

$$- \frac{\lambda}{\xi-a} - \frac{A-\lambda}{b-\xi} = 0 \qquad (4.3.2)$$

Hence equation (4.9) is obtained by solving equation (4.3.2) for η in terms of ξ :

$$\eta = \eta(\xi) = \frac{3(\mu-\xi\lambda)}{(\xi-a)^2} - \frac{3[(\beta-\mu) - \xi(A-\lambda)]}{(b-\xi)^2}$$

$$+ \frac{2\lambda}{\xi-a} + \frac{2(A-\lambda)}{b-\xi} \qquad (4.9)$$

SECTION 4.4

By differentiating equation (4.2) with respect to ξ we obtain:

$$\frac{\partial}{\partial\xi} I(\alpha,\beta,\eta,\xi) = -\frac{2\alpha}{\xi-a}\int_a^\xi [\alpha x+\eta+\alpha\xi-f(x)]dx + \frac{1}{\xi-a}[\alpha\xi+\eta-\alpha\xi-f(\xi)]^2$$

$$- \frac{2\beta}{b-\xi}\int_\xi^b [\beta x+\eta-\beta\xi-f(x)]dx - \frac{1}{b-\xi}[\beta\xi+\eta-\beta\xi-f(\xi)]^2$$

$$- \frac{1}{(\xi-a)^2}\int_a^\xi [\alpha x+\eta-\alpha\xi-f(x)]^2 dx$$

$$+ \frac{1}{(b-\xi)^2}\int_\xi^b [\beta x+\eta-\beta\xi-f(x)]^2 dx \qquad (4.4.1)$$

where

$$-\frac{2\alpha}{\xi-a}\int_a^{\xi}[\alpha x+\eta-\alpha\xi-f(x)]dx = -\frac{2\alpha}{\xi-a}\left[\frac{\alpha}{2}(\xi^2-a^2) + (\eta-\alpha\xi)(\xi-a)\right] + \frac{2\alpha\lambda}{\xi-a}$$

$$= -2\alpha\left[\frac{\alpha\xi}{2} + \frac{a\alpha}{2} + \eta - \alpha\xi\right] + \frac{2\alpha\lambda}{\xi-a}$$

$$= \alpha^2(\xi-a) - 2\alpha\eta + \frac{2\alpha\lambda}{\xi-a} \qquad (4.4.2)$$

and

$$-\frac{2\beta}{b-\xi}\int_{\xi}^{b}[\beta x+\eta-\beta\xi-f(x)]dx$$

$$= \frac{-2\beta}{b-\xi}\left[\frac{\beta}{2}(b^2-\xi^2) + (\eta-\beta\xi)(b-\xi)\right] + \frac{2\beta[A-\lambda]}{b-\xi}$$

$$= -2\beta\left[\frac{b\beta}{2} + \frac{\beta\xi}{2} + \eta - \beta\xi\right] + \frac{2\beta(A-\lambda)}{b-\xi}$$

$$= -\beta^2(b-\xi) - 2\beta\eta + \frac{2\beta(A-\lambda)}{b-\xi} \qquad (4.4.3)$$

and

$$-\frac{1}{(\xi-a)^2}\int_a^{\xi}[\alpha x+\eta-\alpha\xi-f(x)]^2dx$$

$$= -\frac{1}{(\xi-a)^2}\left[\frac{\alpha^2}{3}(\xi^3-a^3) + (\eta-\alpha\xi)^2(\xi-a) + \nu + \alpha(\eta-\alpha\xi)(\xi^2-a^2)\right.$$
$$\left. - 2\alpha\mu - 2(\eta-\alpha\xi)\lambda\right]$$

$$= -\frac{1}{\xi-a}\left[\frac{\alpha^3}{3}(\xi^2+a\xi+a^2) + (\eta-\alpha\xi)^2 + \alpha(\eta-\alpha\xi)(\xi+a)\right]$$

$$= -\frac{1}{(\xi-a)^2}[\nu-2\alpha\mu-2(\eta-\alpha\xi)\lambda]$$

$$= -\frac{1}{\xi-a}\left[\frac{\alpha^2\xi^2}{3} + \frac{a\alpha\xi}{3} + \frac{a^2\alpha^2}{3} + \eta^2 - 2\alpha\eta\xi + \alpha^2\xi^2 + \alpha\eta\xi + a\alpha\eta\right.$$
$$\left. - \alpha^2\xi^2 - a\alpha^2\xi\right] - \frac{1}{(\xi-a)^2}[\nu - 2\alpha\mu - 2(\eta-\alpha\xi)\lambda]$$

$$= -\frac{1}{\xi-a}\left[\frac{\alpha^2}{3}(\xi^2-2a\xi+a^2) + \eta^2 - \alpha\eta(\xi-a)\right]$$
$$- \frac{1}{(\xi-a)^2}[\nu - 2\alpha\mu - 2(\eta-\alpha\xi)\lambda]$$

$$= -\frac{\alpha^2}{3}(\xi-a) - \frac{\eta^2}{\xi-a} + \alpha\eta - \frac{1}{(\xi-a)^2}[\nu - 2\alpha\mu - 2\lambda(\eta-\alpha\xi)] \quad (4.4.4)$$

and

$$\frac{1}{(b-\xi)^2}\int_{\xi}^{b}[\beta x+\eta-\beta\xi-f(x)]^2dx$$

$$= \frac{1}{(b-\xi)^2}\left[\frac{\beta^2}{3}(b^3-\xi^3) + (\eta-\beta\xi)^2(b-\xi) + c-\nu + \beta(\eta-\beta\xi)(b^2-\xi^2)\right.$$
$$\left. - 2\beta(\beta-\mu) - 2(\eta-\beta\xi)(A-\lambda)\right]$$

$$= \frac{1}{(b-\xi)}\left[\frac{\beta^2}{3}(b^2+b\xi+\xi^2) + (\eta-\beta\xi)^2 + \beta(\eta-\beta\xi)(b+\xi)\right]$$
$$+ \frac{1}{(b-\xi)^2}[c - \nu - 2\beta(\beta-\mu) - 2(\eta-\beta\xi)(A-\lambda)]$$

$$= \frac{1}{(b-\xi)}\left[\frac{b^2\beta^2}{3} + \frac{b\beta^2\xi}{3} + \frac{\beta^2\xi^2}{3} + \eta^2 - 2\beta\eta\xi + \beta^2\xi^2 + b\beta\eta\right.$$
$$\left. + \beta\eta\xi - b\beta^2\xi - \beta^2\xi^2\right] + \frac{1}{(b-\xi)^2}[c - \nu - 2\beta(\beta-\mu)$$
$$- 2(\eta-\beta\xi)(A-\lambda)]$$

$$= \frac{1}{(b-\xi)}\left[\frac{\beta^2}{3}(b^2-2b\xi+\xi^2) + \eta^2 + \beta\eta(b-\xi)\right] + \frac{1}{(b-\xi)^2}[c - \nu$$
$$- 2\beta(\beta-\mu) - 2(\eta-\beta\xi)(A-\lambda)]$$

$$= \frac{\beta^2}{3}(b-\xi) + \frac{\eta^2}{b-\xi} + \beta\eta + \frac{1}{(b-\xi)^2}[c - \nu - 2\beta(\beta-\mu)$$
$$- 2(\eta-\beta\xi)(A-\lambda)] \quad (4.4.5)$$

where

$$\nu = \nu(\xi) = \int_a^{\xi}[f(x)]^2dx \quad (4.4.6)$$

$$c = \nu(b) = \int_a^{b}[f(x)]^2dx \quad (4.4.7)$$

Hence

$$\frac{\partial}{2\xi}I(\alpha,\beta,\eta,\xi) = \alpha^2(\xi-a) - 2\alpha\eta + \frac{2\alpha\lambda}{\xi-a} + [\eta-f(\xi)]^2\left[\frac{1}{\xi-a} - \frac{1}{b-\xi}\right]$$

$$- \beta^2(b-\xi) - 2\beta\eta + \frac{2\beta(A-\lambda)}{b-\xi} - \frac{\alpha^2}{3}(\xi-a) - \frac{\eta^2}{\xi-a}$$

$$+ \alpha\eta - \frac{1}{(\xi-a)^2}[\nu - 2\alpha\mu - 2\lambda(\eta-\alpha\xi)] + \frac{\beta^2}{3}(b-\xi)$$

$$+ \frac{\eta^2}{b-\xi} + \beta\eta + \frac{1}{(b-\xi)^2}[c - \nu - 2\beta(\beta-\mu)$$

$$- 2(\eta-\beta\xi)(A-\lambda)]$$

$$= \frac{2}{3}[\alpha^2(\xi-a) - \beta^2(b-\xi)] - (\alpha+\beta)\eta + \{[f(\xi)]^2$$

$$- 2\eta f(\xi)\}\left[\frac{1}{\xi-a} - \frac{1}{b-\xi}\right] + \frac{2\alpha\lambda}{\xi-a} + \frac{2\beta(A-\lambda)}{b-\xi}$$

$$- \frac{1}{(\xi-a)^2}[\nu - 2\alpha\mu - 2\lambda(\eta-\alpha\xi)]$$

$$+ \frac{1}{(b-\xi)^2}[c - \nu - 2\beta(\beta-\mu) - 2(\eta-\beta\xi)(A-\lambda)]$$

However

$$\frac{2}{3}[\alpha^2(\xi-a) - \beta^2(b-\xi)] - \eta(\alpha+\beta)$$

$$= \frac{2}{3}\left[\alpha\left(\frac{3\eta}{2} + \frac{3(\mu-\xi\lambda)}{(\xi-a)^2}\right) - \beta\left(-\frac{3\eta}{2} + \frac{3[(\beta-\mu) - \xi(A-\lambda)]}{(b-\xi)^2}\right)\right] - \eta(\alpha+\beta)$$

$$= \frac{2\alpha(\mu-\xi\lambda)}{(\xi-a)^2} - \frac{2\beta[(\beta-\mu) - \xi(A-\lambda)]}{(b-\xi)^2}$$

Thus

$$\frac{\partial}{\partial\xi}I(\alpha,\beta,\eta,\xi) = f(\xi)[f(\xi)-2\eta]\left[\frac{1}{\xi-a} - \frac{1}{b-\xi}\right] + \frac{1}{(\xi-a)^2}[2\alpha\mu-2\alpha\xi\lambda-\nu$$

$$+2\alpha\mu+2\eta\lambda-2\alpha\xi\lambda+2\alpha\xi\lambda-2\alpha\lambda a] + \frac{1}{(b-\xi)^2}[-2\beta(\beta-\mu)$$

$$+2\beta\xi(A-\lambda)+c-\nu-2\beta(\beta-\mu)-2\eta(A-\lambda)+2\beta\xi(A-\lambda)+2b\beta(A-\lambda)$$
$$-2\beta\xi(A-\lambda)]$$

$$= f(\xi)[f(\xi)-2\eta]\left[\frac{1}{\xi-a}-\frac{1}{b-\xi}\right]+\frac{1}{(\xi-a)^2}[2\alpha(2\mu-\xi\lambda-a\lambda)$$
$$-\nu+2\eta\lambda]+\frac{1}{(b-\xi)^2}[2\beta(-2[\beta-\mu]+\xi(A-\lambda)+b(A-\lambda)$$
$$+c-\nu-2\eta(A-\lambda)]$$

$$= f(\xi)[f(\xi)-2\eta]\left[\frac{1}{\xi-a}-\frac{1}{b-\xi}\right]+\frac{1}{(\xi-a)^2}\left\{2[2\mu-\lambda(a+\xi)]\right.$$
$$\left.\left[\frac{3\eta}{2(\xi-a)}+\frac{3(\mu-\xi\lambda)}{(\xi-a)^3}\right]-\nu+2\eta\lambda\right\}+\frac{1}{(b-\xi)^2}\left\{2[-2(\beta-\mu)\right.$$
$$\left.+(A-\lambda)(\xi+b)]\left[\frac{-3\eta}{2(b-\xi)}+\frac{3[(\beta-\mu)-\xi(A-\lambda)]}{(b-\xi)^3}\right]\right.$$
$$+c-\nu-2\eta(A-\lambda)$$

which in turn equals

$$\eta\left\{\frac{2f(\xi)}{\xi-a}+\frac{2\lambda}{(\xi-a)^2}+\frac{3[2\mu-\lambda(a+\xi)]}{(\xi-a)^3}+\frac{2f(\xi)}{(b-\xi)}-\frac{2(A-\lambda)}{(b-\xi)^2}\right.$$
$$\left.-\frac{3[-2(\beta-\mu)+(A-\lambda)(\xi+b)]}{(b-\xi)^3}\right\}+\frac{[f(\xi)]^2}{\xi-a}-\frac{\nu}{(\xi-a)^2}$$
$$+\frac{6(\mu-\xi\lambda)[2\mu-\lambda(a+\xi)]}{(\xi-a)^5}-\frac{[f(\xi)]^2}{b-\xi}+\frac{c-\nu}{(b-\xi)^2}$$
$$+\frac{6[(\beta-\mu)-\xi(A-\lambda)][-2(\beta-\mu)+(A-\lambda)(\xi+b)]}{(b-\xi)^5}$$

$$= \eta(\xi)\phi_1(\xi)+\phi_2(\xi)$$

Equation 4.10 is obtained by equating this partial derivative to zero:

$$\Lambda(\xi) = \eta(\xi)\phi_1(\xi)+\phi_2(\xi) = 0 \qquad (4.10)$$

CHAPTER FIVE

SECTION 5.1 - PROGRAM DESCRIPTION

A computer program, in the FORTRAN language, was developed to incorporate an algorithm, A1, described in Section 3.2 of this thesis, into a utility package suitable for the comprehensive automated analysis of the SBN_2 curve's characteristics.

The program has a modular structure which improves its clarity and simplifies modification of its code. It contains:

A1) The program's main algorithm which fits the experimental data to two lines. This algorithm calculates the slopes (α,β) of these lines and their point of intersection (ξ,η) in accordance with equations: 3.8,3.9,3.18,3.19,3.20.

A2) An algorithm which extracts the latter half of the expired vital capacity (VC_{EE}) and stores it for further use by A3.

A3) An algorithm which calculates the following subdivisions of lung volume: vital capacity (VC), inspired VC(VC_I), total lung capacity (TLC), and residual volume (RV). It also calculates: CV, closing capacity (CC) and the ratios: CC/TLC, CV/VC as well as the angle, Ψ, between the phase III and IV segments of the curve. In its calculations A3 applies A1 to the data file obtained from either A2 or A7.

A4) An algorithm which uses A1 to calculate the anatomical dead space ($V_{D_{anat}}$) from phase II of the SBN_2 curve.

A5) A routine which calculates the approximate flow-rate $\bar{V}$ throughout the expiratory phase of the SBN_2 manoeuvre. The program informs the user of peak, mean, and minimum flow rates, as well as noting any grossly non-uniform expiratory flow.

A6) A data screening sector to assess the technical quality of the data file should:

1) the expiratory volume differ from that inspired (i.e., $|VC_I - VC_I| - VC_E$) by more than 5%,

2) the expiratory flow rate, $\bar{V}$, (calculated disregarding the first 500 ml. of expirate) exceed 0.5 liter/sec., [~~149~~,8,80],

3) any expiratory flow transients exceeding 0.7 liter/sec. persist for more than 300 ml. of expiration.

Whenever a data file fails to meet these standardized criteria [151] further calculations are interrupted, a diagnostic message is printed, and the program transfers control to the user. In such a case, the user still has the option of forcing the program to continue the analysis of the rejected data file.

Section 5.2. Program Restraints

Under the program's restraints it will print an error message and automatically terminate further calculations on a data file when:

R1) the denominator of equation of 3.18 equals zero in the evaluation of $n(\xi)$;

R2) the difference between two consecutive values of $\xi(r)$ in equation 3.20 is less than the value specified by the parameter EPSILON 2;

R3) the denominator of the recursive formula employed in equation 3.20 equals zero;

R4) the program has failed (after the number of iterations specified by the parameter ITMAX) to find a value of $\xi(r)$ in equation 3.20 which reduces the value of $\phi(\xi)$ in equation 3.19 to less than that specified by the parameter EPSILON 1.

Furthermore, should the calculated slope of phase III exceed that estimated for phase IV (i.e., CI:$\beta>\alpha$) the program will print a diagnostic message and enter into a more complex iterative routine. This auxiliary routine , A7, continues to delete the initial 10% of the data analysed by the algorithm until it either calculates a satisfactory estimate of CV or it encounters a program restraint and terminates further calculations. The program will also enter this routine if it fails to detect the onset of phase IV (i.e., C2:$\beta=\alpha$). Under these two constraints (i.e., C1, C2), the algorithm may be successfully applied to data files which contain a markedly irregular alveolar plateau. However, when in this auxiliary routine, two further restraints (R5, R6) are required.

R5). the maximum number of iterative reductions of the data file specified by the parameter ITRUNK has been completed;

R6) it no longer contains the minimum number of points specified by the parameter INUM.

Section 5.3. Data Requests

During its interaction with the user the program requests:

D1) the machine temperature and barometric pressure under which the test was administered. (This permits the calculation of the BTPS lung volume correction factor) [5];

D2) the individual's age, height, and sex. (This permits the calculation of appropriate predicted values of the SBN_2 parameters from standard regression equations [15,65];

D3) the name of the data file which contains the sequentially acquired values of both lung volume and nitrogen concentration observed during the manoeuvre.

Section 5.4. Anatomical Dead Space

The amount of nitrogen expired ($V_{E_{N_2}}$) prior to the onset of phase III is the result of the changing mixture of alveolar and dead space gas observed during the early expiratory phases of the SBN_2 test, [11,46,24]. In theory this amount of nitrogen has been expired with alveolar gas only. As such it is possible to calculate $V_{D_{anat}}$ from the model proposed by Aitken and Clark-Kennedy [2] in which the transition between alveolar and dead space gas concentrations is sharpened to a theoretically valid vertical boundary front. In their model, described in Figure 5.1, this boundary front is graphically constructed so as to maintain the

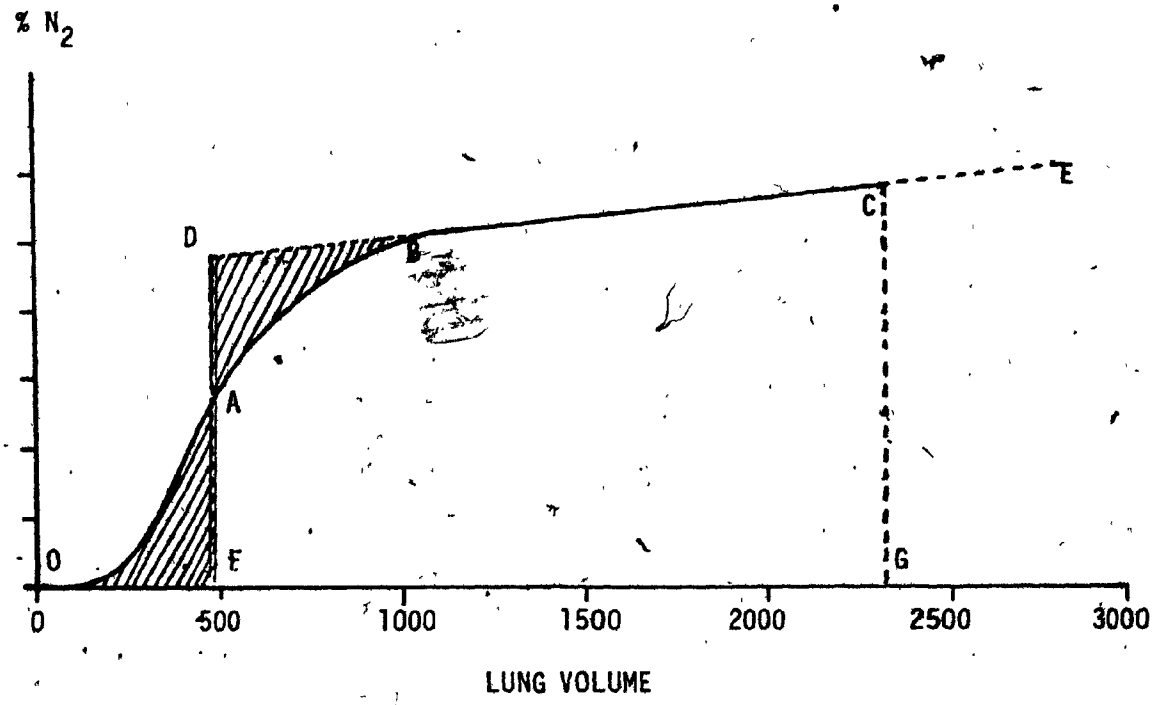

Figure 5.1. Diagram of the method used by Aitken and Clark-Kennedy to compute the lung's anatomical dead space from the single breath washout curve.

Abscissa: Expired volume.

Ordinate: CO_2 concentration (vol per cent) in expired air. The area under the experimental curve (OABCG) represents the amount of CO_2 expired during one expiration. If a perpendicular DF is drawn, so that area FDCG equals area OABCG, DF represents the volume of the dead space. From [11].

amount of N_2 expired during phase II. Once this theoretical boundary front has been constructed, the $V_{D_{anat}}$ is simply the volume expired up to that point. A4, the algorithm described in this subsection of the program, calculates $V_{D_{anat}}$ in accordance with the methodology described in Figure 5.1. It calculates the $V_{E_{N_2}}$ expired from TLC (the point Δ in Figure 5.1) to the onset of phase III (the point ∇ in Figure 5.1) as:

$$V_{E_{N_2}} \Big|_{\nabla}^{\Delta} = \int_{\nabla}^{\Delta} [N_2]dV = J \qquad (5.1)$$

A4 makes use of a six point Lagrange interpolator [52] to augment the quality of the numerical integral obtained from the Cote integration formula [52] used in our evaluation of equation 5.1.

This interpolation routine was required due to the technical characteristics of our data acquisition system in which the analogue to digital conversion of the experimental data occurs at a timed interval of 100 msec. As the result of the rapid concentration gradient observed through phase II, the system acquires sequential data points from that portion of the curve which exhibits large concentration increments.

Applying an integration routine directly to such data would needlessly introduce substantial error into our calculations. The Lagrange interpolater circumvents this problem by using our experimental data to estimate nitrogen concentration values throughout phase II at much finer decrements of lung volume than were recorded. The incremental

concentration differences are thereby reduced to a point where the Cote's integration routine may be accurately applied to such a preprocessed data segment. Having calculated the value of J, A4 proceeds to calculate the slope (m) and y-intercept (e) of a straight line fitted to that part of phase III contained within the first half of the VC_E. These coefficients are obtained by applying the program's main algorithm, A1, to the appropriate section of the VC_E data file. For our purposes, that section was taken to contain the lung volume and concentration data from that part of the first half of the VC_E in which the nitrogen concentration exceeded 5%. The predicted nitrogen concentration $[\hat{N}_2]$ during the initial portion of phase III may then be calculated as:

$$[\hat{N}_2] = mV + e \qquad (5.2)$$

Our method then proceeds to extrapolate the line of fit drawn through the initial portion of phase III in Figure 5.1 beyond its junction at point Θ with phase II to some point . This point Θ is determined so that the area contained under the extrapolated portion of this line equals the value of J obtained from equation 5.1. Explicitly integrating equation 5.2 to obtain the area under the extrapolated portion of this line as:

$$\int_{\Theta}^{\nabla} [\hat{N}_2]dV = \frac{mV^2}{2}\Bigg|_{\Theta}^{\nabla} + (\Theta - \nabla)me \qquad (5.3)$$

and equating it to the value of J. The algorithm determines the point Θ as:

$$\Theta = -\sqrt{m \pm m^2 + 4\,(2J/m + \nabla^2 - 2e\nabla)} \qquad (5.4)$$

where $\Theta > 0$, $V_{D_{anat}} = \nabla$ ~~Θ~~.

Section 5.5. Calculations: Closing Volume Determination

CV is determined by applying the non-linear least squares procedure, encoded in A1 and described in Section 3.2 of this thesis, to the latter half of VC_E. The structure of the algorithm that we developed to implement this procedure is shown in Figure 5.2. This algorithm is incorporated into the overall program structure outlined in Figure 5.3 in accordance with the constraints and restraints we have just outlined. Figure 5.4 describes the rules which control the operation of the arithmetic algorithm, A1.

Under most circumstances CV, α, β, and the angle ψ are determined by the application of A1 to the data file obtained from A2 under restraints R1, R2, R3 and R4. However under certain conditions, specified by the constraints C1 and C2, the closing volume parameters are determined by the application of A1 to the data file produced by A7 until either an acceptable result is obtained or the data is rejected on other grounds (i.e., R1, R2, R3, R4, R5, R6).

In any case, the angle ψ is determined as the supplement of the acute angle Ω where:

$$\tan(\Omega) = \frac{\alpha - \beta}{1 + \alpha\beta} \qquad (5.5)$$

given that $(\alpha - \beta) \neq 0 \neq (1 + \alpha\beta)$.

LEAF 97 OMITTED IN PAGE NUMBERING

CONDITION STUBS													
$\phi < \varepsilon$ 1	Y	N	N	-	-	Y	N	N	N	N	N	N	N
ITER > 2	-	-	-	-	-	Y	-	Y	-	-	N	Y	Y
$[\phi(N) - \phi(N-1)] = 0$	Y	N	N	-	N	N	Y	N	N	N	-	N	N
$[\xi(N)-\xi(N-1)] \leq 2$	Y	N	N	-	N	N	-	N	Y	N	-	N	N
ITER > ITMAX	Y	Y	Y	-	N	N	-	N	-	Y	-	N	Y
$\beta > \alpha$	-	-	-	Y	Y	N	-	N	-	-	-	Y	N
IRID > ITRUNK	Y	Y	N	-	N	N	-	N	-	-	-	Y	Y
N ≤ INUM	Y	-	N	-	N	N	-	N	-	-	-	-	Y

ACTION STUBS													
Print "ITMAX EXCEEDED"	●	●	●					●					
Print "[ϕ(N) - ϕ(N-1)] = 0"						●							
Print "NO SIGNIFICANT VARIATION IN ξ (N)"									●				
Print "WITHIN SPECIAL ROUTINES (C1 or C2)"	●	●									●	●	
Print "NUMBER OF TRUNCATIONS EXCEEDED"		●									●		
Print "NUMBER OF POINTS INSUFFICIENT"	●											●	
Print "BETA > ALPHA"	●		●										
Print "ENTERING SPECIAL ROUTINE, $\phi < \varepsilon$ 1"	●	●	●										
Calculate ξ(ITER + 1)-ξ(ITER) + Y *										●			
Calculate EQUATION 20							●	●	●				
ITER = ITER + 1							●			●			
GOTO	●	●			●	●		●	●		●	●	
RETURN TO TABLE 1 (CALCULATE A + B)			●	●			●			●			
DELETE INITIAL 10% OF DATA FILE			●	●									
PRINT RESULTS (IN REPORT FORM)					●								

Figure 5.2. Decision table illustrating the logic of the overall implementation of the non-linear least squares method for the analysis of the SBN_2 data.

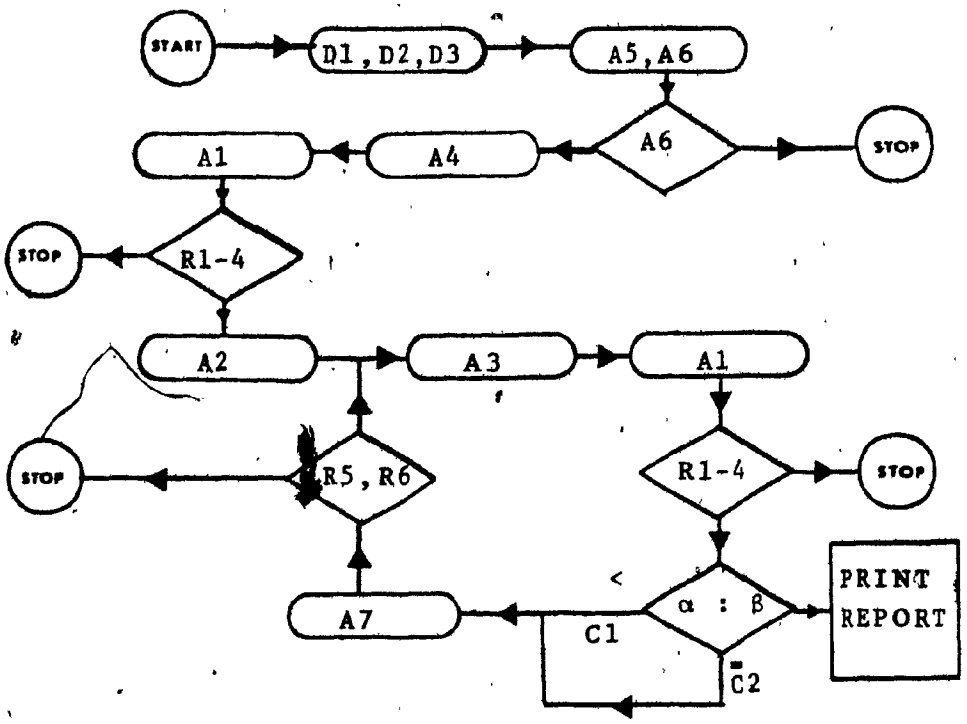

Figure 5.3. Flowchart of the Program's Overall Structure.

CONDITION STUBS	RULES						
Start, I = N	N	N	N	N	N	Y	Y
T > 0	N	Y	Y	Y	Y	Y	N
T ≤ 0		N	N	N	N	N	Y
K = 0		Y	Y	N	N	N	N
K ≠ (N-1)		N	N	Y	Y	N	N
K = (N)		Y	N	Y	N	Y	–
ACTION STUBS							
I = I + 1	X						
T = (X(I) - (ITER))	X						
Return to start	X						
KPLUS1 = I		X	X	X	X	X	X
K = (I - 1)		X	X	X	X	X	X
K = I = N							X
Set: $Q^2=\alpha=\lambda=N=Q=0=\mu$		X	X				
Equations 3.14, 3.15		X	X		X		
Equation 3.18		X	X	X	X	X	X
Equation 3.19		X	X	X	X	X	X
Equation 3.9			X		X		
Equations 3.16,3.17,3.12,3.13				X	X	X	X
B(ξ) = R = T = 0				X		X	X
Equation 3.8				X	X	X	X

Figure 5.4. Decision Table Illustrating the Detailed Logic of the Program's Main Numerical Routine, A1.

The variable secant method [164] utilized in this procedure is initialized by assigning arbitrary values to $\xi(1)$ and $\xi(2)$ in equation 3.20.

Section 5.6. Program Calculations: Lung Volumes

The algorithm A3 searches the entire data file to find VC_E and VC_I. A3 then calculates the total $V_{E_{N_2}}$ as:

$$V_{E_{N_2}} = J + \int_{\nabla}^{RV} [N_2]dv \qquad (5.6)$$

The integral on the right hand side of equation 5.6 is evaluated as the simple sum of the incremental area calculated between consecutive data points from the onset of phase III to the end of phase IV. TLC may then be calculated [7] as:

$$TLC = \frac{VC_I \; F_{A_{N_2}} - V_{E_{N_2}} \left(\frac{V_D}{(VC_E - V_D)} \right)}{F_{A_{N_2}} \; \frac{V_{E_{N_2}}}{VC_E - V_D}} \qquad (5.7)$$

where $F_{A_{N_2}}$ is the alveolar nitrogen concentration.

In our computations $F_{A_{N_2}}$ is the arithmetic mean nitrogen concentration value calculated within the domain of lung volume specified from the onset of phase III to its end (i.e., from the points ∇ to ξ in Figure 5.1). RV is then calculated as the difference between TLC and VC_E. CC was calculated as the sum of CV and RV. All of the above lung volumes were then multiplied by the BTPS correction factor and the remaining lung volume ratios are then calculated.

CHAPTER SIX

The first six figures of this chapter are examples of single breath washout curves published in the literature.

Figures 6.1 [102], 6.2 [101] and 6.3 [99] are samples of tracings obtained using Zenon, Argon and Xenon gas washout.

These curves illustrate the wide range of shape and the effects of cardiogenic oscillations [54, 41] on the washout data. The effects of cardiac activity and airflow rate on these tracings may be more clearly seen in Figure 3.4 [51]. This study [51] simultaneously recorded airflow, gas concentration and the subject's electrocardiogram.

Figures 6.4 [34] and 6.5 [61] are tracings taken from the reports of other researchers who have attempted to develop computer programs for the automated analysis of closing volume. These two figures were published to illustrate the types of curves that were either poorly interpreted or misinterpreted by their programs.

The remaining thirty-seven figures in this chapter demonstrate the results of the discrete non-linear algorithm's analysis of 13 test cases. The raw data for these cases is presented as the first plate in each figure. The subsequent plates in each of these figures show the results of our analysis superimposed on various segments of the phase III - phase IV data. As we can see from these figures, the algorithm is capable of simultaneously fitting the phase III and phase IV portions of these curves in a way that closely matches the eye's ability

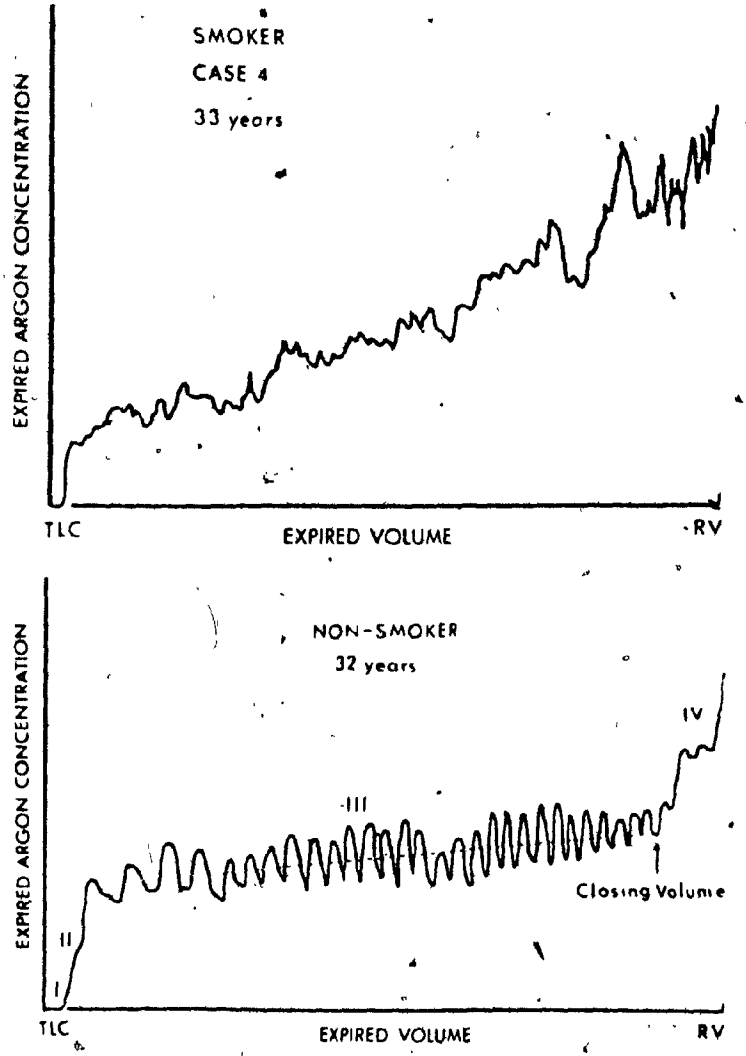

Figure 6.1. Top, relationship between Argon concentration in expired air and expired volume following an inspiratory vital capacity (VC) maneuver during which a bolus of Argon was inhaled at residual volume (RV), in a seated nonsmoker thirty-two years of age. The plateau (phase III) shows a small gradual rise with well marked cardiogenic oscillations followed by a steeper rise with reduced oscillations (phase IV). Arrow indicates "closing volume," which in this subject amounted to 9.6 per cent of his vital capacity. Bottom, as on top, in a seated smoker thirty-three years of age, in whom conventional lung function data disclosed abnormalities. Note that in this patient the slope of the "alveolar plateau" is very steep, indicating gross abnormalities of ventilation distribution. The "closing volume" in this subject could not be determined. From [102].

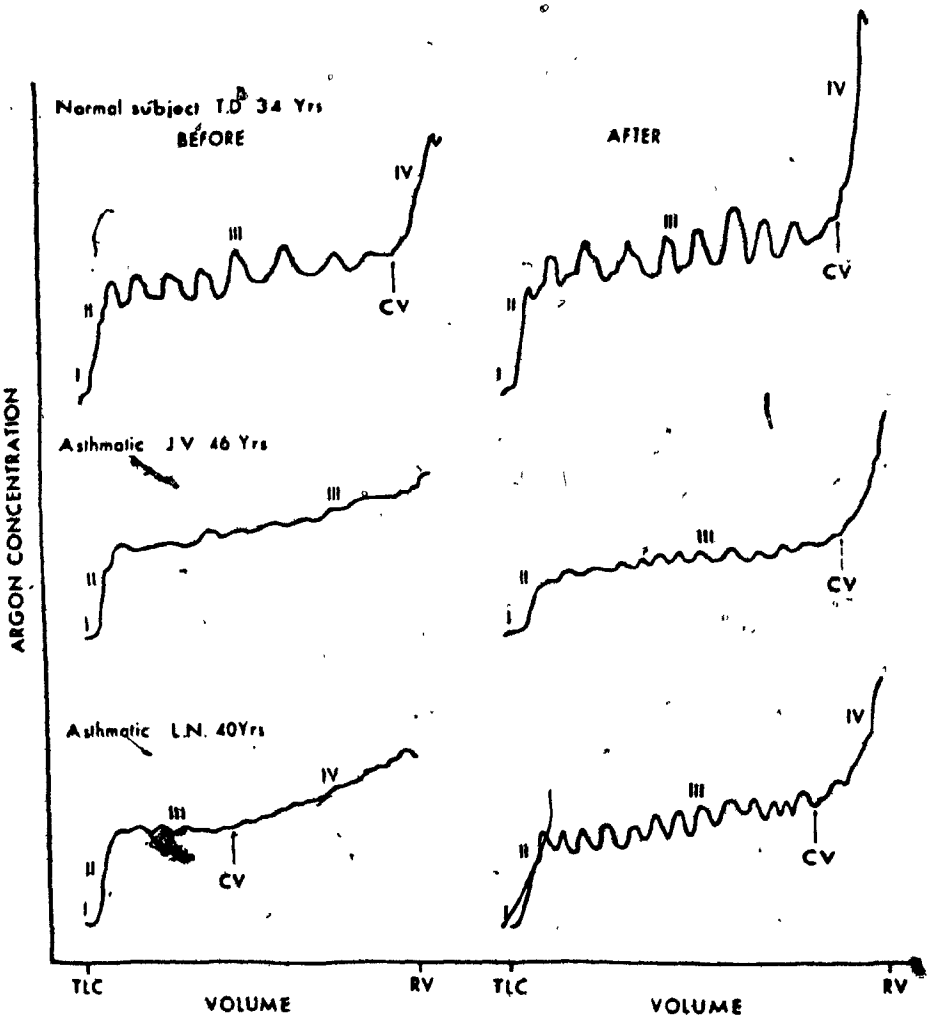

Figure 6.2. Relationship between argon concentration in expired air and expired volumes after an inspiratory maneuver during which a bolus of argon was inhaled at residual volume (RV). The upper left panel depicts the expired argon concentration record in a normal subject. Middle left panel is an example of a rising expired argon record. Lower left panel shows a quantitative abnormality, i.e., closing volume is occurring early in the expired vital capacity maneuver. The lower 2 panels on the right illustrate normalization of the traces after inhalation of aerosol isoproterenol. In the normal subject (upper right panel), isoproterenol produced accentuation of the cardiogenic oscillations and a steeper Phase IV. Arrows indicate beginning of closing volume (CV). From [101].

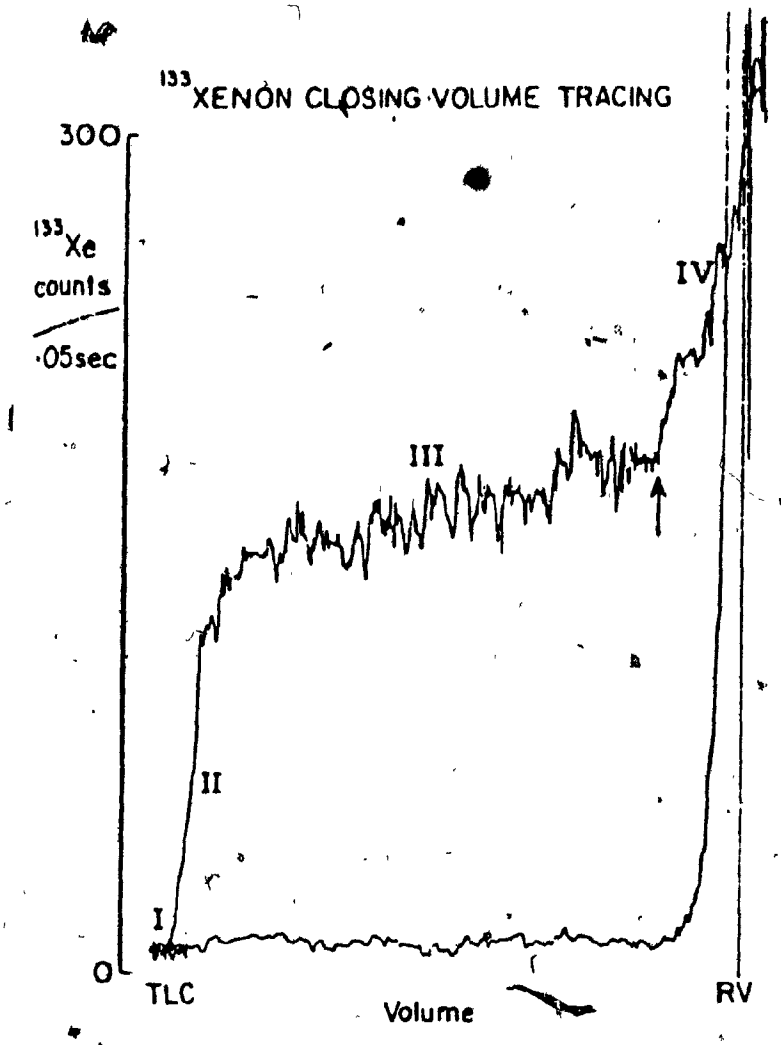

Figure 6.3. Volume is represented on the abscissa; from Residual Volume on the right side to Total Lung Capacity on the left side. On the ordinate, is Xenon concentration measured at the mouth. Also represented on that tracing are the four subdivisions or stages that occurred when Xenon was monitored at the mouth and plotted against simultaneously expired volume from Total Lung Capacity to residual volume. The arrow represents onset of Phase IV or the point of closing volume. From [99].

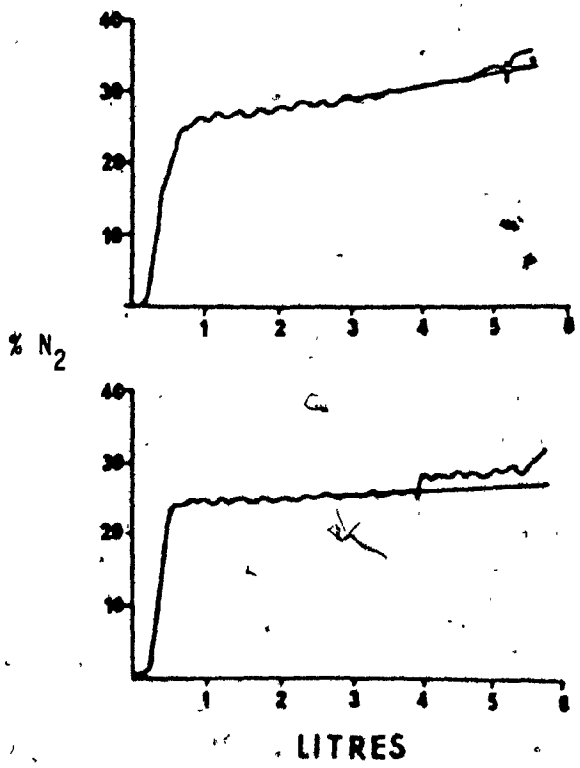

Figure 6.4. Examples of types of curves with which a computer program has difficulty. The dip in the N_2 concentration is interpreted as a cardiogenic and closing volume is underestimated. The step increase in N_2 concentration in the lower trace is interpreted incorrectly as the onset of closing volume. From [34].

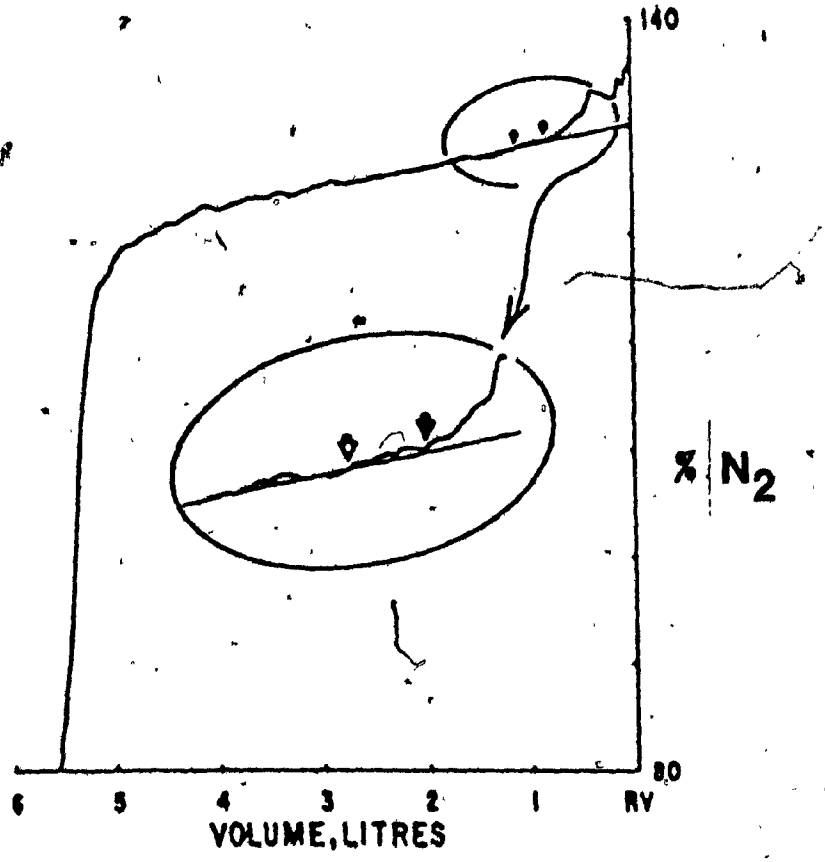

Figure 6.5. A Published Curve [61] Illustrating the Difficulty of Adequately Automating the Analysis of the SB Washout Procedure.

Portion of "closing volume" tracing. The final point of crossing of the data curve and the computer-fitted line is indicated by the light arrow. A more acceptable "point of departure" to the human eye is indicated by the dark arrow. From [61].

to determine their juncture. The algorithm successfully analyses cases similar to those previously considered intractable [61,34,169] for a machine. A detailed quantitative comparison of these results with a properly constructed double-blind manual analysis is underway [127]. While there is good qualitative agreement between the algorithm's performance and the visual analysis of these curves, there are many problems inherent in the quantitative analysis of these results. These problems will be discussed in detail in Chapter Seven of this thesis.

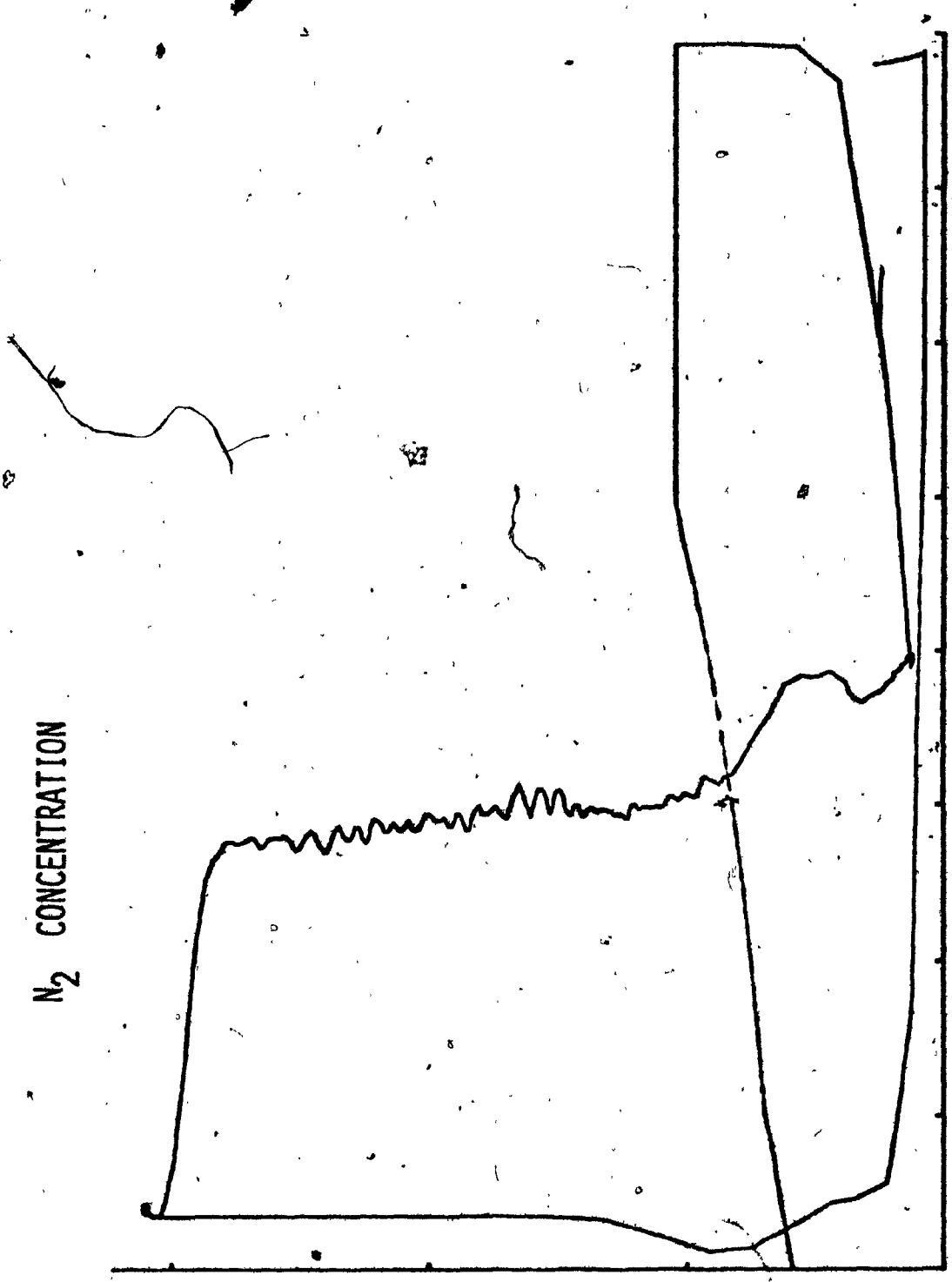

Figure 6.6a. Case 1. Raw Data.

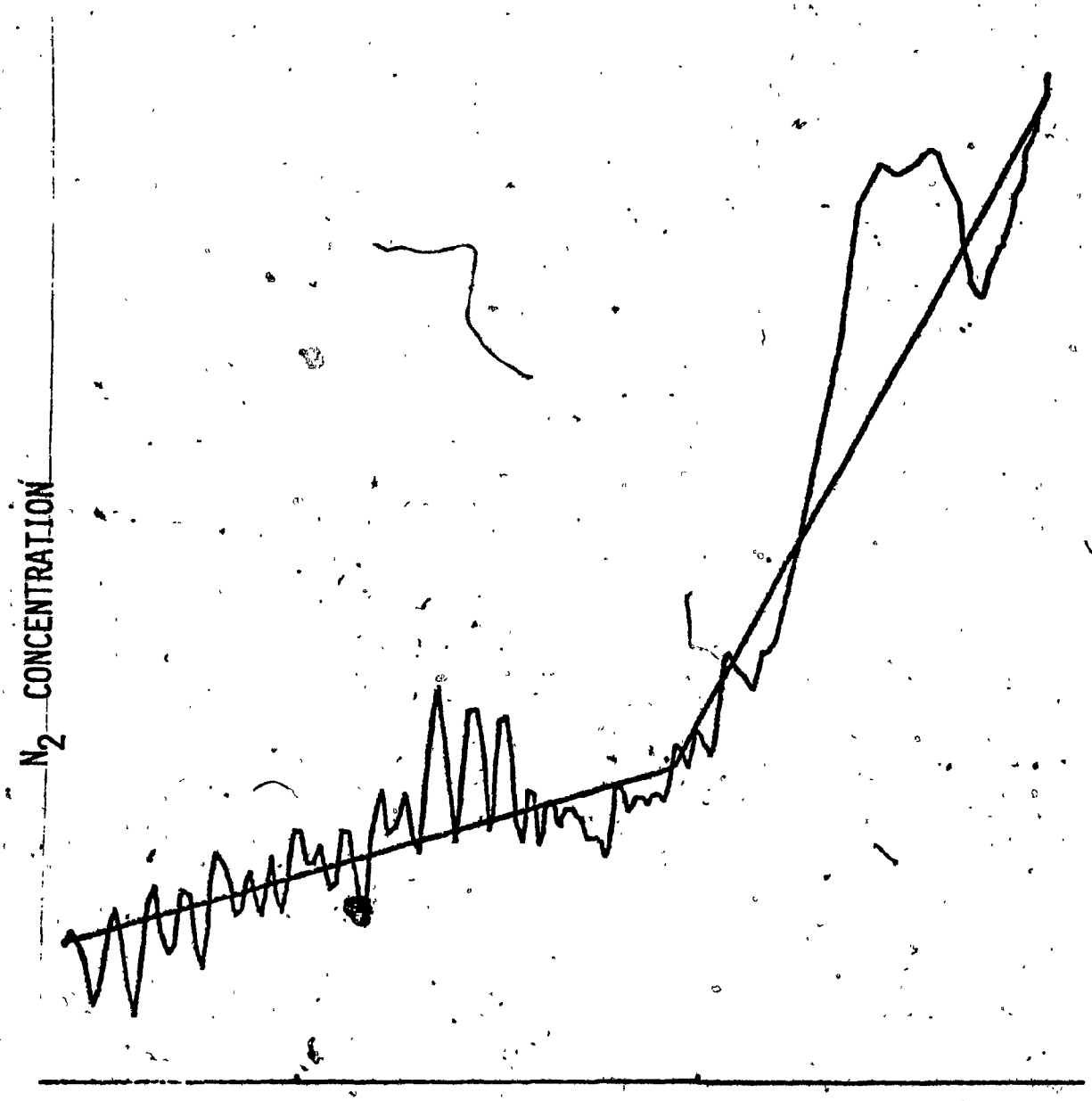

Figure 6.6b. Case 1. Analysis and Raw Data.

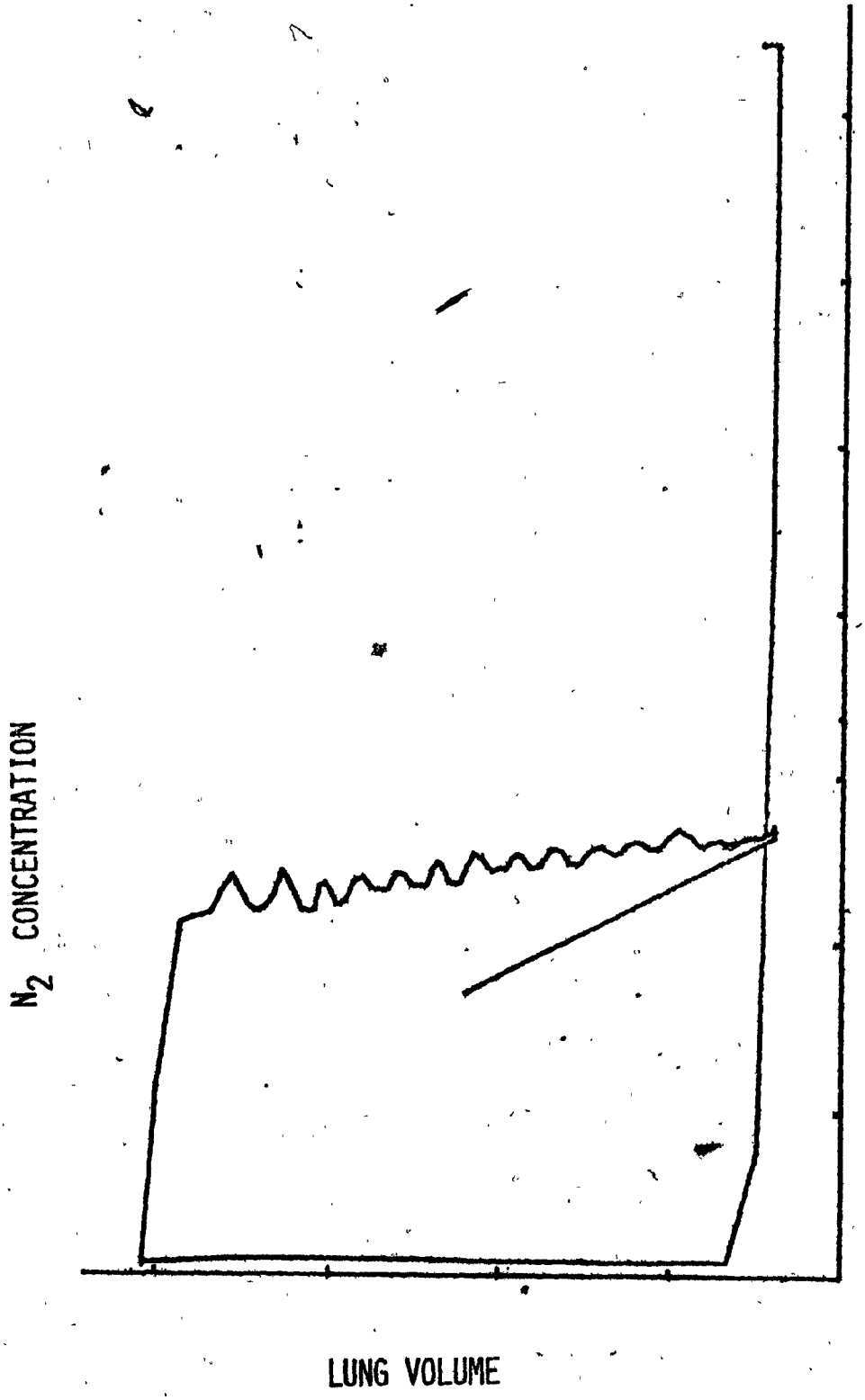

Figure 6.7a. Case 2. Raw Data.

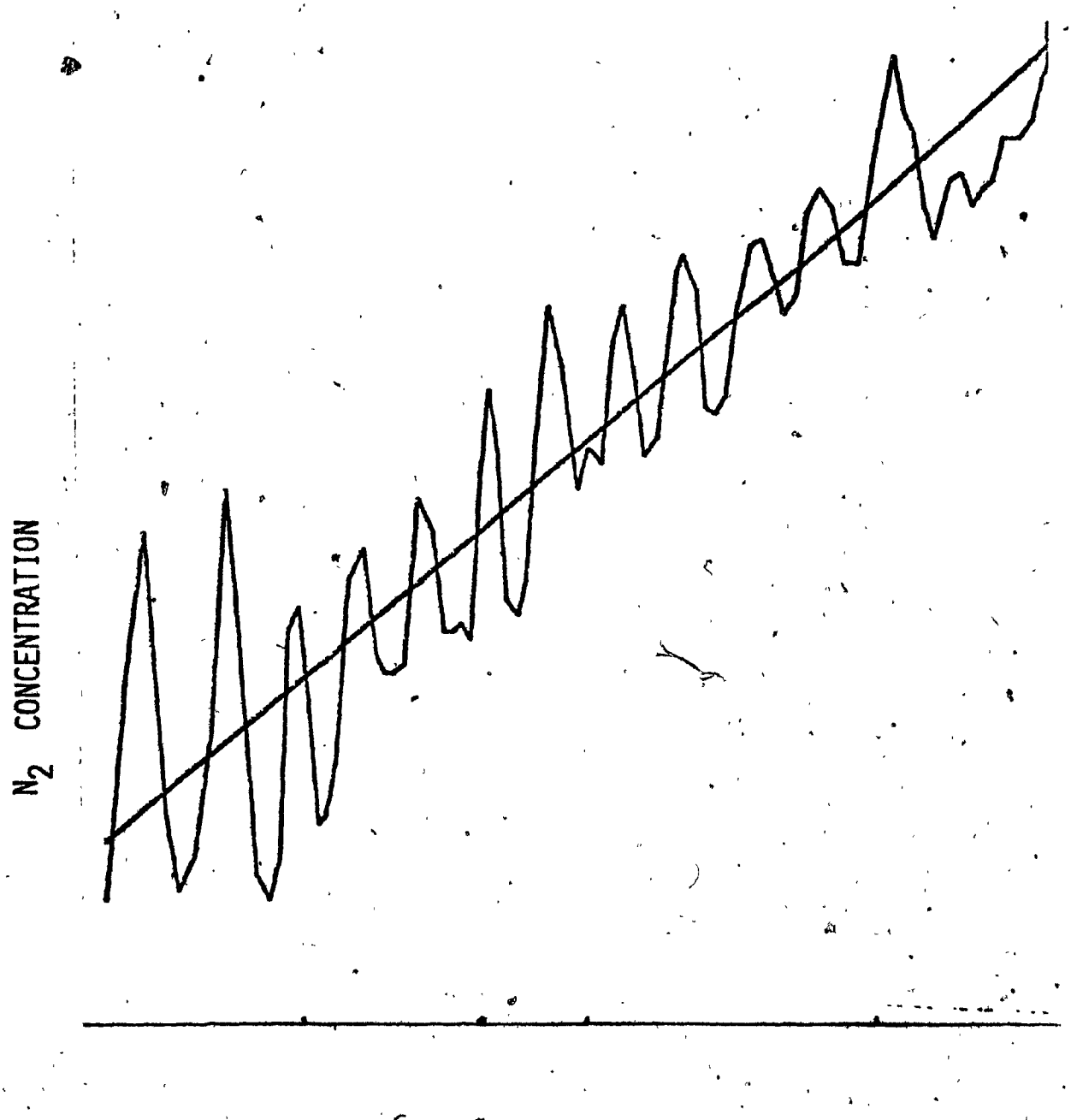

Figure 6.7b. Case 2. Analysis and Raw Data "Closing Volume" Not Found.

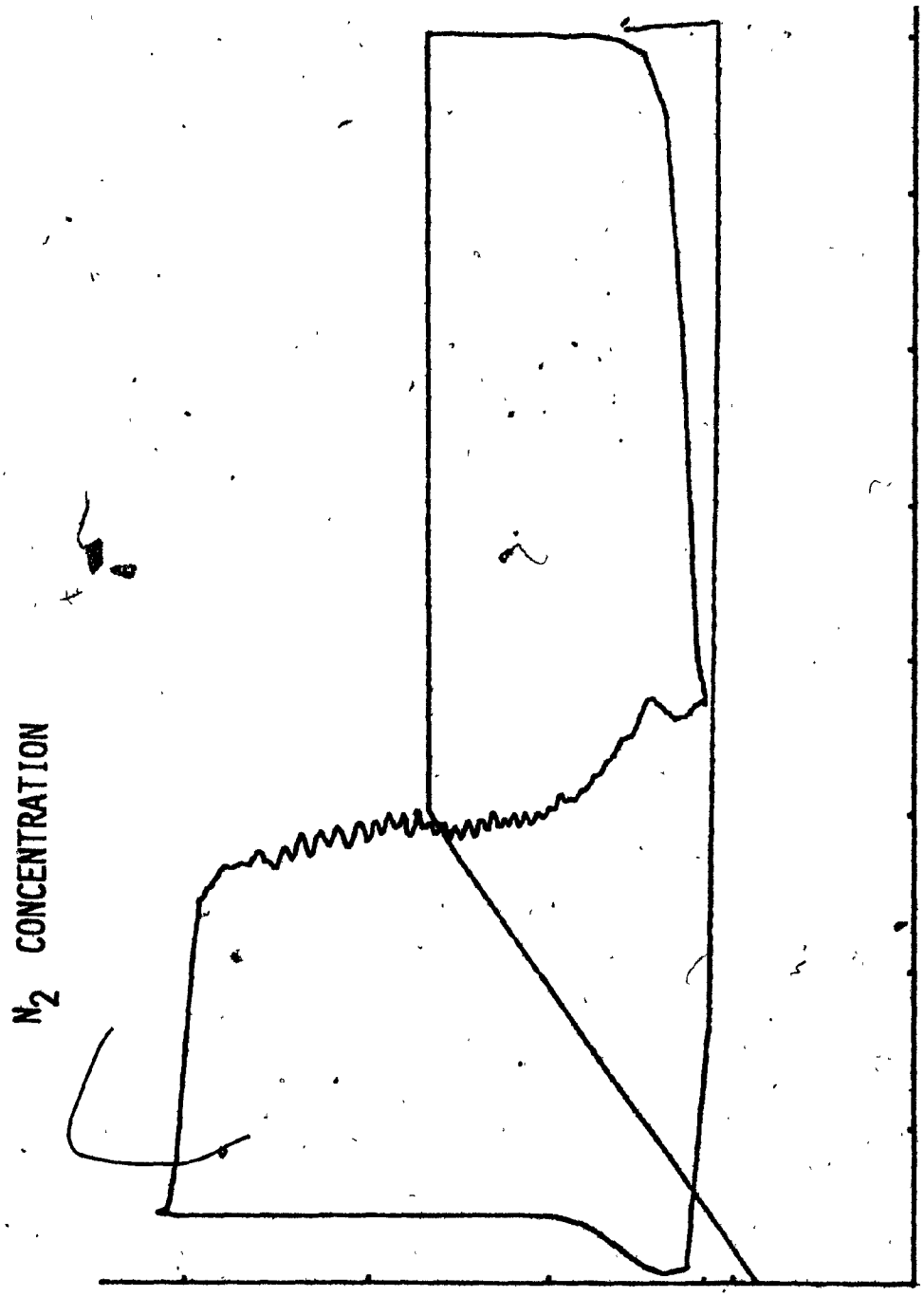

Figure 6.8a. Case 3. Raw Data.

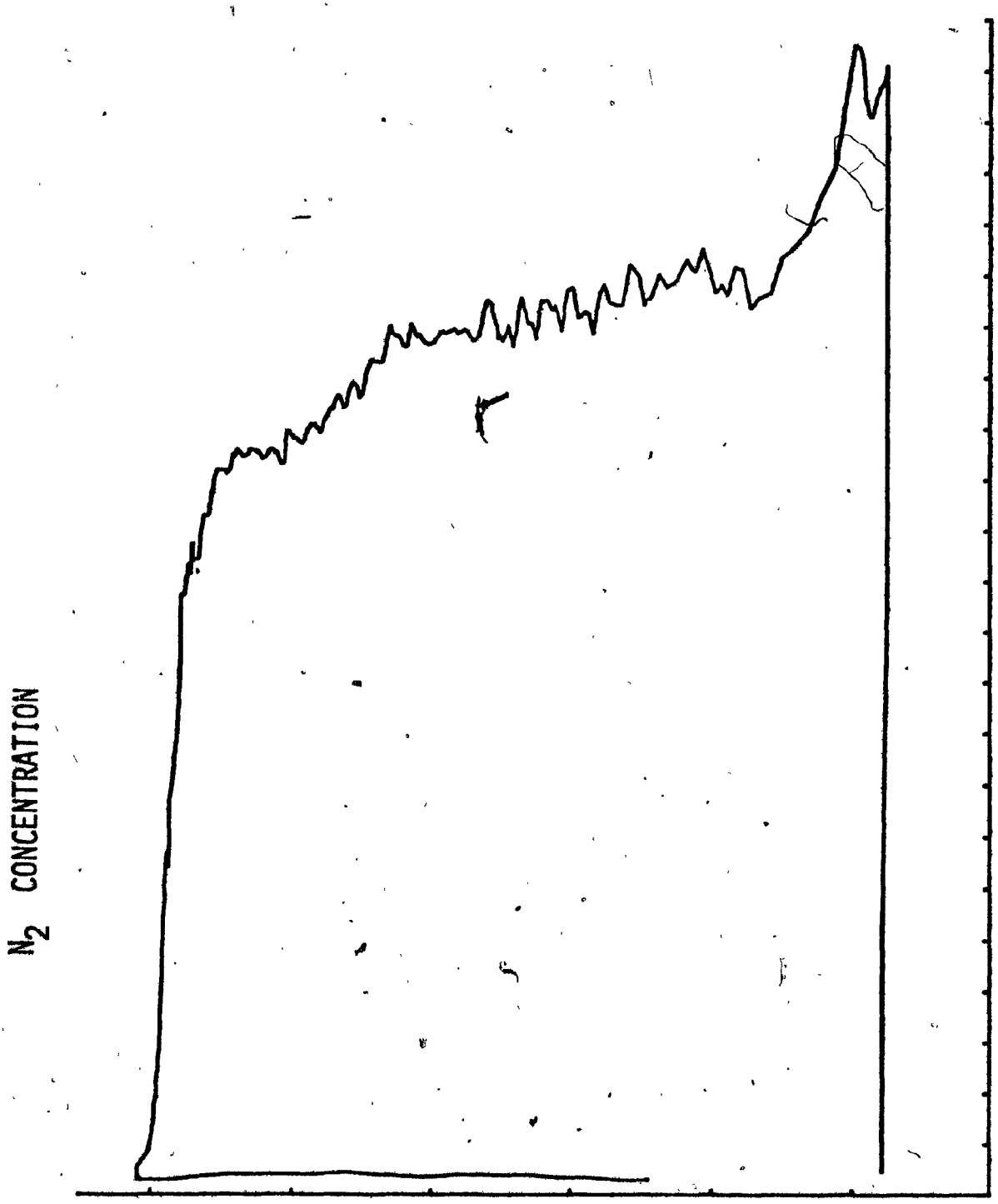

Figure 6.8b. Case 3. Magnified Raw Data.

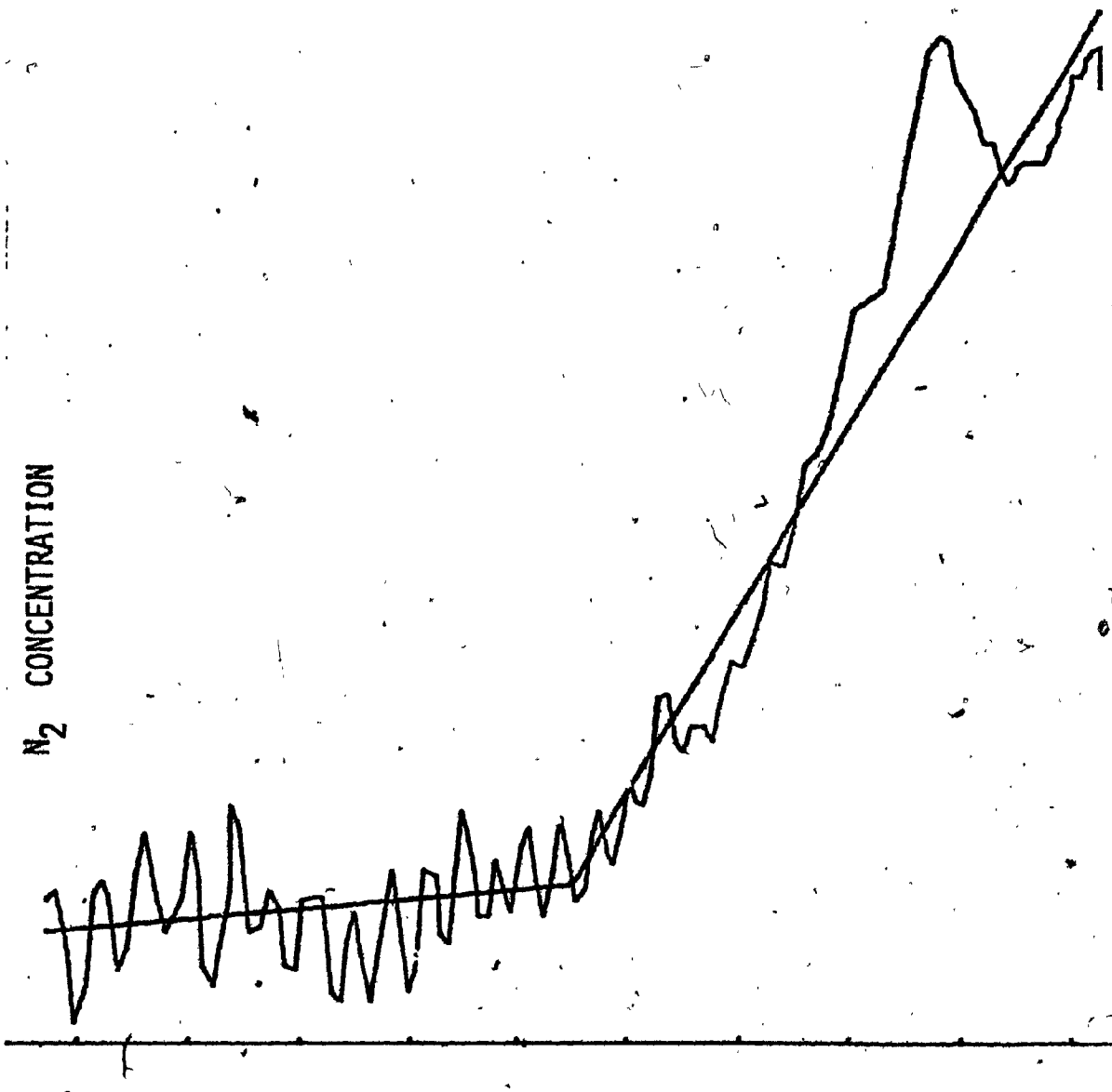

Figure 6.8c. Case 3: Raw Data and Analysis

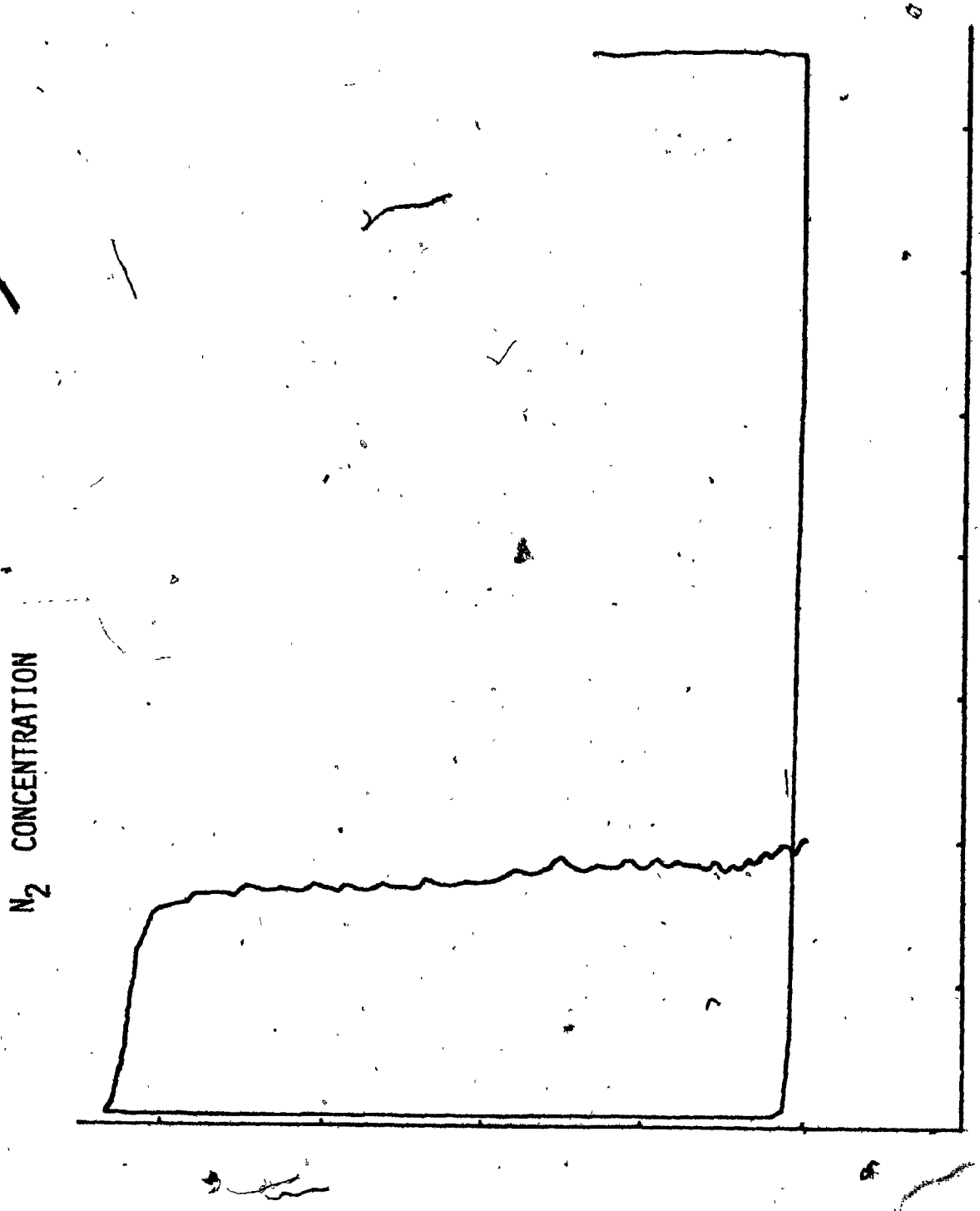

Figure 6.9a. Raw Data. Case 4.

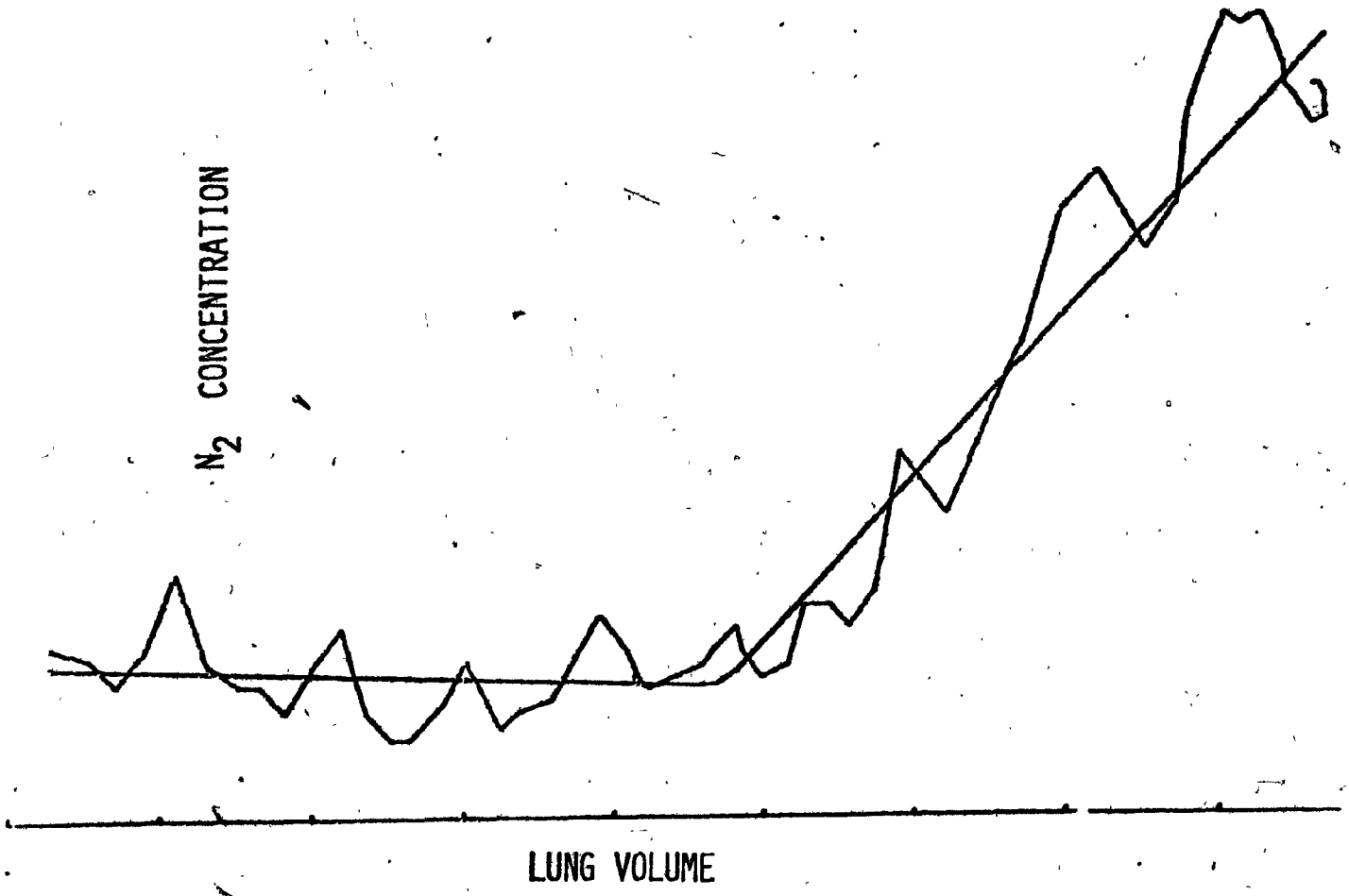

Figure 6.9b. Case 4. Raw Data and Analysis.

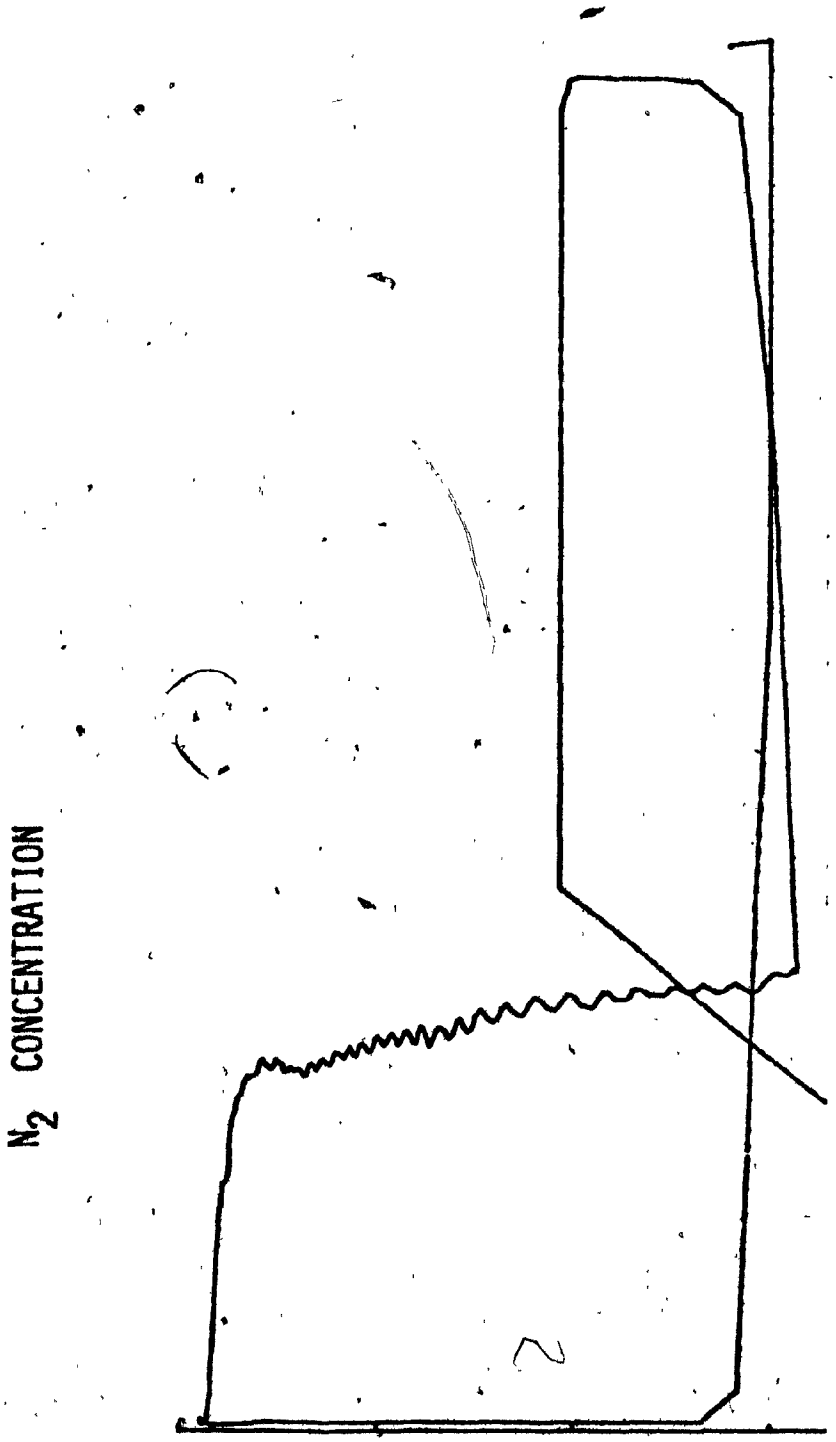

Figure 6.10a. Case 5. Raw Data.

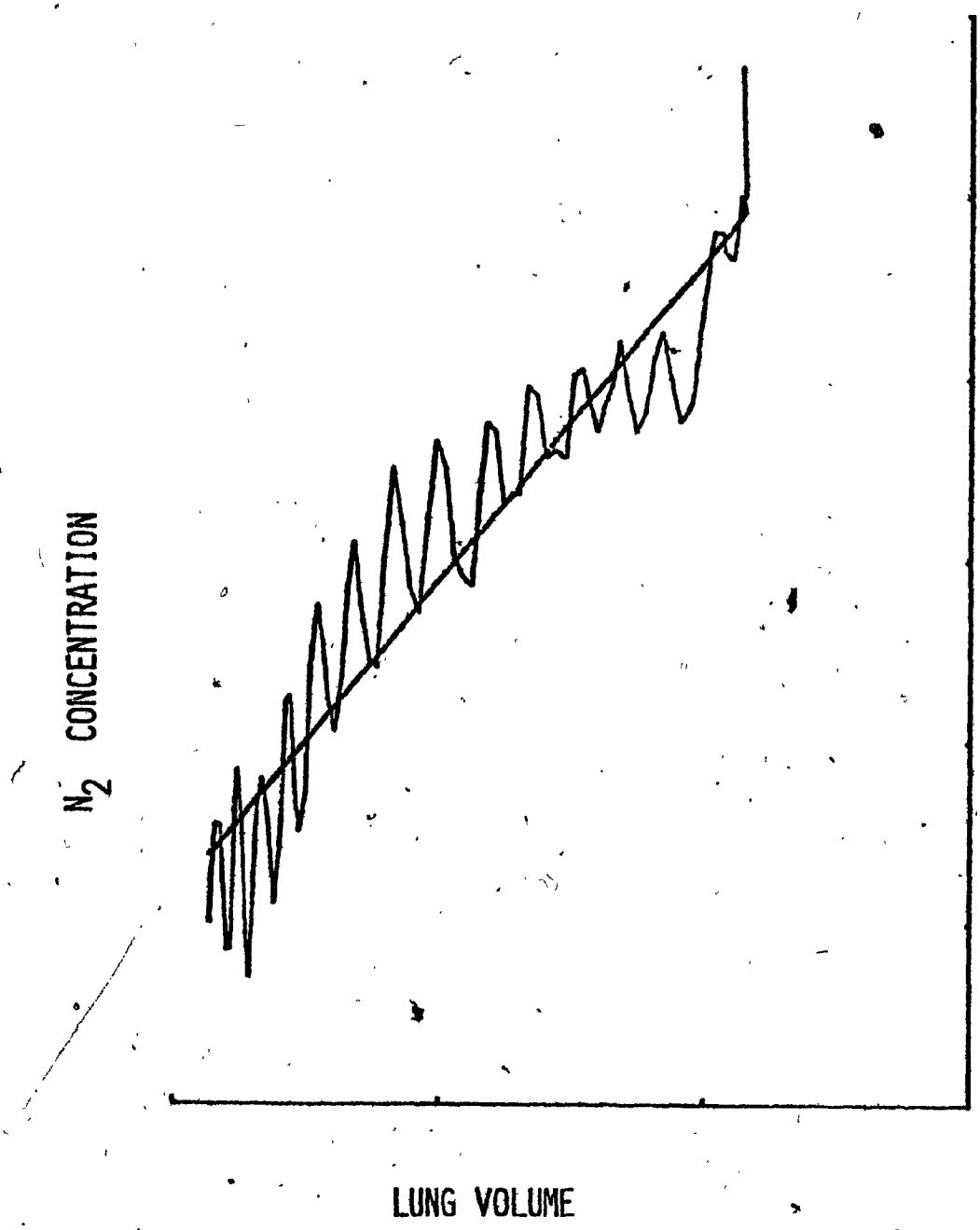

Figure 6.10b. Case 5. Raw Data and First Analysis Closing Volume Not Found.

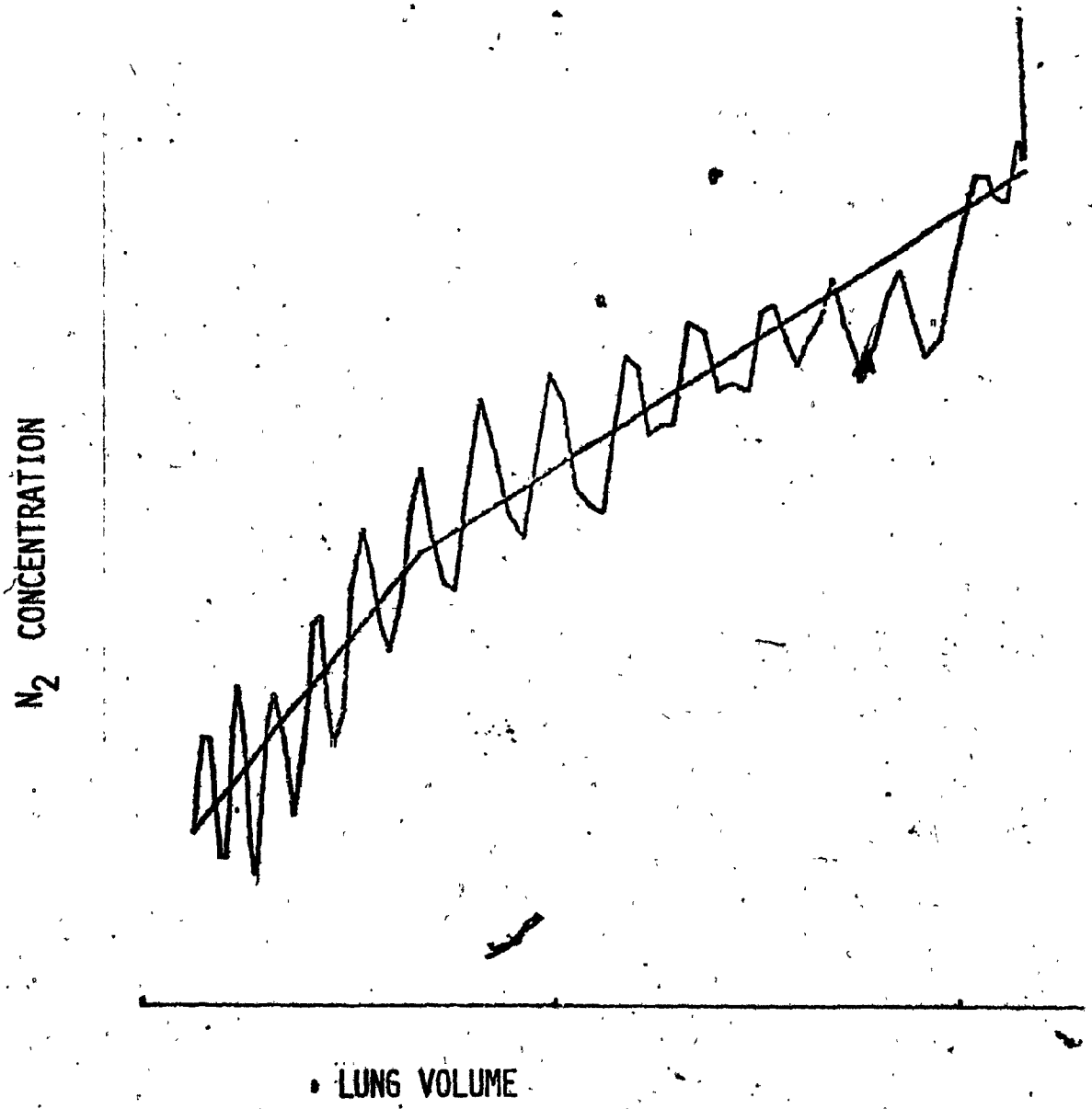

Figure 6.10c. Case 5. * Raw Data and Second Analysis Closing Volume Still Not Found.

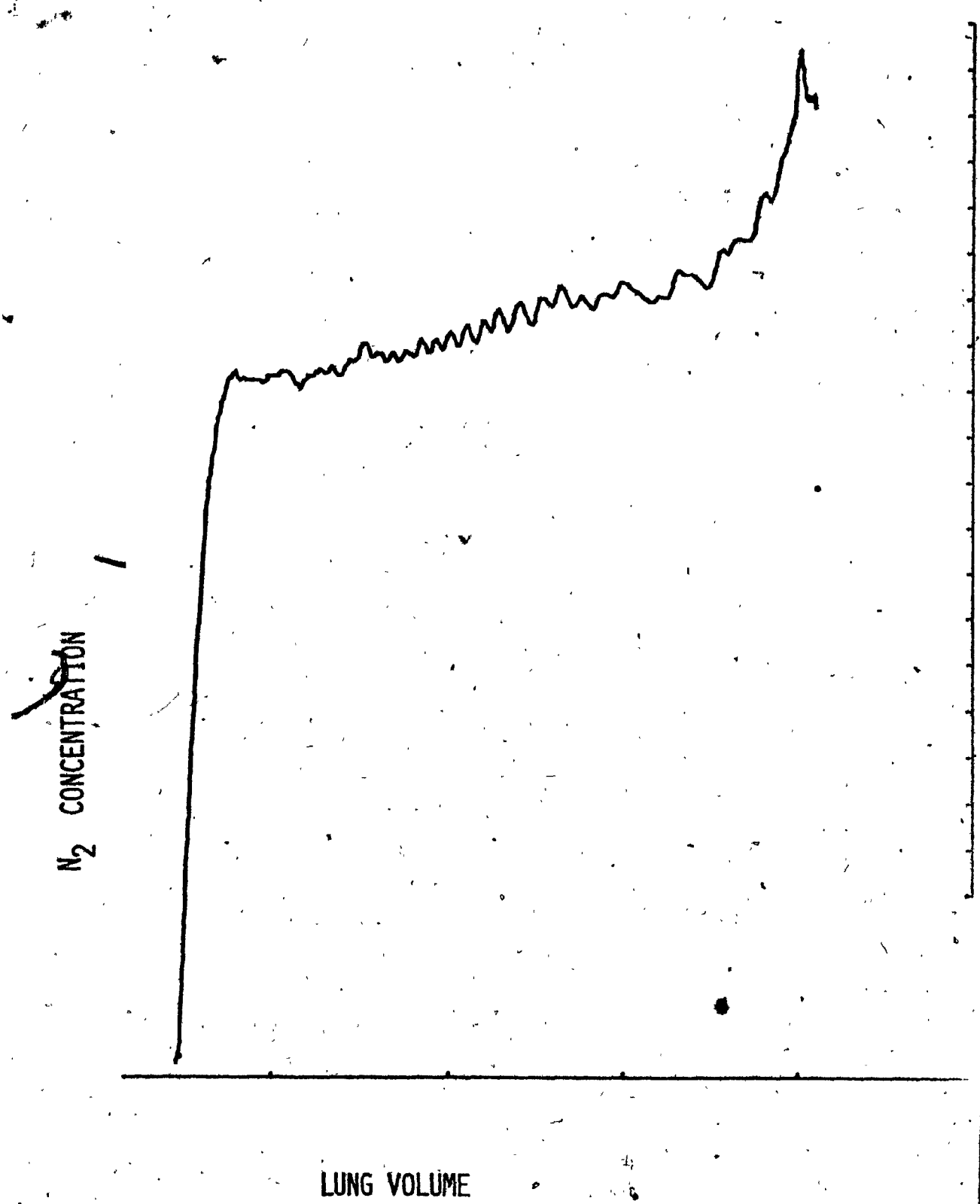

Figure 6.11a. Case 6. Raw Data.

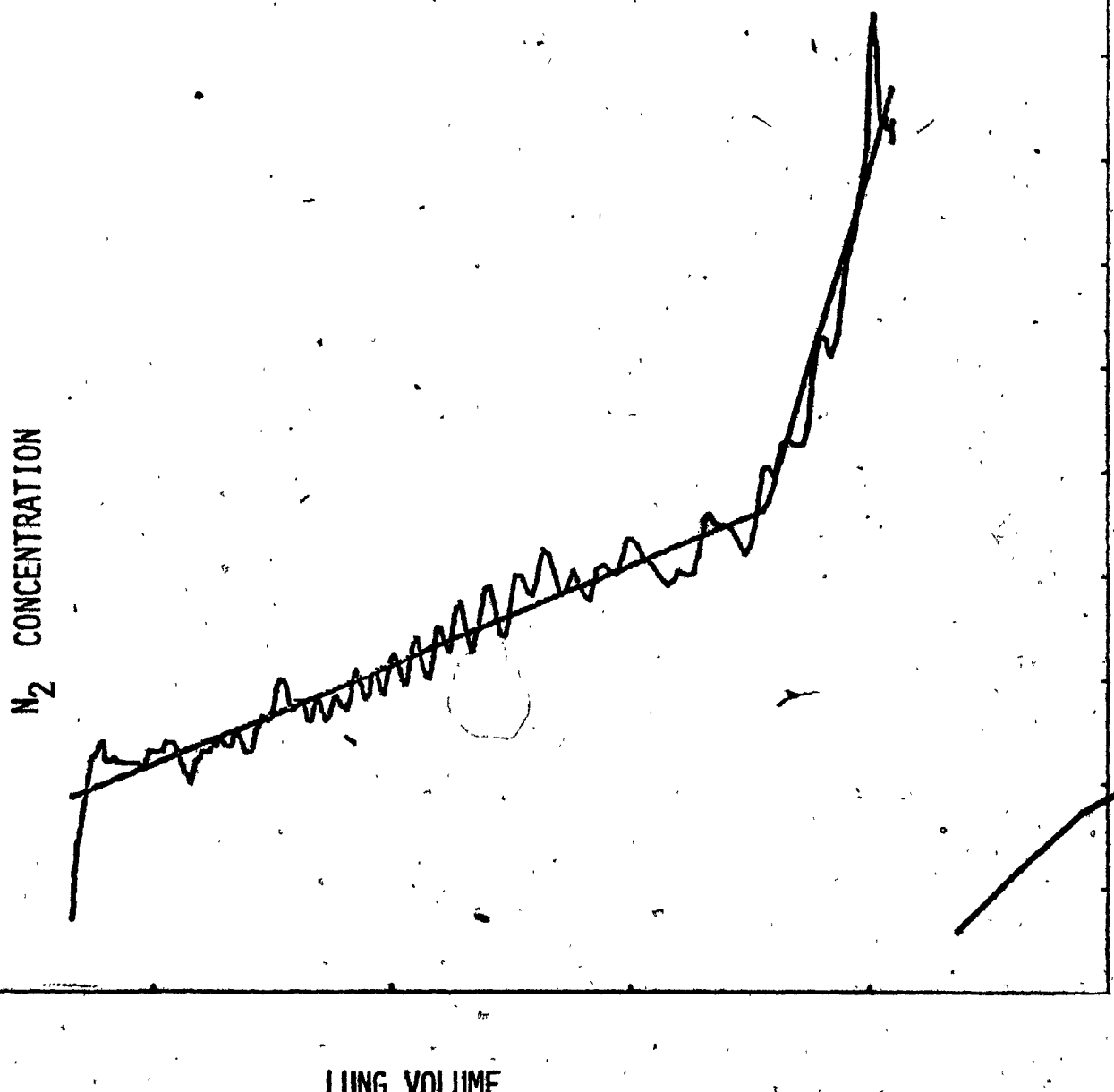

Figure 6.11b. Case 6. Raw Data and Analysis.

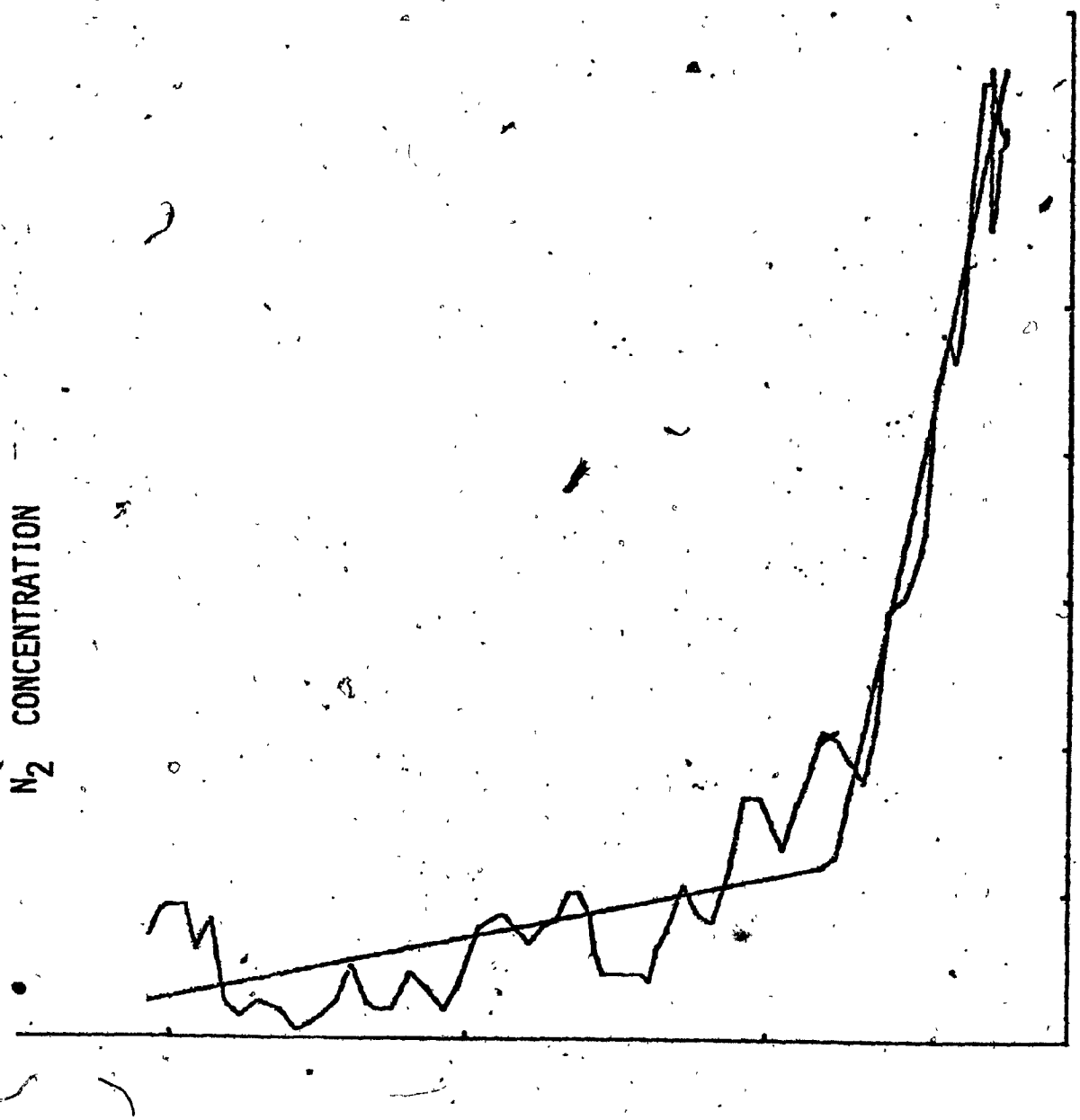

Figure 6.11c. Case 6. Raw Data and Second Analysis.

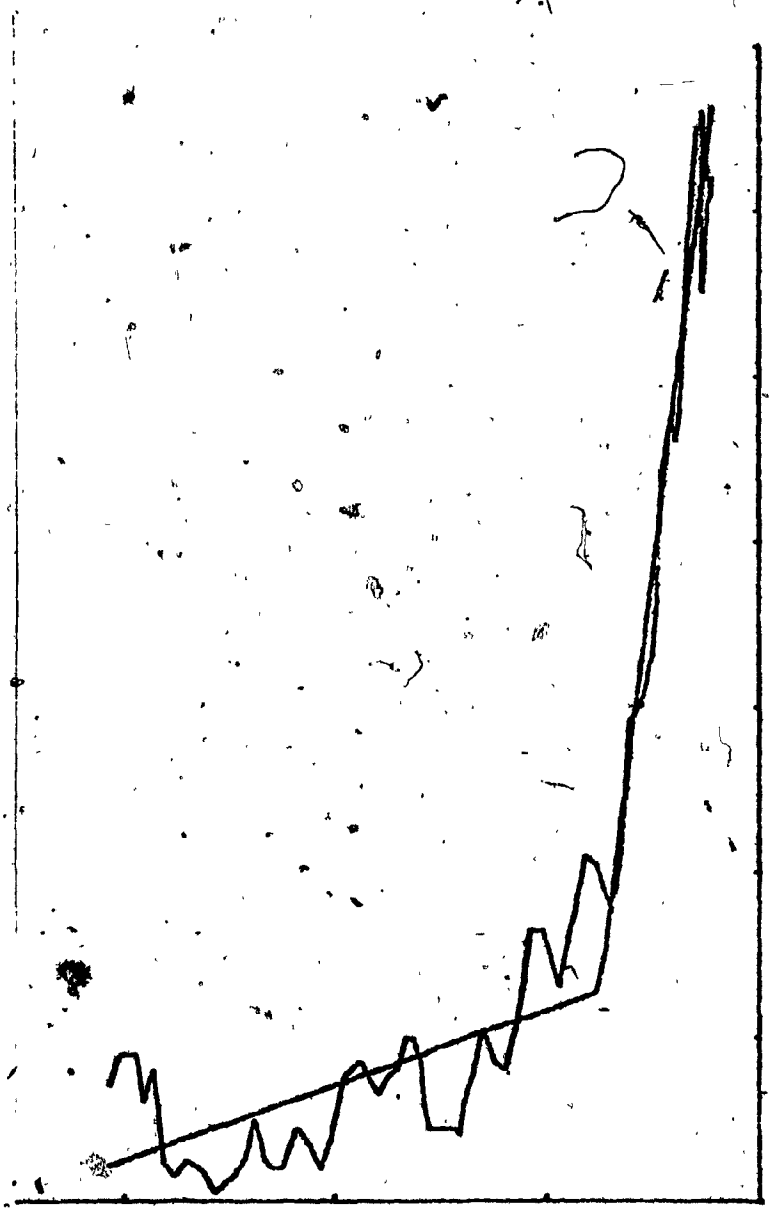

Figure 6.11d. Case 6. Raw Data and Thrid Analysis on Truncated Data File.

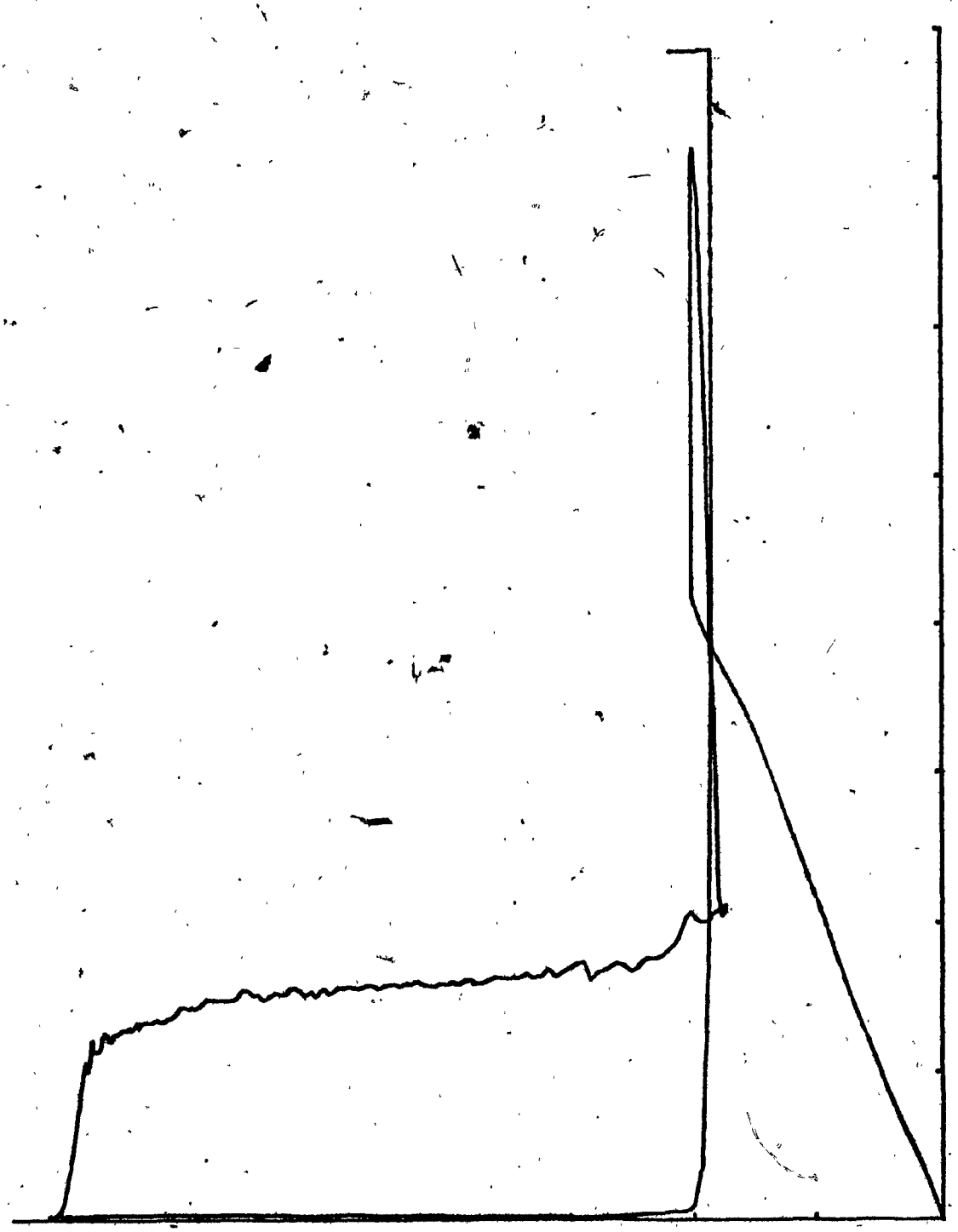

Figure 6.12a. Case 7. Raw Data.

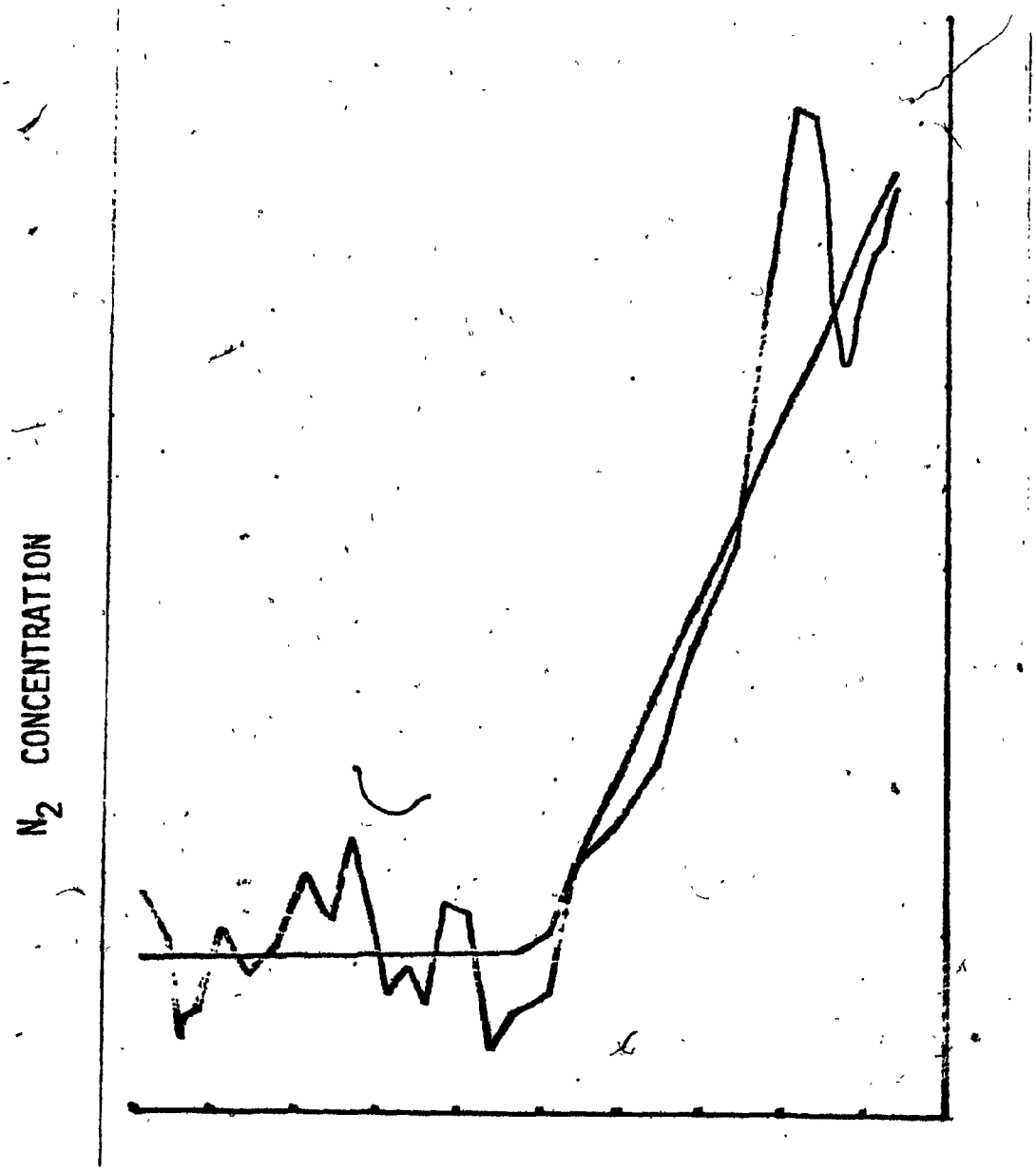

Figure 6.12b. Raw Data and Analysis.

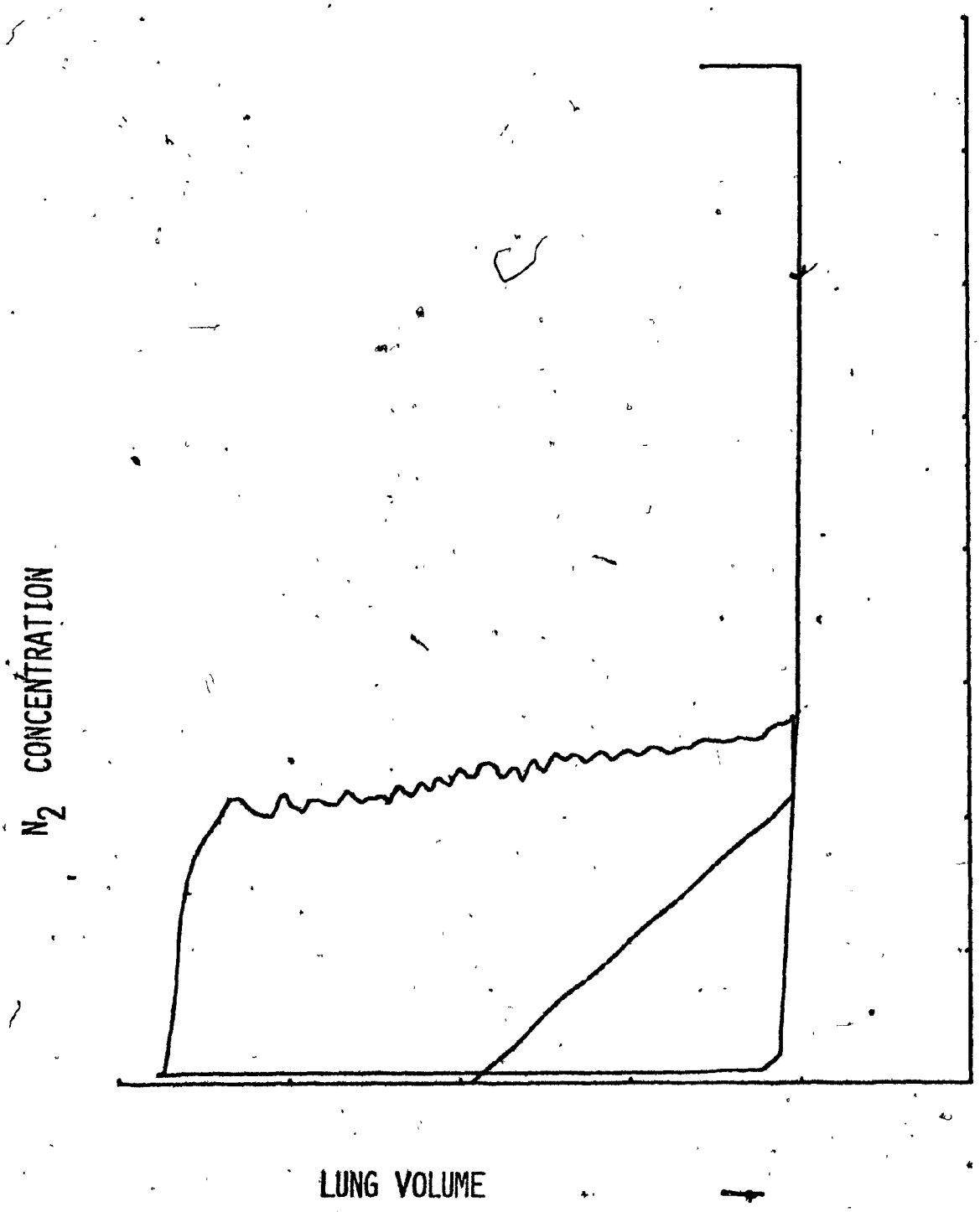

Figure 6.13a. Case 8. Raw Data.

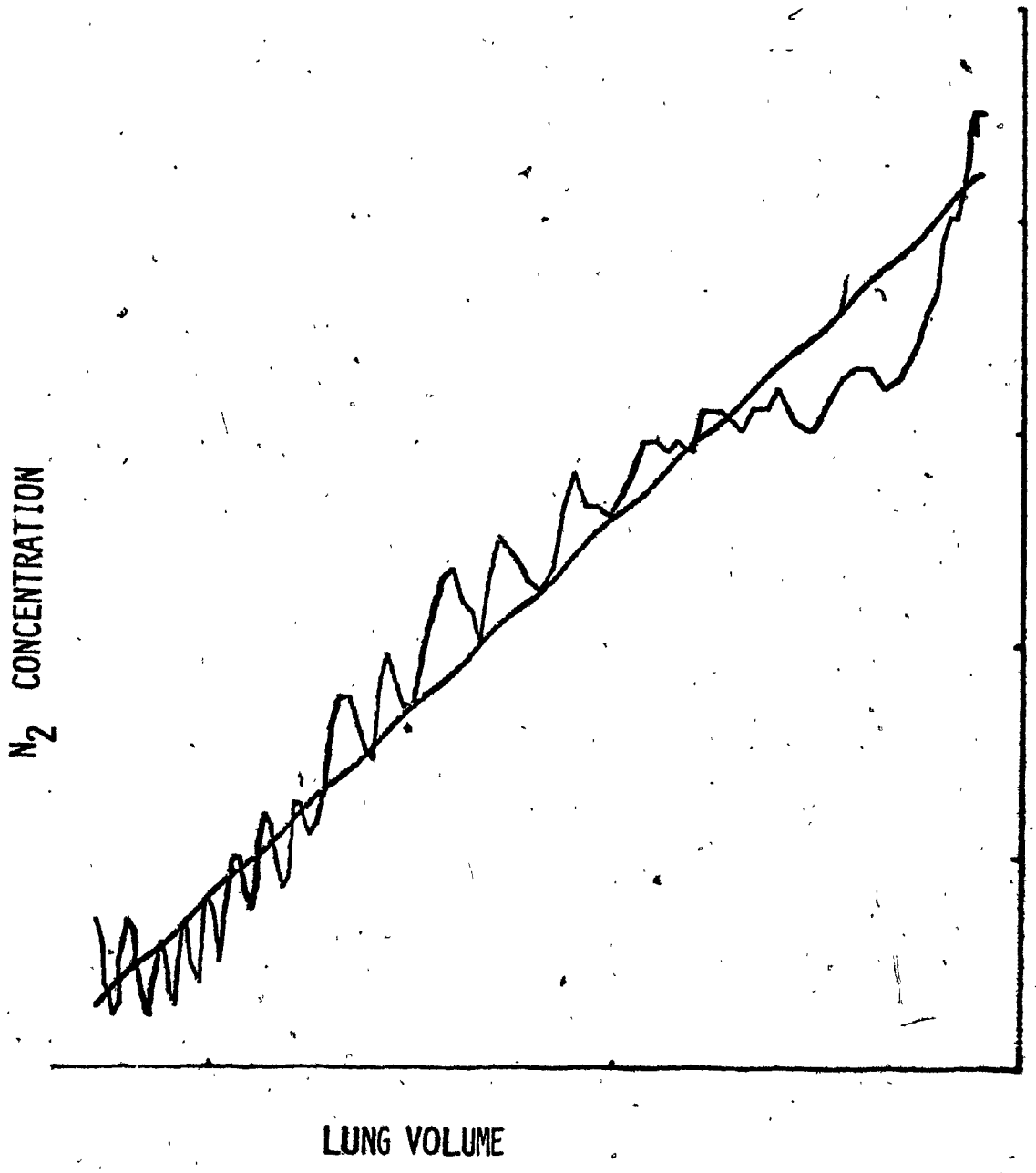

Figure 6.13b. Case 8. Raw Data and Analysis Closing Volume Not Found.

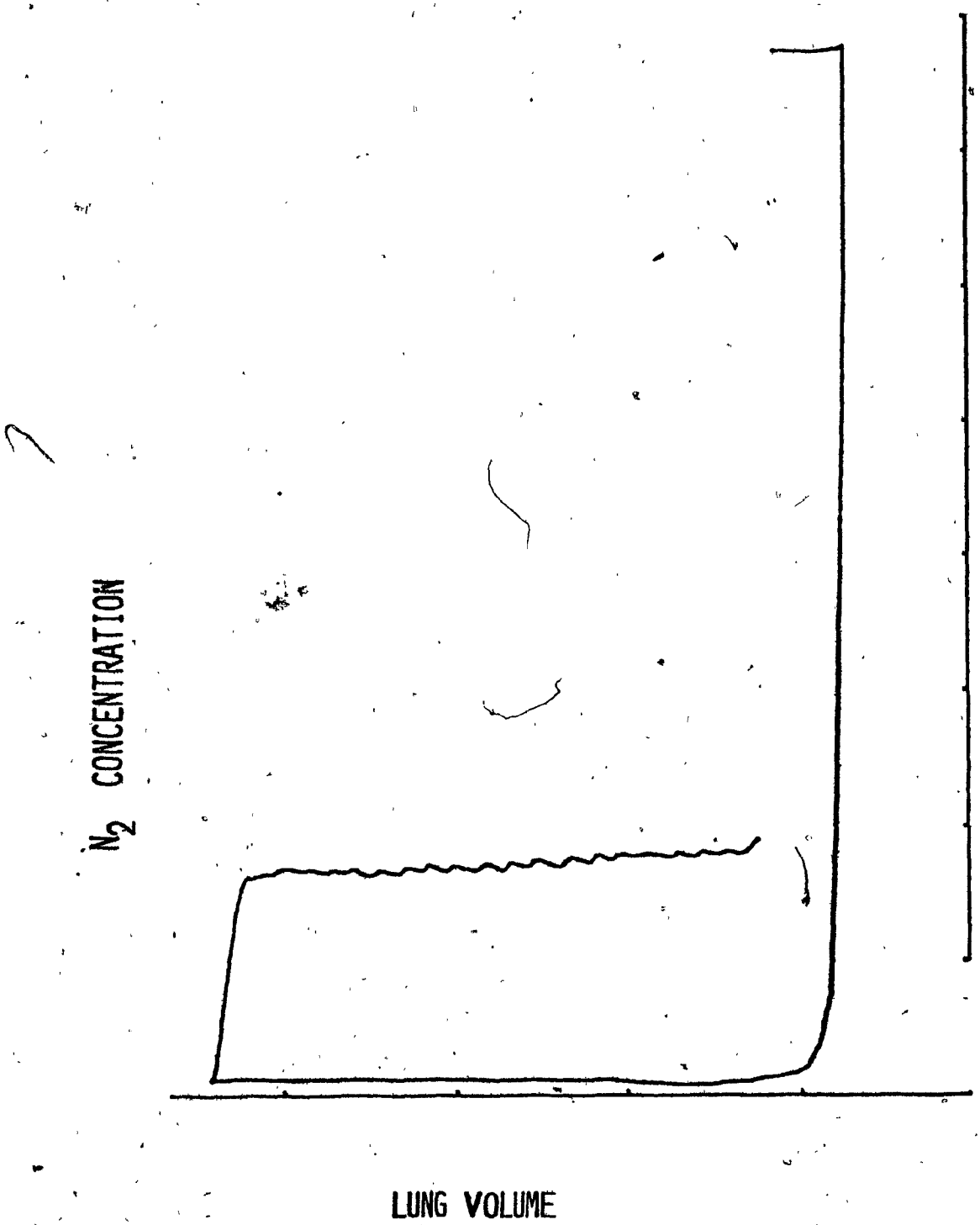

Figure 6.14a. Case 9. Raw Data.

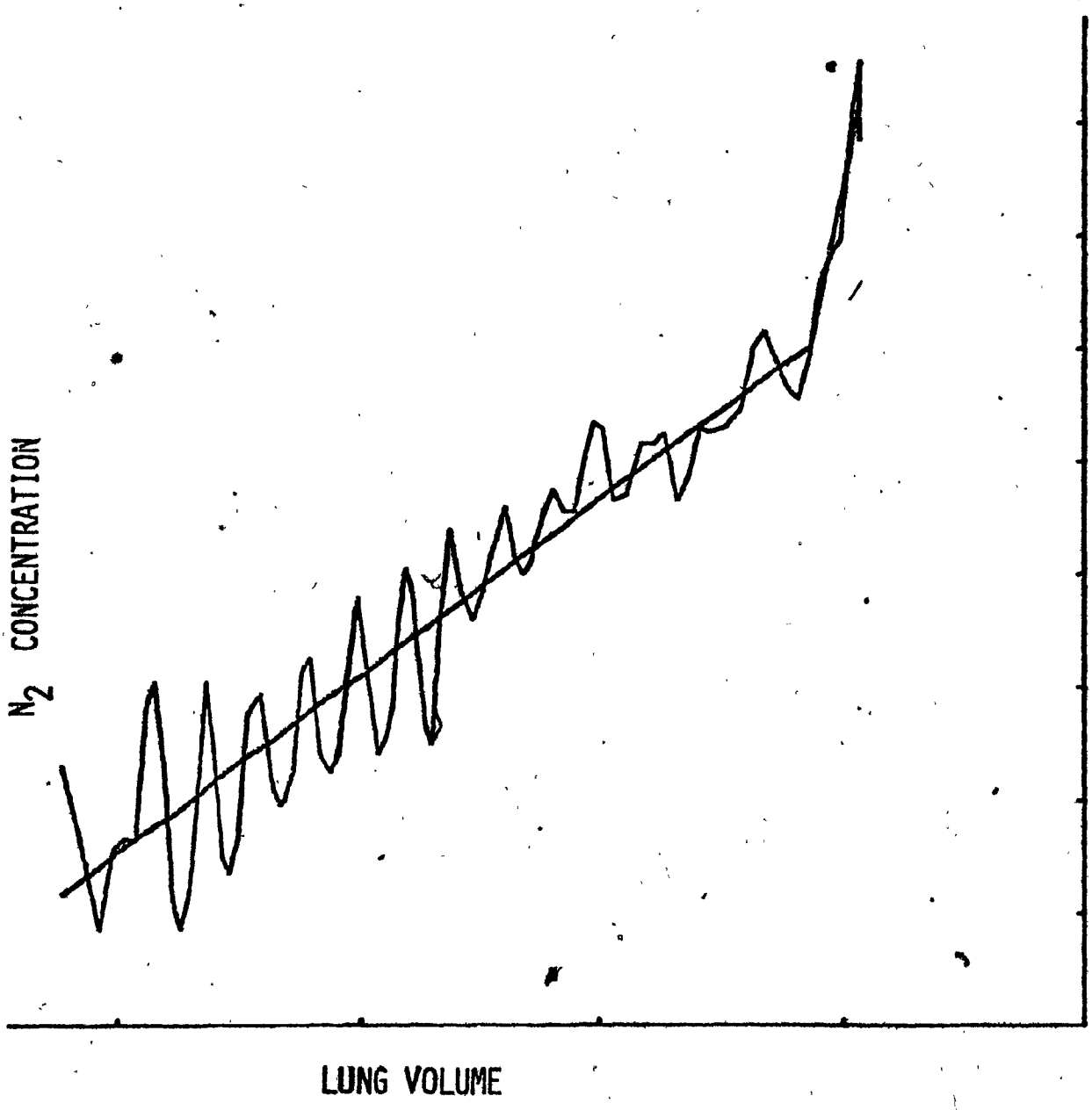

Figure 6.14b. Case 9. Raw Data and Analysis.

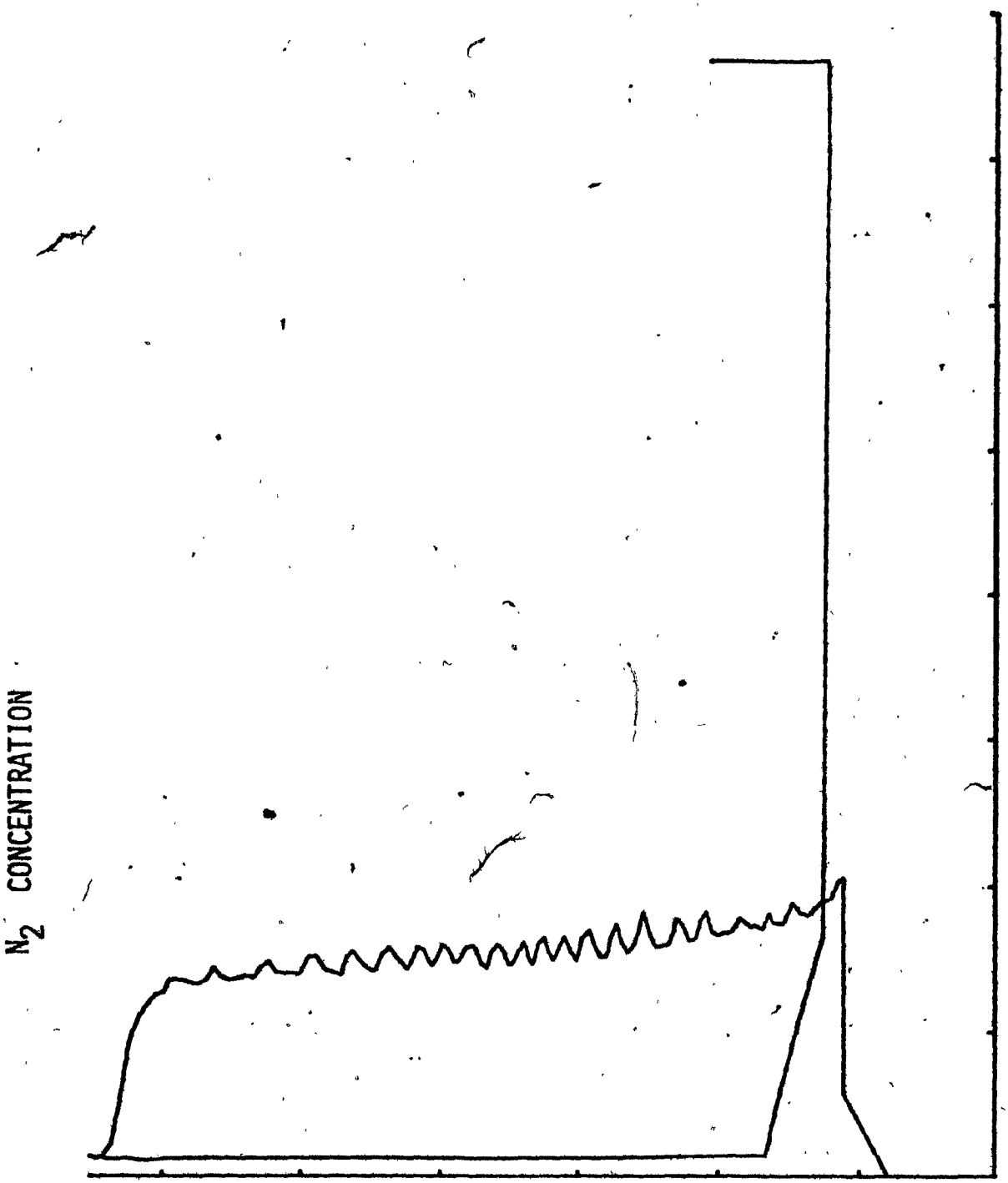

Figure 6.15a. Case 10. Raw Data.

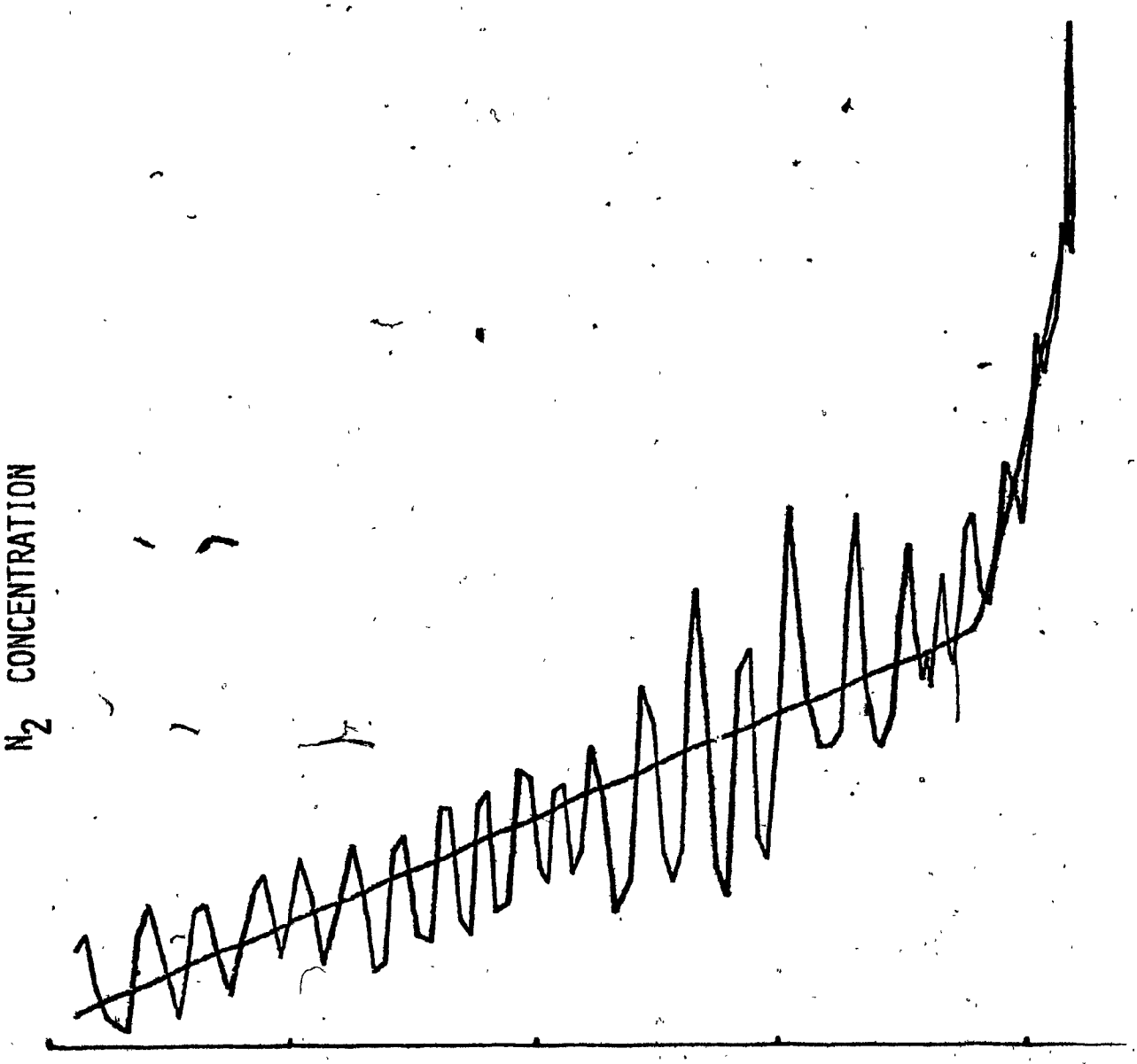

Figure 6.15b. Case 10: Raw Data and Analysis.

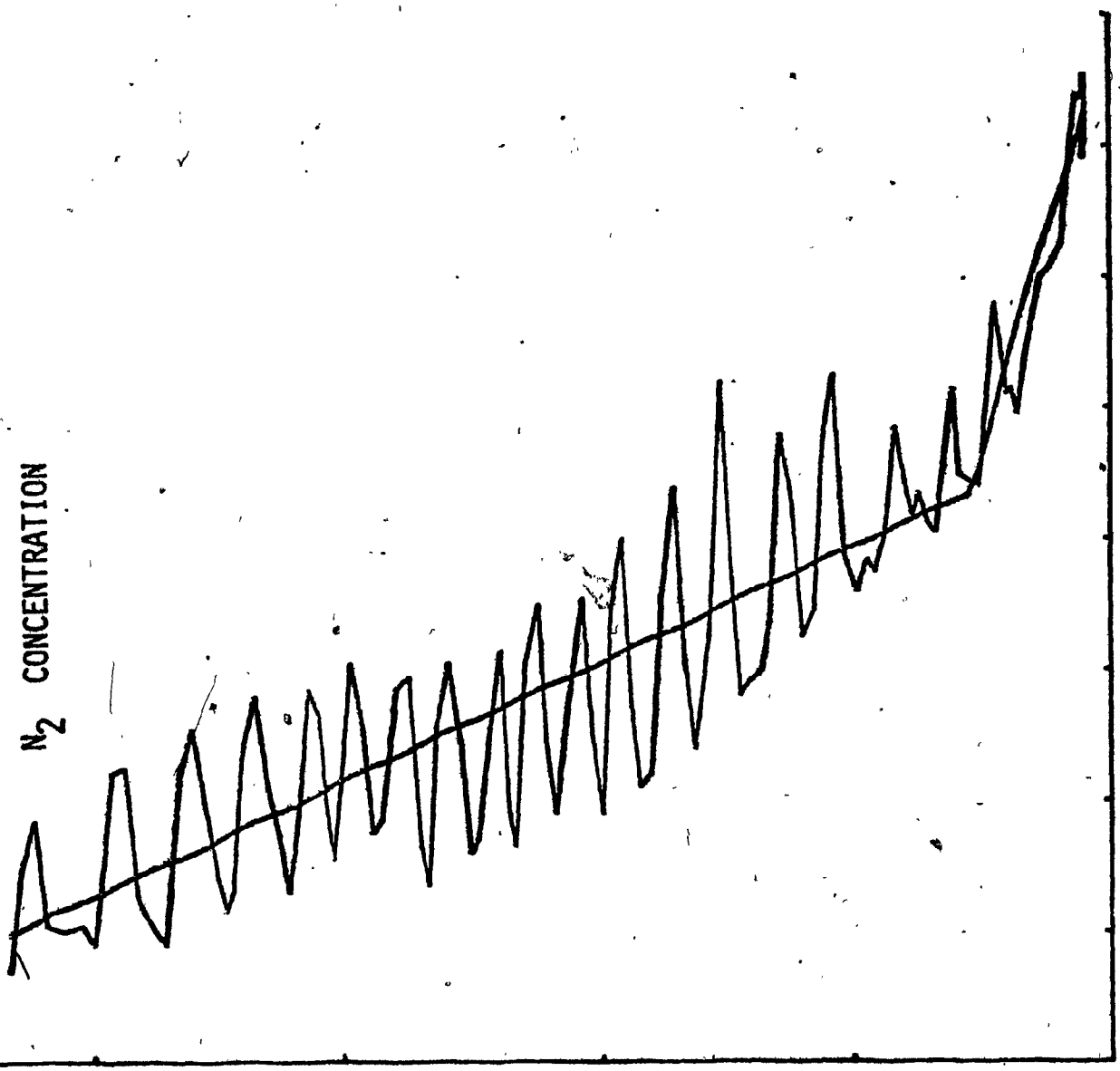

Figure 6.15c. Case 10. Raw Data and Analysis.

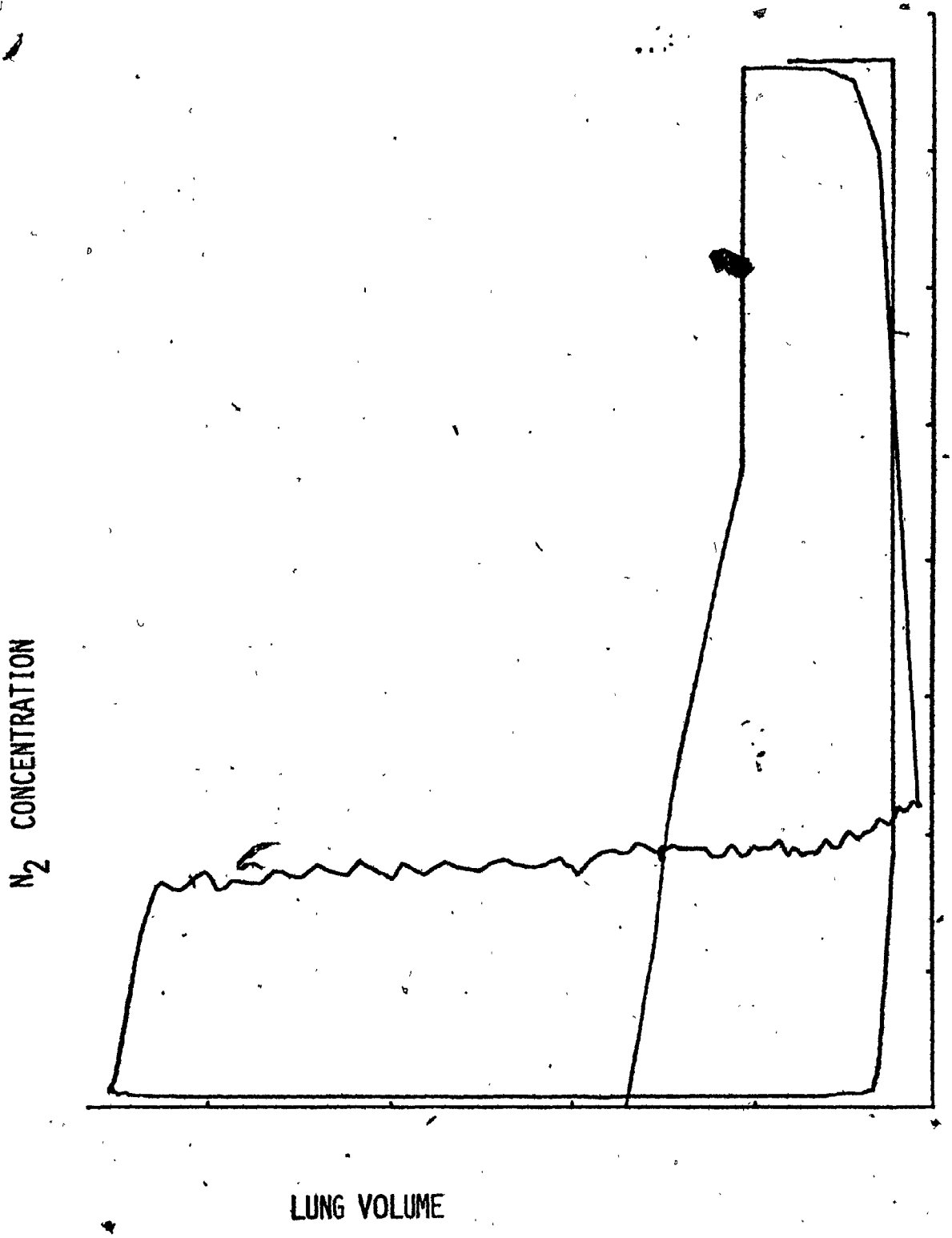

Figure 6.16a. Case 11. Raw Data.

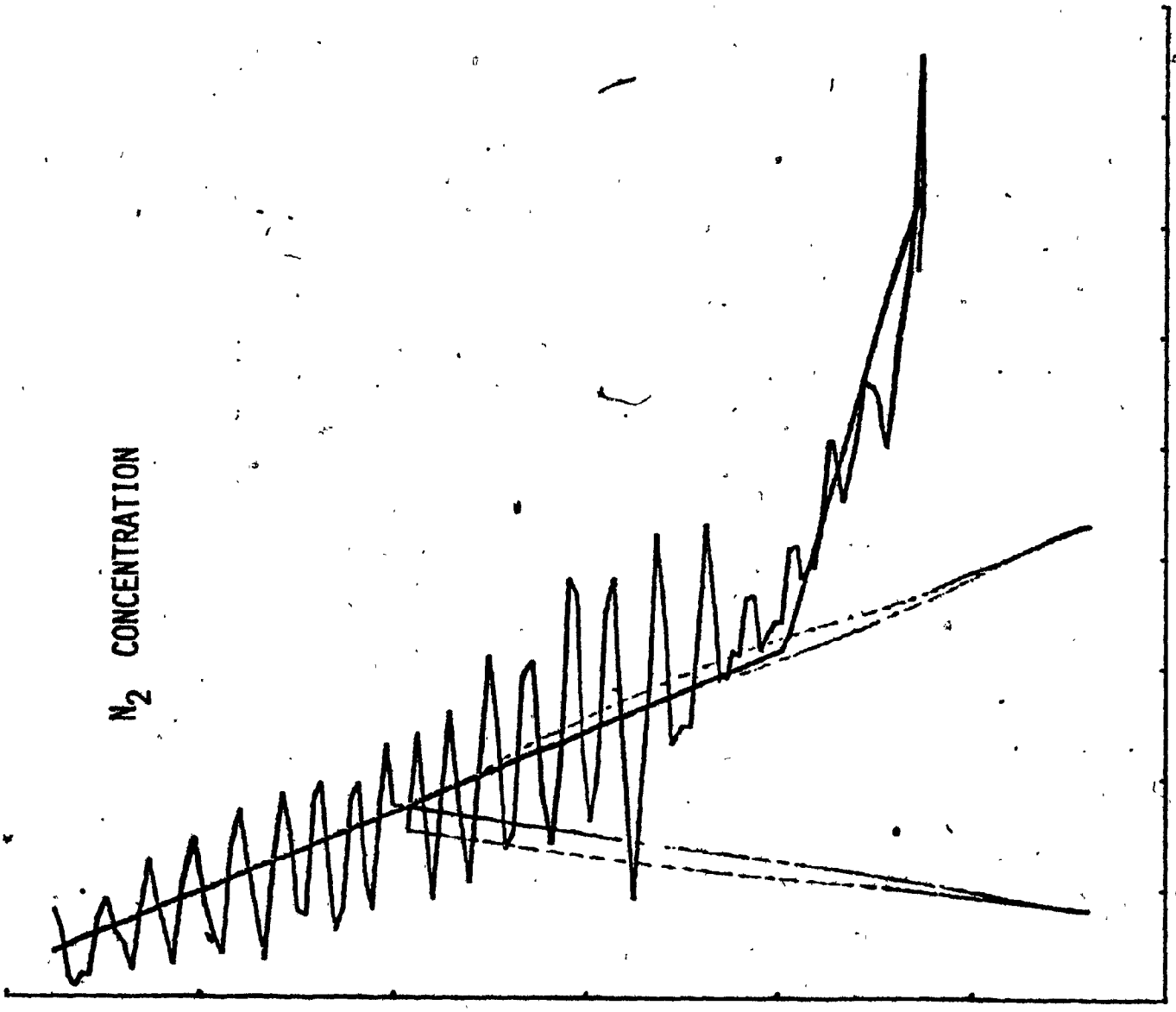

Figure 6.16b. Case 11. Raw Data and First Analysis.

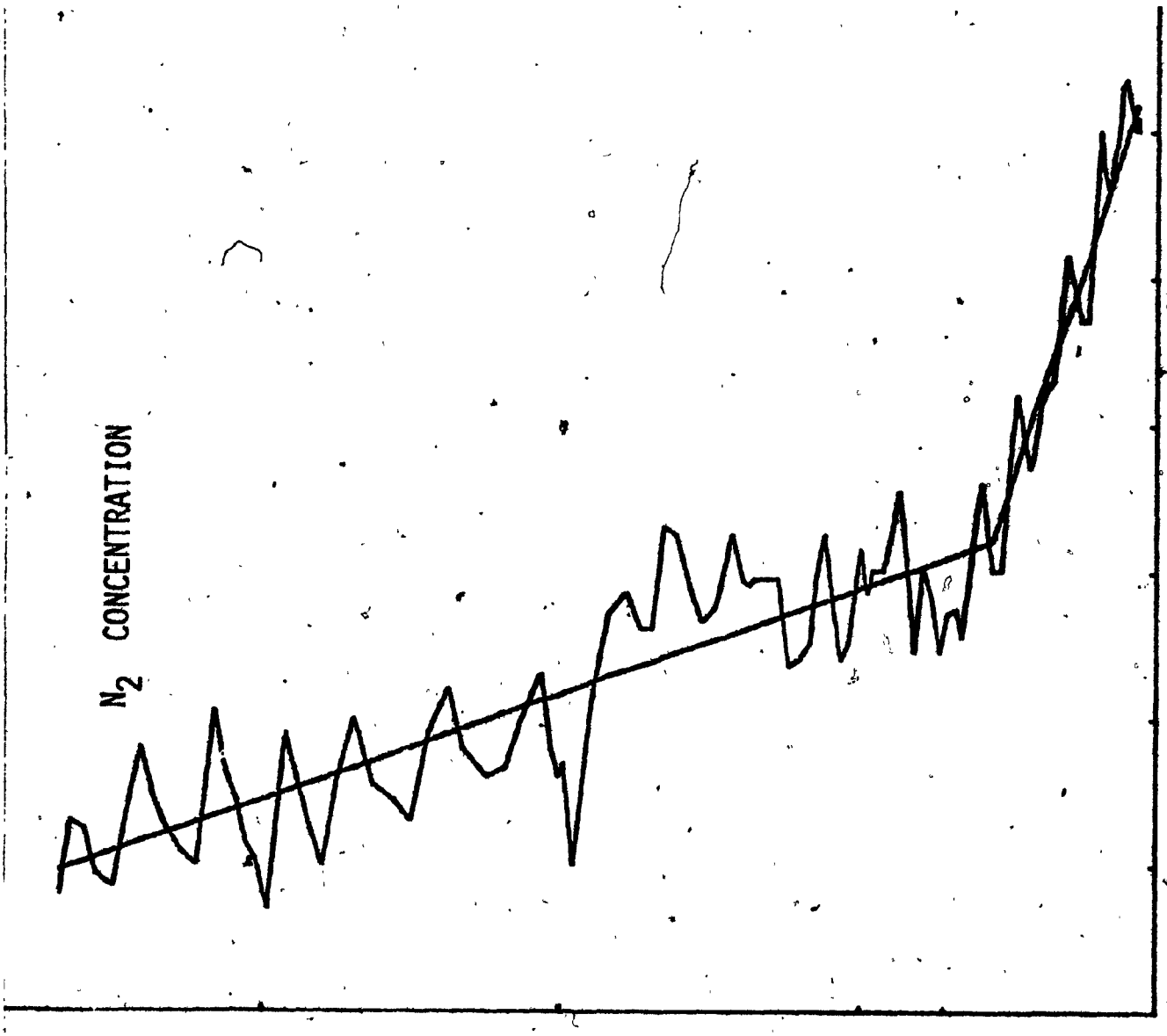

Figure 6.16c. Case 11. Raw Data and Second Analysis.

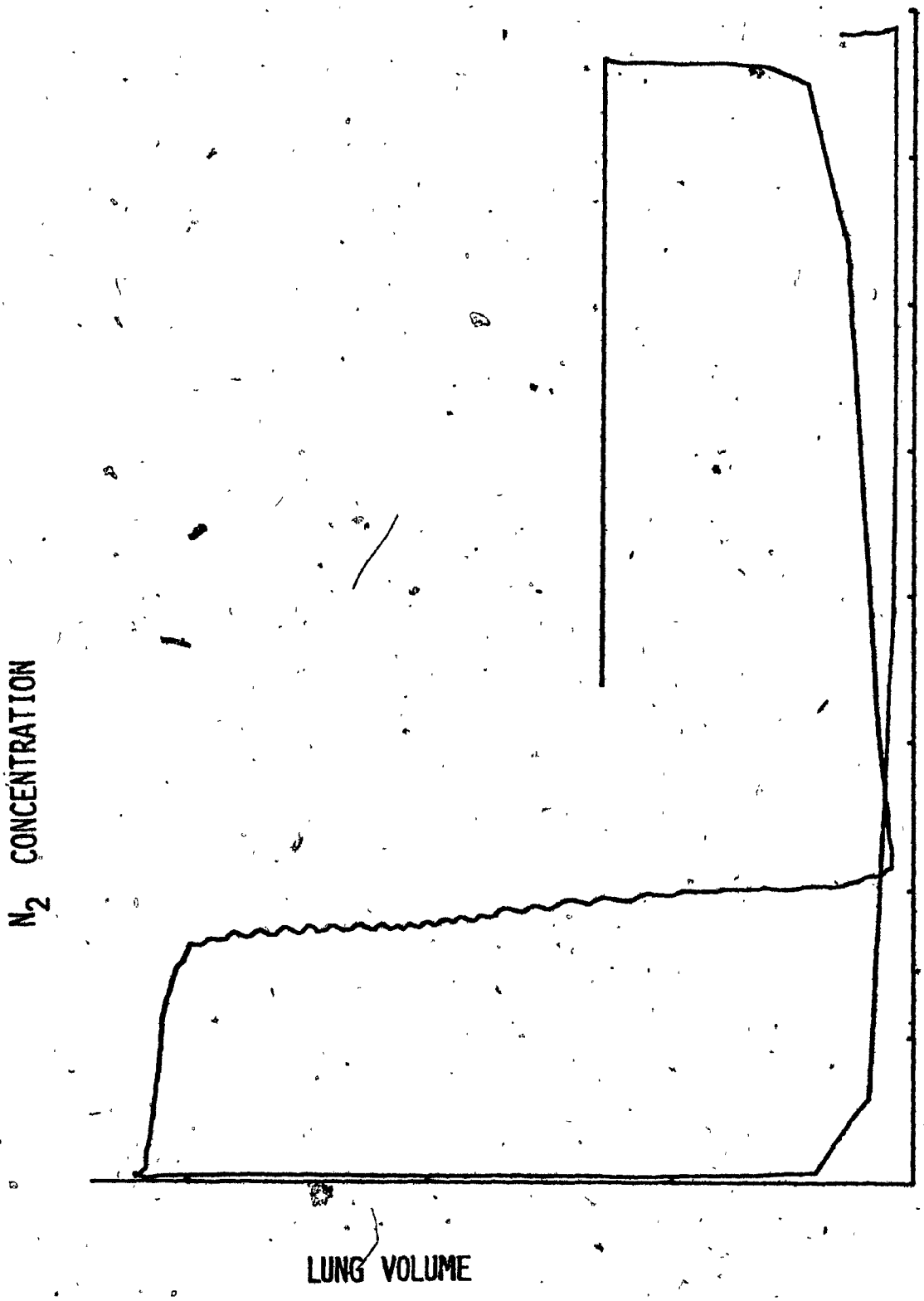

Figure 6.17a. Case 12. Raw Data.

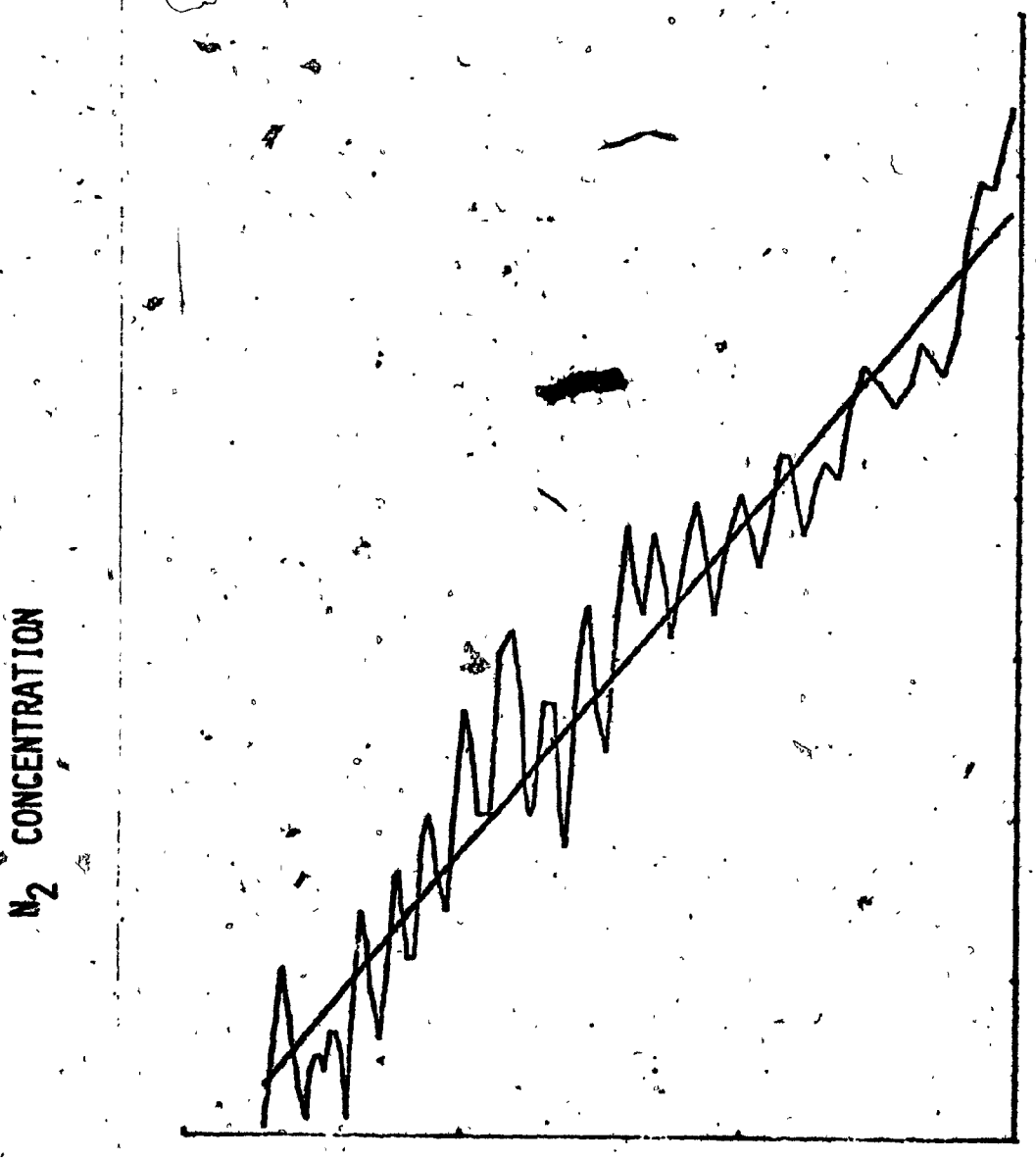

Figure 6.17b. Case 12. Raw Data and Analysis Closing Volume Not Found.

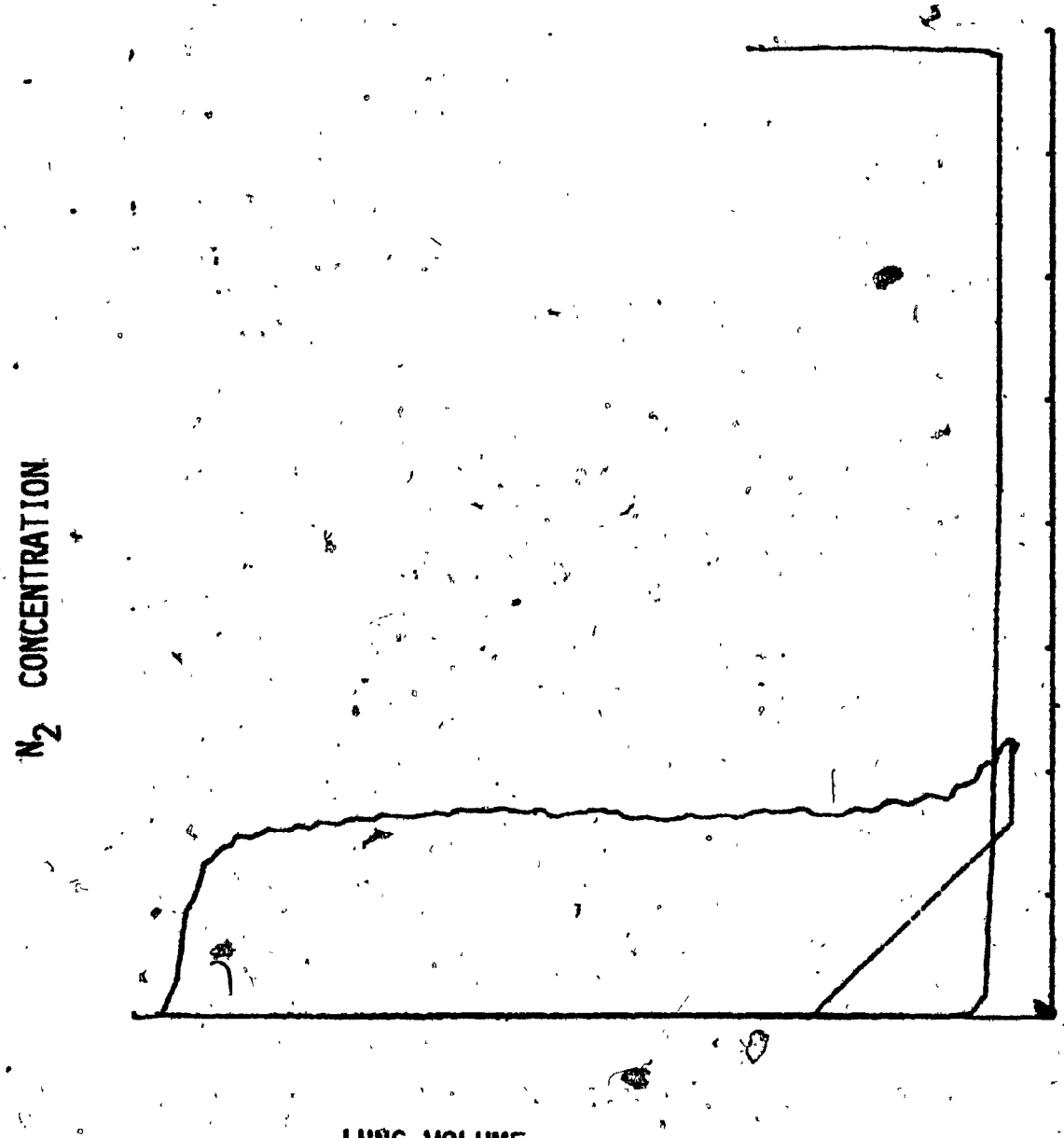

Figure 6.18a. Case 13. Raw Data.

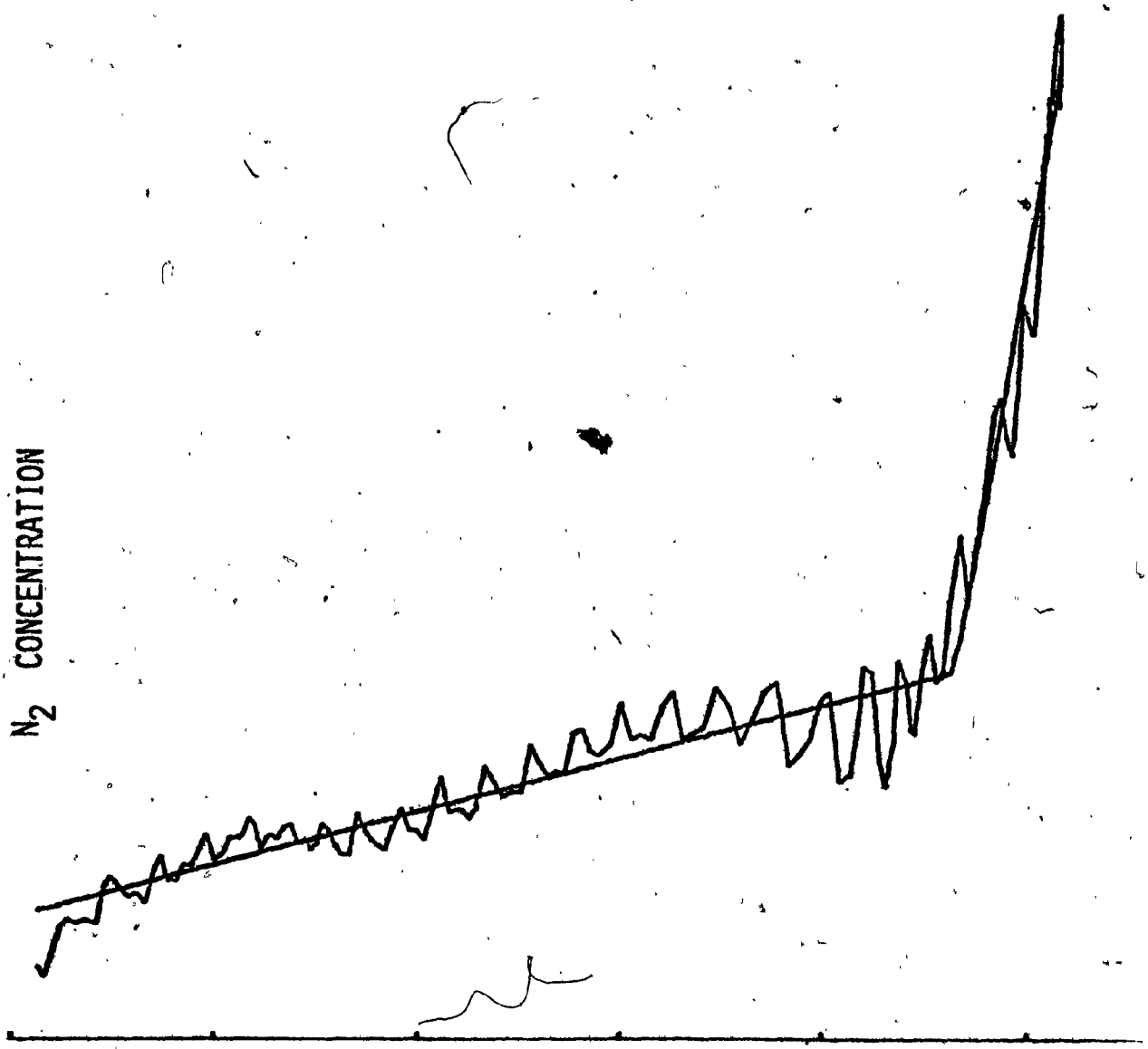

Figure 6.18b. Case 13. First Analysis and Raw Data.

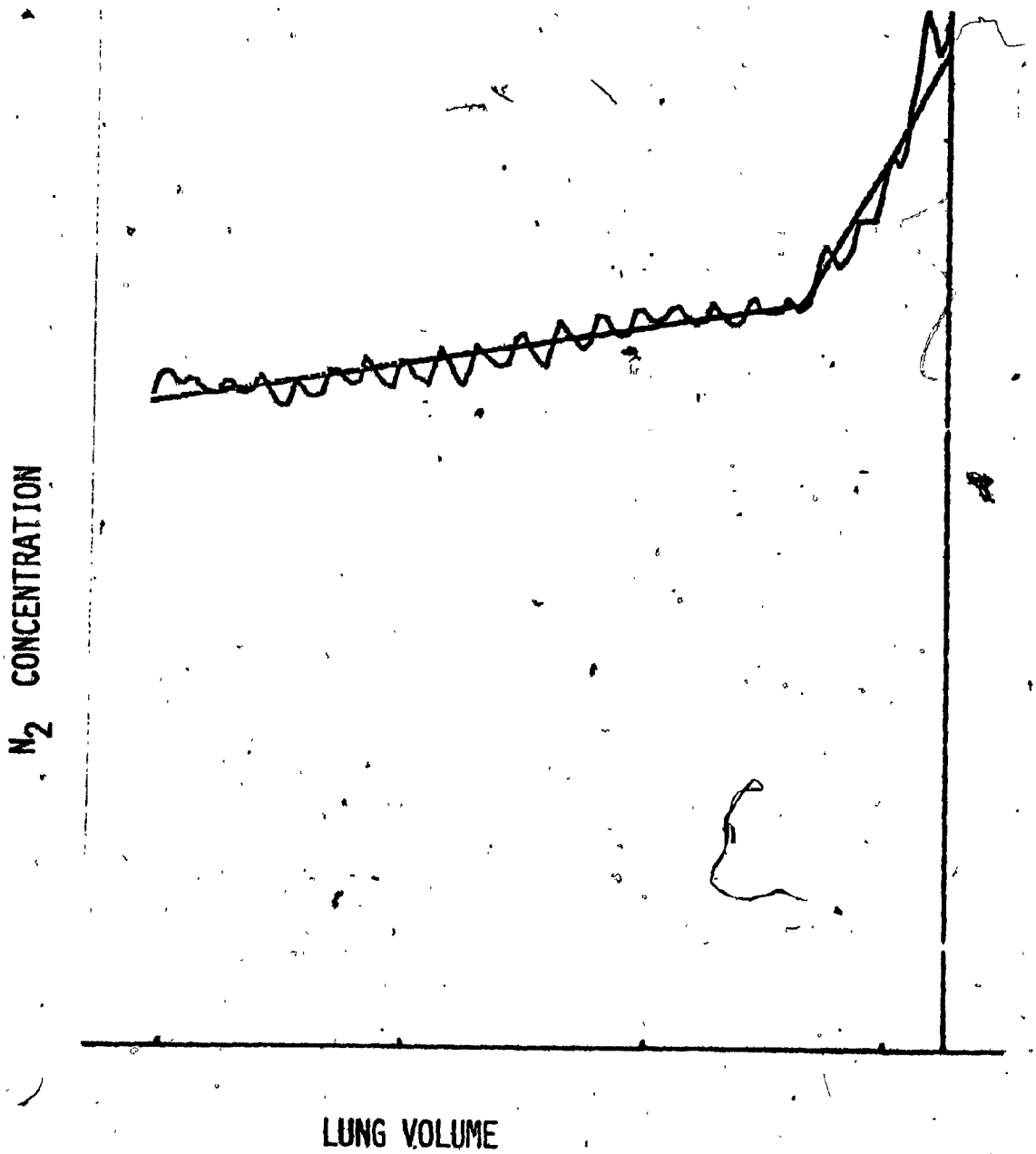

Figure 6.18c. Case 13. Second Analysis and Raw Data.

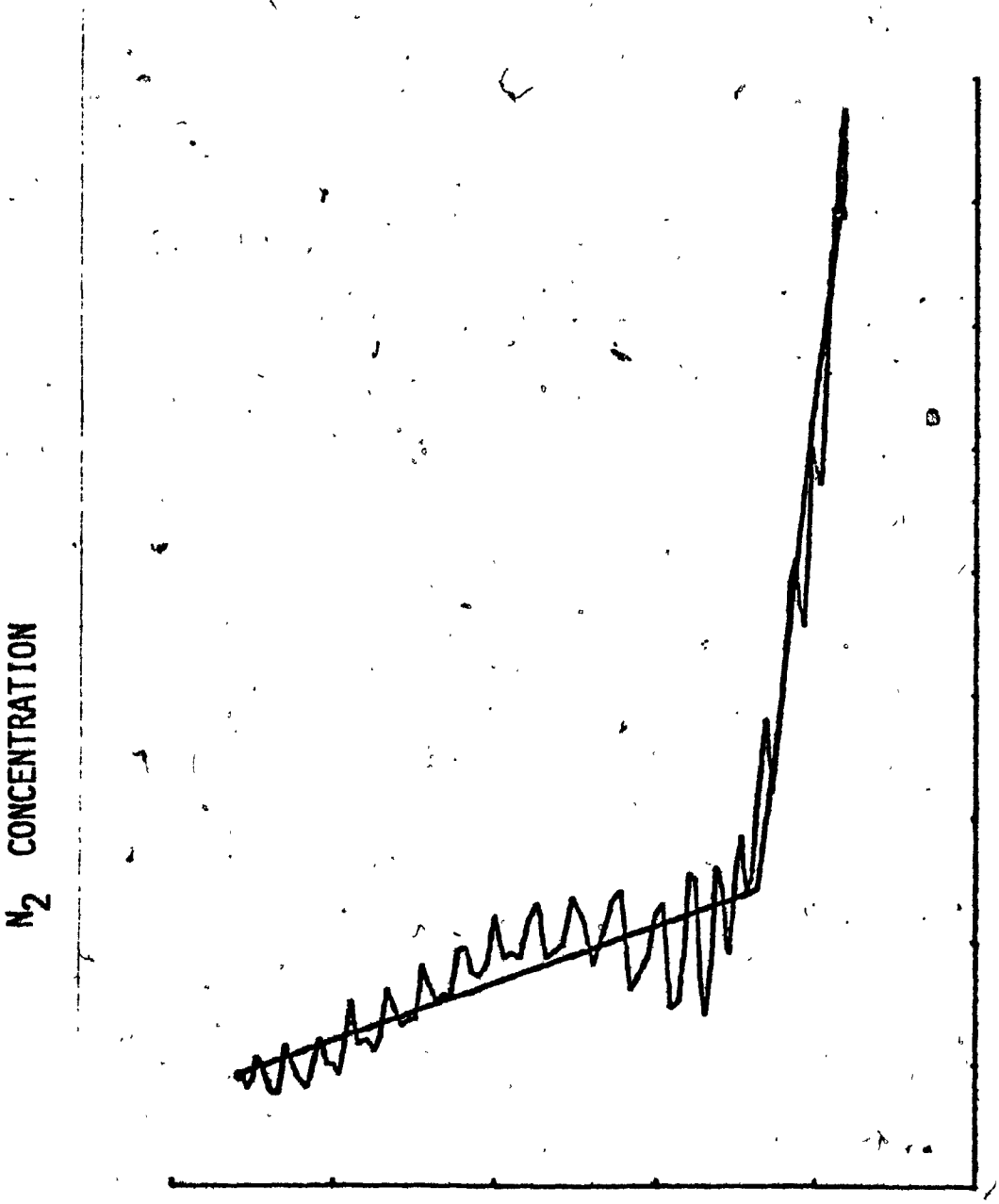

Figure 6.18d. Case 13. Fourth Analysis and Raw Data.

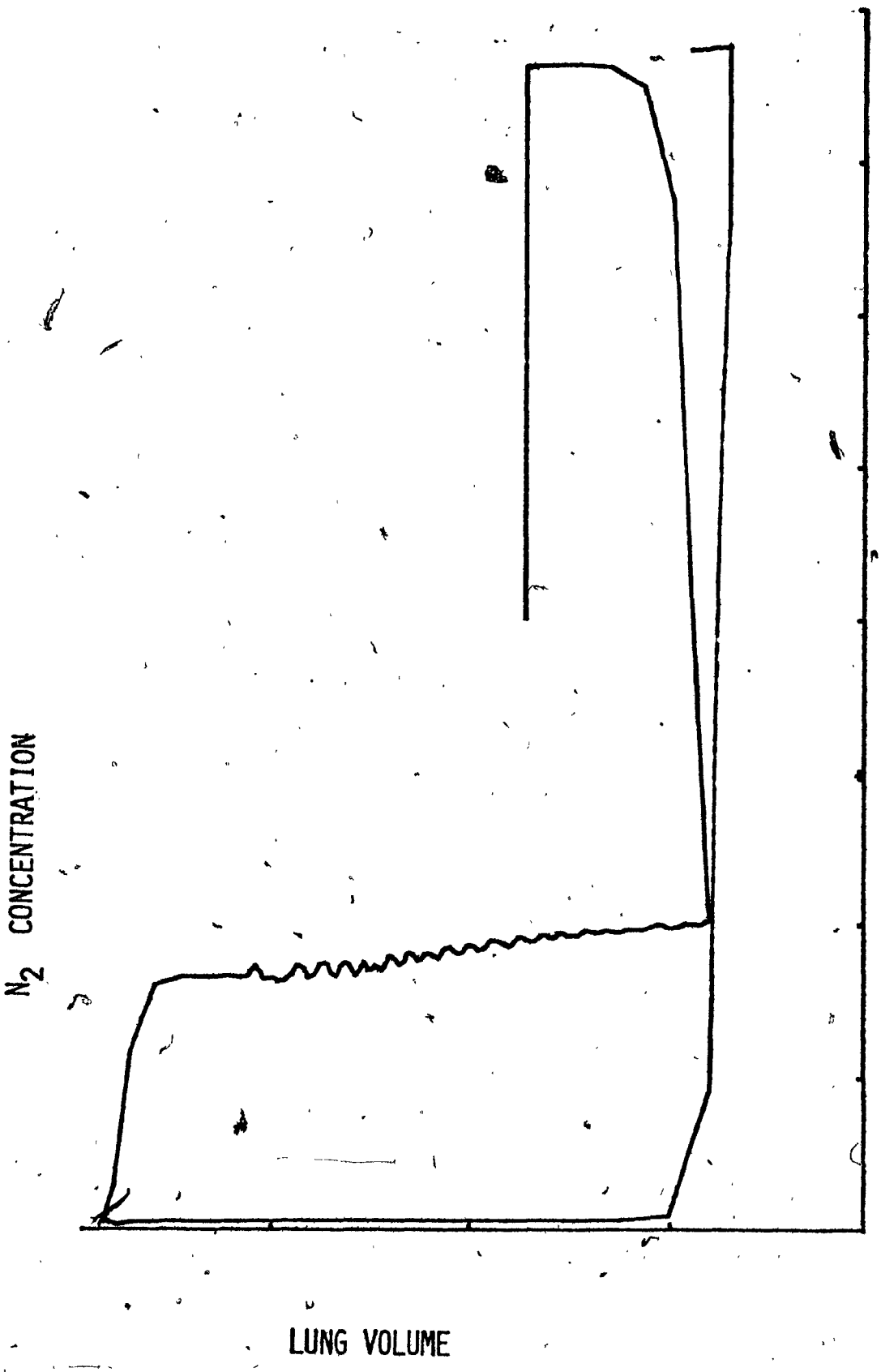

Figure 6.19a. Case 14. Raw Data.

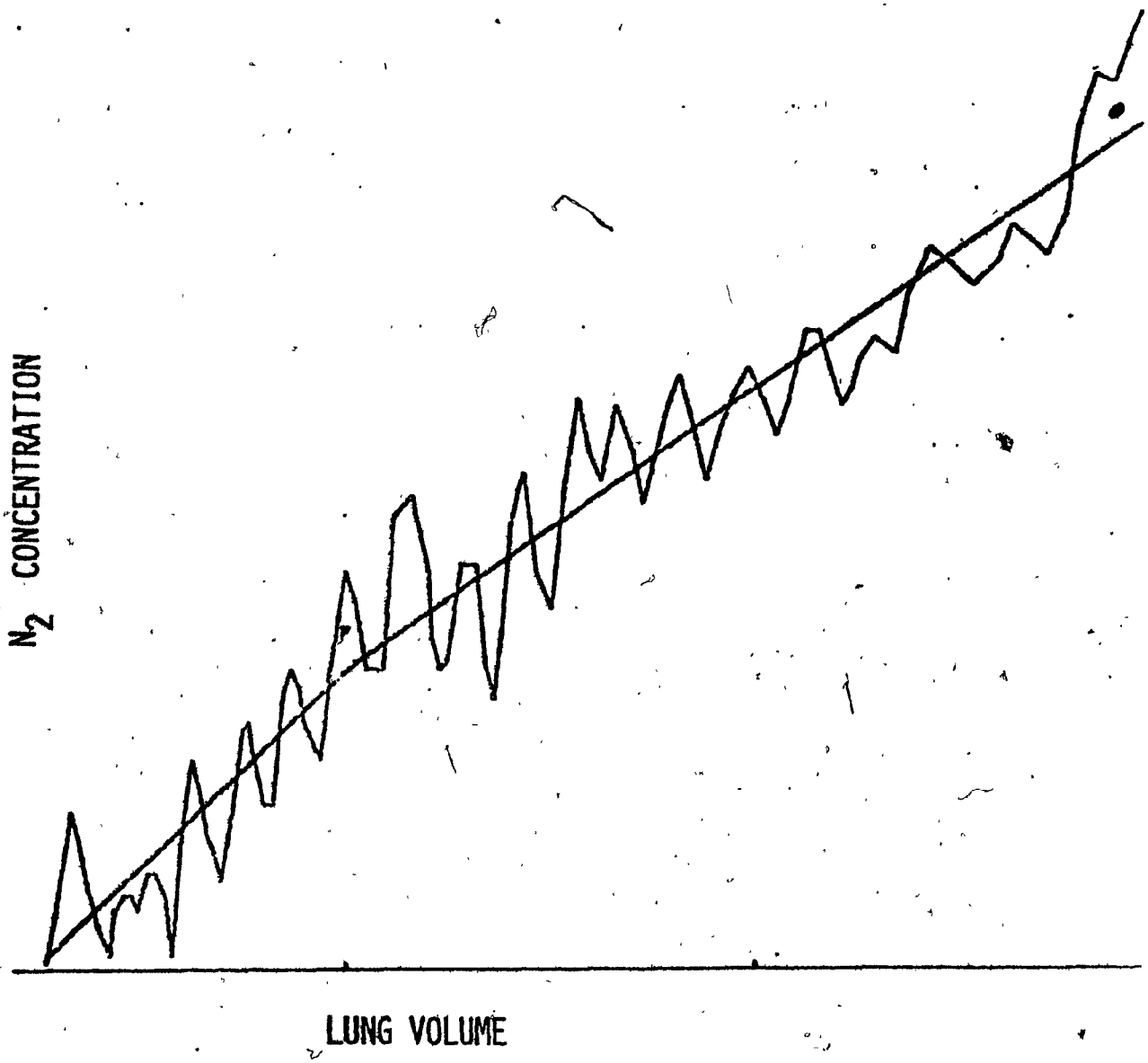

Figure 6.19b. Case 14. Raw Data and First Analysis. Closing Volume Not Found.

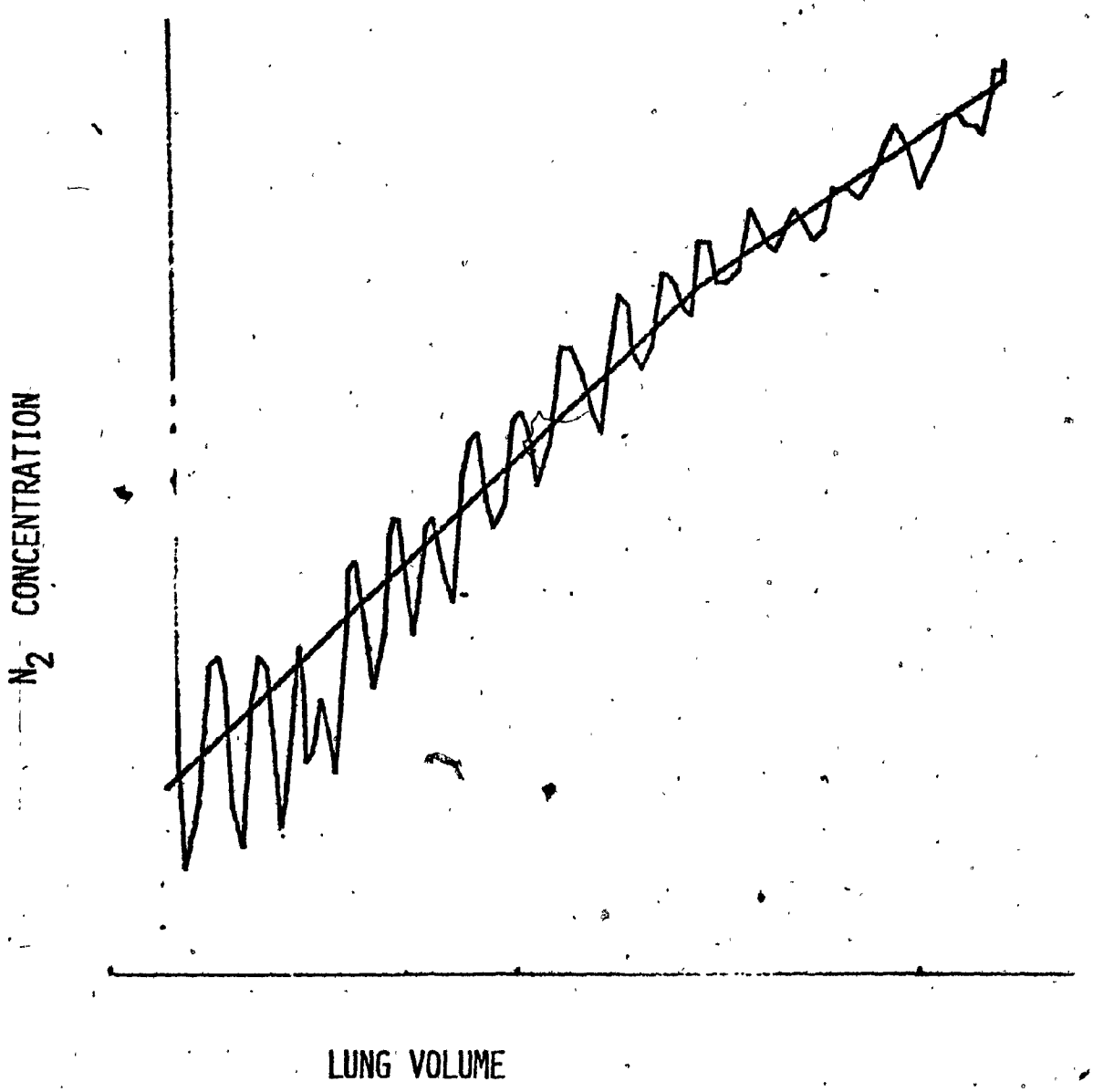

Figure 6.19c. Case 14. Raw Data and Second Analysis. Closing Volume Not Found.

CHAPTER SEVEN

7.1 A SURFEIT OF PROTOCOLS

The results of various computer programs developed for the consistent automated determination of CV have demonstrated [33, 161, 169] the insufficiency of the methodology [151] published for its evaluation by the United States National Heart and Lung Institute (NHLI).

Guy et al. [61] found that while their computer program was capable of fitting a line to phase III that 'few would fault' their algorithm's literal use of the standardized criteria [151] for the determination of CV produced estimates that systematically differed from those made by trained experts. They suggested that the human observer may identify the phase III-IV junction in accordance with more flexible criteria than those published by the NHLI. The protocol distributed by the NHLI advocates determining the slope of phase III from the latter 70% of the phase III data while estimating the onset of phase IV from data observed only in the latter half of phase III. This methodology has been successfully applied only in the analysis of 'easy to read' SBN_2 curves. Computer programs, written in strict accordance with the 1973 guidelines, are simply incapable of satisfactorily determining CV in 'more difficult to read' cases.

Various authors [33, 34, 61, 169, 153] have reported simple modifications of the 1973 protocol which have attempted to improve the

results of their programs' calculations of CV. These modifications essentially involve running linear regression analyses on data contained within an interval other than 'the latter half of phase III' as the NHLI guidelines specify.

Such technical changes in procedure can markedly affect computed estimates of CV and the calculated slope of Phase III. However, while such estimates are different, they are in no better agreement with the manual interpretation of the data [61].

As such it is not surprising but rather unfortunate that, since 1973, five new sets of criteria for the determination of CV have appeared in the literature [126]. In fact, the initial difficulties surrounding the delineations of the phase III and IV segments of the SBN_2 curve are now compounded by the numerous partially effective methods that have been advocated for the determination of CV.

7.2 The NHLI Protocol

It is surprising that in the face of these difficulties, the very definition and suggested methodology of CV published by the NHLI has neither been critically reviewed nor criticized.

Upon consideration it may easily be argued that a critical review of the methodology distributed by the NHLI would require a committee of experts to objectively assess the various methodologies and algorithms available for the analysis of the SBN_2 washout curve. It is true that such a committee would be best suited to the prerequisite task of compiling an extensive reference library of carefully recorded

and reproducible SBN_2 tracings. The manual interpretation of the wide spectrum of both "hard" and "easy to read" tracings included in this library could then be undertaken by a panel of experts whose opinions would be canvassed first individually and then collectively.

The need for such a reference library is pressing in that it is futile to attempt a comprehensive comparative study of the alternative methods and programs available for the analysis of washout data without such a database. At present only two studies [169,34] have documented the results of their program's performance in the analysis of CV on a sample population not composed of carefully selected, comparatively "easy-to-read", cases.

Problems inherent in program comparisons are particularly complex when the programs in question are developed in an attempt to reduce the large intra- and inter-observer variance documented in the manual analysis of the data [33 ,39].

At the moment, the only way to evaluate these different computer programs is to compare correlation coefficients which attempt to summarize the results obtained from applying different algorithms to different reference samples with different groups of readers. It is our belief that such an uncontrolled, multifactoral study should not be undertaken. From the outset, the results of such a comparative exercise are questionable on so many grounds that they could not help but muddle the task of program comparisons.

There is an urgent need to establish an effective standard protocol for the analysis of single breath washout data. It is very unwise to compare either manual or automated CV determinations to predicted normals and population limits established by different observers applying different protocols [33]. The utility of the six available computer programs in epidemiological and clinical use is severely hampered by this problem in that each algorithm effectively represents yet another protocol.

7.3 The Definition of Closing Volume

While a critical review of the methodology distributed by the NHLI may be difficult, it is certainly easy to constructively criticize the NHLI's definition of CV on theoretical grounds. This definition considers CV to be the volume from the onset of phase IV to RV. It can forcefully be argued, in accordance with the position first taken by Hamosh and Taveira da Silva [64] in 1974, that CV should be calculated neither from the onset of phase IV nor the end point of phase III but rather from the junction point of these two continuous phases.

The protocol distributed by the NHLI advocates determining the onset of phase IV in terms of data observed only in the latter half of phase III. Even if one adopts the view that such a boundary point should be used in calculating CV, then surely, in that it is literally computed entirely from phase III data, this boundary point logically represents the end point of the phase III interval rather than the onset of phase IV. If, on the other hand, CV is calculated from the junction

of two phases of the washout curve, then it certainly cannot be described in terms of the data contained in only one of these phases.

7.4 The Calculation of Closing Volume

These apparently theoretical difficulties compound further problems that are immediately encountered when attempting to successfully instruct a computer to analyze the SBN_2 washout curve in accordance with the protocol published by the NHLI.

The suggested methodology for determining the onset of phase IV is so qualitative that upon writing a computer program for the determination of CV one is forced to establish at least one ad hoc quantitative threshold which must be used to determine what is a significant departure from the observed phase III data. Such fixed threshold criteria when incorporated into utility programs for the routine evaluation of SBN_2 tracings limit their accuracy and reliability [34,169,61,42,139]. Such simple methods have shown themselves to be sensitive to cardiogenic oscillations [169], non-linear or multi-sloped alveolar plateaus [169], the size of both the VC_E [34,169] and alveolar plateau [169] and sudden steps in nitrogen concentration [34]. These difficulties have not been reported by other authors [61, 33] of similar algorithms.

Even the simple task of segmenting the latter half of phase III for further analysis forces one to define what is to be considered either as the onset of phase III, the end of phase II, or the phase II-III juncture [169].

Anatomomical Dead Space Calculations

The $V_{D_{anat}}$ calculations have been described as hardly worth human effort, but of use when computed by machine [61]. Besides being essential in the accurate calculation of the single breath TLC, $V_{D_{anat}}$ may be used as an index of change in large airway caliber [46]. Fortunately, in that the classic methodology described by Aitken and Clark-Kennedy [2] for the determination of $V_{D_{anat}}$ is explicit, it is a comparatively easy matter to successfully apply numerical techniques to its literal determination.

Our non-linear program's main numerical algorithm, A1, is ideally suited to the task of determining the slope of the alveolar plateau used in the $V_{D_{anat}}$ calculations. This program calculates this slope from that portion of the phase III segment contained within the initial half of the VC_E. When applying A1 to this data segment, the program deletes from the data the initial part of phase II which contained N_2 concentration values which were less than 5%. The arbitrary threshold value of 5% has little effect on the estimate of the phase III slope used in the $V_{D_{anat}}$ calculations. Because the mid-portion of the phase II segment is relatively linear, any arbitrary threshold value that succeeds in isolating the convex foot of the sigmoidal phase II curve from our data would suffice.

The decision to estimate the slope of the alveolar plateau, used in the $V_{D_{anat}}$ calculations, from data contained in the first half of the VC_E is both arbitrary and important. Bouhuys [11] has

pointed out that single breath procedures for the estimation of dead space volume are particularly sensitive to the method's estimation of $F_{A_{N_2}}$. In that the $V_{D_{anat}}$ calculations involve the linear extrapolation of phase III data, we have chosen to perform this extrapolation from a smaller data segment than that originally proposed by Aitken and Clark-Kennedy [2]. This means that these calculations are less sensitive to any non-linearities in the phase III data while utilizing the method of least squares to estimate the slope of the initial portion of the alveolar plateau. The $V_{D_{anat}}$ calculations are thus made on the basis of an extrapolation that faithfully reflects the phase III data contained within the first half of the VC_E.

This methodology differs from that developed by Fowler [49]. Fowler's calculation of $V_{D_{anat}}$ involves the extrapolation of a line of zero slope from the estimated value of $F_{A_{N_2}}$. $F_{A_{N_2}}$ is taken to equal the N_2 concentration at the transition point between the second and third phase of the record. While these calculations are straightforward [61], the physiological validity of either approach in the calculation of anatomical dead space remains a philosophical question [46].

7.5 The Role of Modeling in the Recognition of Closing Volume

In general, "hard to read" SBN_2 tracings are interpreted so admirably by human observers that some researchers [61] have attributed the difficulties they observed in developing a reliable algorithm for the analysis of the SBN_2 tracing to the complexity of the pattern

recognition task involved in assessing CV.

Guy et al. [61] found that the human observer, when estimating the slope of the alveolar plateau by eye, tends to weigh the points near the curve's inflection to a varying extent. While recognizing the non-linear nature of this problem they were unable to re-define the onset of phase IV in a manner that would augment the agreement they observed between their results and those obtained from the manual evaluation of "hard to read" curves.

Our work would suggest that the problems involved in developing an accurate and reliable program for the automatic determination of CV are inherent in its definition and standardized methodology. Neither are sufficient for the rigorous routine analysis of the SBN_2 curve.

We would suggest that it is the phase III-IV junction point, in conjunction with slope estimates, which best describe in a mathematical and physiological sense the latter half of the SBN_2 curve in normal reference samples.

7.6 Our Model's Assumptions, Performance and Limitations

The theoretical approach that we have taken in this thesis makes no attempt to model, from first principles, the complex physiological processes underlying the observed relationship of gas concentration [25,24, 30,32] to lung volume described by the SBN_2 washout data. Rather we have adopted a simple model which attempts to describe the nitrogen concentration observed throughout phase IV and the latter half of phase

III as two intersecting linear functions of lung volume. Our work suggests that in evaluating the juncture of these two phases it is necessary to give equal consideration to both phase III and phase IV data.

This approach is empirical and its limitations are many. It should be adequate for practical use in epidemiological studies and screening programs aimed at the early detection and assessment of small airway disease.

This model does not offer an adequate description of the SBN_2 washout data observed in cases of more complex gas dynamics concomitant with advanced patho-physiology. Individuals who exhibit a grossly non-linear alveolar plateau or phase IV segment cannot be adequately characterized in terms of such a simple model's parameters. As such, the algorithms that we have presented in this thesis will be as inadequate in this regard as any other, based on the assumption of gas concentration effects which are linearly dependent on lung volume regardless of the state of pulmonary impairment.

The non-linear least squares algorithm that we have described in this thesis provides estimates of lung function which appear to be insensitive to cardiogenic oscillation, the lung volume at which the phase III-IV junction occurs and the size of both VC_E and the alveolar plateau. This non-linear procedure is a modification of an earlier one [90] which biased its estimates in proportion to the relative size of the phase IV segment [126].

7.7 Refining our Model

It should prove possible to account for the effects of variation in expiratory flow on estimates of this model's parameters in terms of a further modification to the method we have described in Chapter Three. Such a modification would thereby reduce the necessity for stringent control on expiratory flow rate during the test.

We could revise the present model's form by incorporating quadratic, rather than linear, approximations of the phase III and IV components of the SBN_2 curve. Such a major revision would greatly improve the model's utility in characterizing multi-sloped, non-linear, alveolar plateaus. However it is our opinion that any major revision of the model's form should only be undertaken in conjunction with the development of a mathematical model of the physiological processes underlying the empirical data.

From the brief overview of the system, presented in the first three chapters of this thesis, one may begin to appreciate the scope of such an undertaking.

7.8 A Mandate to Formalize an Official Protocol

Considering the seriousness of the shortcomings we have described it would seem appropriate for the National Heart and Lung Institute to establish a committee to review and refine the protocol [151] it has distributed since 1973.

If agreement can be reached on a universally acceptable protocol for CV determinations that can be rigidly applied to at least normal

reference samples, then it would be a simple matter to develop an official, reliable, computer program for the protocol's implementation. Widespread distribution of a such a computer program for the analysis of single breath washout data could effectively dispell much of skepticism surrounding the reliability of CV analysis [33].

Most of the algorithms published for CV determination have treated their task with expedience, taking little note of other available algorithms or the proliferation of presently used protocols. To date only one author [169] has even cited the existence of another algorithm available for the determination of CV and he did so in the addendum to his paper!

It is of some importance that the NHLI or some other organization of suitable authority studies and finally adopts an official position on the protocol to be used in determining CV. For without careful study and the subsequent adoption of an acceptable protocol for the determination of CV, the continued proliferation of different algorithms for the analysis of single breath washout data could not help but produce further skepticism over the reliability of such analyses. This task is of pressing importance in that recent research [134] has finally shown that small airway pathology is related to increasing closing capacity in excised human lungs. This study also demonstrated a correlation between small airway pathology and an abnormal slope of the phase III segment of the SBN_2 curve. Furthermore, once an official protocol has been adopted it should be made imperative for

researchers to report further studies which involve CV measurements in accordance with this protocol as well as any other they may have devised or adopted.

7.9 Consideration of Cost, Complexity and Reliability

A refined protocol would undoubtedly increase the complexity of the algorithms used in the analysis of single breath washout data. However computational complexity and its associated cost cease to be of even the minor importance given them by Cramer [33] when algorithms similar to the ones described in this thesis can be handled by small, cheap microprocessors.

An ideal system would incorporate a microprocessor driven plotter which would enable the results of a suitable numerical analysis of the SBN_2 data to be immediately superimposed on the raw data obtained from the spirometer. Such a system would not only speed the processing of test results, but would allow the technician to immediately spot any unusual patterns involving step-jump in nitrogen concentration, [169] a multi-sloped alveolar plateau or artifact.

A simplified version of the non-linear algorithm described in this thesis has been implemented on a M6809 microprocessor [170].

This implementation provides an adequate analysis of the SBN_2 curve but has a turnabout time of over forty-five minutes due to the use of virtual arrays in interpreted Basic with a slow disk system. It should be soon possible to provide the clinician with a microprocessor for the on-line analysis of these curves based on refinements to the non-linear algorithm presented in this thesis.

Even simpler interactive systems in which the technician can immediately spot difficulties saves time for both the laboratory and the subject, and eliminates the error involved in hand calculation [33, 34]. Such a system is of great use in epidimiological studies where the volume of data makes the time required for manual interpretation and statistical analysis of the curves almost prohibitive [34, 35].

REFERENCES

1. Ainsworth, M, Eveleigh, J.W. A method of estimating lung resistance in humans. Tech. Paper No. 320, Chemical Defense Experimental Establishment, Ministry of Supply, Porton, Wistshire, England, 1952.

2. Aitken, R.S., Clark-Kennedy,A.E. On the fluctuation in the composition of the alveolar air during the respiratory cycle in muscular exercise. J. Physiol., London 65: 380-411, 1928.

3. Alkawa, J.K., Pinfield, E.R. Computerizing a Clinical Laboratory. Charles C. Thomas Ltd., Springfield, Illinois, 1973.

4. Arbus, G.S., Herbert, L.A., Levesque, P.R., et al. Characterization and clinical application of the "significant band" for acute respiratory alkalosis. N. Eng. J. Med., 280, 117-123, 1969.

5. Bates, D.V., Macklem, P.T., Christie, R.V. Respiratory Function in Disease, 2nd Ed., Saunders, Philadelphia, 1971.

6. Becklake, M.R., Permutt, S. Evaluation of tests of lung function for "screening" for early detection of chronic obstructive lung disease. In The Lung in Transition Between Health and Disease, Macklem, P.T., Permutt, S. (Eds.), Dekker, New York, 1979.

7. Becklake, M.R., M. Leclerc, H. Strobach, Swift, J. The N_2 closing volume test in population studies: Sources of variation and reproductivity. Am. Rev. Respirat. Diseases III, 141-147, 1975.

8. Begin, R., Renzett, A.D., Bigler, A.H., Watanabe, S. Flow and age dependence of airway closure and dynamic compliance. J. Appl. Physiol., 38, 199-207, 1975.

9. Bobbaers, H., Clement, J., Pandaens, J., Van de Woestijne, P. Simulation of frequence dependence of compliance and resistance in healthy man. J. of Appl. Physiol., 38, #3, 427-435, 1975.

10. Bouhuys, A. Breathing. New York: Grune and Stratton, 1974.

11. Bouhuys, A. Respiratory dead space. Handbook of Physiology. Respiration. Washington, D.C.: Am. Physiol. Soc., 1964, sect. 3, vol. I, chapt. 28, 699-714.

12. Bouhuys, A., Jonson, B. Alveolar pressure, airflow rate and lung inflation in man. J. Appl. Physiol. 22, 6, 1086-1100, 1967.

13. Branscomb, B.V., Larsen, R.I. Lung function models and indices. 7th Conf. Res. in Emphysema, Aspen 1965; Med. thorac 22: 382-398, 1965.

14. Brundin, A., Tammivaara-ilty, R. Clinical and physiological follow-up of severe chronic obstructive lung disease. Scan. J. of Resp. Dis. Suppl., 79, Munksgaard, Copenhagen, 1972.

15. Buist, A.S., Ross, B.B. Predicted values for closing volumes using a modified single breath nitrogen test. Am. Rev. Respirat. Diseases 107, 744-752, 1973.

16. Buist, A.S., Ross, B.B. Quantitative analysis of the alveolar plateau in the diagnosis of early airway obstruction. Am. Rev. Respirat. Diseases 108, 1078-87, 1973.

17. Buist, A.S., Van Fleet, D.L., Ross, B.B. A comparison of conventional spirometric tests and the test of closing volume in an emphysema screening center. Am. Rev. Respirat. Diseases 107, 735-743, 1973.

18. Buist, S., Nagy, J. A longitudinal study of smoker's and non-smokers. 5-6 year follow-up using spirometry and the single breath N2 test. Chest, 77 (2 Suppl), 259, 1980.

19. Clement, J., Van de Woestinjne, K.P. Validity of simple physical models in interpreting maximal expiratory flow-volume curves. Respiratory Physiol. 15, 70-86, 1972.

20. Clement, J., Van de Woestinjne, K.P., Pardaens, J. A general theory of respiratory mechanics applied to forced expiration. Respir. Physiol. 19, 60-79, 1973.

21. Comroe, J.H. Jr., Forster, R.E. II, Dubois, A.B., Briscoe, W.A., Carlsen, E. The Lung, 2nd ed., Chicago: Year Book, 1962.

22. Cook, C.D., Sutherland, J.M., Segal, S., Cherry, R.B., Mead, J., McIlroy, M.B., Smith, C.A. Studies of respiratory physiology. III. Measurements of mechanics of respiration. J. Clin. Invest. 36, 440-448, 1957.

23. Cooper, E.A. A comparison of the respiratory work done against an external resistance by man and by a sine wave pump. Quart. J. Exptl. Physiol. 45:179-191, 1960.

24. Cormier, Y.F., Belanger, J. The influence of active gas exchange on the slope of phase III at rest and after exercise. Am. Rev. Respir. Dis. 123, 213-216, 1981.

25. Cormier, Y., Mitzner, W., Menkes, H. Reverse nitrogen gradients in the study of phase III and cardiogenic oscillations of the single breath nitrogen test. Am. Rev. Respir. Dis. 120, 15-20, 1979.

26. Cormier, Y., Nadeau, D. Ventilation, perfusion, and cardiogenic oscillations of the single-breath N2 test. J. Appl. Physiol. 49(4):552-557, 1980.

27. Cosio, M.G., Ghezzo, H., Hogg, J.C., Corbin, R., Coveland, M., Dosman, J., Macklen, P.T. The relation between structural changes in small airways and pulmonary function tests. N. Engl. J. Med. 298, 1277-81, 1978.

28. Cosio, M.G., Hale, K.A., Hiewoehner, D.E. Morphologic and morphometric effects of prolonged cigarette smoking on the small airways. Am. Rev. Respir. Dis. 122, 265-271, 1980.

29. Cumming, G. Gas mixing efficiency in the human lung. Resp. Physiol. 2, 213-224, 1967.

30. Cumming, G., Horsfield, K., Preston, S.B. Diffusion equilibrium in the lungs examined by nodal analysis. Resp. Physiol. 12, 329-345, 1971.

31. Cumming, G., Crank, J., Horsfield, K., Parker, I. Gaseous diffusion in the airways of the human lung. Resp. Physiol. 1, 58-74, 1966.

32. Cumming, G., Horsfield, K., Jones, J.G., Muir, D.C.F. The influence of gaseous diffusion on the alveolar plateua at different lung volumes. Resp. Physiol. 2, 386-398, 1967.

33. Cramer, W.O., Miller, W.C. A computerized approach to closing volume determination. Ann. Allergy 38, 22-26, 1976.

34. Craven, N., Sidwall, G., West, P., McCarthy, D.S., Cherniack, R.M. Computer analysis at the single-breath nitrogen washout curve. Am. Rev. Respirat. Diseases 113, 445-449, 1976.

35. Dell, R.B., Engel, K., Winters, R.W. A computer program for the blood pH-logP_{CO_2} nomogram. Radiometer, 72 Emdrupveg, Copenhagen, 1972.

36. Dolluss, R.E., Milic-Emili, J., Bates, D.V. Regional ventilation of the lung, studied with boluses of ^{133}xenon. Respiration Physiol. 2, 234-246, 1976.

37. Dosman, J.A., Cotton, D.J., Graham, B.L., Hall, D.L., Li, R., Froh, F., Barnett, G.D. Sensitivity and specificty of early diagnostic tests of lung function in smokers. Chest 79(1), 6-11, 1981.

38. Dosman, J.A., Cotton, D.J., Graham, B.L., Hall, D., Froh, F., Barnett, G.D. Sensitivity of variables derived from the single breath nitrogen test in smokers. Chest 1980 (2 Suppl):286-289, 1977.

39. Ducic, S., Swift, J., Martin, R., Macklem, P. Appraisal of a new test: Between-technician variation in the measurement of closing volume. Am. Rev. Respirat. Diseases 112, 621-627, 1975.

40. Engel, L.A., Grassino, A., Anthonisen, N.R. Demonstration of airway closure in man. J. Appl. Physiol. 38, 1117-1125, 1975.

41. Engel, L.A., Macklem, P.T. Gas mixing and distribution in the lung. In Widdicombe, J.G., ed. MTP international review of physiology. Respiratory physiology II. Baltimore: University Park Press, 14:37-82, 1977.

42. Fairley, M.B. Airway closure. Anesthesiology. Vol. 36, No. 6, 529-532, 1972.

43. Farrell, E.J., Siegel, J.H. Simulation of respiratory regulation of blood gases in the ciritically ill patient. Computer Applications in Medical Care, 1976.

44. Feinberg, B.N., Chester, E.H., Schveffler, J.D. Parameter Estimation: A diagnostic aid for lung diseases. Instrumentation Technology, 40-46, July 1970.

45. Ferguson, G.A. Statistical Analysis in Psychology and Education 2nd Ed., McGraw Hill, New York, 1966.

46. Fletcher, R., Jonson, B., Cumming, G., Brew, J. The concept of deadspace with special reference to the single breath test for carbon dioxide. Br. J. Anaesth. 53, 77-87, 1981.

47. Fletcher, C.M. The problem of observer variation in medical diagnosis with special reference to chest diseases. Methods Int. Med., 3, 98-103, 1964.

48. Fletcher, C., Petro, R., Tinker, C., Speizer, F.E. The natural history of chronic bronchitis and emphysema. New York, Oxford University Press, 70-105, 1976.

49. Fowler, W.S. Lung function studies, III. Uneven pulmonary ventilation in normal subjects and in patients with pulmonary disease. J. Appl. Physiol., 2, 283-299, 1949.

50. Fraser, R.G., Pare, J.A.P. Structure and function of the lung, 2nd ed. Philadelphia, Saunders, 1971.

51. Frazier, A.R., Rehder, K., Sessler, A.D., Rodarte, J.R., Hyatt, R.E. Single-breath oxygen tests for individual lungs in awake man. J. Appl. Physiol. 40(3), 305-11, 1976.

52. Froberg, C.E. Introduction to Numerical Analysis. Reading: Addison-Wesley, p.198-203, 1969.

53. Fry, D.L., Hyatt, R.E. Pulmonary mechanics. A unified analysis of the relationship between pressure, volume and gas flow in the lungs of normal and diseased human subjects. Am. J. Med., 29, 672-689, 1960.

54. Fukuchi, Y., Cosio, M., Kelly, S., Engel, L.A. Influence of pericardial fluid on cardiogenic gas mixing in the lung. J. Appl. Physiol. Respirat. Environ. Exercise Physiol. 42(1), 5-12, 1977.

55. Fukuchi, Y., Roussos, C.S., Macklem, P.T., Engel, L.A. Convection, diffusion and cardiogenic mixing of inspired gas in the lung; an experimental approach. Resp. Physiol., 26, 77-89, 1976.

56. Glazier, J.B., Huges, J.M.B., Maloney, J.E., West, J.B. Vertical gradient of alveolar size in lungs of dogs frozen intact. J. Appl. Physiol., 23, 694-705, 1967.

57. Glaister, D.H., Schroter, R.C., Sudlow, M.F., Milic-Emili, J. Transpulmonary pressure gradient and ventilation distribution in excised lungs. Resp. Physiol. 17, 365-385, 1973.

58. Goldberg, M., Green, S.B., Moss, M.L., Marbach, C.B., Carfinkel, D. Computer-based instruction and diagnosis of acid-base disorders. J. Am. Med. Assoc., 223(3), 269-76, 1973.

59. Grene, M. Means, ends, and functions: Some problems with mechanism in biology. Am. Rev. Respir. Dis., 112, 325-28, 1975.

60. Guthrie, D. A History of Medicine. London: Nelson, 1945.

61. Guy, J., Gaines, R.A., Hill, P.M., Wagner, P.D., West, J.B. Computerized, noninvasive tests of lung function. Am. Rev. Respirat. Diseases, 113, 737-44, 1976.

62. Hale, K.A., Niewoehner, D.E., Cosio, M.G. Morphologic changes in the muscular pulmonary arteries: Relationship to cigarette smoking, airway disease, and emphysema. Am. Rev. Respir. Dis., 122, 273-278, 1980.

63. Hamming, R.W. Numerical Methods for Scientists and Engineers. New York: McGraw Hill, p.230-236, 1973.

64. Hamosh, P., Taveira da Silva, A.M. Air bolus method compared to single breath method for determination of closing volume. Am. Rev. Respirat. Diseases, 110, 518-20, 1974.

65. Hart, M.C., Orzalesi, M.M., Cook, C.D. Relation between anatomic respiratory dead space and body size and lung volume. J. Appl. Physiol., 18, 519-522, 1963.

66. Higgins, M.W., Keller, J.B. Seven measures of ventilatory function. Am. Rev. Respir. Dis., 108, 258-272, 1973.

67. Hildebrandt, J., Young, A.C. Anatomy and Physics of respiration; Section VIII, Chapter 39,. In Physiology and Biophysics, Ruch, T.C. and Patton, H.D. (Eds), W.B. Saunders, Philadelphia, 19th edition, 1965.

68. Hogg, J.C., Macklem, P.T., Thurlbeck, W.M. Site and nature of airway obstructure in chronic obstructive lung disease. N. Engl. J. Med., 278, 1355-60, 1968.

69. Holland, C.S. A linear dynamic model of the lung, including the effect of tissue interdependence. Masters Thesis, Dept. of Mechanical Engineering, McGill University, 1972.

70. Hoppin, F.G., Jr., Hildebrandt, J. Mechanical properties of the lung. In: Bioengineering Aspects of the Lung, edited by J.B. West. New York: Dekker, Vol. 3, p.83-162, 1977.

71. Horsfield, K. The relation between structure and function in the airways of the lung. Brit. J. Dis. Chest, 68, 145-160, 1974.

72. Horsfield, K., Cumming, G. Angles of branching and diameters of branches in the human bronchial tree. Bull. Math. Biophys., 28, 245-59, 1967.

73. Horsfield, K., Cumming, G. Functional consequences of airway morphology. J. Appl. Physiol., 24, 384-390, 1968.

74. Horsfield, K., Dart, G., Olson, D.E., Filley, G.F., Cumming, G. Models of the human bronchial tree. J. Appl. Physiol., 31, 207, 1971.

75. Hughes, J.M.B., Glazier, J.B., Maloney, J.E., West, J.B. Effect of lung volume on the distribution of pulmonary blood flow in man. Resp. Physiol., 4, 58-72, 1968.

76. Hyatt, R.E., Okeson, G.C., Rodarte, J.R. Influence of expiratory flow limitation on the pattern of lung emptying in normal man. J. Appl. Physiol., 35, 411-419, 1973.

77. Ingram, R.H., Jr., O'Cain, C.F. Frequency dependence of compliance in apparently healthy smokers versus non-smokers, lung and airways mechanics in normal man and in chronic lung diseases. Entretiens de Physiopathologie Respiratoire, Nancy, 8e Series (Peslin, R. Ed), Paris, Masson and Cie, 1971.

78. Irving, H. An interactive decision table interpreter for use in computer aided medical diagnosis. Masters Thesis, School of Computer Science, McGill University, 1976.

79. Jackson, A.C., Milhorn, H.T. Digital computer simulation of respiratory mechanics. Comput. Biomed. Res., 6, 27-56, 1973.

80. Jacquez, J. Respiratory Physiology. McGraw Hill, Washington, 1979.

81. Jansen, J.M., Peslin, R., Bohadana, A., Racineux, J.L. Usefulness of forced expiration slope ratios for detecting mild airway abnormalities. Am. Rev. Respir. Dis., 122, 221-230, 1980.

82. Katz, M. A probability graph describing the predictive value of a highly sensitive diagnostic test. N. Engl. J. Med. 294, 1115-1116, 1974.

83. Knopp, K. Infinite Sequences and Series. Dover Publications, Inc., N.Y., 1956.

84. Knudson, R.J., Lebowitz, M.D. Comparison of flow-volume and closing volume variables in a random population. Am. Rev. Respir. Dis. 116, 1039-46, 1977.

85. Knuth, D.E. Searching and Sorting. Addison-Wesley, Reading, 1973.

86. Lambert, R.K., Wilson, T.A. A model for the elastic properties of the lung and their effect on expiratory flow. J. Appl. Physiol. 34(1), 34-48, 1973.

87. Leblanc, P., Ruff, F., Milic-Emili, J. Effects of age and body position on airway closure in man. J. Appl. Physiol. 28, 1448-51, 1970.

88. Lecocq, H.F. A theoretical analysis of the continuous distribution of specific tidal volume throughout the lung with special reference to anatomical dead space. IEEE Trans. Biomed. Eng., Vol. BME-23, 2, 110-17, 1976.

89. Leung, K.V., O'Mara, K. The development of a model with time lag of human ventilation. Proc. 2nd International Conference on Medical and Biological Engineering, Ottawa, August 1976.

90. Leung, K.V., O'Mara, K. A mathematical analysis of the single breath gas washout curve. Proc. First Mediterranean Conference on Medical and Biological Engineering, Naples, Italy, Sept. 1977.

91. Linn, W.S., Hackney, J.D. Nitrogen and helium "closing volume": Simultaneous measurement and reproducibility. J. Appl. Physiol. 34, 396-399, 1973.

92. Lourenco, R.V. (Ed.). Clinical methods for the study of regulation of breathing. Chest, 70(1), Suppl. 109-45, 1976.

93. Macklem, P.T. Airway obstruction and collateral ventilation. Physiol. Rev. 51, 368-436, 1971.

94. Macklem, P.T. Respiratory mechanics. Annu. Rev. Physiol. 40, 157-184, 1978.

95. Macklem, P.T. Obstruction in small airways a challence to medicine. Amer. J. Med. 52, 721-724, 1972.

96. Macklem, P.T., Mead, J. The physiological basis of common pulmonary function tests. Arch. Env. Health 14, 5-9, 1967.

97. Macklem, P.T., Permutt, S. (Eds.). The lung in the transition between health and disease. Dekker, N.Y., 1979.

98. Margaria, R., Milic-Emili, G., Petit, J.M., Cavagna, G. Mechanical work of breathing during muscular exercise. J. Appl. Physiol. 15, 354-358, 1960.

99. Martin, R.R., Lemelin, C., Zuffer, M., Anthonisen, N.R. Measurement of "closing volume": Application and limitations. Bull. Physiol-Pathol. Respirat. 9, 979-995, 1973.

100. McAlister, N.H., Smith, I.D., Jennings, B.H., Mullin, J.K., Handforth, F.R., Toogood, J.H. Interactive programs for statistical computations and information display in chronic obstructive pulmonary disease research. Computers and Biomedical Research 7, 496-512, 1974.

101. McCarthy, D., Milic-Emili, J. Closing volume in asymptomatic asthma. Am. Rev. Respir. Dis. 107, 559-69, 1973.

102. McCarthy, D.S., Spencer, R., Green, R., Milic-Emili, J. Measurement of "closing volume" as a simple and sensitive test for early detection of small airway disease. Am. J. Med. 52, 747-753, 1972.

103. McFadden, E.R., Ingram, R.H. Clinical application and interpretation of airway physiology. In Nadel, J.A. (Ed.), Physiology and Pharmacology of the Airways, Dekker, 1980.

104. Mead, J. Personal communication.

105. Mead, J. Control of respiratory frequency. J. Appl. Physiol. 15, 325-336, 1960.

106. Mead, J. Mechanical properties of lungs. Physiol. Rev. 41, 281-330, 1961.

107. Mead, J. Respiration: Pulmonary mechanics. Ann. Rev. Physiol. 169-192, 1973.

108. Mead, J., Agostoni, E. Dynamics of breathing. In Handbook of Physiology. Section 3, Respiration, (W.O. Fenn & H. Rahn, Eds.), Vol. I. American Physiological Society, Washington, D.C., 1964.

109. Mead, J., Martin, H. Principles of respiratory mechanics. J. Am. Physical Therapy Association, Vol. 18, No. 5, 478-95, 1968.

110. Mead, J., Milic-Emili, J. Theory and methodology in respiratory mechanics with glossary of symbols. In Handbook of Physiology, Section 3, Respiration, (W.O. Fenn & H. Rahn, Eds.), Vol. I, American Physiological Society, Washington, D.C., 1964.

111. Menn, S.J., Barnett, G.O., Schmechel, D., Owens, W.D., Pontoppidan, H. A computer program to assist in the care of acute respiratory failure. J. Am. Med. Assoc. 223(3), 308-12, 1978.

112. Michaelson, E.D., Grassman, E.D., Peters, W.R. Pulmonary mechanics by spectral analysis of forced random noise. J. Clinical Investigation 56, 1210-1230, 1975.

113. Milic-Emili, J. The use of radioactive xenon in diagnostic procedures for pulmonary disease. Scan. J. Clin. Lab. Invest. 30, 1-4, 1972.

114. Milic-Emili, J., Henderson, A.M., Kaneko, K. Distribution of ventilation as investigated with radioactive bases. J. Biol. Nucl. Med. 11, 63-68, 1967.

115. Milic-Emili, G., Petit, J.M. Il lavoro meccanico della respirazione a varia frequenza respiratoria. Arch. Sci. Biol. 43, 326-330, 1959.

116. Milne, E.N. Correlation of physiologic findings with chest roentgenology. Radiologic Clinics of North America, Vol. XI, No. 1, 17-45, 1973.

117. Mitchell, R.S., Stanford, R.E., Johnson, J.M., Silvers, G.W., Dart, G., George, M.S. The morphologic features of the bronchi, bronchioles, and alveoli in chronic airway obstruction: A clinicopathologic study. Am. Rev. Respir. Dis. 114, 137-45, 1976.

118. Murray, C.D. The physiological principle of minimum work I. Proc. Nat. Acad. Sci. 12, 204-214, 1926a.

119. Murray, C.D. The physiological principle of minimum work II. Proc. Nat. Acad. Sci. 12, 299-304, 1926b.

120. Nash, E.S., Briscoe, W.A., Cournand, A. The relationship between clinical and physiological findings in chronic obstructive disease of the lungs. Med. Thorac 22, 305-27, 1965.

121. Nathan, S.P., Lebowitz, M.D., Knudson, R.J. Spirometric testing: number of tests required and selection of data. Chest, 76, 384-388, 1979.

122. Olson, D.E., Dart, G.A., Filley, G.F. Pressure drop and fluid flow regime of air inspired into the human lungs. J. Appl. Physiol. 28, 482-484, 1970.

123. O'Mara, K. The development of an algorithm for the diagnosis of pulmonary function. Proc. 5th Canadian Medical and Biological Engineering Conference, Montreal, Sept. 1974.

124. O'Mara, K., Fancott, T., Bezevin, J., Jaworski, W. A decision table acid-base interpreter. Proc. 2nd International Conference on Medical and Biological Engineering, Ottawa, August 1976.

125. O'Mara, K., Leung, K.V. Pulmonary function and its interpretation in lung disease. Proc. 13th International Conference on Internal Medicine, Helsinki, August 1976.

126. O'Mara, K., Leung, K.V., Fancott, T., Klasa, S. An algorithm for the non-linear lest-squares analysis of the single breath nitrogen washout curve. In G. Lasker (Ed.), Applied Systems and Cybernetics, Pergamon Press, New York, 1980.

127. O'Mara, K., Leung, K.V., Fancott, T., Klasa, S., Becklake, M. A mathematical analysis of the single breath nitrogen washout curve, to be published.

128. O'Mara, K., Leung, K.V., Fancott, T., Klasa, S., Frank, H. A model of acid-base balance in man, to be published.

129. Otis, A.B. The work of breathing. In Handbook of Physiology, Sec. 3, Respiration, Vol. 1, edited by W.O. Fenn, H. Rahn. Washington, D.C.: American Physiological Society, Chap. 17, 1964.

130. Otis, A.B., McKerrow, C.B., Bartlett, R.A., Mead, J., McIlroy, M.B., Selverstone, N.J., Radford, E.P. Mechanical factors in distribution of pulmonary ventilation. J. Appl. Physiol. 8, 427-443, 1956.

131. Paiva, M. Hypotheses underlying a continuous analysis of gas transport in a lung model. The Institute of Mathematics and its Applications, 17-21, 1978.

132. Pardaens, J., Van de Woestijne, P., Clement, J. A physical model of expiration. J. Appl. Physiol. 36(4), 479-490, 1972.

133. Pedley, T.J., Schroter, R.C., Sudlow, M.F. Gas flow and mixing in the airways. In Bioengineering Aspects of the Lung, Vol. 3, West, J.B. (Ed.), 1977.

134. Petty, T.L., Silver, G.W., Stanford, R.E., Baird, M.D., Mitchell, R.S. Small airway pathology is related to increased closing capacity and abnormal slope of phase III in excised human lungs. Am. Rev. Respir. Dis. 121, 449-456, 1980.

135. Petty, T.L. (Ed.). Chronic obstructive pulmonary disease. Dekker, N.Y., 1978.

136. Rahn, H., Farhi, L. Ventilation, perfusion, and gas exchange - V_A/Q concept. In Handbook of Physiology, Sec. 3, Respiration, Vol. I, Chap. 30, edited by W.O. Fenn, H. Rahn. Washington, D.C.: American Physiological Society, 1964.

137. Rashevsky, N. Mathematical Biophysics, 3rd ed. Dover, 1960.

138. Rasmussen, F., Solusteen, P., Andersen, L.H. Epidermiological limitations of the nitrogen closing volume test, closing volume physiology, methodology, epidemiology and clinical investigations. Scand. J. Respirat. Diseases Suppl. 95, 102-107, 1976.

139. Rehder, K., Marsh, H.M., Rodarte, J.R., Hyatt, R.E. Airway closure. Anesthesiology, 47, 40-52, 1977.

140. Richter, J.P. The notebooks of Leonardo da Vinci. Dover, N.Y., 1970.

141. Rohrer, F. Der Stromungswiderstand in den menschlieben Atemwegen und der Einfluss der unregelmässigen Verzweigung des Bronchial-systems auf den Atmungsverlauf in verschiedenen Lungenbrzirken. Arch. Ges. Physiol. 162, 225-299, 1915.

141. Rosen, R. Optimality principles in biology. London: Butterworths, pp.41-60, 1967.

142. Ruch, T.C., Patton, H.D. (Eds.). Physiology and Biophysics. Saunders, Philadelphia, 1965.

143. Sahni, S., Horowitz, E. Fundamentals of data structures. Computer Science Press, 1976.

144. Scheffe, The analysis of variance. Wiley, N.Y., 1959.

145. Sorensen, J.B., Morris, A.H., Crapo, R.O., Gandner, R.M. Selection of the best spirometric values for interpretation. Am. Rev. Respir. Dis., Vol. 122, 802-805, 1980.

146. Strobech, H. Unpublished data.

147. Tammeling, G., Quanjer, Ph., Visser, B., Lende, R.V.D. Airway closure and expiratory flow limitations in relation to smoking habits and symptoms on CNSLD, closing volume physiology, methodology, epidemiology and clinical investigations. Scan. J. Respirat. Diseases Suppl. 95, 73-79, 1976.

148. Thompson, D'Arcy. On growth and form. Bonner, J.T. (Ed.), Cambridge University Press, Cambridge, 1966.

149. Travis, D.M., Green, M., Don, H.F. Expiratory flow rate and closing volumes. J. Appl. Physiol. 35, 626-630, 1973.

150. Uhl, R.R., Lewis, F.J. Digital computer calculation of human pulmonary mechanics using a least squares F,t technique. Comput. Biomed. Res. 7, 489-95, 1974.

151. U.S. Department of Health, Education, and Welfare. National Heart and Lung Institute, Division of Lung Diseases. Suggested standardized procedures for closing volume determinations (nitrogen method). Bethseda:National Heart and Lung Institute, 1973.

152. Van Meerten, R.J., Duринck, J.R., De Wit, C. Computer-guided diagnosis of asthma, asthmatic bronchitis, chronic bronchitis and emphysema. Respiration 28, 399- , 1971.

153. Vogel, J., Muller, E., Merker, G., Visser, B.F., Kowalski, J., Wuthe, H. EDV-gerechte Residualvolumenbestimmung und alveolargas-analytische Verteilungsanalyse bei epidemiologischen Reihenuntersuchungen. Z. Erkrank. Atm.-Org. 146, 3-11, 1976.

154. Wagner, P.D., West, J.B. Changes in ventilation-perfusion relationships and gas exchange. In The lung in the transition between health and disease. Macklem, P.T. & Permutt, S. (Eds.), Dekker, N.Y., 1979.

155. Wartak, J. Mathematical model for medical diagnosis. Comp. Biol. Med., Vol. 4, No. 2, 79-84, 1974.

156. Warner, H.R. Computer-assisted medical decision-making. New York: Academic Press, 1979.

157. Weibel, E.R. Morphological basis of alveolar-capillary gas exchange. Physiol. Rev. 53, 419-495, 1973.

158. Weibel, E.R. Morphometry of the human lung. New York: Academic Press, 1963.

159. Weibel, E.R., Gomez, D.M. Architecture of the human lung. Science, 137, 573, 1962.

160. West, J.B. Ventilation/blood flow and gas exchange. Blackwell, London, 3rd edition, 1977.

161. Wilson, ¢. Relations among recoil pressure, surface area, and surface tension in the lung. J. Appl. Physiol. Respirat. Environ. Exercise Physiol., 50(5), 921-926, 1981.

162. Woolcock, A.J., Vincent, N.F., Macklem, P.T. Frequency dependence of compliance as a test for obstruction in the small airways. J. Clin, Invest. 48, 1097, 1969.

163. Bezevin, J., Fancott, T., O'Mara, K., Jaworski, W. Interactive decision based diagnosis by computer. Proc. 6th Annual Conference of the Society for Computer Medicine, Boston, Nov. 1976.

164. Blum, E.K. Numerical Analysis Theory and Practice. Addison Wesley, p.108-109, 1972.

165. Gomez, D.M. A physico-mathematical study of lung function in normal subjects and in patients with obstructive pulmonary diseases. 7th Conf. Res. in Emphysema, Aspen 1964, Med. Thorac. 22, 274-294 (1965).

166. West, J.B. (Ed.). Bioengineering Aspects of the Lung. Dekker, New York, 1977.

167. Oderr, C. Architecture of the lung parenchyma. Am. Rev. Respir. Dis. 90(3), 401-410, 1964.

168. Reynolds, O. An experimental investigation of the circumstances which determine whether the motion of water shall be direct or sinuous, and of the law of resistance in parallel channels. Philos. Trans. R. Soc. London, 194, 935-982, 1883.

169. Hankinson, J.L. Computer determined closing volumes. Computers and Biomedical Research 10, 247-257, 1977.

170. O'Brien, A. 491 Project.
Dept. of Computer Science, Concordia University.

APPENDIX B

A MATHEMATICAL ANALYSIS OF THE SINGLE BREATH GAS WASHOUT CURVE

Leung, K.V., O'Mara, K.

Department of Computer Science, Concordia University, Montreal, Quebec, Canada.

In: F. Denoth (Ed.). Digest of Papers, First Mediterranean Conference on Medical and Biological Engineering, Sorrento [Napoli], ITALY. Sept. 1977, p. 6.25-6.28.

INTRODUCTION

In 1967 Dollfuss, Milic-Emili & Bates first described a method, using ^{133}xenon as a tracer gas, for determining the lung volume at the onset of closure, or closing volume (CV), in gravitationally dependent airways [5]. Since then other inert gases such as helium and nitrogen have been used in extensive studies of closing volume measurements [2], their reproducibility [1] [11] and diagnostic use [3] [12] in health and disease.

The closing volume test is of clinical interest in that it is an easily performed, non-invasive measurement related to small airway function. As such it has been proposed as a simple sensitive test for the detection and assessment of early obstructive lung disease [9] [10].

While this test has been shown to be well-suited to use in a respiratory disease screening program, the prognostic implications of an increased closing volume are not yet known [13]. In fact, while the closing volume test may be considerably more sensitive than any other single

test of small airway function, it is not yet known if individuals with abnormally large closing volumes will eventually manifest irreversible airway obstruction [4] [12].

A major difficulty in the application of the single breath gas washout tests to the clinical evaluation of lung function is that visual examination is a very subjective method for determining the onset of airway closure [8] [11]. More reliable techniques involving the mathematical analysis of these curves are essential for the quantitative evaluation of closing volumes in the study of small airway function [6].

In this paper we outline the development of a numerical technique giving an optimal least squares estimate of the slopes of the phase III, alveolar plateua, and phase IV component of single breath gas washout curves.

The best broken line fit of the phase III and phase IV components of the gas washout curves is then used to determine the point of onset of small airway closure.

METHOD & THEORY

The single breath nitrogen washout curve shown in Fig. I will be considered for our purposes to be a tabulated function of N discrete observations of nitrogen concentration, Y_n, at a given lung volume, x_n: (x_1,Y_1), $(x_2,Y_2),\ldots,(x_N,Y_N)$, with $x_1 \leq x_2 \leq \ldots, \leq x_N$.

We wish to estimate the nitrogen concentration at any lung volume within the domain specified by the phase III and phase IV components of the gas washout curve as:

$$y = \begin{cases} \alpha x + \eta - \alpha\xi & \text{if } a \leq x \leq \xi, \\ \beta x + \eta - \beta\xi & \text{if } \xi \leq x \leq b, \end{cases}$$

where α, β are the slopes of the phase III and phase IV segments of the washout curve, a and b are the boundary points of the experimental data, and η and ξ specify the nitrogen gas concentration and lung volume components at the onset of closing volume.

In order to obtain optimal estimates of the slopes of the phase III and phase IV components of single breath gas washout curves and the point of onset of closing volume, we wish to determine the parameters α, β, ξ, η so as to reduce their sum of squares of errors, $\Gamma(\alpha, \beta, \xi, \eta)$, to a minimum. The sum of squares of errors Γ, for a given set of parameters, α, β, ξ, η, may be calculated as:

$$\Gamma(\alpha,\beta,\xi,\eta,x_n,Y_n) = \sum_{n=1}^{N} [y(\alpha,\beta,\xi,\eta,x_n) - Y_n]^2$$

$$= \sum_{n=1}^{K} [\alpha x_n + \eta - \alpha\xi - Y_n]^2 + \sum_{n=K}^{N} [\beta x_n + \eta - \beta\xi - Y_n]^2, \quad (1)$$

with K dependent on ξ such that $x_K \leq \xi \leq x_{K+1}$.

The set of parameters, α, β, ξ, η, that reduce (1) to a minimum are a solution of the following 4 equations which are obtained by equating each of four partial derivatives of (1) with respect to these parameters to zero:

$$\frac{1}{2}\frac{\partial}{\partial\alpha}\Gamma(\alpha,\beta,\xi,\eta,x_n,Y_n) = \sum_{n=1}^{K}[(x_n-\xi)\alpha+\eta-Y_n][x_n-\xi] = 0 \qquad (2)$$

$$\frac{1}{2}\frac{\partial}{\partial\beta}\Gamma(\alpha,\beta,\xi,\eta,x_n,Y_n) = \sum_{n=K+1}^{N}[(x_n-\xi)\beta+\eta-Y_n][x_n-\xi] = 0, \qquad (3)$$

$$\frac{1}{2}\frac{\partial}{\partial\eta}\Gamma(\alpha,\beta,\xi,\eta,x_n,Y_n) = \sum_{n=1}^{K}[(x_n-\xi)\alpha+\eta-Y_n] + \sum_{n=K+1}^{N}[(x_n-\xi)\beta+\eta-Y_n] = 0, \qquad (4)$$

$$\frac{1}{2}\frac{\partial}{\partial\xi}\Gamma(\alpha,\beta,\xi,\eta,x_n,Y_n) = \sum_{n=1}^{K}\alpha[\alpha(x_n-\xi)+ \quad -Y_n] + \sum_{n=K+1}^{N}\beta[\beta(x_n-\xi)+\eta-Y_n] = 0. \qquad (5)$$

Solving (2) and (3) for α and β in terms of ξ and η, we obtain:

$$\alpha = \alpha(\xi,\eta) = -\frac{P(\xi)}{Q(\xi)} + \frac{\mu(\xi) - \xi\lambda(\xi)}{Q(\xi)}, \qquad (6)$$

$$\beta = \beta(\xi,\eta) = -\frac{S(\xi)}{T(\xi)} + \frac{[B-\mu(\xi)] - \xi[A-\lambda(\xi)]}{T(\xi)}, \qquad (7)$$

where

$$A = \sum_{n=1}^{N} Y_n, \quad B = \sum_{n=1}^{N} x_n Y_n, \quad P(\xi) = \sum_{n=1}^{K}(x_n-\xi), \quad Q(\xi) = \sum_{n=1}^{K}(x_n-\xi)^2$$

$$S(\xi) = \sum_{n=K+1}^{N} (x_n - \xi) , \quad T(\xi) = \sum_{n=K+1}^{N} (x_n - \xi)^2 , \quad \lambda(\xi) = \sum_{n=1}^{K} Y_n ,$$

$$\mu(\xi) = \sum_{n=1}^{K} x_n Y_n$$

with $K = K(\xi)$ such that

$$x_k \leq \xi \leq x_{K+1} .$$

Eliminating α and β from (4), we get η in terms of ξ only:

$$\eta = \eta(\xi) = \frac{\frac{P(\xi)}{Q(\xi)}[\mu(\xi) - \xi\lambda(\xi)] + \frac{S(\xi)}{T(\xi)}[B - \xi A + \xi\lambda - \mu] - A}{\frac{[P(\xi)]^2}{[Q(\xi)]^2} + \frac{[S(\xi)]^2}{[T(\xi)]^2} - N} \tag{8}$$

Hence from (6) and (7) α and β become functions of ξ only, and (5) may be rewritten as follows:

$$\Phi(\alpha(\xi), \beta(\xi), \xi, \eta(\xi), x_n, Y_n) = \alpha^2 P(\xi) + \beta^2 S(\xi)$$

$$+ \{K(\xi)\alpha + [N - K(\xi)]\beta\} - \alpha\lambda(\xi) - \beta[A + \lambda(\xi)] - 0 . \tag{9}$$

The zeros of (9) may then be obtained by an iterative algorithm employing the variable secant method. This method uses two arbitrarily chosen values of ξ to generate a sequence of ξ that may converge to the zeros of (9) by using the iterative formula:

$$\xi_{r+1} = \xi_r - \frac{\Phi(\xi_r)}{\Phi(\xi_r) - \Phi(\xi_{r-1})}[\xi_r - \xi_{r-1}] .$$

The zero of (9) that reduces the sum of squares of errors $\Gamma(\alpha,\beta,\xi,\eta,x_n Y_n)$, to a global minimum optimally specifies the value of ξ at the point of onset of airway closure.

RESULTS

Starting from either end of the single breath nitrogen washout curve shown in Fig. I it took our algorithm 11 iterations to converge to two estimates of closing volume that were in agreement to within 1% of the vital capacity.

The method outlined here provides numerically optimal estimates of onset of airway closure and is insensitive to the gross cardiogenic oscillations which can hamper the evaluation of closing volume curves.

The objective numerical evaluation, provided by this method, should enhance the application and acceptability of closing volume determinations in epidemiological and clinical studies of small airway functions.

REFERENCES

[1] Becklake, M. R., Leclerc, M., Strobach, H., and Swift, J.: The N_2 closing volume test in population studies: Sources of variation and reproductivity,

Am. Rev. Respir. Dis., 1975, 111, 141.

[2] Buist, A. S., and Ross, B.B.: Predicted values for closing volumes using a modified single breath nitrogen test, Amer. Rev. Resp. Dis., 1973, 197, 744.

[3] Buist, A. S., and Ross, B. B.: Quantitative analysis of the alveolar plateau in the diagnosis of early airway obstruction, Am. Rev. Resp. Dis., 1973, 108, 1078.

[4] Buist, A. S., Van Fleet, D. L., and Ross, B. B.: A comparison of conventional spirometric tests and the test of closing volume in an emphysema screening center, Am. Rev. Resp. Dis., 1973, 197, 735.

[5] Dollfuss, R. E., Milic-Emili, J., and Bates, D. V.: Regional distribution of ventilation of the lung studied with boluses of ^{133}xenon, Resp. Physiol., 1967, 2, 234.

[6] Ducic, S., Swift, J., Martin, R., and Macklem, P.: Appraisal of a new test: Between-technician variation in the measurement of closing volume, Am. Rev. Resp. Dis., 1975, 112, 621.

[7] Fletcher, C. M.: The problem of observer variation in medical diagnosis with special reference to chest diseases, Methods inf. Med., 1964, 3, 97.

[8] Linn, W. S., and Hackney, J. D.: Nitrogen and helium "closing volume": Simultaneous measurement and reproducibility, J. Appl. Physio., 1973, 34, 396.

[9] Macklem, P. T.: Obstruction in small airways: a challenge to medicine, Amer. J. Med., 1972, 52, 721.

[10] McCarthy, D. S., Spencer, R., Greene, R., and Milic-Emili, J.: Measurement of "closing volume" as a simple and sensitive test for early detection of small airway disease, Amer. J. Med., 1972, 52, 747.

[11] Martin, R. R., Lemelin, C., Zutter, M., and Anthonisen, N. R.: Measurement of "closing volume": Application and limitations, Bull. Physiopathol. Respir. (Nancy), 1973, 9, 979.

[12] Rasmussen, F., Solvsteen, P., and Andersen, L.: Epidemiological limitations of the nitrogen closing volume test, Closing volume physiology, methodology, epidemiology and clinical investigations, Scan. J. Resp. Dis. Supp., 1976, 95, 192.

[13] Tammeling, G., Quanjer, Ph., Visser, B., and Lende, R. V. D.: Airway closure and expiratory flow limitations in relation to smoking habits and symptoms of CNSLD, Closing volume physiology, methodology, epidemiology and clinical investigations, Scan. J. Resp. Dis. Supp., 1976, 95, 73.

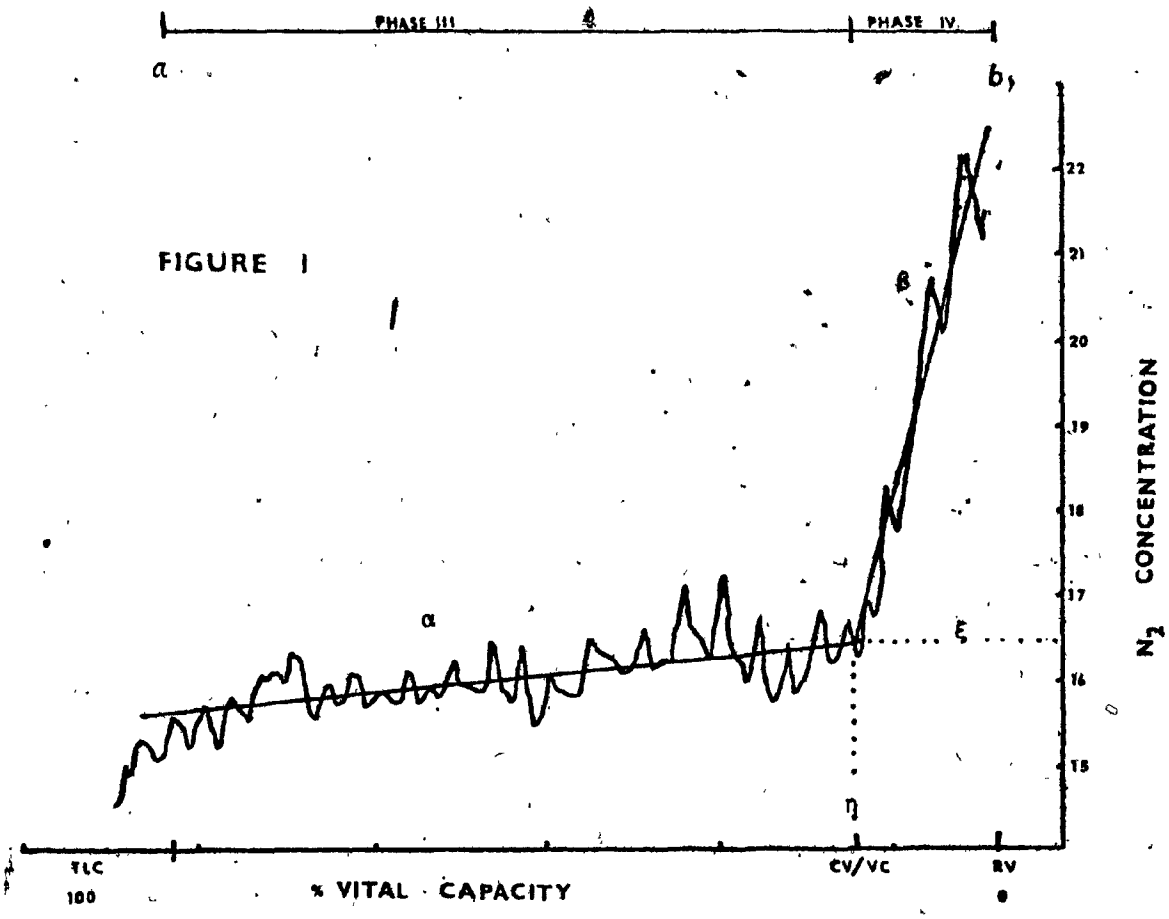
PHASE III
PHASE IV
a
b
α
β
γ
ξ
η
22
21
20
19
18
17
16
15
N_2 CONCENTRATION
TLC
100
% VITAL CAPACITY
CV/VC
RV
0

FIGURE 1

ACKNOWLEDGEMENTS

This work was based on an analysis of clinical data supplied by McGill University's Dept. of Epidemiology and Health through the courtesy of Dr. Margaret Becklake and Helen Strobach.

APPENDIX 1 PROGRAM FLOWCHART

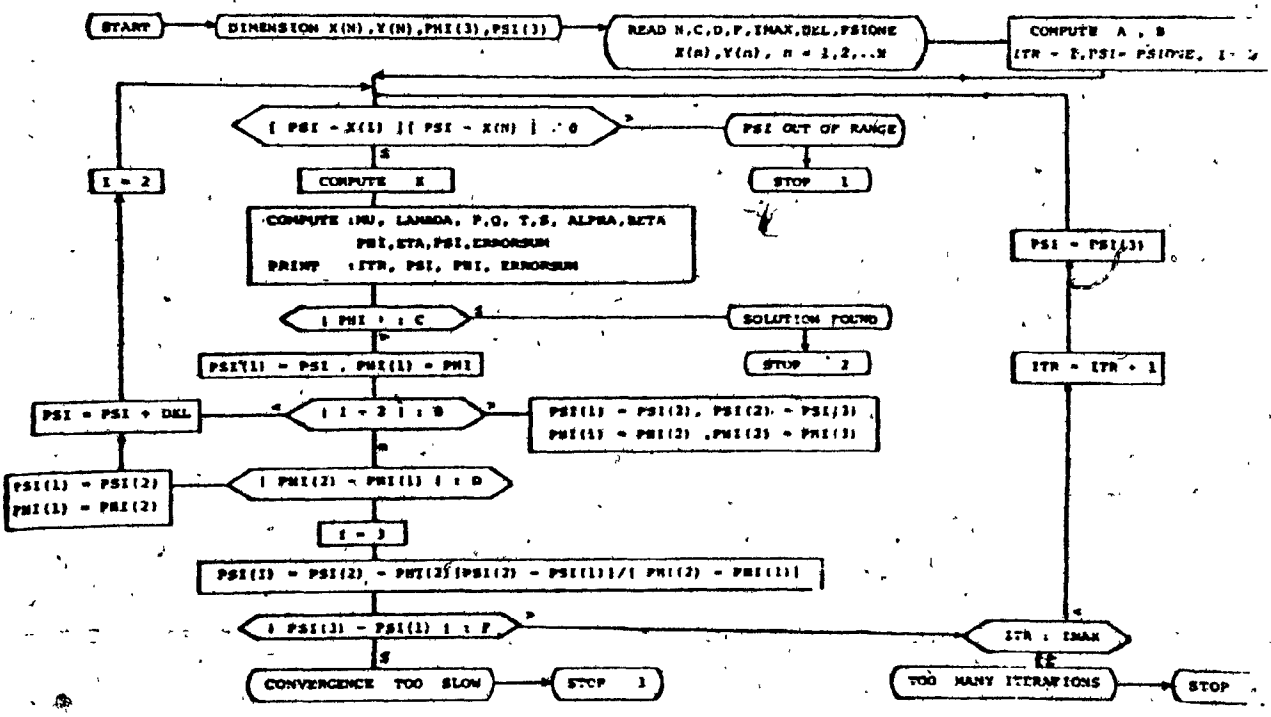

APPENDIX 2

SUGGESTED STANDARDIZED PROCEDURES

FOR

CLOSING VOLUME-DETERMINATIONS (NITROGEN METHOD)

July 1973

Distributed by:

Division of Lung Diseases
National Heart and Lung Institute

TABLE OF CONTENTS

FOREWORD

As part of a continuing effort to provide the pulmonary biomedical communi with topical reports, the Division of Lung Diseases is distributing the following protocol for closing volume measurements, prepared by Drs. Richard Martin and Peter Macklem in collaboration with other investigators participating in a Division of Lung Diseases contract program on the early diagnosis of chronic airways obstruction.

Representing the results of an effort to develop a common methodology for the performance and interpretation of closing volume tests, these procedures were developed as part of a multi-center, collaborative epidemiologic study of the reliability, reproducibility, sensitivity and possible long-term significance of closing volume abnormality. While they do not represent the only method of closing volume measurement nor do they reflect any official position of the National Heart and Lung Institute, it is hoped that this suggested protocol will provide a useful basis for any investigators contemplating studies of this physiologic measurement using the nitrogen method.

I. Introduction

In September 1971, the Division of Lung Diseases sponsored an Epidemiology Workshop which reviewed the Division's grant and contract programs dealing with pulmonary disease epidemiology and made recommendations for new program initiatives. Representing expertise in epidemiology both from this country and abroad, the consultants at the workshop placed highest priority on recommendations for new research programs focusing on methods of early detection as a first step towards documenting the natural history of chronic lung disease in populations, and ultimately as an approach to prevention.

The Division acted upon this recommendation with the issuance of a request for contract proposals (RFP) in February of 1972. The RFP focused on issues of major importance to national health: chronic obstructive lung diseases, smoking, and early diagnosis as a step towards documenting possible reversibility. It was hoped that the contract mechanism would provide a useful aid to collaboration between institutions engaged in this type of study.

Four contracts were awarded under this program in September 1972 (see Appendix A) after an extensive scientific review by an ad hoc review committee of peer scientists. All four institutions are studying physiologic abnormalities of peripheral or small airways as an early, and possibly reversible, manifestation of chronic obstructive lung disease. Various physiologic measurements may reflect dysfunction in this region of the lung, including the determination of closing volume. One group (Rancho Los Amigos) is developing a new type of apparatus for making this measurement, using boluses of methane and is applying it to a well-defined population of smokers and nonsmokers. Three other institutions (McGill University, University of Oregon, and University of Manitoba) are part of an investigator-initiated collaboration which seeks to demonstrate: 1) the usefulness of the measurement of closing volume as a simple reliable screening test for detecting obstruction in small airways; 2) the prevalence of small airways obstruction at a stage when other routine tests of lung function are not clearly abnormal; and 3) the natural history of this abnormality and how it may be modified by the cessation of smoking.

The following methodology represents an effort by the latter three institutions to develop a standardized procedure for administering and reading closing volume curves.

For their collaborative, epidemiologic study the investigators chose to use the nitrogen method of closing volume determinations (i.e., resident nitrogen as the test gas; vital capacity of pure oxygen). Factors influencing this choice included: portability of equipment; relative procedural simplicity compared to other techniques; the fact that all centers had some field survey experience with this method; and the possibility of also obtaining a measure of total lung capacity from the closing volume single breath record. For other investigators, the choice between this method and various bolus techniques will largely depend on the setting and goals of individual studies.

Figure 1. EQUIPMENT SCHEMATIC

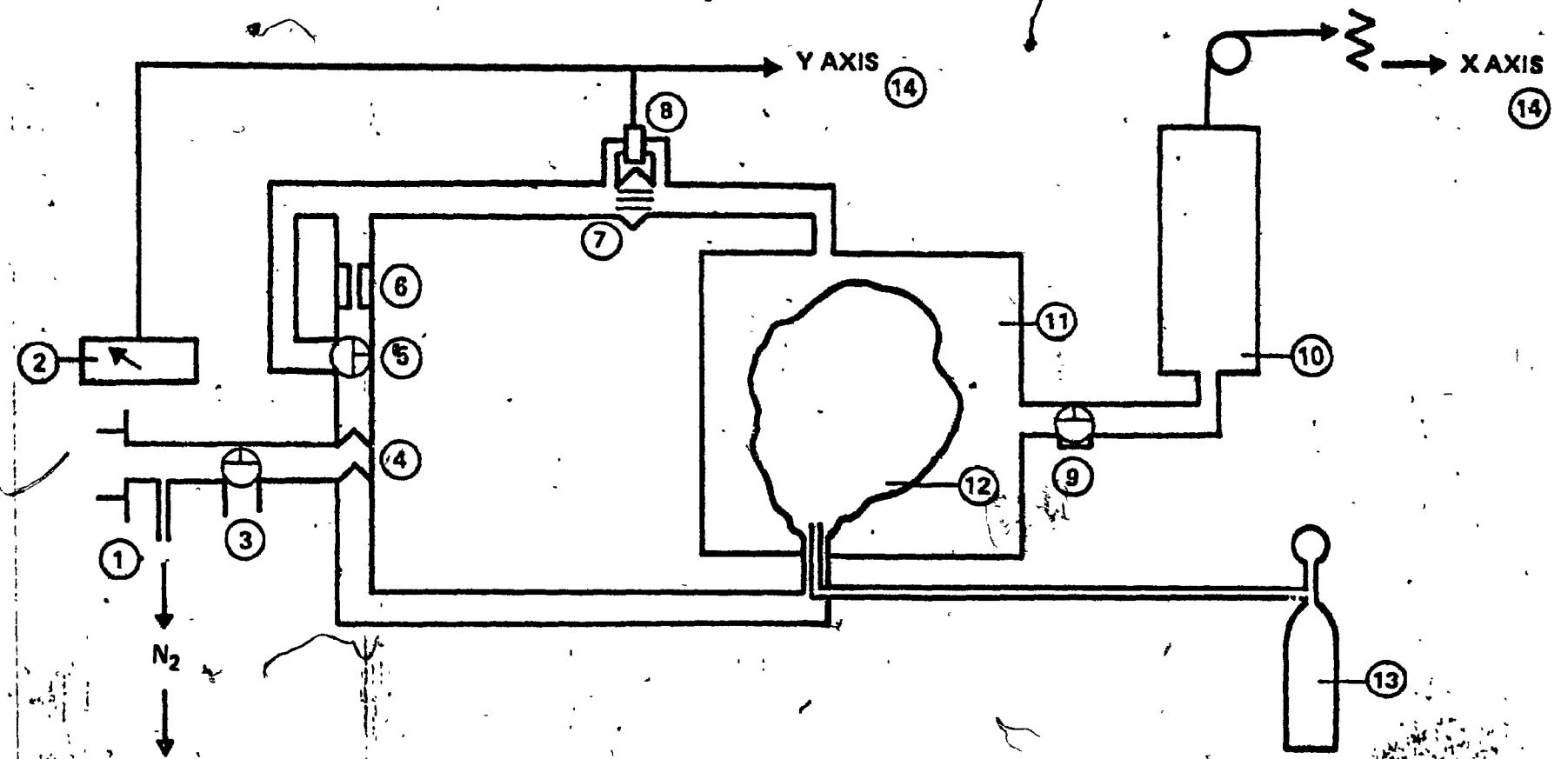

LEGEND

(See text for complete description)

1. MOUTHPIECE WITH NITROGEN METER SIDE PORT
2. GALVANOMETER FOR FLOW DISPLAY
3. 3-WAY VALVE
4. BREATHING VALVE-ONE WAY
5. 3-WAY VALVE
6. ALINEAR RESISTANCE
7. PNEUMOTACHYGRAPH
8. DIFFERENTIAL TRANSDUCER
9. 3-WAY VALVE
10. 9 L. SPIROMETER
11. 35 L. BOX
12. 30 L. RUBBER BAG
13. OXYGEN SUPPLY
14. XYY RECORDER

In pilot studies thus far, this nitrogen method protocol has been found to be reliable, reproducible and simple enough to be directed completely by trained technicians.

II. Suggested Nitrogen Method Closing Volume Protocol

A. Equipment (see Figure 1)

The numbers (#) correspond to those in the equipment schematic, figure 1.

1. Mouthpiece (not of dixie cup type); port for the nitrogen meter. The specific nitrogen analyzer has not yet been chosen but possibilities include:

   a. Med-Science 505-B
   b. CPI Linear Model 410
   c. Hewlett Packard 47302A

   Output of the nitrogen analyzer activates one Y axis of an XYY recorder.

2. Galvanometer attached to the output of the amplified pneumotachygraph signal. This galvanometer should be calibrated so that mid-range is equal to 0.5 lps. It is used to help the subject control his expired flow rate.

3. #5 Standard 3-way tap (e.g., Collins)

4. Breathing valve. Possibilities include:

   The standard Hans Rudolph valve has a very small dead space but does offer some resistance which will damp peak flow. However, the rest of the flow volume curve should be accurately transcribed.

   A modified Otis-McKerrow valve with negligible resistance, very small opening pressure (even when parts are wet) and a reasonably low dead space.

   Note: A P-312 Lloyd valve is not recommended due to high opening pressure requirements and problems with sticking of the valve flaps.

5. Three-way valve to allow the subject to exhale through the resistance during closing volume measurements or through no resistance for maximum expiratory rates.

6. Alinear resistance (approximately 12 cm H_2O/lps) to assist control of expiratory flow during closing volume maneuvers.

7. Fleisch #3 pneumotachygraph. The screen should be heated as it is in the expired line where condensation could be a major problem. A #3 pneumotachygraph was chosen rather than a #4 because of a better signal/noise ratio at very low flow rates. (Peak expiratory flows will not be accurately recorded, but it is doubtful that the frequency response of the XYY recorder would be adequate to record them accurately anyway).

8. Sanborn differential transducer #270 coupled to a pneumotachygraph and amplified by a Sanborn 8805-A carrier preamplifier. Two parallel outputs will be taken; one for the galvamometer in front of the subject and one to activate one of the Y axes of the recorder. Validyne differential pressure transducer Model MP45 or DP15 and transducer indicator Model CD12 could be used in place of the equivalent Sanborn Transducer and Carrier preamplifier.

9. Three-way valve, without its stopping pin to allow connection between box and spirometer; box and atmosphere or spirometer and atmosphere.

10. 9-liter spirometer, with a potentiometer to generate an electrical signal that will activate the common X axis of the XYY recorder.

11. 35 liter box.

12. 30 liter rubber bag. The bag filled with pure oxygen is the only place from which the subject can inhale when valve #3 is turned and he is in the circuit.

13. Oxygen supply.

14. Recorder. Honeywell #150 XY_1Y_2 recorder allowing for simultaneous recording of the flow volume curve and the N_2 volume curve.

    One can also use Hewlett Packard XY_1 Y_2 recorder No. 7046 A.

    For all intents and purposes, these two machines are identical in accuracy on the XY_1 Y_2 as regard to linearity; repeatability and FS accuracy. The choice between these two types of recorder should be made on the availability of service in the area.

Optional Modifications:

- A waterless spirometer (wedge Med-Sci; rolling seal - CPI) may be substituted for the pneumotachygraph, Sanborn 270 transducer and Collins Spirometer.

- An electrical integrator which measures the area under the N_2 - volume curve can be added.

B. Calibration

1. Twice daily
   - Balancing of the transducer

2. Daily
   - volume calibration with a known standard over a 5 liter range
   - nitrogen meter with 2 points, i.e., 0 and 80% N_2 dry gas
   - Pneumotachygraph with electrical calibration signal

3. Weekly
   - Nitrogen meter with concentrations of 0, 5, 10, 20, 50, 80%, all dry N_2 from either tonometered or calibrated tanks. With sufficient experience, monthly calibrations may prove adequate.

4. Every 3 months
   - Pneumotachygraph calibration check with rotameters over flow range of 0 to 0.8 lps.
   - Spirometer calibrations check over volume range 0-9 liters.

C. Procedure

(All numbers in parentheses refer to equipment schematic, figure 1).

1. Nitrogen washout of the circuit

At the beginning of the day, with valve (3) in the mouth-to-air position and valve (9) in the box-to-air position, O_2 should be flushed into the bag and gas allowed to evacuate freely at valve (9) so that nitrogen is washed out of circuit between the O_2 bag and valve (4). From then on there should be no contamination of that part of the circuit during the day.

2. Preparation for each test

The bag (12) is filled with oxygen (13). Valve (9) is then turned to connect the spirometer (10) to air and the bell is raised to approximately 80% of its capacity. Valve (9) is then turned to connect the spirometer to the box (11).

3. Performance of the test

The subject comes onto the mouthpiece (1) with valve (3) turned so that he is breathing room air. After a few quiet breaths, the subject takes two deep breaths and exhales to residual volume. As he approaches RV, the tap (3) is turned connecting him with the circuit and $F_{A_{N_2}}$ is measured. The operator urges the subject to breathe out until the volume tracing shows no further changes. At this point, he inspires a vital capacity breath of pure O_2 from the bag and, without breath holding, he expires a second time to residual volume. Tap (3) is then turned so that the subject breathes room air again. The subject monitors expiratory flow rates through

the voltage output display (2) of the transducer (8) connected to the pneumotachygraph (7). He is instructed to maintain expiratory flow at 0.4 lps.

The operator urges the subject repeatedly at both extremes of vital capacity; during exhalation for the measurement, however, it must be only after the phase IV deflection has appeared.

4. Number of measurements per subject

A minimum of 3 and a maximum of 6 measurements are made. The number of measurements is determined by eyeballing criteria for acceptance of the curves (see next section).

Complete O_2 washout is not necessary between measurements. This of course necessitates accurate F_{AN_2} measurements. However, it is advisable to delay repeating the test if, during preliminary phase breathing air, inspiratory and expiratory nitrogen concentration differ by more than 5%.

D. Criteria for Acceptability of Single Breath N_2 Closing Volume Curves

The following criteria must be met for acceptability; failure to satisfy any one of these leads to rejection of the curve:

1. Mean expiratory flow after the first 500 ml is expired must equal or be less than 0.5 lps (the subject is instructed to aim for 0.4 lps).

2. Except for the first 500 ml of expiration during closing volume measurement, expiratory flow transients must not exceed 0.7 lps. Unacceptable flow transients are defined as deviation from the required flow which persists during expiration of more than 300 ml.

3. Difference between inspired and expired VC must be less than 5%.

4. Differences in VC between blows must not exceed 10%.

5. There must not be a step change in the expired N_2 concentration with continued cardiogenic oscillations after the step. The causes of such step changes are obscure but are probably not related to airway closure. If such curves are accepted the onset of Phase IV will frequently be read as the volume at which the step occurs.

E. Measurements to be Made From Acceptable Curves

Ideally on all subjects 3 acceptable tracings will be obtained. The mean of the 3 values of each measurement is taken as the final value. When only 2 readable tracings are obtained, the mean of the

2 values is used. When only one readable tracing is obtained, the subject is discarded from the series. Readers must keep a careful track of the number of individuals with 3, 2, 1 and 0 readable curves.

Figure 2 depicts a sample closing volume tracing.

1. Closing Volume (CV)

The onset of phase IV should be determined by the best-fit line drawn by eye through the latter half of phase III. The point of final departure from this line is the onset of phase IV. In some subjects there is a sharp drop in N_2 concentration after the onset of phase IV. Occasionally this can intersect the line drawn through phase III. Under these circumstances the onset of phase IV istaken as the first definite point of departure of the N_2 tracing from the best-fit line. The closing volume is the volume from the onset at phase IV to residual volume (RV). CV is usually expressed as % of the expired vital capacity (VC).

2. Closing Capacity (CC)

Closing capacity is defined as closing volume plus residual volume (CV + RV) and is usually expressed as % of total lung capacity (TLC).

3. Total Lung Capacity (TLC)

TLC can be calculated from the alveolar dilution equation using V_{EN_2} determined by planimetry or by electrical integration of the area under the single breath curve:

$$TLC = \frac{V_I F_A N_2 - \overline{V_E N_2}\left(\frac{V_D}{V_E - V_D}\right)}{F_A N_2 - \frac{\overline{V_E N_2}}{V_E - V_D}}$$

4. Residual Volume (RV)

RV can be derived by subtracting the recorded vital capacity from TLC.

5. Slope of phase III

The slope of phase III is determined by the best-fit line, between 70% VC and the onset of phase IV.

The analysis of these curves cannot always be made in a totally objective manner. On some curves in particular the onset of phase IV is difficult to

Figure 2. SAMPLE CLOSING VOLUME TRACE

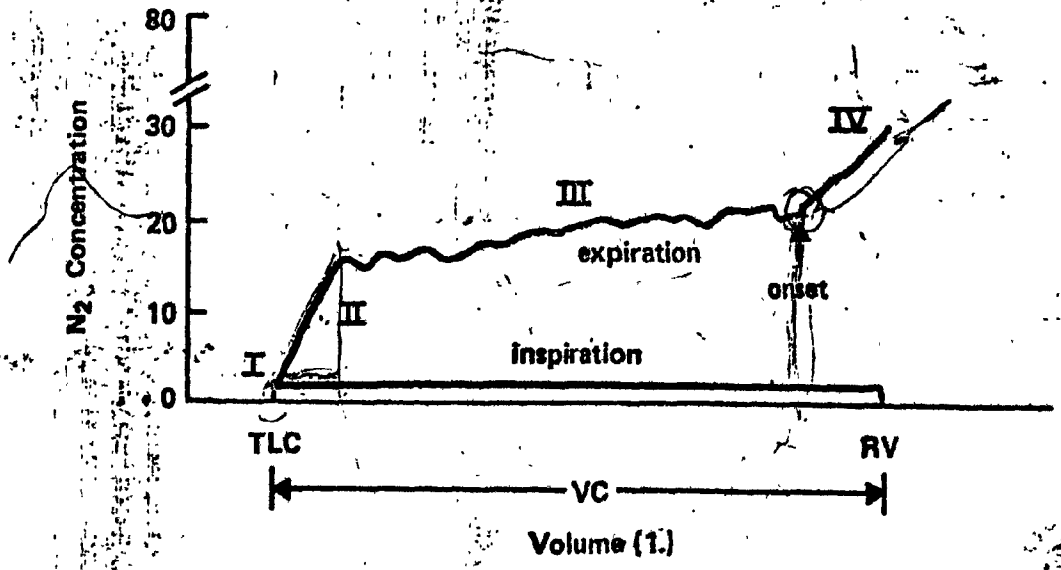

determine and when the same reader blindly reads such curves twice, there is not a very good agreement between the two measurements. This appears to be due to differences between individuals, because when a subject generates such a curve, it is likely that all curves that he generates will be difficult to analyze. On the other hand, if a subject generates a curve which is easy to analyze, in all likelihood, all curves obtained from him will be easy to analyze. Obviously curve readers will have to use good judgement and they may decide that some curves, although conforming to the criteria of acceptability, are unreadable and therefore must be rejected. It is impossible at present to establish a set of rigid rules governing such cases.

III. Appendix

Contracts Awarded Under RFP-NHLI-72-24

NHLI-73-2903
*Reuben M. Cherniack, M.D.
University of Manitoba

Epidemiologic and Physiologic Studies of Small Airways Disease

NHLI-73-2901
Jack D. Hackney, M.D.
Rancho Los Amigos Hospital

The Individual and Combined Effects of Smoking and Other Atmospheric Pollutants in Chronic Airways Obstruction

NHLI-73-2902
*Peter T. Macklem, M.D.
McGill University

Smoking and Chronic Airways Obstruction

NHLI-73-2900
*Benjamin B. Ross, M.D.
University of Oregon

Closing Volume Test of Small Airways Disease and Smoking

*These three contracts constitute a collaborative study.